

THERMODYNAMIC STUDIES OF BINARY MIXTURES
INVOLVING AROMATIC FLUOROCARBONS

A thesis presented for the degree of
DOCTOR OF PHILOSOPHY
in the
FACULTY OF SCIENCE
of the
UNIVERSITY OF LEICESTER
by
Philip R. Jackson

The Chemistry Department,
Leicester University,
LEICESTER
LE1 7RH
Oct. 1986

UMI Number: U526600

All rights reserved

INFORMATION TO ALL USERS

The quality of this reproduction is dependent upon the quality of the copy submitted.

In the unlikely event that the author did not send a complete manuscript and there are missing pages, these will be noted. Also, if material had to be removed, a note will indicate the deletion.



UMI U526600

Published by ProQuest LLC 2015. Copyright in the Dissertation held by the Author.
Microform Edition © ProQuest LLC.

All rights reserved. This work is protected against
unauthorized copying under Title 17, United States Code.



ProQuest LLC
789 East Eisenhower Parkway
P.O. Box 1346
Ann Arbor, MI 48106-1346

STATEMENT

Work presented in this thesis has been carried out by the author in the department of Chemistry at Leicester University between October 1983, and September 1986 unless stated.

This work has not been presented and is not currently being presented for any other degree.

October 1986

Philip R. Jackson

P.R.Jackson

ACKNOWLEDGEMENTS

I would like to thank my supervisor, Dr.K.W.Morcom, for his considerable help and encouragement during the past three years.

I would also like to express my thanks to Dr.D.A.Armitage at Leicester Polytechnic for his willingness to provide assistance when required, and to Dennis, Dennis, Phil and Bill in the workshop.

A special thank you is due to my mother and father for their interest and support throughout the years, and to my wife Corinne for her encouragement.

Thanks also to Chelsea F.C. for providing a means of escaping the laboratory! Again, thanks to Don, Jeremy, Tony, Steve,Gerald, et al for their friendship.

The award of an SERC research grant is acknowledged.

Finally, thanks to Rosemary for typing the thesis.

TO MY WIFE, CORINNE

Philip R. Jackson

Thermodynamic studies of
binary mixtures involving
aromatic fluorocarbons

SUMMARY

Solid-liquid phase diagrams have been determined for binary systems of hexafluorobenzene + naphthalene-type compounds, and indicate strong 1:1 congruently melting point complexes. Hexafluorobenzene + cis- and + trans-decalin were found to give simple eutectic phase diagrams.

Excess enthalpies, excess volumes and excess Gibbs functions have been measured for the same hexafluorobenzene + naphthalene-type compound mixtures and are large and negative, which is characteristic of systems where specific interactions take place. This contrasts with the large positive excess functions found with hexafluorobenzene + decalin systems, where only dispersion forces are assumed present.

The excess Gibbs function for hexafluorobenzene + trans- and cis-decalin have been determined theoretically from freezing point data as well as directly from vapour pressure measurements.

A batch calorimeter, besides being used for excess enthalpy measurements, has been employed in determining heats of solution, which lead to a value for the enthalpy change for the process, solid + solid \rightarrow complex.

The possibility of charge-transfer interactions occurring in hexafluorobenzene + naphthalene-type compound systems has been discussed in terms of HOMO/LUMO overlap considerations and is supported by the observation that pentafluorocyanobenzene forms stronger (higher melting point) complexes with 1- and 2-methylnaphthalene, than hexafluorobenzene does.

CONTENTS

	Page No.
CHAPTER 1. INTRODUCTION	
1.1 History of aromatic-fluorocarbon/ aromatic-hydrocarbon complexes	1
1.2 Aim of present research	9
CHAPTER 2. MATERIALS	
2.1 Sample preparation	11
2.2 Purity determination	13
2.3 Materials	15
CHAPTER 3. PHASE DIAGRAMS (SOLID-LIQUID EQUILIBRIA)	
3.1 Introduction	19
3.2 The apparatus	21
3.3 Operation of apparatus	22
3.4 Calibration curve	24
3.5 Results	25
CHAPTER 4. EXCESS VOLUMES	
4.1 Introduction	26
4.2 Capillary calibration	28
4.3 Batch dilatometer	28
4.4 Loading the batch dilatometer	29
4.5 Operation	30
4.6 Pressure corrections	31
4.7 Dilution dilatometer: loading	32
4.8 Dilution dilatometer: operation	34
4.9 Results	36

CHAPTER 5. ENTHALPY MEASUREMENTS

5.1	Introduction	38
5.2	Operation of calorimeter for excess enthalpy measurements (H^E liq)	38
5.3	Endothermic measurements of excess enthalpies	39
5.4	Exothermic measurements of excess enthalpies	40
5.5	Measurement of deflections $\Delta 1, \Delta 2, \Delta 3, \Delta 4$.	42
5.6	Excess enthalpy results	43
5.7	Enthalpies of solution	44
5.8	Operation of calorimeter for enthalpies of solution	47
5.9	Results	48
5.10	Calculation of enthalpy of solid complex from solid-liquid phase diagrams	48
5.11	Application	51

CHAPTER 6. EXCESS GIBBS FUNCTIONS

6.1	Introduction	53
6.2	Determination of the vapour space volume	53
6.3	Excess Gibbs function determination by Barker	55
6.4	The sample preparation line	68
6.5	Bouyancy corrections to the weight of involatile component in the cell.	69
6.6	The vapour pressure apparatus	72
6.7	The loading procedure	73
6.8	The run	75
6.9	Results	76

6.10	The theoretical determination of excess Gibbs function, ' G^E ', from simple eutectic phase diagrams	78
6.11	Results	82
CHAPTER 7. DISCUSSION		
7.1	Solid-liquid phase equilibria	83
7.2	Excess volumes	86
7.3	Excess enthalpies	89
7.4	Enthalpies of solution	92
7.5	Excess Gibbs functions	95
7.6	Excess Gibbs functions determined from solid-liquid phase diagrams	96
7.7	Preliminary spectroscopic studies	98
7.8	Conclusion	99

CHAPTER 1

INTRODUCTION

1.1. History of aromatic-fluorocarbon/
aromatic-hydrocarbon complexes.

Fluorocarbon-hydrocarbon mixtures were first studied by Scott(1,2), who found that in general such binary mixtures exhibited large positive deviations from ideality.

Upon the production of high purity aromatic fluorocarbons (due to vapour chromatography(3)), it was seen that if hexafluorobenzene replaced the aliphatic or alicyclic perfluorocarbon in a given fluorocarbon-alicyclic hydrocarbon mixture, then the excess functions were reduced in magnitude by about fifty per cent (4); they are reduced even further if the alicyclic hydrocarbon is replaced by an aromatic hydrocarbon.

The aromatic fluorocarbon-aromatic hydrocarbon complex was first noted by Patrick and Prosser (5). They reported that hexafluorobenzene and benzene gave a complex with a melting point 18 K above that of the individual components. In the same year of 1960, Brooke (6), whilst working on reactions of aromatic polyfluoro compounds with nitrogen containing bases, saw that aniline and hexafluorobenzene formed a white precipitate; an addition complex was postulated.

Work on aromatic fluorocarbon-aromatic hydrocarbon systems soon established that they were generally characterised by congruent melting point phase diagrams (16) and G^E, V^E, H^E values that were less positive than mixtures containing non-aromatic (aliphatic and alicyclic) hydrocarbons (7,8,14,15,17,45). This, together with positive C_p^E values suggested an enhanced fluorocarbon-aromatic hydrocarbon interaction. Initially a $\pi-\pi^*$ acceptor-donor interaction was put forward as an explanation.

Powell et al. (7) showed that in hexafluorobenzene + methylated benzene systems, as the number of methyl groups increased the excess volume V^E decreased. This was explained by the ability of the methyl groups to push more electrons into the π -ring of the electron donating benzene, thus creating a better partner for the electron accepting hexafluorobenzene. However, a similar trend emerged for hexafluorobenzene + methylated cyclohexane systems, even though cyclohexane has no π -character. In each case, the decrease in V^E may be due to dispersion forces which increase as more methyl groups are added. Dispersion forces cannot however account for the overall lower V^E values in aromatic fluorocarbon-aromatic hydrocarbon systems (figure 1.1.1). Morcom et al. (8) noticed the same trend in excess enthalpies for these systems.

The absence of bands in ultra-violet spectroscopy (9,10) cast further doubt on the existence of

charge-transfer interactions. Bands were noticed though in hexafluorobenzene + 'n' donor systems (examples of 'n' donors used being N,N-dimethylaniline (DMA) and N,N,N',N'-tetramethyl-p-phenylenediamine).

Foster (46,47) reported that using ^{19}F n.m.r., no detectable shift in the absorption due to hexafluorobenzene occurred, when large excesses of electron donors (aromatic hydrocarbons) were added. This does not imply the absence of charge-transfer interactions, since the shift could be undetectable if only partial charge-transfer occurs. Shifts were noticed however with other electron acceptors like 1,3 - difluoro - 2,4,6 tri-nitrobenzene.

Armitage and Morcom (13) used highest occupied molecular orbital (HOMO) - lowest unoccupied molecular orbital (LUMO) interactions to explain why charge-transfer interactions were present in complexes involving 'n' donors and not π -donors (like benzene). Consider the latter case. The LUMO of the electron accepting hexafluorobenzene interacts with the HOMO of the electron donating benzene (figure 1.1.2). The best HOMO/LUMO overlap is a partial one (figure 1.1.3). If the benzene and hexafluorobenzene molecules overlap exactly, the overlap of donor and acceptor orbitals is zero. Although the partial overlap means some charge-transfer interactions could arise, it also minimizes dispersion, polarisation and hydrogen bond forces. So a total overlap of the molecule may be preferred. In the case of

Figure (1.1.1)

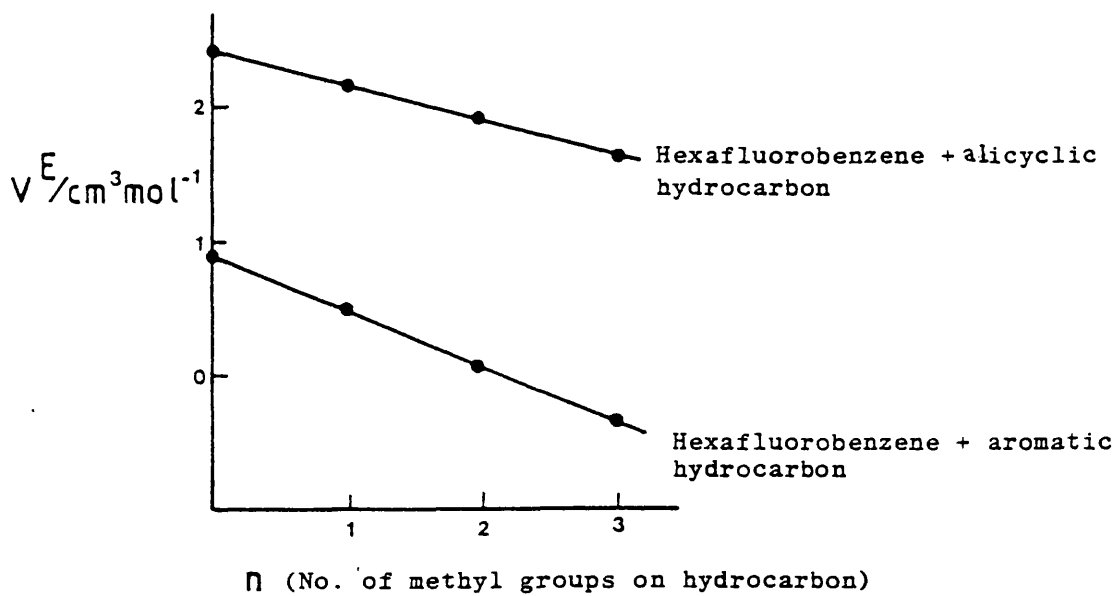
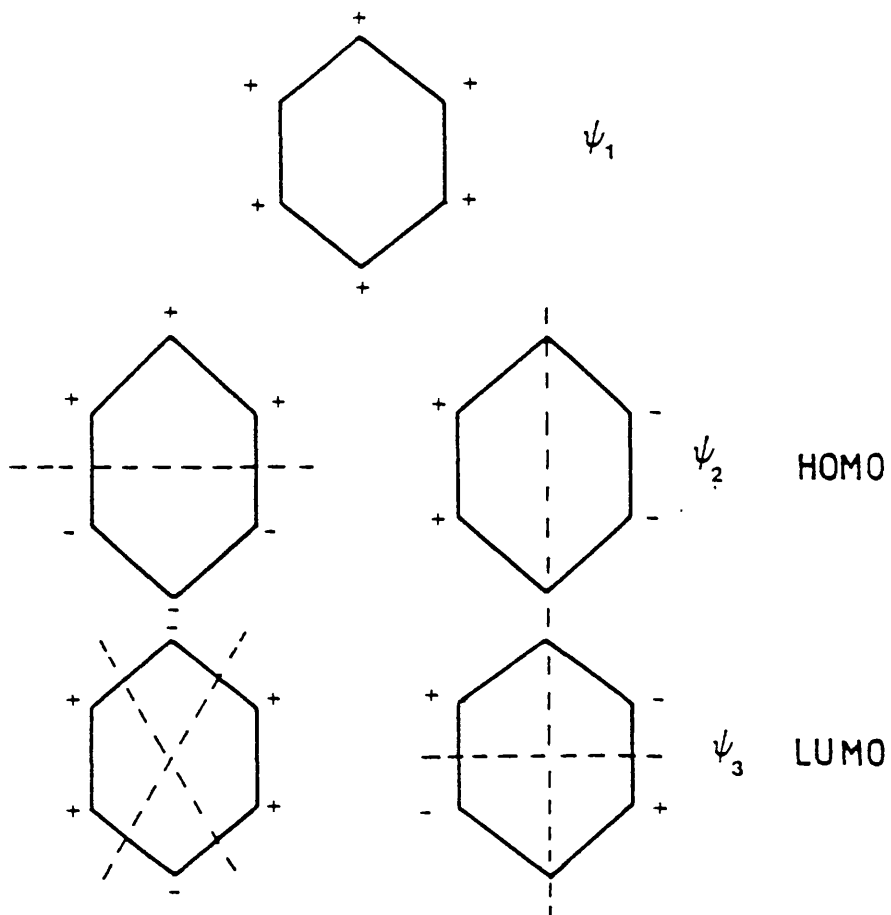


Figure (1.1.2)

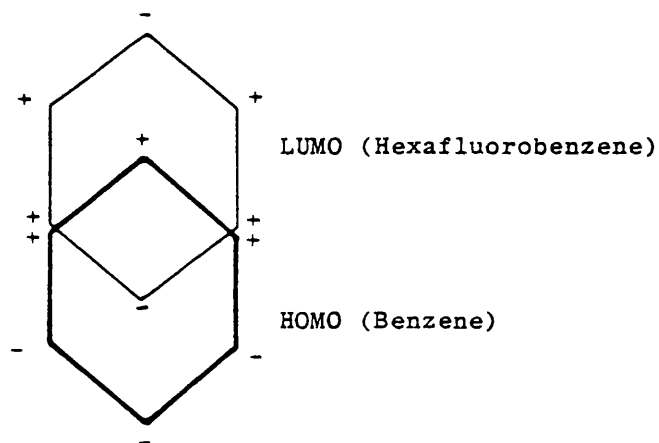


hexafluorobenzene + DMA, an altogether more favourable interaction involving partial overlap of molecules (figure 1.1.4) allows charge-transfer to occur. This offset configuration is born out by X-ray crystallography work (44).

Fenby, McLure and Scott (11,12) studied both hexafluorobenzene and pentafluorobenzene + benzene (noting s-shaped excess enthalpy curves) at different temperatures. It was seen that the excess enthalpy, H^E , became more positive as the temperature increased. They postulated that an excess function, x^E , (where $x^E = H^E, V^E, \text{ or } G^E$) was made up of two parts: x_p^E (a positive, physical contribution due to dispersion forces) that was present in any mixture, and x_c^E (a negative specific contribution due to $\pi-\pi^*$ interactions, or a direct interaction between C-H and C-F bond dipoles) present in aromatic fluorocarbon + aromatic hydrocarbon mixtures. x_p^E for aromatic fluorocarbon + aromatic hydrocarbon mixtures can be estimated by the value of the excess function for the equivalent aromatic fluorocarbon + alicyclic hydrocarbon mixtures, where no specific forces are assumed to exist; this is a dubious assumption though, as non-specific interactions are unlikely to be the same in both systems due to differences in shape and polarizability. Nevertheless, it allows an idea of x_c^E to be deduced.

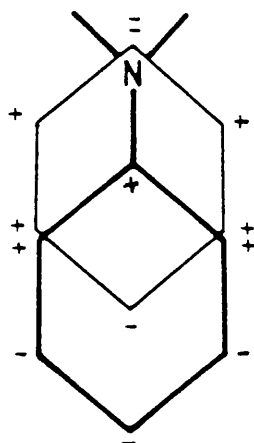
Hanna (18) suggested that H_c^E was due to electrostatic forces between the C-F bond dipole and the π -quadrupole of

Figure (1.1.3)



The best HOMO-LUMO interaction for hexafluorobenzene + benzene.

Figure (1.1.4)



HOMO-LUMO interaction for hexafluorobenzene + DMA.

the aromatic hydrocarbon, and that π - π^* interactions played little if any part in the stabilization of the complex. Gaw and Swinton (14,15) measured the vapour pressures of hexafluorobenzene + cyclohexane, + benzene, + toluene and + p-xylene. They favoured the proposal of Hanna, pointing out that in aromatic fluorocarbon-aromatic hydrocarbon interactions, although ionization potentials decrease and dispersion forces increase as more methyl groups are added to the hydrocarbon, there is also a corresponding increase in the π -quadrupole moment, thus improving C-F dipole/ π -quadrupole interactions.

Brown and Swinton (88) calculated the contribution of quadrupole/quadrupole interactions to intermolecular potentials in benzene, hexafluorobenzene and benzene + hexafluorobenzene mixtures. The quadrupole interaction potentials calculated (which ignored contributions from dispersion forces or quadrupole/dispersion forces) were dependent on the angle the molecules made to each other; in the pure substances a perpendicular arrangement of molecules was favourable, whereas in the 1:1 complex a parallel arrangement was preferred.

The solid-liquid phase diagram for pentafluorobenzene + benzene (19) surprisingly shows an incongruent melting point complex. This could be due to the fluorines attracting the electrons and leaving a highly positive hydrogen in pentafluorobenzene. Instead of the usual face-to-face configuration predicted by X-ray crystallography, the hydrogen may be attracted to the

electrons in the benzene π -ring, resulting in the pentafluorobenzene molecule lying at 90° to the benzene molecule.

Kelly et al. (41) constructed solid-liquid phase diagrams for pentafluorobenzene with various methyl substituted benzenes. 1,2- and 1,3-dimethylbenzenes both give congruent melting point complexes with pentafluorobenzene, but 1,4-dimethylbenzene does not. This may be due to the poor packing ability of 1,4-dimethylbenzene.

Skillerne de Bristowe et al. (20,21) studied pentafluorobenzene + aromatic hydrocarbon mixtures, noting similar trends in excess enthalpies and volumes as for hexafluorobenzene mixtures. In a paper with Howell (22) they too proposed the π -quadrupole / C-F bond dipole interaction as being the reason for the decrease in H^E as the number of methyl groups on the aromatic hydrocarbon increased.

Much attention has been focussed on pentafluorocyanobenzene (PFCB) complexes, where, if charge-transfer interactions are important, the cyanide, being a superior electron withdrawing group to fluorine, should lead to even stronger interactions. Morcom (23) showed that the phase diagram with benzene was unique in having two maxima at PFCB mole fractions of 0.5 and 0.625. Excess enthalpy measurements for PFCB + methylated benzene systems (24) showed that H^E becomes more negative as more

methyl groups are introduced into benzene (as was found with hexafluorobenzene). H_C^E values were calculated for PFCB + benzene, + toluene and + xylene (using cyclohexane as the non-aromatic in each case) and suggested that PFCB formed stronger complexes than hexafluorobenzene. Hall, Morcom and Brindley (25) had shown that PFCB formed stronger complexes than hexafluorobenzene with aromatic amines (again by calculating H_C^E values), but charge-transfer interactions were thought to be irrelevant in aromatic fluorocarbon + aromatic hydrocarbon mixtures. Leong, Jones and Fenby (26) measured the corresponding excess volumes, but the V_C^E value arrived at for PFCB mixtures differed little from those for hexafluorobenzene mixtures.

In 1965, Boeyens and Herbststein (27) first looked at the solid 1:1 complexes using X-ray crystallography. Their work supported the charge-transfer theory, indicating that all molecular compounds had a face to face arrangement, with the two components in alternate layers. Tor Dahl (28-31,44) continued the research, finding that the molecular planes were almost parallel to each other but that the distance between planes and the relative orientation of molecules varied from complex to complex. This suggested the presence of other intermolecular forces besides $\pi-\pi^*$. Dahl reported that the hexafluorobenzene + hexamethylbenzene complex showed properties much more like charge-transfer complexes than hexafluorobenzene + mesitylene (28), or + p-xylene (29). The hexafluorobenzene + hexamethylbenzene complex had two forms: Triclinic (30),

(stable below 273.2 K) and trigonal (31). In this complex the two rings do not overlap as much as in the others (see Armitage et al. (13), HOMO/LUMO overlap) and the interplanar distance is smaller.

Goates, Ott and Reeder have also been active in this field, presenting the congruent melting point phase diagram for hexafluorobenzene + pyridine (32), and phase diagrams for hexafluorobenzene + cyclohexene, + 1,5-cyclo-octadiene and + 1,3-cyclohexadiene (33). The latter paper indicated that at least 2π -bonds were needed in the hydrocarbon (though not necessarily conjugated) in order to form a complex with an aromatic fluorocarbon. They also recognised the possibility that packing geometry was important, noticing that the cyclic p-dioxane gave a complex with hexafluorobenzene, but that 1,2-dimethoxyethane (p-dioxane with a C-C bond severed) did not (34). Replacing the oxygen by nitrogen gave similar results (35): The cyclic N-methylpiperidine complexed with hexafluorobenzene, whilst N,N-dimethylpiperazine did not. Goates, Ott, and Reeder (35) concluded that there were three criteria for compounds that would complex with hexafluorobenzene.

1. A cyclic structure
2. Multiple interaction site. (At least 2π -bonds in the case of aromatic hydrocarbons, or two oxygens, nitrogens etc.)
3. Favourable packing geometry with

electrostatic interactions.

Andrews and Morcom (36) noticed that benzene formed complexes with p-dioxane and then went on to complement the work of Goates by measuring the excess enthalpies of hexafluorobenzene + 1,4-dioxane (37). Osborne and Morcom (42) later carried out vapour pressure measurements on a variety of cyclic ether + hexafluorobenzene systems. Murray (38) measured the excess volumes for hexafluorobenzene + non-cyclic ethers, finding positive V^E values that became more positive as the chain length increased.

1.2 Aim of present research.

The aim of this research is to look at hexafluorobenzene + naphthalene type complexes; the only previous work has been a mention of a complex existing between hexafluorobenzene and 2-methylnaphthalene (5) and a more detailed phase diagram of hexafluorobenzene with naphthalene itself (39). (Benzene + naphthalene systems have recently been studied however (43) and Milgrom (48) and Masterton (49) have both noted that 2-methylnaphthalene forms inclusion compounds with aliphatics, like n-heptane.) Following the discovery of a very strong 1:1 complex between hexafluorobenzene and 1-methylnaphthalene (40), (melting point of complex=373 K) it was decided that a whole range of phase diagrams,

excess volumes, excess enthalpies and vapour pressure measurements on hexafluorobenzene + naphthalene, + tetralin and + decalin compounds would cast further light upon the nature of the aromatic fluorocarbon-aromatic hydrocarbon interaction.

CHAPTER 2

MATERIALS

2.1 Sample Preparation.

Although some of the chemicals used were pure enough not to necessitate further purification, others (namely 1- and 2-methylnaphthalene, quinoline, isoquinoline and 2,3-cyclohexenopyridine) were not.

In the case of 2-methylnaphthalene, zone refining was employed in an attempt to improve purity. Consider a pure substance 'A' (equivalent to 2-methylnaphthalene) made impure by 'B', which lowers the melting point of 'A', resulting in a diagram of the type shown in figure (2.1.1). When liquid of composition z is cooled, the formation of a solid composition x is expected. If the equilibrium is not reached though, layers of solid varying in composition from x to z will be formed. Figure (2.1.2) shows the apparatus used, which was filled with crude 2-methylnaphthalene that was left to solidify. Only 2-methylnaphthalene in the volume of the tube covered by the heater could be melted. The heater was positioned at the base of the tube and moved slowly upwards. As it did so, the molten zone created by it moved upwards too, the impurities 'B' accumulating in it. Below the heater re-solidification occurred, the solid supposedly containing a purer form of 2-methylnaphthalene. After one run, the top third of material was discarded (whilst still liquid) and the process repeated. However, zone refining was found to have little, if any, effect on the compound's purity.

Figure (2.1.1)

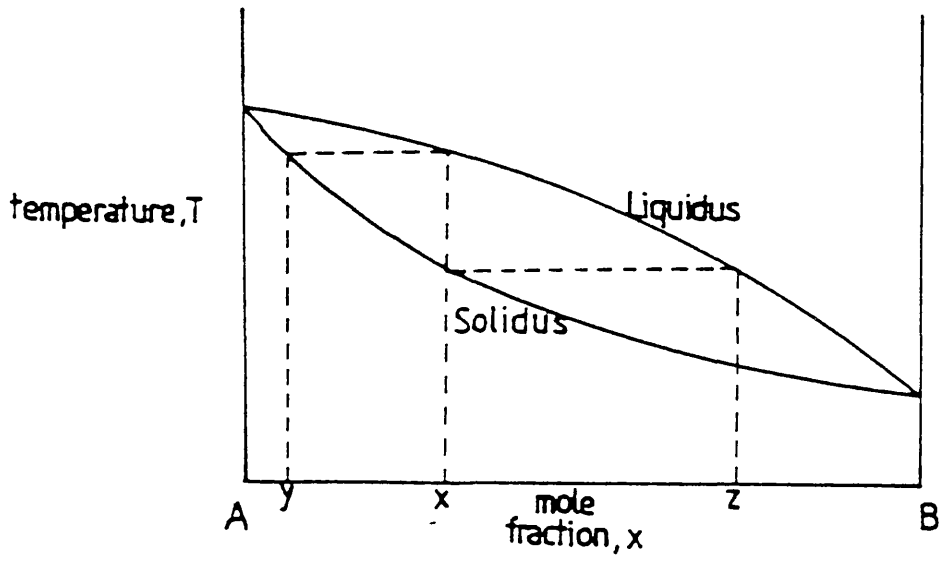
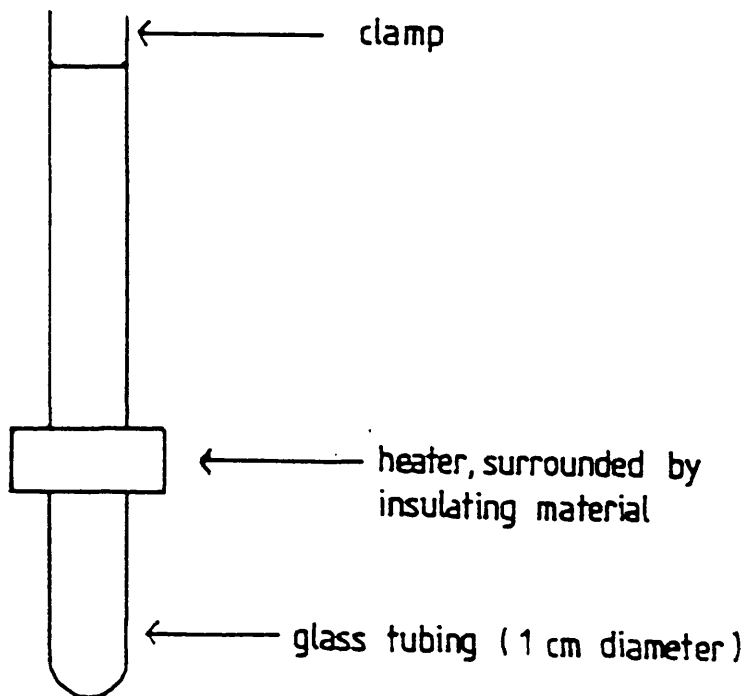


Figure (2.1.2)

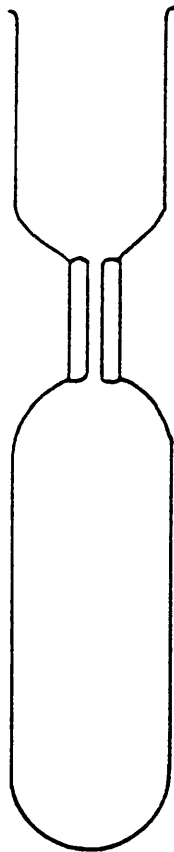


Fractional distillation was then performed under reduced pressure using a 1.5 m electrically heated column (50) and gave considerable improvements in purity as determined from freezing-point runs (section 2.2). Several fractions were collected and analysed, and in all cases, the middle fractions proved to be the purest. All liquids needing purification were treated this way.

After purification the liquids were dried. The removal of water is important, as the relative molecular mass of water is very small in comparison to that of aromatic fluorocarbons and hydrocarbons and so even a small mass of water means a significant number of moles. Liquids used in phase diagram, enthalpy and volume work were dried using Molecular Sieve (Type 4A, B.D.H. Chemicals Ltd). The sieve was activated by heating under vacuum at 453 K for several hours. 2-methylnaphthalene and isoquinoline are both solids at room temperature, but were stored at higher temperatures as liquids and dried with Molecular Sieve. Liquids used in vapour pressure measurements had to be more thoroughly dried, and P_2O_5 acted as the drying agent (see Chapter 6).

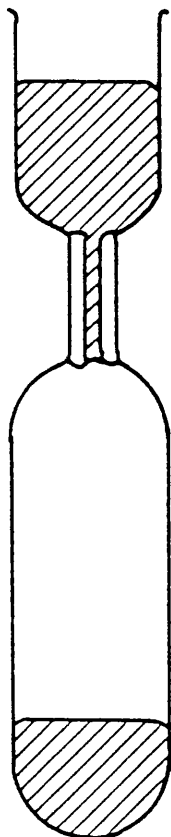
Degassing is important for enthalpy measurements and essential for volume measurements, where no air bubbles must be present if wildly spurious results are to be avoided. The ampoule (figures 2.1.3 and 2.1.4) was filled (to about three quarters of its capacity) with the relevant dried liquid, using a syringe fitted with an 8"

Figure (2.1.3)



Empty Ampoule

Figure (2.1.4)



Full Ampoule

needle. After freezing the sample with liquid nitrogen, the ampoule was attached to the vacuum line and the sample pumped on. The sample was allowed to thaw and then frozen and pumped on again. This process was repeated (generally three or four times) until no air bubbles were present. Double-distilled mercury was then run into the top of the ampoule to seal the degassed material before the vacuum was released. The degassed liquid was removed as required by syringe and the mercury in the top portion of the ampoule fell down the capillary to replace the withdrawn liquid. The liquid will remain degassed in the ampoule almost indefinitely. The ampoules must be stored at a constant temperature to prevent material loss due to expansion.

2.2 Purity determination.

Gas-liquid chromatography was used in an attempt to determine the purity of crude and fractionally-distilled 2-methylnaphthalene samples. The samples were made up to 10% solutions with alcohol and analysed using a PYE 104/P.E. F.11 G.L.C. Instead of registering a 2-methylnaphthalene and impurity peak(s), (the relative areas of which yield an estimate of purity) only a single peak was seen. This implied that the impurity peak was hidden under the main peak and that 1-methylnaphthalene was the major impurity. It was realised that a similar situation may arise over compounds like quinoline and isoquinoline, so checks on purity were made using freezing

temperature measurements.

At a melting point, if we assume that the pure solid A separates out and that $\Delta_{fus} H$ is constant, then using the Gibbs-Helmholtz equation we can obtain the familiar expression:

$$-\ln x_A \gamma_A = \frac{\Delta_{fus} H_A}{R} \left[\frac{1}{T_A} - \frac{1}{T_A^*} \right] \quad (2.2.1)$$

where T_A = the actual melting point; T_A^* = melting point of A.

If x_A is the mole fraction of the pure substance, A, then x_B represents the impurity mole fraction.

$$\ln(1-x_B) = -x_B - \frac{x_B^2}{2} - \frac{x_B^3}{3} \dots \quad (2.2.2)$$

Assuming the activity coefficient, $\gamma_A = 1$.

$$\ln x_A = \ln(1-x_B) \approx -x_B = -\frac{\Delta_{fus} H_A}{R} \left[\frac{1}{T_A} - \frac{1}{T_A^*} \right] \quad (2.2.3)$$

If it is further assumed that $T_A \approx T_A^*$, equation (2.2.3) becomes

$$x_B = \frac{\Delta_{fus} H_A}{R} \left[\frac{T_A^* - T_A}{T_A^{*2}} \right] \quad (2.2.4)$$

Where values of T_A^* were taken from the literature (67).

The purity of a sample can also be determined from an analysis of freezing temperature / time curves (51), where

it is assumed that the concentration of impurities is related to the amount of curvature of the curve corresponding to the actual freezing. However, the shape of our curves did not lend itself to this treatment.

2.3 Materials.

1. HEXAFLUOROBENZENE.

Hexafluorobenzene of Bristol Organics Ltd. (stated purity = 99.5%) was dried with Molecular Sieve 4A and used without further purification. The freezing point = 278.44 K (compared with a literature value of 278.23 K (65)). The vapour pressure of the same material dried with P_2O_5 at 303.15 K was 14305 N m^{-2} . (Compared with a literature value of 14322 N m^{-2} at 303.15 K (15)).

2. PENTAFLUOROCYANOBENZENE

Pentafluorocyanobenzene of Bristol Organics Ltd. (stated purity = 99+%) was dried using Molecular Sieve type 4A and used immediately. The freezing point of 274.35 K did not compare well with the value of Hall and Morcom (23), (275.75 K). However, supercooling with this compound made measurements of its freezing temperature difficult.

3. 2-METHYLNAPHTHALENE

2-Methylnaphthalene supplied by Fluka Chemicals had a stated purity of 97%. Freezing temperature measurements revealed the purity to be almost 98%. Fractional distillation and drying gave a final purity of 99%. The freezing point = 306.15 K.

4. 2-ETHYLNAPHTHALENE

2-Ethyl-naphthalene of Aldrich Chemical Co. had a stated purity of 99+% and was dried using Molecular Sieve and used immediately. The freezing point = 265.22 K.

5. QUINOLINE

Quinoline of Aldrich Chemical Co. (99% pure) was fractionally distilled to remove a slight brown colouration and dried with Molecular Sieve. The final purity was 99+%. The freezing point = 257.82 K.

6. ISOQUINOLINE

Isoquinoline of Aldrich Chemical Co. (stated purity = 97%) also suffered from a brown colouration that disappeared after fractional distillation. The material was dried and the new purity measured as 99%. The freezing point = 298.48 K.

7. CIS- AND TRANS-DECAHYDRONAPHTHALENE

Both cis- and trans-decahydronaphthalene had a stated purity of 99+% and were used after drying with Molecular Sieve. The vapour pressures of cis- and trans-decalin at 303.15 K were 453 N m⁻², and 893 N m⁻² respectively. This compares with literature values of 400 N m⁻², and 809 N m⁻² (67).

8. 1-METHYLNAPHTHALENE

1-Methylnaphthalene of Aldrich Chemical Co. (stated purity 97%) was fractionally distilled and dried, yielding

98.5% pure material. A further distillation and drying had no effect and the material was then used.

9. 2,3-CYCLOHEXENOPYRIDINE

2,3-Cyclohexenopyridine of Aldrich Chemical Co. was supplied without a quoted purity. Fractional distillation removed a deep red/brown colour, yielding a colourless liquid, which when dried had a purity of 99%.

10. BENZENE

Benzene (B.D.H.) of stated purity 99% was dried with Molecular Sieve and used without further purification.

11. PENTAFLUOROBENZENE

Pentafluorobenzene (Fluka Chemicals) (99% purity) was fractionally distilled and dried with Molecular Sieve before use.

12. TETRAHYDRONAPHTHALENE

Tetrahydronaphthalene of Aldrich Chemical Co. (stated purity 99%) was dried with Molecular Sieve and used immediately.

13. MERCURY

Mercury was used in calorimetry, excess volumes, vapour pressure measurements and for the storage of degassed materials. The mercury was filtered through a pierced filter paper before being washed with acetone and filtered a second time; it was then passed through a continuous recycling nitric acid column under reduced

pressure for a day. The mercury was then washed with water and dried using filter paper. Finally, the mercury was distilled twice, under reduced pressure.

CHAPTER 3

PHASE DIAGRAMS (SOLID-LIQUID EQUILIBRIA)

3.1 Introduction

Solid-liquid equilibria are normally considered under atmospheric pressure so that the remaining variables (temperature and composition) can be plotted in an equilibrium diagram. The phase rule states:

$$P + F = C + 2$$

(where P = number of phases, F = number of independent variables and C = number of components)

In a two component system, if only one phase exists (say liquid) then from the above equation, $F = 3$. One of these variables is pressure, which leaves two variables and so one phase is depicted by an area on the diagram. If two phases are present, just one degree of freedom remains (excluding pressure) and this is represented by a line. If three phases co-exist, $F = 0$ (excluding pressure) and a point is used to represent it.

Solid-liquid systems can be divided into three categories.

1. Eutectic systems
2. Completely miscible solid solutions
3. Partially miscible solid solutions

The first category can be sub-divided into the following types:

(a) Eutectic formation, with liquids miscible: The components are miscible in the liquid state, but pure components make up the solid phases. Addition of 'A' to pure 'B' will lower the melting point of 'B' and vice versa. A typical diagram is shown in figure (3.1.1).

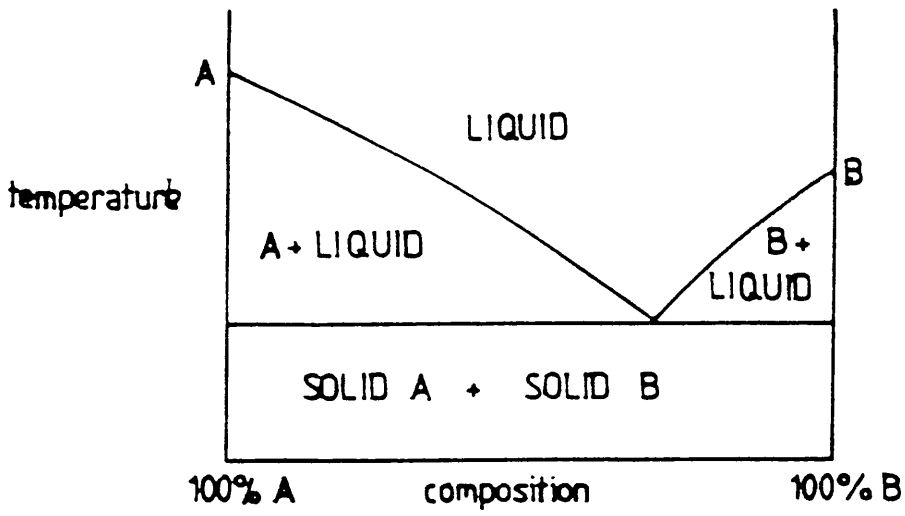
(b) Eutectic formation, with liquids partially miscible.

(c) Congruently melting compound formation. 'Congruent' implies that the solid substance can exist in equilibrium with the liquid of the same composition.

Compounds of the type AB , AB_2 , A_2B etc. can be formed, the composition being given by the maximum of the curve (1:1 complex in the example, figure 3.1.2). The melting point corresponding to 'D' may be above, or below the melting point of the pure components and the shape of the curve in the region 'CDE' gives a fair indication of the compound's stability (figures 3.1.3 and 3.1.4). 1:1 complexes of this type are commonly encountered in hexafluorobenzene + aromatic hydrocarbon systems (16).

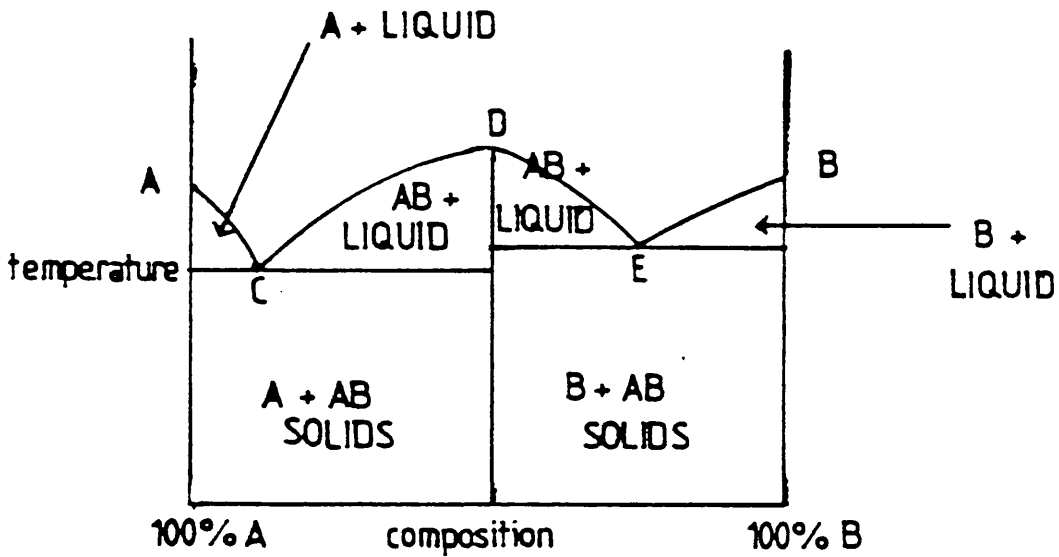
(d) Incongruently melting complexes. These occur when the compound is not very stable, even in the solid state and decomposes below its melting point. An example is shown in figure (3.1.5), the composition of the complex

Figure (3.1.1)



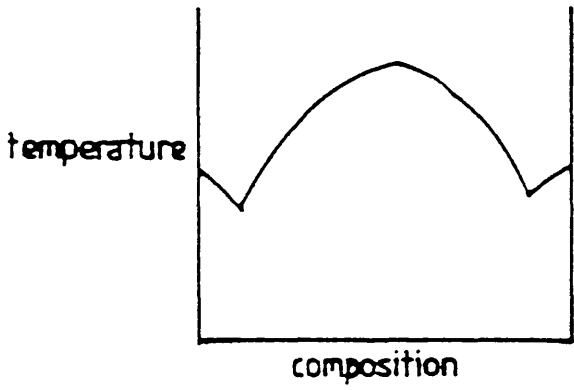
Eutectic phase diagram

Figure (3.1.2)



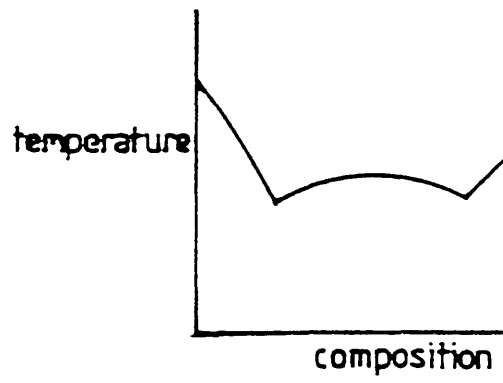
Phase diagram for congruently melting complex

Figure (3.1.3)



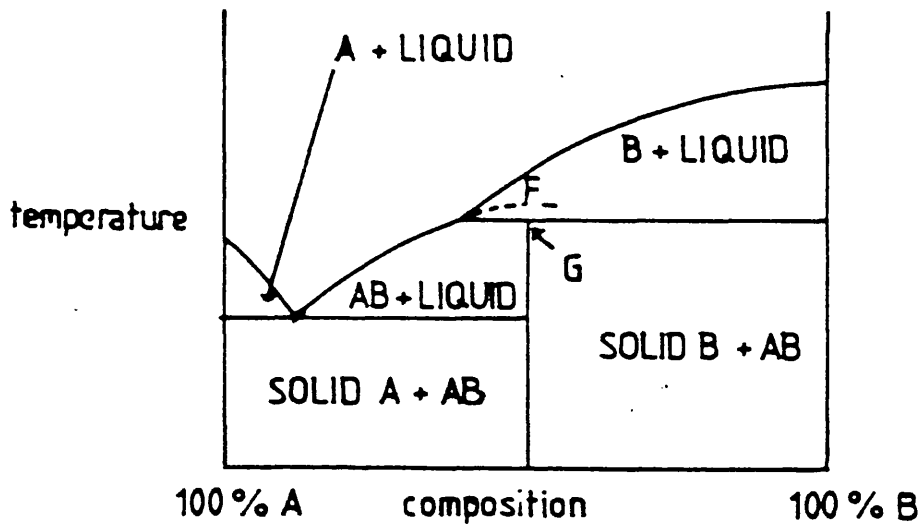
Stable complex

Figure (3.1.4)



Unstable complex

Figure (3.1.5)



Phase diagram for Incongruently melting complex

being indicated by point 'F' (the maximum of the extrapolated portion). True melting is solid \rightarrow liquid. Peritectic (or meritectic) melting is solid I \rightarrow liquid + solid II and this arises at point 'G', where the 1:1 complex breaks up into its components.

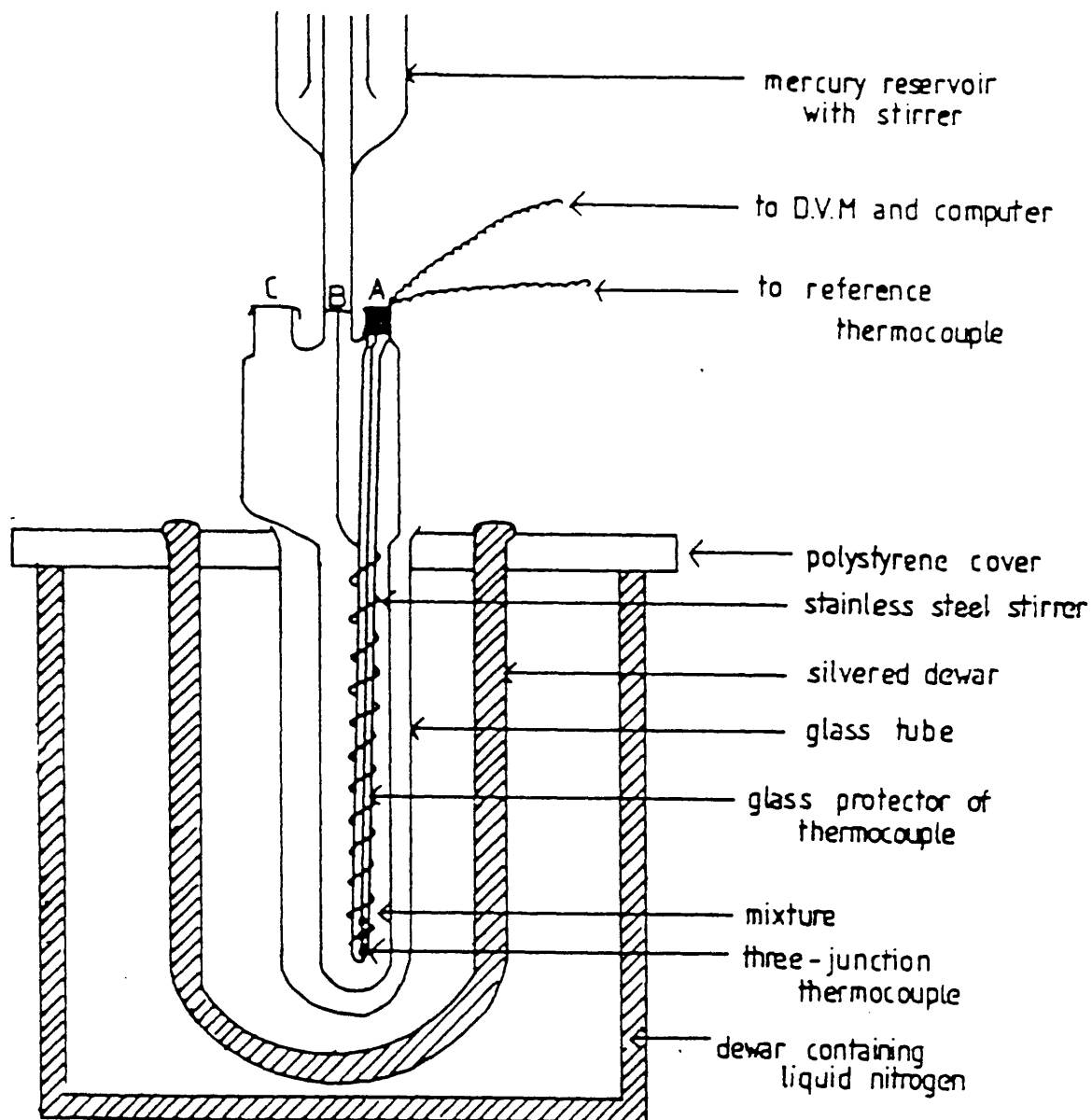
Kendall (52) looked at the solubility of a compound 'A' in different solvents 'B' which had a gradually increased ability to form compounds with 'A'; the phase diagrams slowly changed from simple eutectic, to incongruent and finally to congruent.

3.2 The apparatus

This is shown in figure (3.2.1) and is similar in design to the apparatus employed by Duncan and Swinton (16), and Osborne (53). Other types of phase diagram apparatus include models where stirring is effected by means of a pulsating gas pressure applied to the liquid surface. These have an advantage over mechanically stirred equipment (like the one to be described here) where the stirrer ceases to function when the mixture is half frozen (which affects the cooling curve).

The cell is depicted in figures (3.2.2) and (3.2.3). The Quickfit joint 'A' accommodates a glass tube that in turn contains a three junction copper/constantan thermocouple; the tube reaches to the bottom of the cell's finger. The thermocouple is linked to a digital voltmeter (D.V.M.) which gives the electromotive force (E.M.F.)

Figure (3.2.1)



Phase diagram apparatus

Figure (3.2.2)

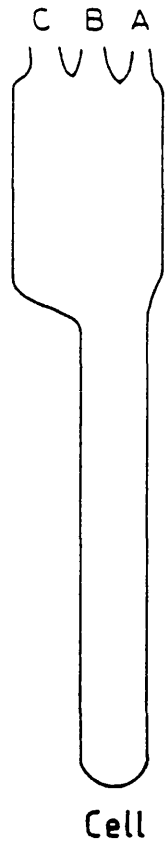
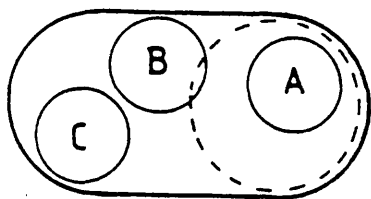


Figure (3.2.3)



Top view of cell.

readings. The outlet 'C' holds a rubber Suba seal (frequently changed due to perishing), through which components are injected into the finger. The entire cell is connected to the stirrer portion of the apparatus via 'B'. The D.V.M. is linked to a Commodore 'Pet' (Model 3032) computer and plotter, enabling an E.M.F. against time graph to be constructed as the run progresses.

3.3 Operation of Apparatus

The glass cell (figure 3.2.2) was cleaned using chromic acid, water and finally acetone, before being dried in the oven. It was then attached to the stirrer at 'B' and the thermocouple and Suba seal put in place. The reference thermocouple was placed in an ice/distilled water bath, which was frequently stirred to ensure a steady temperature of 273.15 K. The mechanical stirrer was then briefly operated to ensure that the stainless steel stirrer had a free vertical movement of about 1 cm without disturbing the glass tube it surrounded.

In any run, the chosen compound was injected through 'C' at the base of the cell's finger, using a pre-weighed syringe (with 8" needle). The syringe was then re-weighed in order to obtain the weight of liquid introduced and the new mole fraction. The liquid, once injected, had to at least cover the three junctions of the thermocouple. Dry nitrogen gas was injected through the cell (again via 'C') to ensure an inert atmosphere. Stirring in the cell was then commenced and the cooling performed using liquid

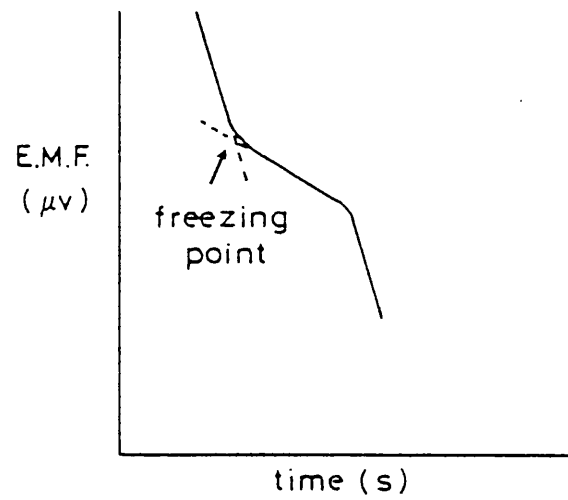
nitrogen. (The glass tube and silvered dewar placed around the finger allowed a uniform rate of cooling.) A plot of E.M.F. against time was produced, from which an E.M.F. corresponding to the freezing point was obtained.

The first run was usually performed on one of the pure components and in subsequent runs more and more of the second component was added until a mole fraction of at least 0.5 was attained.

The other side of the diagram was produced in the same way, but by first performing a run on the pure second component and then gradually adding more and more of component one.

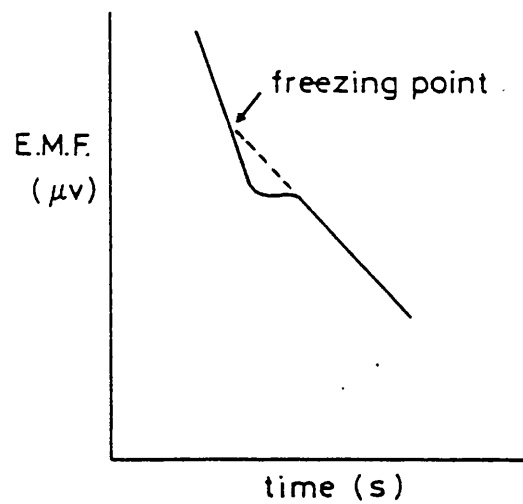
Typical E.M.F. against time plots are shown in figures (3.3.1) and (3.3.2), with the breaks due to freezing of the mixture. At liquid compositions close to the eutectic a slightly more complicated E.M.F. against time plot arises (figures 3.3.3 and 3.3.4). As the liquid of composition I is cooled the temperature falls rapidly along 'jk'. At 'k', liquid of composition I is in equilibrium with solid 'AB' and as further cooling occurs more solid 'AB' separates giving latent heat. This means cooling along 'k' is slower. As more and more solid 'AB' separates out so the composition of the liquid alters along the line 'kc' becoming richer in 'B'. Eventually, the liquid has the eutectic composition (II) and solids 'B' and 'AB' separate. Along 'lm' the temperature is constant until all liquid is frozen. 'lm' is termed the

Figure (3.3.1)



A typical cooling run of a binary mixture, indicating freezing point.

Figure (3.3.2)



Cooling run showing supercooling. Extrapolation indicates freezing point.

Figure (3.3.3)

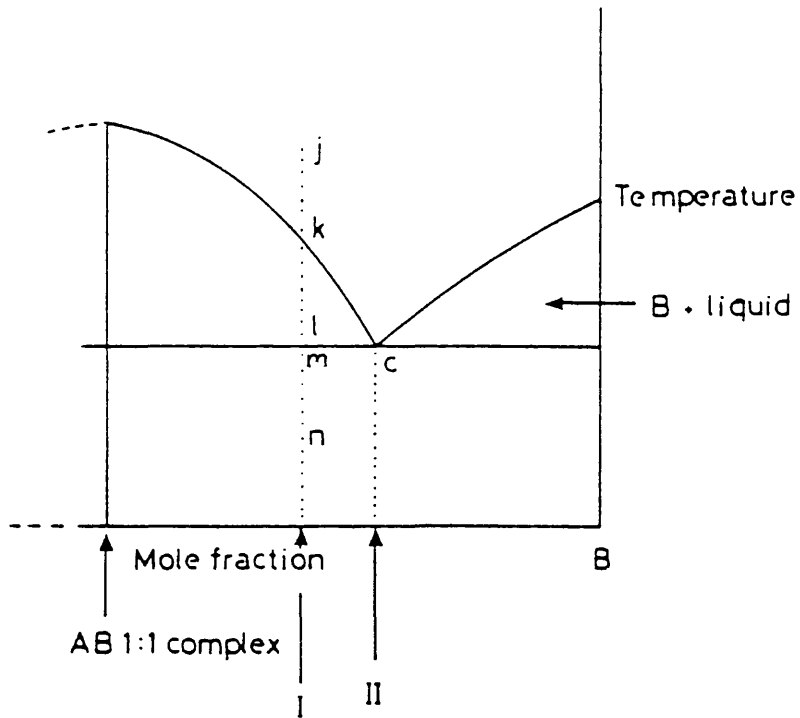
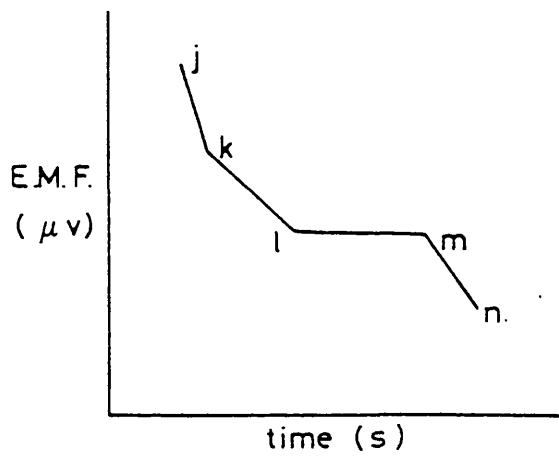


Figure (3.3.4)



E.M.F. v. time plot corresponding to cooling a mixture of composition I (figure 3.3.3).

eutectic arrest.

3.4 Calibration curve

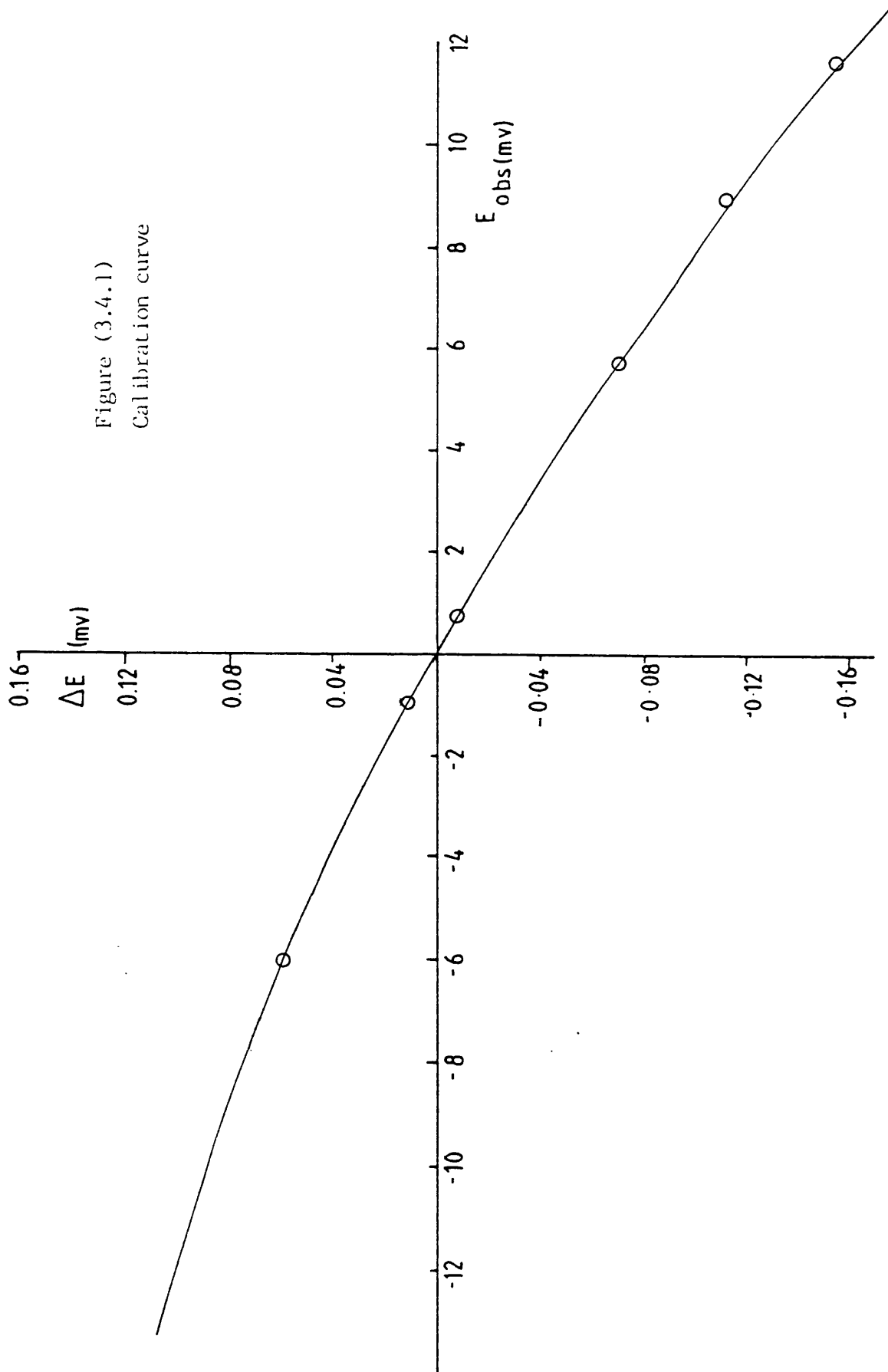
A calibration curve (figure 3.4.1) was constructed as follows. One junction of the thermocouple, along with a platinum resistance thermometer, was placed in a water bath thermostated at, say, 313.15 K. The reference junction rested in an ice/distilled water bath at 273.15 K. The platinum resistance thermometer was connected to a resistance bridge (Automatic Systems Laboratories Model F17) which allowed the temperature of the water bath to be determined to ± 0.001 K. Calibration tables (55) were used to convert the temperatures to an E.M.F. (E_{standard}). E_{observed} values were read from the D.V.M. The water bath was then set at various other temperatures and the procedure repeated.

From the phase diagram experiments, a list of observed E.M.F.s and their corresponding mole fractions were obtained. The observed E.M.F.s were converted to standard E.M.F.s using the equation

$$E_{\text{standard}} = E_{\text{observed}} - \Delta E \quad (3.4.1)$$

and the calibration curve of ΔE versus E_{observed} plotted. Finally, calibration tables were consulted again to convert the E_{standard} values to temperatures.

Figure (3.4.1)
Calibration curve



3.5 Results

Tables (3.5.1) - (3.5.12) show the freezing temperatures, eutectic arrest point temperatures and fluorocarbon mole fraction (X_f) for the systems studied. Freezing temperatures were generally determined from cooling runs and are generally believed to be reliable to ± 0.03 K; an asterisk denotes values obtained from warming runs. The phase diagrams are shown in figures (3.5.1) - (3.5.12).

Table (3.5.1)

Freezing temperatures

Hexafluorobenzene + 2-methylnaphthalene

x_F	Freezing temperature/K	Eutectic/K
0.000	305.76	
0.005	305.70	
0.069	301.62	
0.127	304.55	299.00
0.147	308.83	
0.184	314.23	
0.238	322.73	
0.308	328.84	
0.352	331.39	
0.392	333.37	
0.461	335.54	
0.506	335.66	
0.546	335.56	
0.643	332.64	
0.683	328.10	
0.733	325.49	
0.767	321.56	
0.789	317.48	
0.860	303.45	275.25
0.939	276.68	
0.949	275.28	
0.959	276.52	
0.983	277.43	
1.000	278.44	

Table (3.5.2)

Freezing temperatures

Hexafluorobenzene + 2-ethylnaphthalene

x_F	Freezing temperature/K	Eutectic/K	x_F	Freezing temperature/K	Eutectic/K
0.000	265.22		0.575	306.00	
0.028	262.49		0.609	305.11	
0.048	257.33		0.620	304.77	
0.050	258.03		0.683	301.56	
0.055	260.68		0.720	299.20	
0.058	262.47	257.05	0.749	296.63	
0.061	263.27		0.780	293.36	
0.063	263.56		0.806	289.83	
0.086	270.61		0.870	279.85	
0.101	277.42		0.886	274.51	
0.123	281.21		0.899	272.98	
0.134	283.65		0.918	273.68	272.41
0.170	287.23		0.958	275.94	272.56
0.217	293.63		0.984	277.61	
0.233	294.71		0.993	277.90	
0.271	299.00		1.000	278.44	
0.293	300.39				
0.353	304.06				
0.384	304.88				
0.402	305.41				
0.449	305.03				
0.482	306.43				
0.500	306.65				
0.534	306.60				

Table (3.5.3)

Freezing temperatures

Hexafluorobenzene + quinoline

x_F	Freezing temperature/K	Eutectic/K	x_F	Freezing temperature/K	Eutectic/K
0.000	257.82		0.904	281.52	
0.032	259.06		0.932	275.17	
0.037	265.19		0.952	276.06	274.26
0.043	269.62		0.972	277.22	
0.046	271.60	254.50	1.000	278.44	
0.050	272.30				
0.075	283.01				
0.092	288.55				
0.109	292.25				
0.139	298.15				
0.141	298.34				
0.219	308.07				
0.276	310.62				
0.328	314.19				
0.364	315.64				
0.404	316.57				
0.446	317.34				
0.528	317.64				
0.580	316.91				
0.622	315.71				
0.708	310.63				
0.746	307.70				
0.800	302.91				
0.849	295.22				

Table (3.5.4)

Freezing temperatures

Hexafluorobenzene + isoquinoline

x_F	Freezing temperature/K	Eutectic/K	x_F	Freezing temperature/K	Eutectic/K
0.000	298.48		0.550	284.80	
0.018	297.25		0.604	283.69	
0.060	295.14		0.633	282.82	
0.077	294.15		0.661	281.48	
0.116	292.23		0.707	278.79	
0.167	289.27		0.752	275.33	
0.215	286.55	282.07	0.774	273.28	
0.268	283.28	282.05	0.799	269.57	
0.306	281.98		0.803	269.15	
0.336	282.73	281.57	0.823	267.96	
0.372	283.82	281.53	0.890	271.89	267.65
0.395	284.23		0.948	275.56	
0.420	284.65		1.000	278.44	
0.504	285.36				

Table (3.5.5)

Freezing temperatures

Hexafluorobenzene + tetralin

x_F	Freezing temperature/K	Eutectic/K	x_F	Freezing temperature/K	Eutectic/K
0.000	238.00		0.506	266.69	
0.028	232.65		0.542	266.43	
0.039	230.07	229.66	0.588	265.52	
0.064	231.58		0.611	264.71	
0.068	232.10		0.626	264.11	
0.080	238.10		0.654	262.81	
0.138	248.00		0.676	261.62	
0.180	253.24		0.700	260.09	258.17
0.210	256.56		0.721	258.30	257.55
0.261	259.70		0.737	258.44	
0.307	262.81		0.798	263.62	
0.345	264.24		0.849	267.54	
0.386	265.08		0.897	271.14	
0.423	266.06		1.000	278.44	
0.469	266.56				

Table (3.5.6)

Freezing temperatures

Hexafluorobenzene + cis-decalin

x_F	Freezing temperature/K	Eutectic/K	x_F	Freezing temperature/K	Eutectic/K
0.000	231.41		0.588	268.68	
0.033	230.08	229.90	0.639	268.88	
0.096	230.41	229.91	0.683	269.61	
0.100	253.79		0.719	270.78	
0.110	253.99		0.750	271.13	
0.136	256.61		0.795	271.17	
0.193	261.55		0.828	271.47	
0.242	263.17		0.855	272.72	
0.276	264.73		0.876	273.05	
0.361	266.25		0.894	273.84	
0.399	266.81		0.910	274.67	
0.449	266.97		0.921	274.77	
0.485	267.52		0.951	276.36	
0.517	267.57		0.970	277.20	
0.562	268.27		1.000	278.44	

Table (3.5.7)

Freezing temperatures

Hexafluorobenzene + trans-decalin

x_F	Freezing temperature/K	Eutectic/K	x_F	Freezing temperature/K	Eutectic/K
0.000	244.41		0.542	265.32	
0.044	244.34	242.58	0.574	266.01	
0.065	242.63		0.601	266.70	
0.097	242.11		0.651	267.64	
0.106	242.50		0.692	268.25	
0.143	250.57		0.741	269.32	
0.179	253.89		0.799	270.74	
0.225	257.13		0.839	272.04	
0.286	259.82		0.877	273.28	
0.322	261.26		0.900	274.17	
0.399	263.32		0.928	275.66	
0.483	264.43		1.000	278.44	
0.513	264.91				

Table (3.5.8)

Freezing temperatures

Hexafluorobenzene + 2,3-Cyclohexenopyridine (Incomplete)

x_F	Freezing temperature/K	x_F	Freezing temperature/K
0.000	224.99*	0.649	252.35
0.048	221.31*	0.702	257.21
0.094	217.75*	0.741	261.02
0.148	213.29*	0.781	263.79
0.371	217.73	0.819	266.86
0.391	218.86	0.852	269.32
0.415	224.86	0.899	272.26
0.473	231.43	0.921	273.99
0.510	235.98	0.956	276.24
0.539	240.15	0.987	277.92
0.582	245.59	1.000	278.44
0.615	248.34		

Temperatures with an asterisk beside them were obtained by warming runs.

No Eutectics noted.

Table (3.5.9)

Freezing temperatures

Pentafluorocyanobenzene + 1-methylnaphthalene

x_F	Freezing temperature/K	Eutectic/K
0.000	242.58	
0.033	277.74	
0.044	291.03	
0.054	300.82	240.94
0.061	309.13	242.33
0.084	317.81	
0.132	346.43	
0.209	367.52	
0.305	382.65	
0.414	391.17	
0.495	392.69	
0.554	392.10	
0.638	388.31	
0.733	379.30	
0.754	376.57	
0.777	373.26	
0.849	354.47	
0.887	342.99	
0.913	331.60	
0.937	317.77	
0.950	307.37	272.62
0.961	300.20	273.02
1.000	274.35	

Table (3.5.10)

Freezing temperatures

Pentafluorocyanobenzene + 2-methylnaphthalene

x_F	Freezing temperature/K	Eutectic/K
0.000	306.15	
0.039	303.53	
0.096	299.25	
0.138	305.08	298.03
0.189	318.21	
0.226	325.29	297.83
0.268	334.75	
0.316	340.73	
0.419	348.27	
0.484	350.99	
0.557	349.99	
0.625	346.94	
0.709	338.10	
0.759	330.29	
0.775	328.58	
0.803	322.94	
0.861	312.90	
0.923	295.58	
1.000	274.10	

Table (3.5.11)

Freezing temperatures

Pentafluorobenzene + 2-methylnaphthalene

x_F	Freezing temperature/K	Eutectic/K
0.000	305.06	
0.055	301.33	
0.150	293.80	
0.248	286.12	277.56
0.303	280.67	277.87
0.380	279.79	277.80
0.419	280.90	
0.481	282.01	
0.518	281.96	
0.626	278.96	
0.696	275.38	
0.760	269.46	
0.826	258.75	227.03
0.885	244.24	226.99
1.000	228.51	

Table (3.5.12)

Freezing temperatures

Hexafluorobenzene + Naphthalene (Naphthalene rich side only)

x_F	Freezing temperature/K	Eutectic/K
0.000	353.15	
0.027	351.70	
0.052	350.61	
0.127	346.52	
0.130	346.56	
0.173	350.98	
0.200	354.43	346.04
0.225	358.40	346.43
0.261	363.18	346.54
0.268	361.99	
0.295	364.08	
0.330	366.76	
0.391	369.50	
0.409	370.00	

Figure (3.5.1)
Solid liquid phase diagram
Hexafluorobenzene + 2-methylnaphthalene

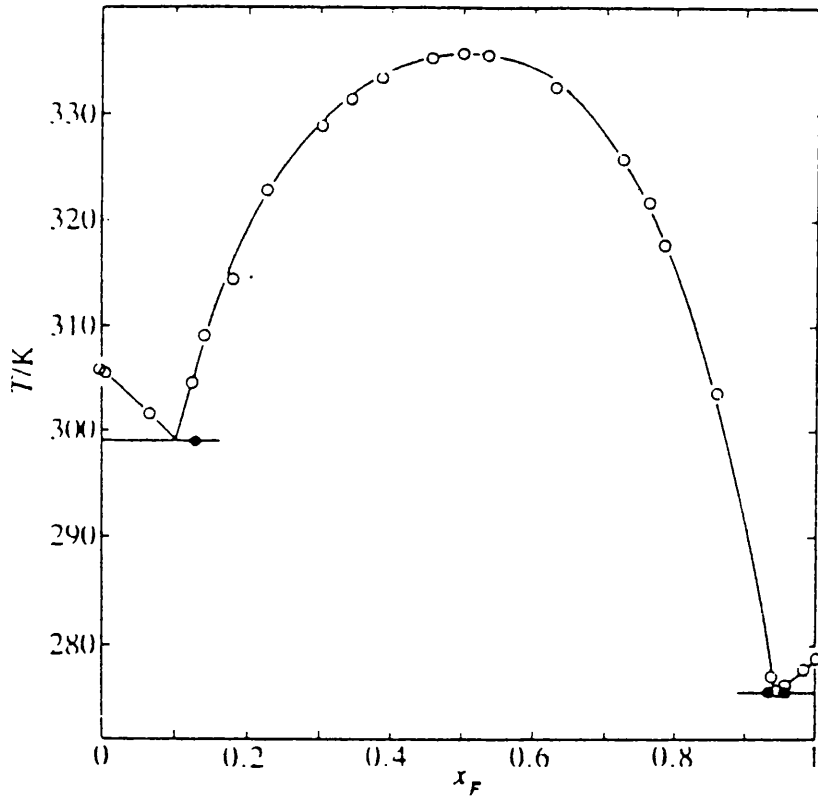


FIGURE (3.5.2)
Solid liquid phase diagram
Hexafluorobenzene + 2-ethylnaphthalene

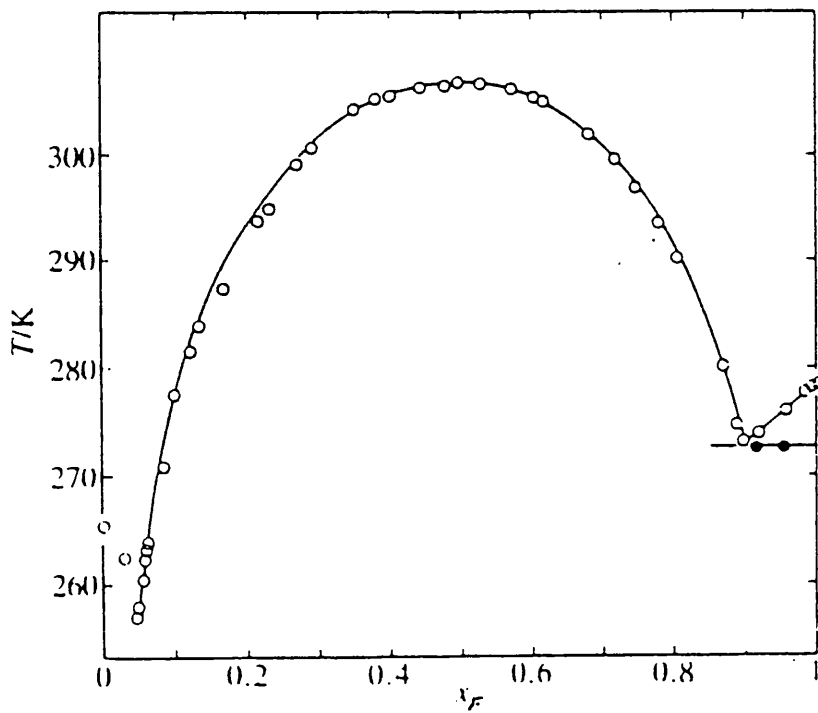


Figure (3.5.3)
Solid liquid phase diagram
Hexafluorobenzene + quinoline

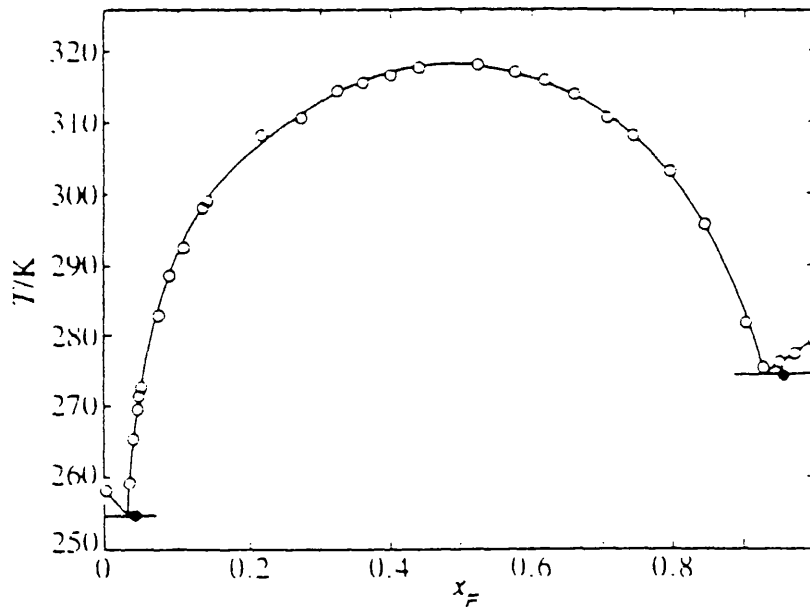


Figure (3.5.4)
Solid liquid phase diagram
Hexafluorobenzene + Isoquinoline

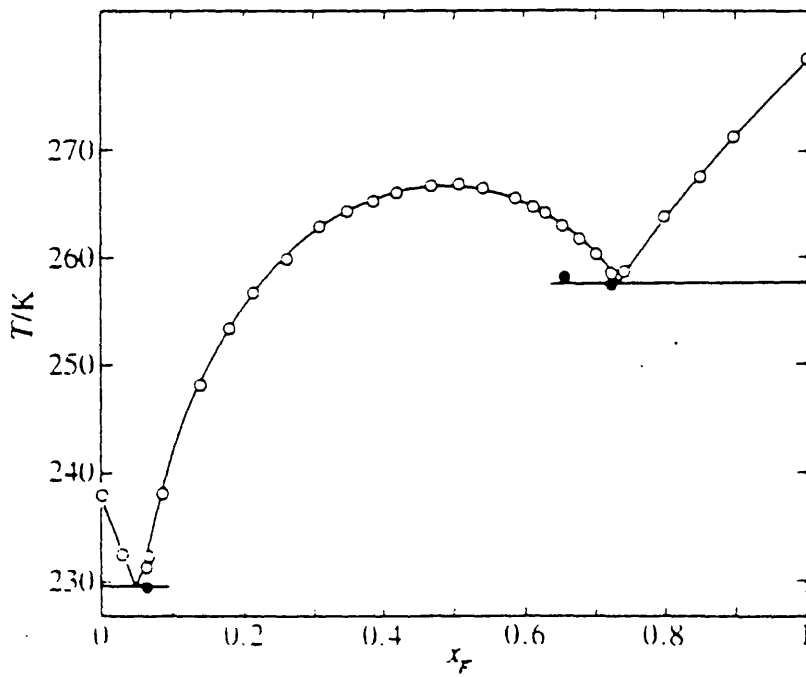


Figure (3.5.5)
Solid liquid phase diagram
Hexafluorobenzene + tetralin

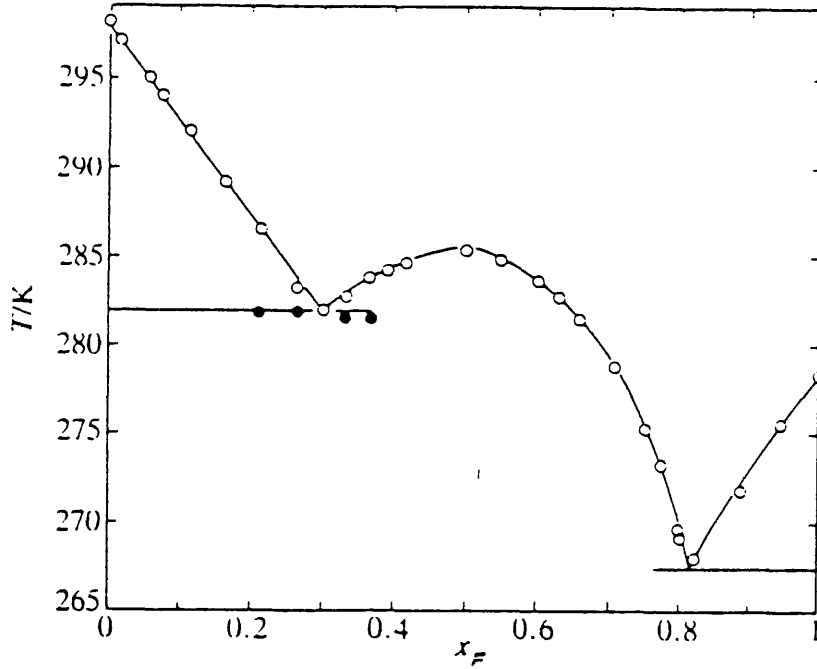


Figure (3.5.6)
Solid liquid phase diagram
Hexafluorobenzene + cis-decalin

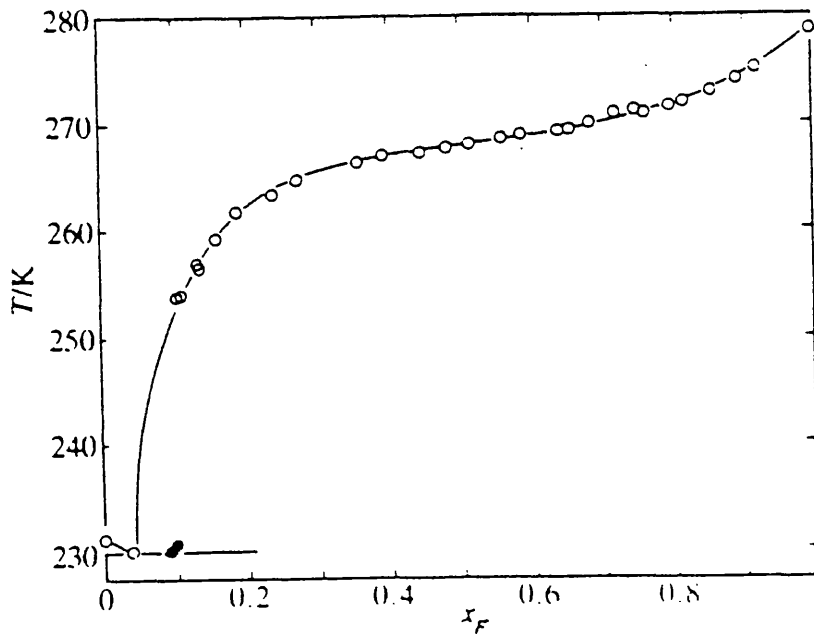


Figure (3.5.7)
Solid liquid phase diagram
Hexafluorobenzene + trans-decalin

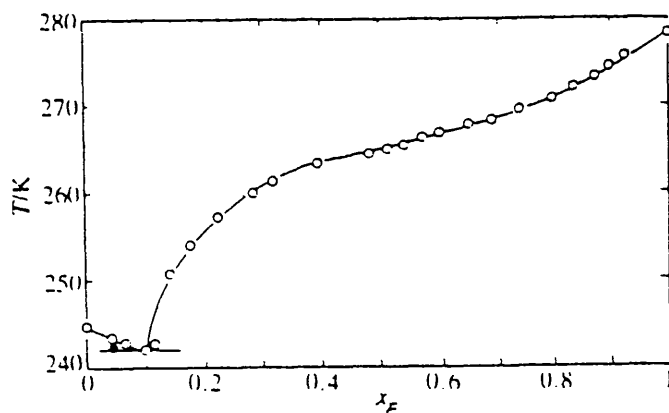


Figure (3.5.8)
Solid liquid phase diagram
Hexafluorobenzene + 2,3-cyclohexenopyridine

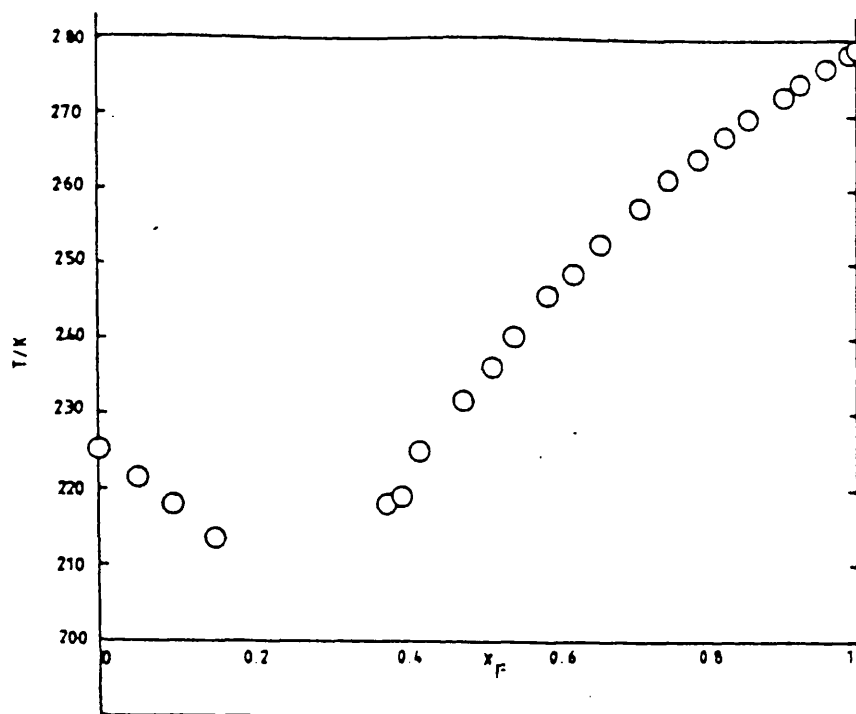
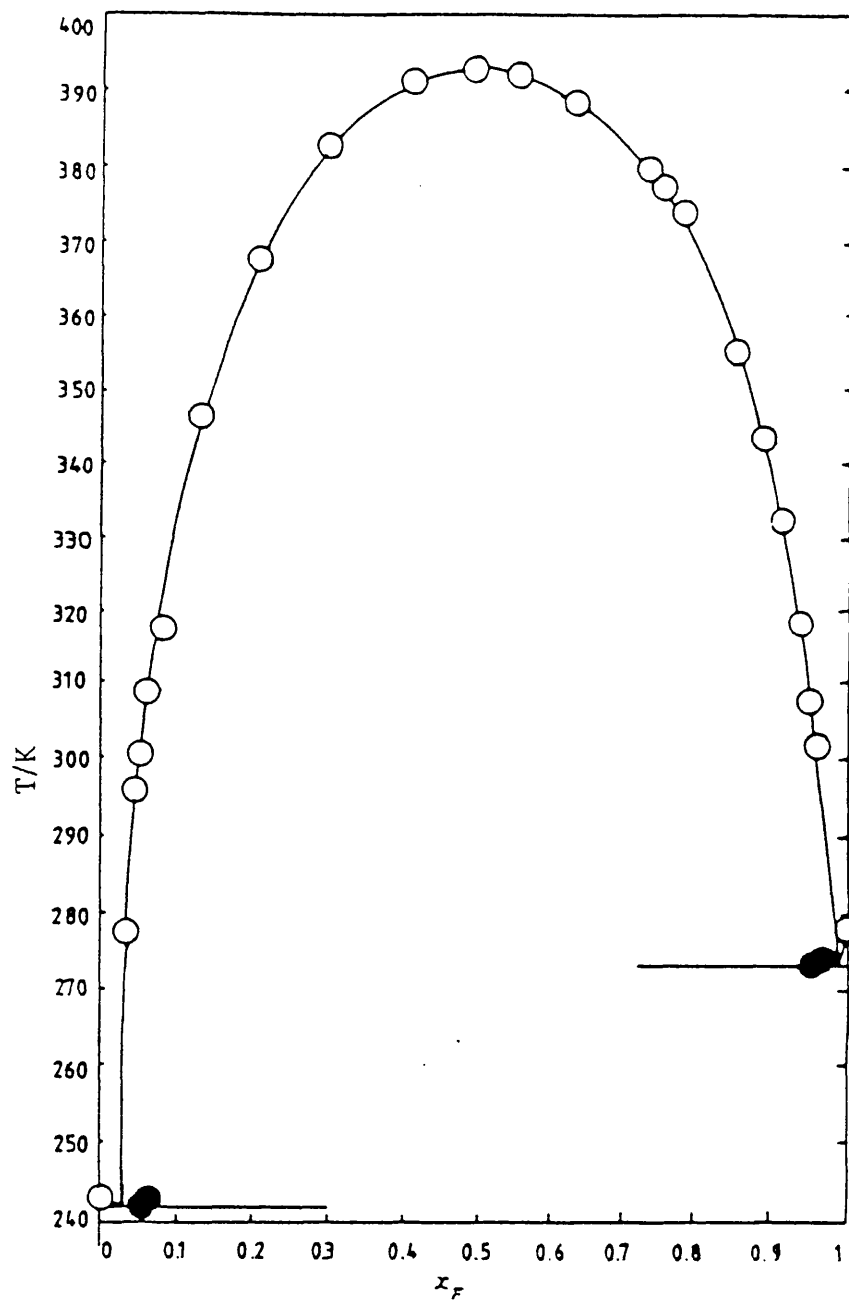


Figure (3.5.9)

Solid liquid phase diagram

Pentafluorocyanobenzene + 1-methylnaphthalene



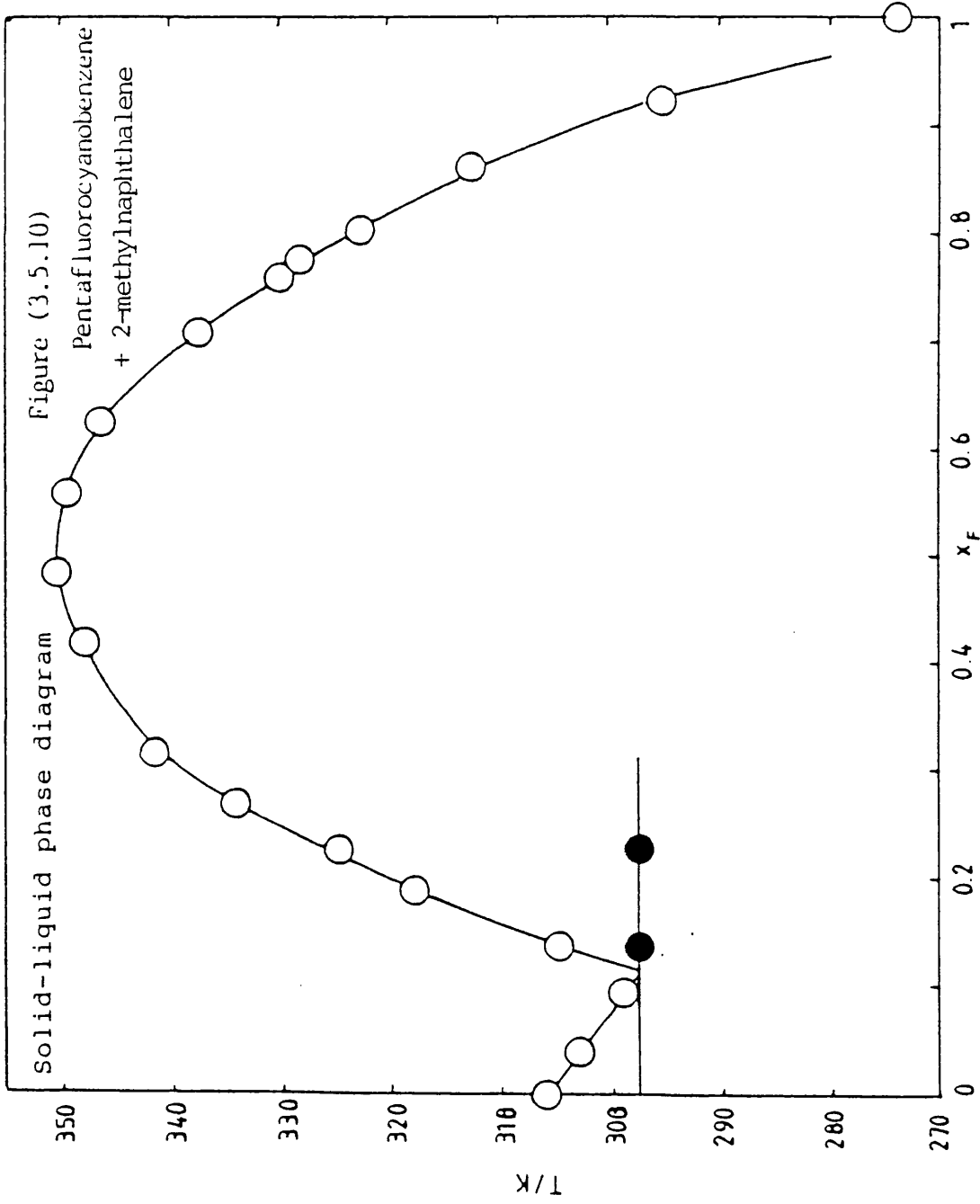


Figure (3.5.11) Solid-liquid phase diagram
Pentafluorobenzene + 2-methylnaphthalene

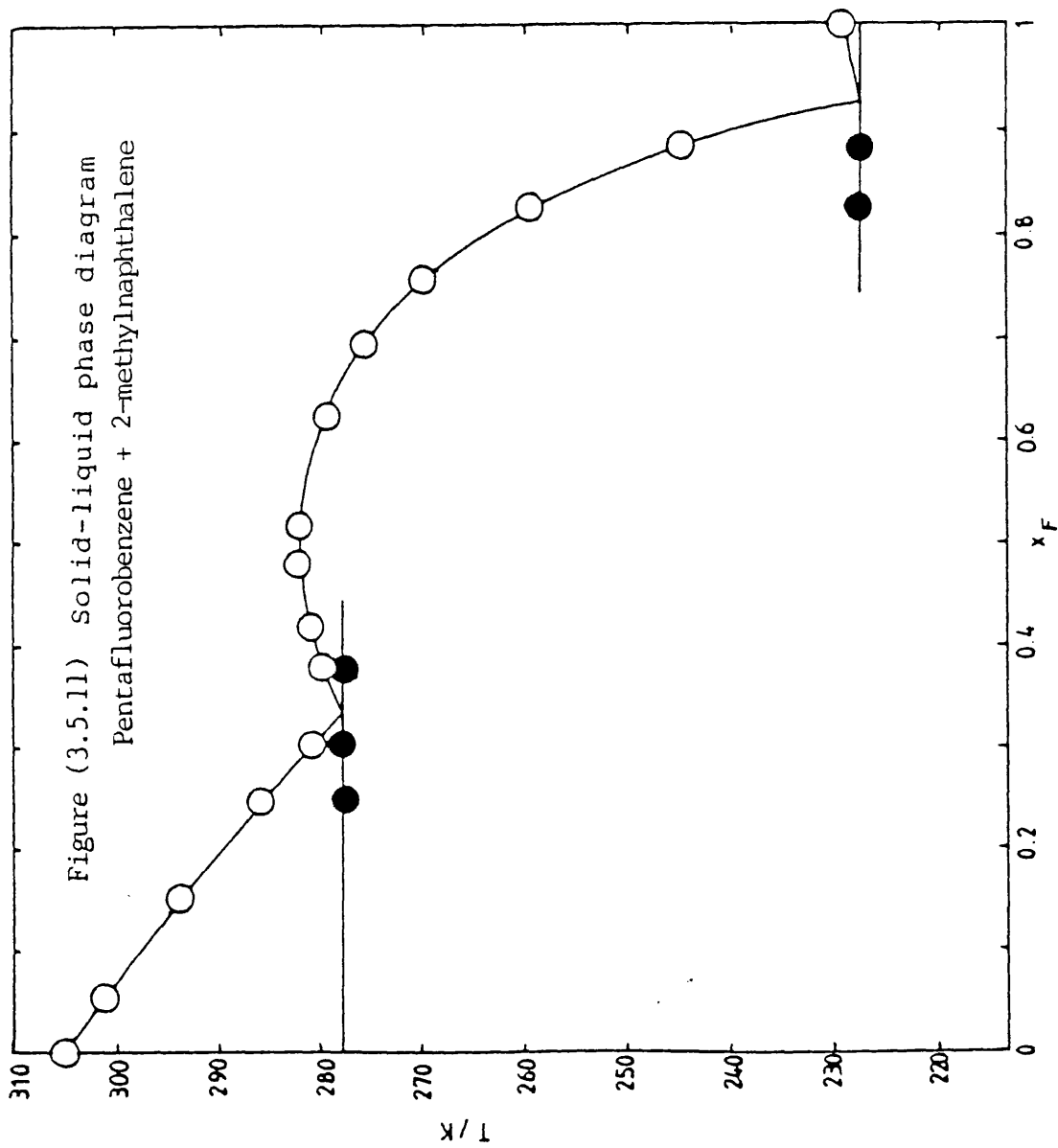
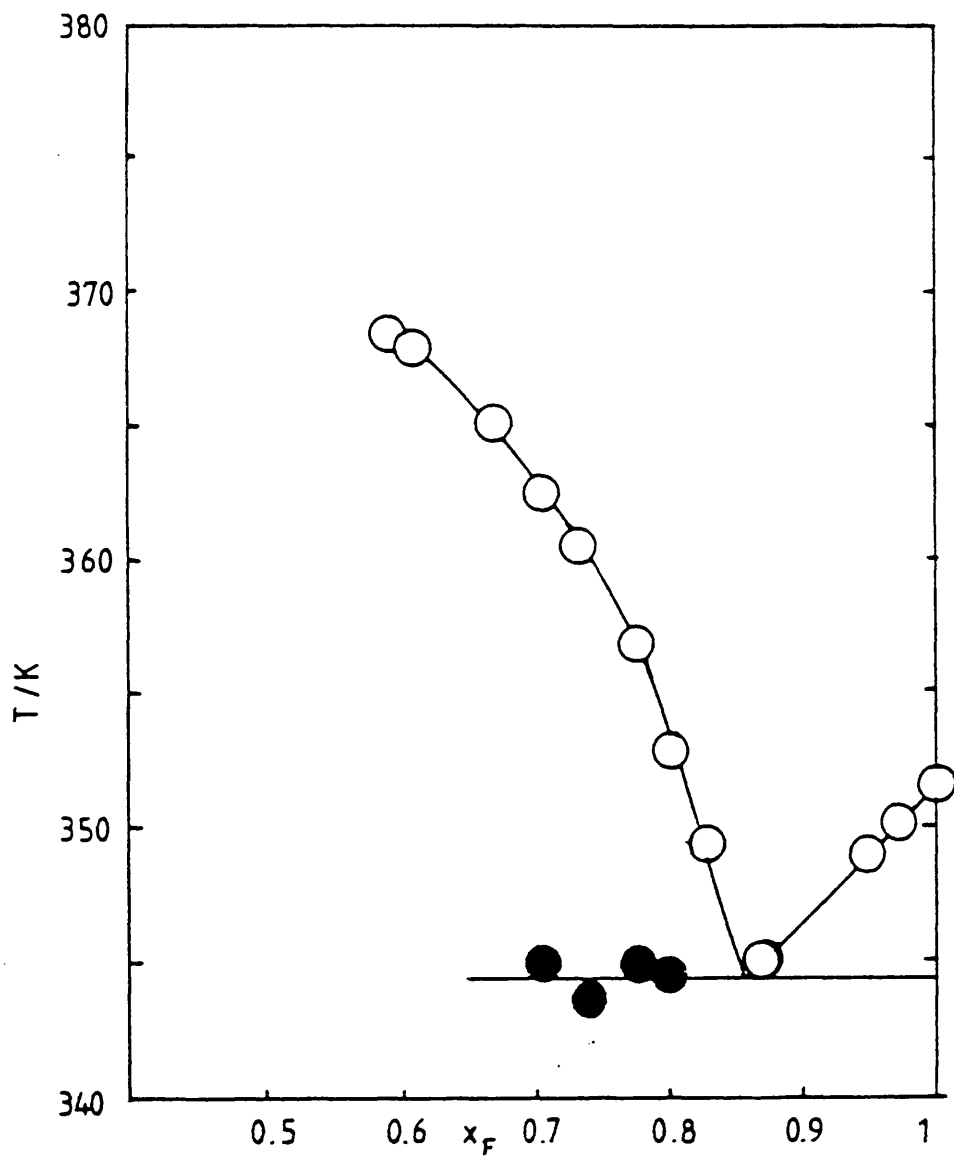


Figure (3.5.12) Solid-liquid phase diagram
Hexafluorobenzene + naphthalene



CHAPTER 4

EXCESS VOLUMES

4.1 Introduction

The change in Gibbs function on forming a solution at constant T and P is given by :

$$\Delta_{\text{mix}} G = G(\text{mixture}) - G(\text{unmixed components}).$$

Then for a binary mixture,

$$\Delta_{\text{mix}} G = n_1 \mu_1 + n_2 \mu_2 - n_1 \mu_1^* - n_2 \mu_2^* \quad (4.1.1)$$

where n = number of moles, μ = chemical potential and '*' signifies a pure component.

$$\text{Also, } \mu_i = \mu_i^* + RT \ln x_i \gamma_i \quad (4.1.2)$$

(Where γ = activity coefficient).

Substituting (4.1.2) into (4.1.1) gives

$$\Delta_{\text{mix}} G = n_1 RT \ln x_1 \gamma_1 + n_2 RT \ln x_2 \gamma_2$$

$$\Delta_{\text{mix}} G_m = \Delta_{\text{mix}} G / (n_1 + n_2) = RT \left\{ x_1 \ln x_1 \gamma_1 + x_2 \ln x_2 \gamma_2 \right\} \quad (4.1.3)$$

or,

$$\Delta_{\text{mix}} G_m = RT \left\{ x_1 \ln x_1 + x_2 \ln x_2 \right\} + RT \left\{ x_1 \ln \gamma_1 + x_2 \ln \gamma_2 \right\} \quad (4.1.4)$$

The excess Gibbs function, G^E , is defined by

$$\Delta_{\text{mix}} G_m = \Delta_{\text{mix}} G_m (\text{ideal}) + G^E \quad (4.1.5)$$

and generally, an excess function X^E is defined by

$$X^E = \Delta_{\text{mix}} X_m - \Delta_{\text{mix}} X_m (\text{ideal}) \quad (4.1.6)$$

$$\text{Since } dG = v dP - S dT, \quad v = \left(\frac{\partial G}{\partial P} \right)_T$$

it follows that

$$\Delta_{\text{mix}} v_m = \left\{ \frac{\partial}{\partial P} (\Delta_{\text{mix}} G_m) \right\}_T \quad (4.1.7)$$

For the ideal case,

$$\Delta_{\text{mix}} v_m (\text{ideal}) = \left[\frac{\partial}{\partial P} \left\{ \Delta_{\text{mix}} G_m (\text{ideal}) \right\} \right]_T \quad (4.1.8)$$

From equations (4.1.4) and (4.1.5), equation (4.1.8)

becomes

$$\Delta_{\text{mix}} v_m (\text{ideal}) = \left[\frac{\partial}{\partial P} \left\{ RT(x_1 \ln x_1 + x_2 \ln x_2) \right\} \right]_T = 0 \quad (4.1.9)$$

Since in equation (4.1.9) the term in brackets is independent of pressure,

$$v^E = \Delta_{\text{mix}} v_m - 0 \quad (\text{from equation (4.1.6)}).$$

The excess volume, v^E , can be determined from precise density measurements (56). However, the excess volumes

listed in this thesis were measured directly using batch and dilution dilatometers. The batch dilatometers were of a type used by Duncan and Swinton (17), and Armitage et al.(62). The dilution dilatometer used in this laboratory was the one previously used by Osborne (53) and by Armitage (57) and Martin (58); it is similar to the dilatometer designed by Marsh (59). Variations on dilution dilatometer design include the tilting dilution dilatometer (60,61) where no greased taps are present in the apparatus, and no opening or closing of taps is necessary during the entire run.

4.2 Capillary calibration

The diameter of the capillary was determined by introducing an unbroken thread of mercury into it. The length of the thread was measured using a travelling microscope, before tipping the mercury into a pre-weighed container in order to determine its weight (to ± 0.0001 g). Table (4.2.1) shows the results of two duplicate calculations of the diameter.

Before using the capillary, a glass knife was used to engrave a reference mark at a suitable position towards the top of the capillary.

4.3 Batch dilatometer

The batch dilatometer and capillary tube are illustrated in figures (4.3.1) and (4.3.2). For work at

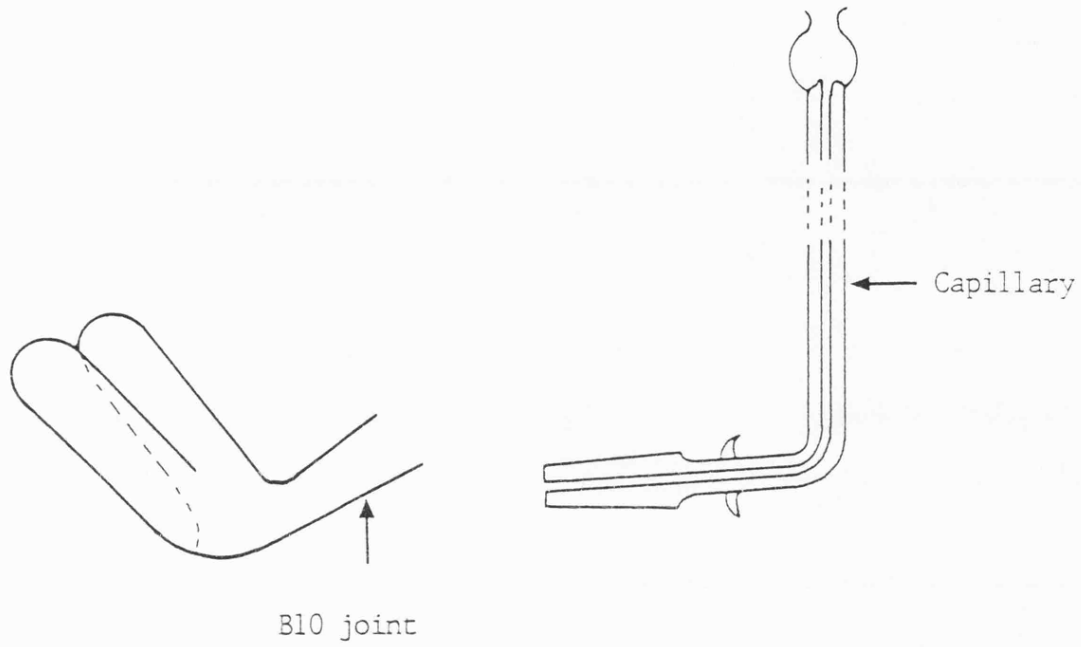
Table (4.2.1)

	RUN 1	RUN 2
Length of mercury thread/cm	2.842	11.895
Weight of mercury/g	0.0765	0.3187
Volume (= weight/density at 295.65 K)/cm ³	5.64988x10 ⁻³	2.35374x10 ⁻²
Cross sectional area (= volume/length)/cm ²	1.98799x10 ⁻³ ✓	1.97876x10 ⁻³
Diameter, D/cm	0.050311	0.050194

Average diameter = $0.05025 \frac{3}{3} \text{ cm} \pm 0.0001 \text{ cm}$
 0.0503 ± 0.0001

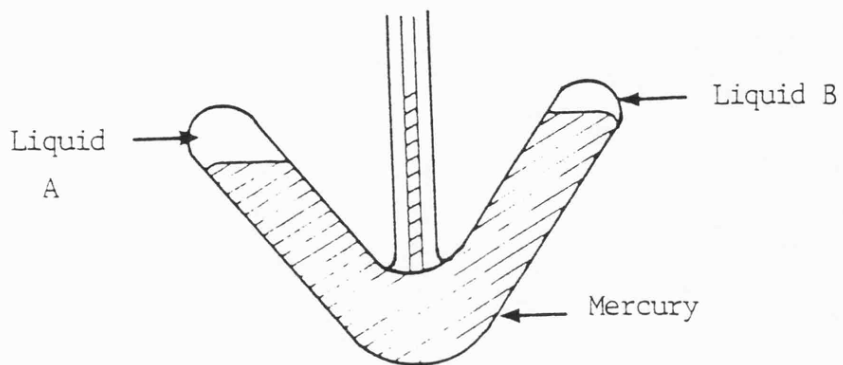
0.

Figure (4.3.1)



Side view of batch dilatometer and capillary

Figure (4.3.2)



Front view of loaded batch dilatometer

extreme mole fractions, a slightly modified form of dilatometer can be used where the capacity of one limb is exaggerated in comparison to the other, so that the large volume of the dominant component can be more satisfactorily accommodated.

4.4 Loading the batch dilatometer

The dilatometer was cleaned with chromic acid, water and acetone, and then dried. It was attached by the B.10 joint to the vacuum line, evacuated and filled with double-distilled mercury from a mercury reservoir. The dilatometer was then firmly clamped in a position whereby the two 'arms' were approaching a vertical stance. The two components were injected (one into each 'arm') using pre-weighed syringes with curved needles (stainless steel luer-lock fitting). Curved needles helped to ensure that the liquids, when injected, went straight to the top of their respective arms. When injecting there was invariably a small volume of air at the end of the needle which appeared as a bubble in the liquids. However, as the liquids were degassed, the bubble disappeared almost immediately. The capillary was then lightly greased (Apiezon high vacuum grease) and worked well into the dilatometer's B.10 joint. An elastic band held the capillary in place. The apparatus was clamped vertically in a thermostated bath and left to equilibrate. A hot air blower was then used to expel mercury from the top of the capillary, so that when placed back in the thermostated bath the mercury level was below the reference level of

the capillary and could be focussed on using the cathetometer.

4.5 Operation

The readings of the reference and mercury levels were taken, using the cathetometer, after re-equilibration (which typically took about fifteen minutes). The dilatometer was removed and rocked judiciously about ten times, until satisfactory mixing had occurred. It was then replaced in the bath, allowed to reach equilibrium again and the new reference and mercury levels were noted. From the readings a change in height ' ΔH ' was calculated.

In the case of 2-methylnaphthalene and isoquinoline (both solid at room temperature) a slightly different approach was adopted. The dilatometer was weighed empty and the 2-methylnaphthalene (or isoquinoline) injected into one 'arm' of the dilatometer, whilst inside a Perspex glove box held at an elevated temperature. The dilatometer was re-weighed. The compound in the 'arm' was then frozen using liquid nitrogen, attached to the vacuum line and pumped on. Mercury was then run in to fill the dilatometer as before. Once the dilatometer had been removed from the line, the second component (hexafluorobenzene) was injected into the other 'arm' as normal. When the apparatus was clamped in the thermostated bath, the 2-methylnaphthalene (or isoquinoline) melted and no air bubble was visible.

v^E is determined using the expression

$$v^E = \frac{\pi d^2 \Delta H}{4(n_A + n_B)} \quad (4.5.1)$$

where d = capillary diameter, ΔH = change in height upon mixing and n_A, n_B = the number of moles of components A and B.

4.6 Pressure corrections

During any excess volume run, the mercury level in the capillary will rise or fall. This means that the pressure applied to the contents of the dilatometer will vary and so pressure corrections must be made. The apparatus employed to make these corrections is depicted in figure (4.6.1). A rubber pipette filler was attached to 'A'. Rubber tubing from 'B' connected the apparatus to the top of the capillary. By opening the tap and squeezing the pipette filler, the dilatometer system was subjected to a pressure, the value of which was read from the difference in manometer levels (P cm). The new reference mark reading and new mercury level reading were taken using the cathetometer.

Consider figure (4.6.2) where there is a drop in the mercury level upon mixing (to H_2), and a further drop due to the applied pressure (to H_3). The uncorrected height

Figure (4.6.1)

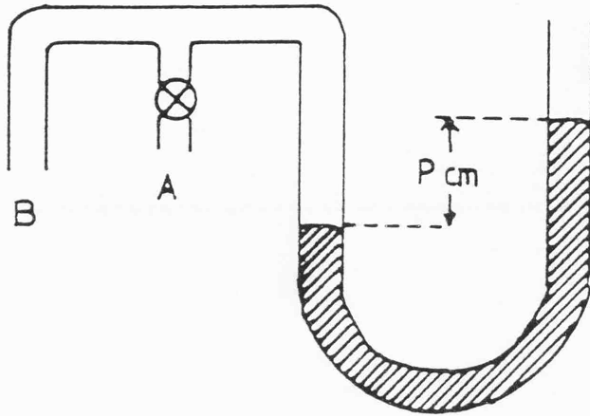
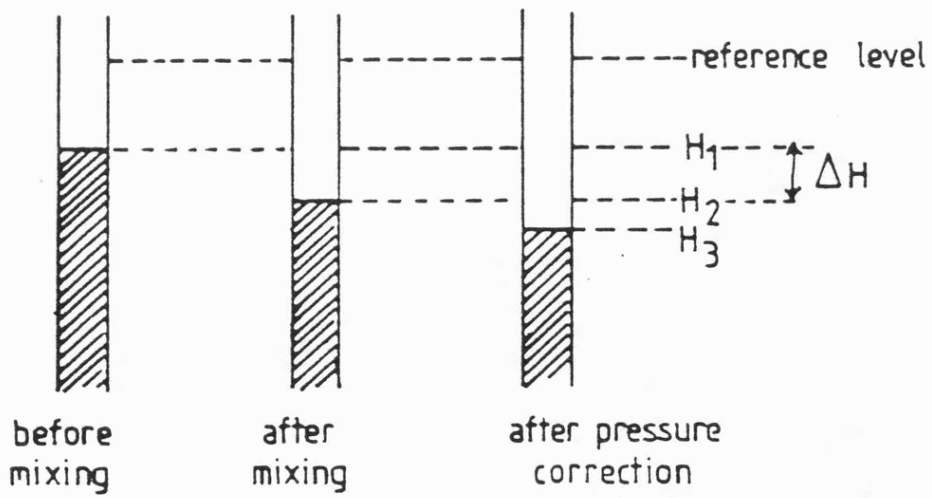


Figure (4.6.2)



change, $\Delta H = H_2 - H_1$. ΔH is corrected using the formula:

$$\Delta H_{\text{corrected}} = \Delta H + \Delta H \times \frac{(H_3 - H_2)}{P} \quad (4.6.1)$$

$\Delta H_{\text{corrected}}$ is then fed into equation (4.5.1) as ΔH .

Batch methods are useful when small amounts of expensive materials are to be used. However, although an accurate method, batch dilatometry is tedious, each run yielding only a single point on the v^E against mole fraction plot; with a dilution dilatometer, two runs adequately cover the whole mole fraction range.

4.7 Dilution dilatometer: loading

The apparatus (figure 4.7.1) is permanently mounted to a metal frame because of its fragility.

Prior to loading, a thorough cleaning of the apparatus was carried out using the usual chromic acid, water, acetone routine. Lightly greased stoppers were inserted into joints '1' and '3', while the connection to the vacuum line was made at joint '2' using flexible pressure tubing. The whole apparatus was evacuated and filled with mercury, with tube 'D' being filled first (achieved by suitable operation of tap 'T'). The tap was then turned to a position 90° from that shown in figure (4.7.1) and the vacuum released. A stopper was placed in joint '2' and the apparatus tilted so that the burette

made an angle of about 70° to the horizontal. Component 1 was injected into chamber 'A' via joint '3' and the weight introduced was noted. A small magnetic stirrer was also placed in 'A' before the stopper was replaced in joint '3'. Stopper '2' was then removed and the second component injected into the burette (the weight was not noted). The capillary was worked into joint '2' and held tightly there by an elastic band. The apparatus was clamped vertically in a thermostated tank and as equilibrium was being attained, mercury dropped from 'A' to the burette 'B', indicating that no premature mixing was taking place.

If negative v^E values were anticipated (that is, falls in the capillary mercury level upon mixing were expected) then the mercury level in 'D' was kept close to the top. Then, when 'D' was connected to the rest of the apparatus (using tap 'T') the level of mercury in the capillary dropped only a little, to the same level as in 'D'.

If positive v^E values were predicted, it was necessary to start with the mercury level in the capillary low down. In this case mercury was removed from 'D' until its level was low, before connecting it to the rest of the apparatus.

Finally, the tap was returned to a position 90° away from that shown in figure (4.7.1).

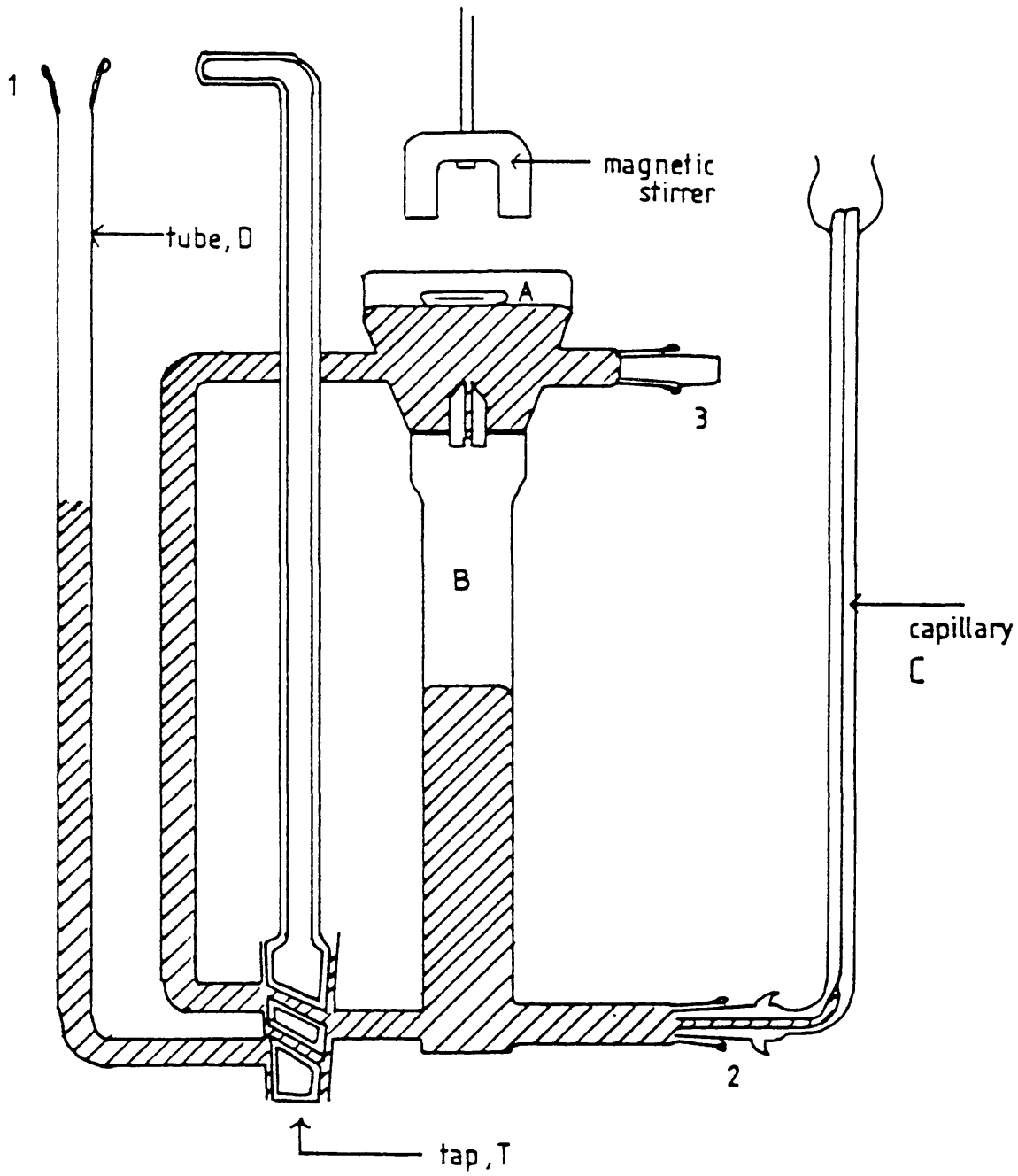
4.8 Dilution dilatometer: operation

The mercury level readings in the burette and capillary, along with their corresponding reference marks, were taken using the cathetometer. By turning the tap 'T' into the position illustrated in figure (4.7.1) a quantity of component 2 was introduced into chamber 'A' where the magnetic stirrer ensured proper mixing. After equilibrium had been established (commonly twenty minutes) the new capillary and burette heights were noted. The amount of component 2 introduced (and so the new mole fraction) could be calculated knowing the internal diameter of the burette, the height change and the density of component 2 at the set temperature. The change in mercury height in the capillary allowed the excess volume to be determined. The process was continued until all of the second component had been run into chamber 'A'.

A second run was then performed with component 2 in chamber 'A' and component 1 occupying the burette 'B'

If contractions in the mercury level of the capillary were involved (negative V^E against mole fraction plot), after several additions the level became so low that it was seen that if another addition was attempted the level would drop below the base of the capillary. In this instance tap 'T' was used to connect 'D' to the rest of the apparatus again and the mercury level in the capillary duly rose to the height of the mercury in 'D'. The tap was turned 90°, the new capillary mercury level noted and the

Figure (4.7.1)



Dilution dilatometer

run continued.

Pressure corrections were performed in exactly the same way as for the batch dilatometer (section 4.6).

The number of moles of component 1 injected in chamber 'A' is given by:

$$n_A = W_A / M_A \quad (4.8.1)$$

Where W = mass and M = molar mass.

As the run progresses, component 2 is added from the burette into chamber 'A' in stages. The burette heights, $Z_1, Z_2, Z_3 \dots Z_i$ are noted. The total number of moles added at any time is:

$$n_{Z_i} = \frac{\pi d^2 (Z_i - Z_1) D}{4 M} \quad (4.8.2)$$

Where D = the density of component 2, d = internal diameter of the burette and M = molar mass of component 2.

The mole fraction after any addition is, therefore

$$x_i = \frac{n_A}{n_A + n_{Z_i}} \quad (4.8.3)$$

Besides noting changes in the burette height after additions, changes in the capillary level are also taken. These need to be pressure corrected. If a pressure of P cm

of mercury is applied, causing a decrease in height of the capillary level of δh cm, then the correction to be added to each capillary mercury height is

$$\frac{\delta H \cdot \Delta H}{\rho} \quad (4.8.4)$$

where ΔH = change in capillary height for each addition.

Suppose as additions occur, the capillary heights are h_1, h_2, \dots, h_i . Then the volume change at a given point is

$$V_{h_i} = \frac{(h_i - h_1) \left(1 + \frac{\delta H}{\rho}\right) \pi (c)^2}{4} \quad (4.8.5)$$

where c = diameter of the capillary.

The excess molar volume, v_i^E is represented by

$$v_i^E = \frac{(h_i - h_1) \left(1 + \frac{\delta H}{\rho}\right) M \pi (c)^2}{(Z_i - Z_1) d^2 \pi D + \frac{n_A}{4}} \quad (4.8.6)$$

4.9 Results

Values for the well-studied system hexafluorobenzene + benzene were obtained using the batch and dilution dilatometer. In both cases results were in good agreement with those obtained by Duncan and Swinton (17). (tables 4.9.1 and 4.9.2).

Six other systems were analysed using batch dilatometry and a further two using dilution dilatometry (tables 4.9.3 - 4.9.10). Measurements were made at 303.15 K where possible.

All volumes were fitted to the function

$$V_i^E = \sum_{j=1}^q x_1 x_2 A_j (x_2 - x_1)^{j-1} \quad (4.9.1)$$

where j = number of parameters needed for the best fit. Parameter values and standard deviations (both in $\text{cm}^3\text{mol}^{-1}$) are listed for each system in tables (4.9.1) to (4.9.10). The smoothed curves with the experimental points are shown in figures (4.9.1) to (4.9.10).

Table (4.9.1)

Excess volumes of mixing

Hexafluorobenzene + benzene

313.2 K

Batch dilatometer

x_F	$V^E/\text{cm}^3\text{mol}^{-1}$
0.104	0.444
0.205	0.688
0.376	0.845
0.450	0.836
0.564	0.766
0.705	0.542
0.765	0.481

$A(1) = 3.269$; $A(2) = 1.478$; $A(3) = 0.358$

standard deviation = 0.019

Table (4.9.2)

Excess volumes of mixing

Hexafluorobenzene + benzene

313.2 K

Dilution dilatometer

x_F	$V^E/\text{cm}^3\text{mol}^{-1}$
0.053	0.233
0.138	0.535
0.189	0.664
0.235	0.746
0.287	0.806
0.303	0.837
0.322	0.833
0.352	0.859
0.379	0.856
0.386	0.867
0.401	0.863
0.441	0.850
0.478	0.823
0.495	0.820
0.566	0.751
0.592	0.720
0.650	0.643
0.734	0.516
0.786	0.419
0.905	0.180

A(1) = 3.268; A(2) = 1.535; A(3) = 0.236

Standard deviation = 0.006

Table (4.9.3)

Excess volumes of mixing results

Hexafluorobenzene + 2-methylnaphthalene

338.2 K Batch dilatometer

x_F	$V^E/\text{cm}^3\text{mol}^{-1}$
0.091	-0.353
0.192	-0.678
0.280	-0.913
0.325	-1.007
0.364	-1.130
0.469	-1.237
0.560	-1.210
0.619	-1.129
0.664	-1.072
0.678	-0.986
0.771	-0.780
0.889	-0.418

A(1) = 4.880; A(2) = 0.025; A(3) = -1.356

Standard deviation = 0.024

Table (4.9.4)

Excess volumes of mixing results

Hexafluorobenzene + 2-ethylnaphthalene

338.2 K Batch dilatometer

x_F	$V^E/\text{cm}^3 \text{mol}^{-1}$
0.174	-0.524
0.195	-0.600
0.266	-0.759
0.357	-0.929
0.416	-0.966
0.424	-0.966
0.468	-0.966
0.554	-1.001
0.555	-0.989
0.587	-0.977
0.670	-0.800
0.791	-0.544
0.873	-0.325

$A(1) = -4.040$; $A(2) = -0.404$; $A(3) = 1.487$

Standard deviation = 0.016

Table (4.9.5)

Excess volumes of mixing

Hexafluorobenzene + isoquinoline

303.2 K Batch dilatometer

x_F	$V^E/\text{cm}^3\text{mol}^{-1}$
0.120	-0.343
0.195	-0.478
0.358	-0.690
0.471	-0.733
0.563	-0.710
0.635	-0.637
0.744	-0.565
0.784	-0.469
0.916	-0.195

A(1) = 2.911; A(2) = 0.262; A(3) = 0.086

Standard deviation = 0.018

Table (4.9.6)

Excess volumes of mixing

Hexafluorobenzene + cis-decalin

303.2 K

Batch dilatometer

x_F	$V^E/\text{cm}^3\text{mol}^{-1}$
0.103	0.659
0.188	1.145
0.266	1.437
0.390	1.808
0.423	1.825
0.523	1.874
0.627	1.869
0.697	1.704
0.759	1.513
0.870	1.020

A(1) = 7.603; A(2) = -0.658; A(3) = 1.012; A(4) = -0.880

Standard deviation = 0.025

Table (4.9.7)

Excess volumes of mixing

Hexafluorobenzene + trans-decalin

303.2 K Batch dilatometer

x_F	$V^E/\text{cm}^3\text{mol}^{-1}$
0.214	1.206
0.345	1.640
0.391	1.752
0.445	1.811
0.496	1.886
0.549	1.943
0.629	1.816
0.736	1.572
0.789	1.370
0.913	0.638

$A(1) = 7.569$; $A(2) = -1.273$; $A(3) = 0.296$; $A(4) = 1.278$

Standard deviation = 0.023

Table (4.9.8)

Excess volumes of mixing

Hexafluorobenzene + 2,3-cyclohexenopyridine

303.2 K Batch dilatometer

x_F	$V^E/\text{cm}^3\text{mol}^{-1}$
0.035	-0.019
0.081	-0.020
0.149	-0.051
0.234	-0.091
0.320	-0.151
0.343	-0.170
0.344	-0.170
0.404	-0.234
0.444	-0.262
0.519	-0.297
0.534	-0.315
0.601	-0.322
0.670	-0.336
0.679	-0.341
0.729	-0.329
0.824	-0.310
0.920	-0.152

$A(1) = -1.141$; $A(2) = 1.189$; $A(3) = -0.121$

Standard deviation = 0.011

Table (4.9.9)

Excess volumes of mixing

Hexafluorobenzene + quinoline

318.2 K Dilution dilatometer

x_F	$V^E/\text{cm}^3\text{mol}^{-1}$
0.039	-0.116
0.066	-0.205
0.158	-0.496
0.230	-0.706
0.299	-0.859
0.347	-0.933
0.411	-1.034
0.417	-1.034
0.470	-1.095
0.514	-1.097
0.532	-1.112
0.614	-1.069
0.627	-1.096
0.651	-1.038
0.730	-0.900
0.803	-0.740
0.871	-0.522

$A(1) = -4.617$; $A(2) = 0.685$; $A(3) = 0.486$

Standard deviation = 0.012

Table (4.9.10)

Excess volumes of mixing

Hexafluorobenzene + tetralin

303.2 K Dilution dilatometer

x_F	$V^E/\text{cm}^3\text{mol}^{-1}$
0.207	0.052
0.376	0.110
0.406	0.118
0.436	0.124
0.485	0.134
0.527	0.135
0.578	0.133
0.649	0.126
0.739	0.101
0.809	0.083
0.910	0.045

A(1) = -0.530; A(2) = 0.179; A(3) = 0.291

Standard deviation = 0.003

Figure (4.9.1)

Excess volumes for hexafluorobenzene + benzene 313.15 K
Batch dilatometer

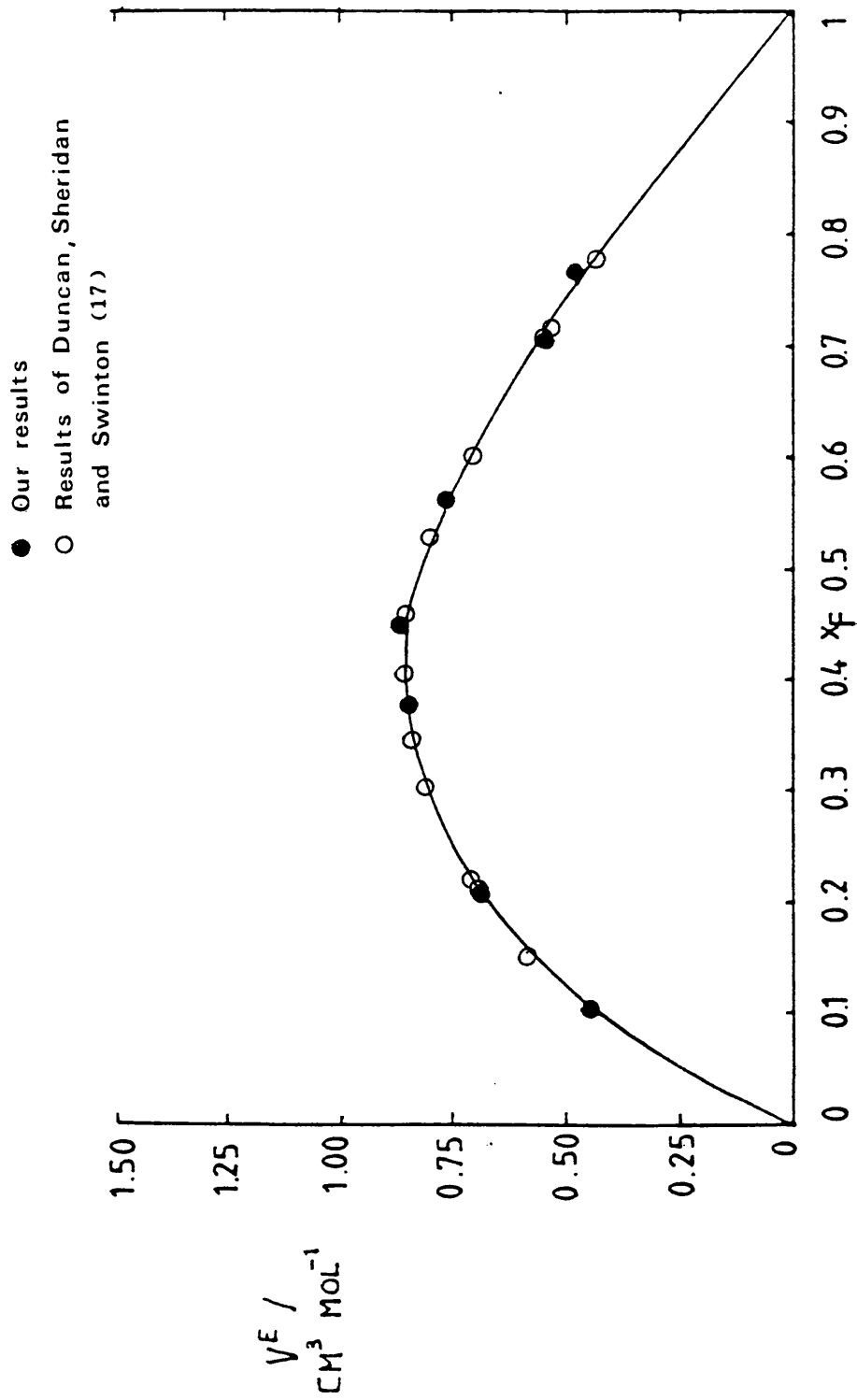


Figure (4.9.2)
Excess volumes for hexafluorobenzene + benzene 313.15 K
Dilution dilatometer

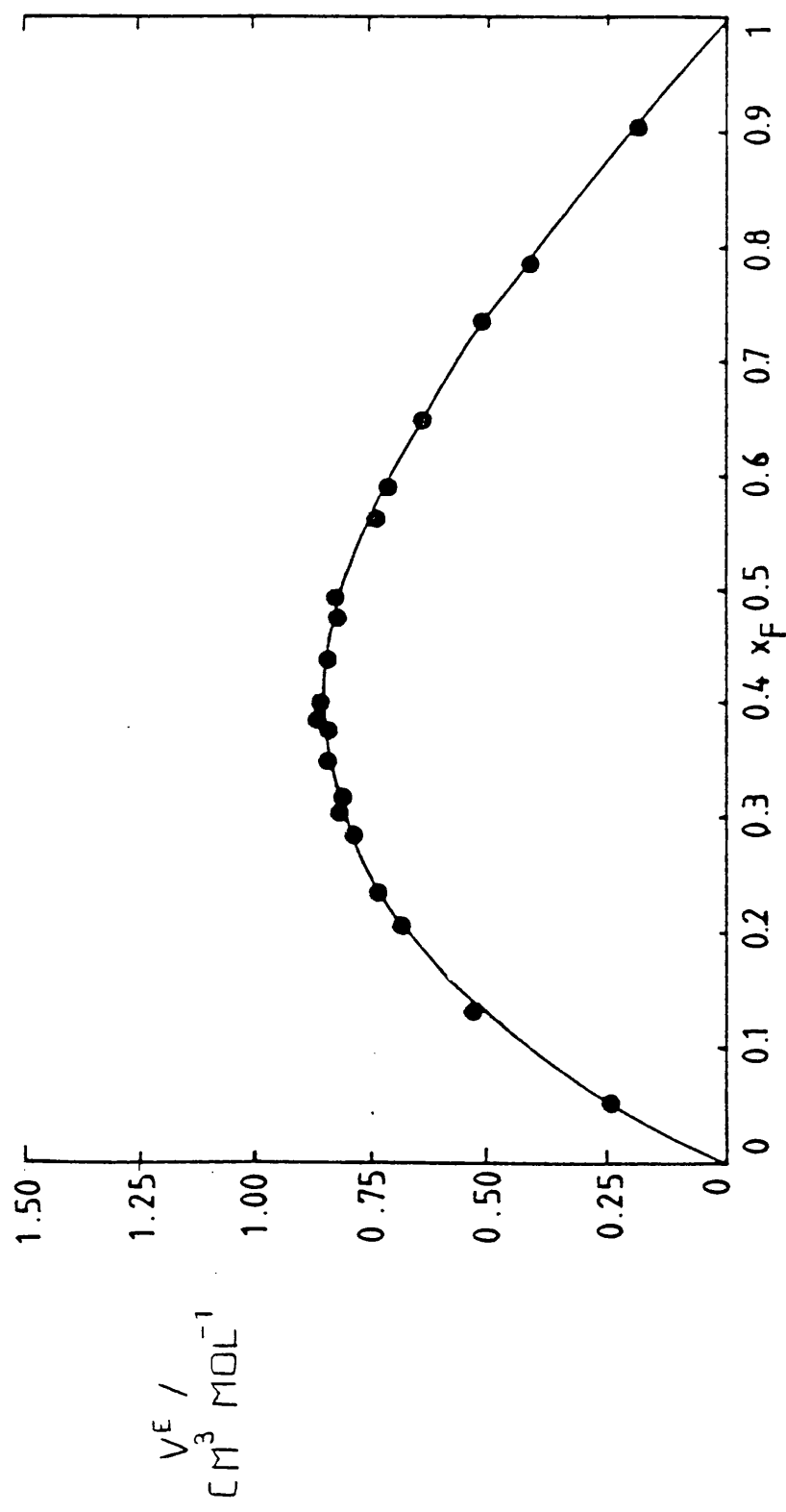


Figure (4.9.3)
Excess volumes for hexafluorobenzene
+ 2-methylnaphthalene 338.15 K
Batch dilatometer

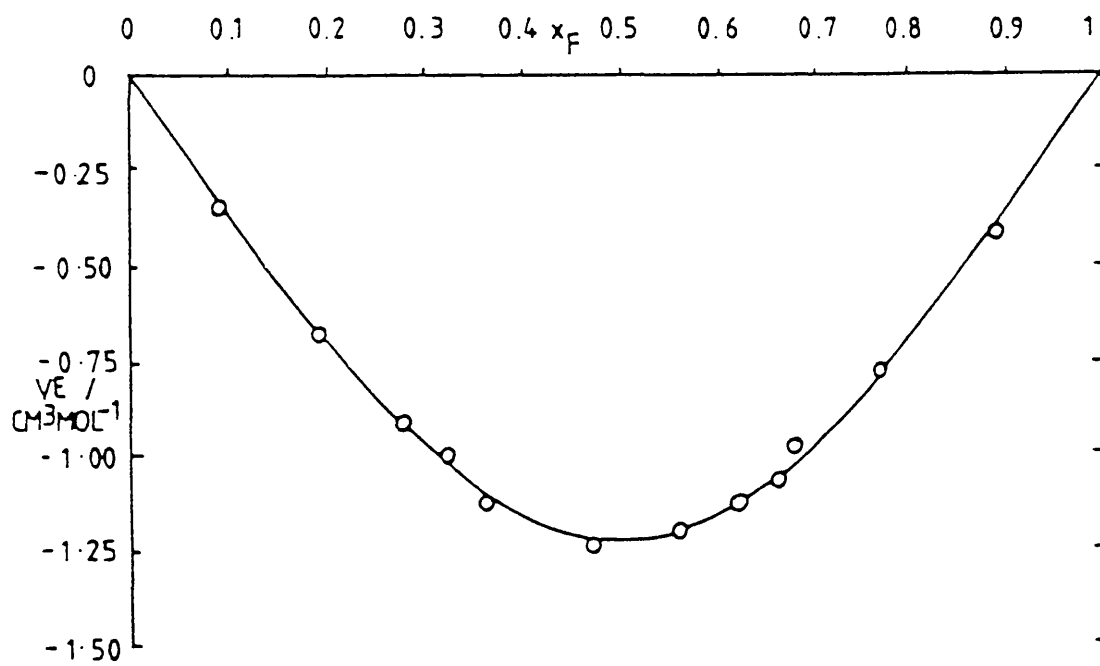


Figure (4.9.4)
Excess volumes for hexafluorobenzene
+ 2-ethylnaphthalene 318.15 K
Batch dilatometer

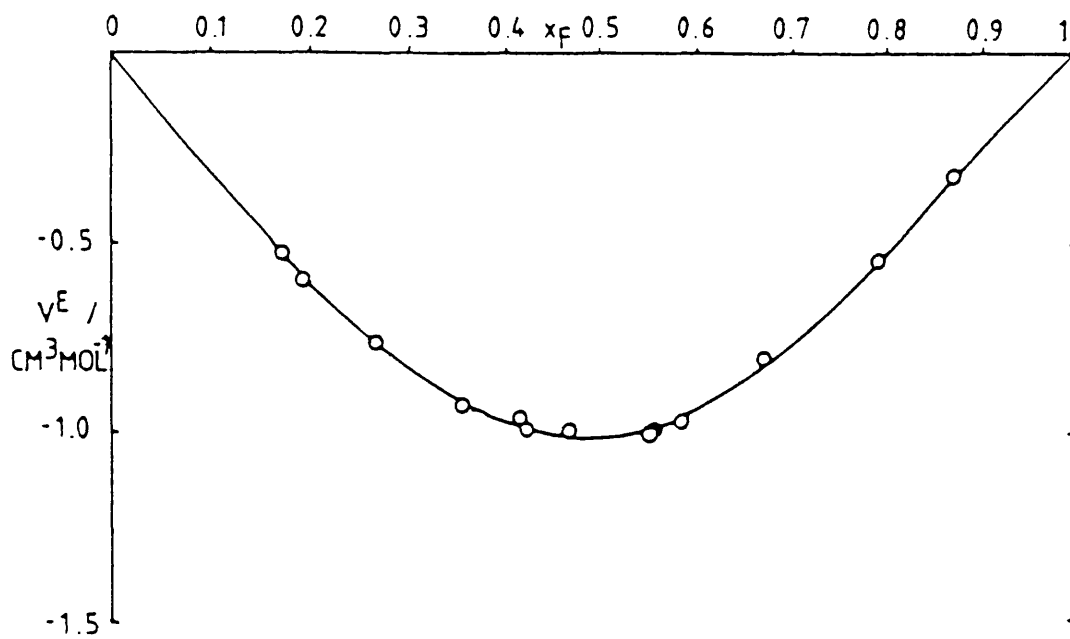


Figure (4.9.5)
Excess volumes for hexafluorobenzene
+ isoquinoline 303.15 K
Batch dilatometer

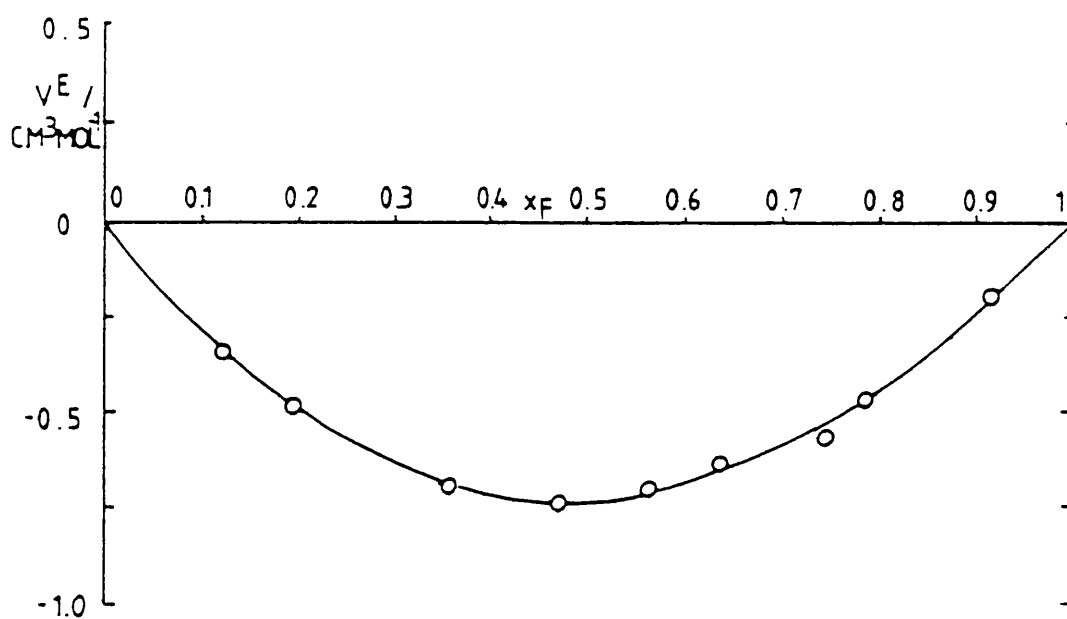


Figure (4.9.6)
Excess volumes for hexafluorobenzene + cis-decalin 303.15 K
Batch dilatometer

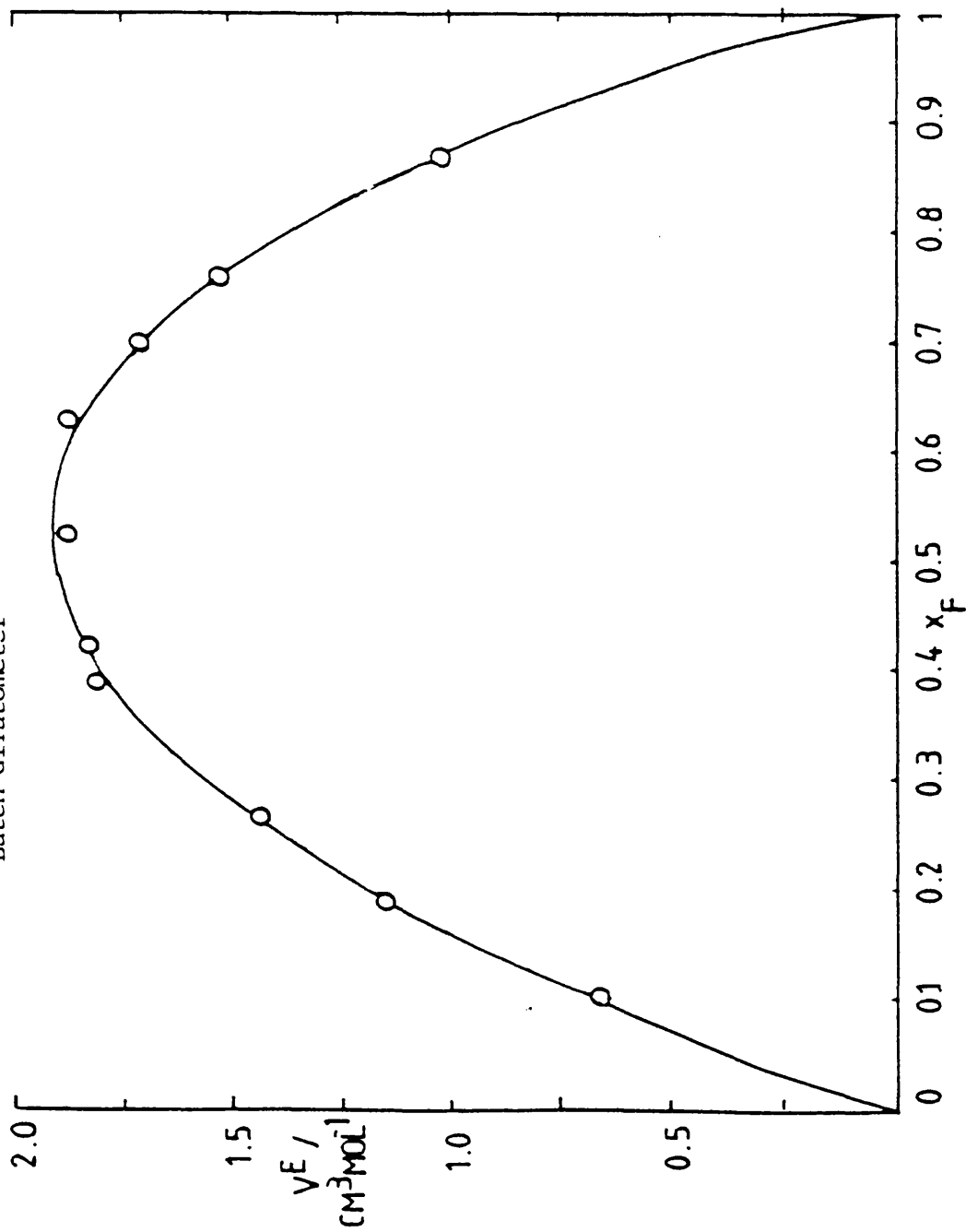


Figure (4.9.7)

Excess volumes for hexafluorobenzene + trans-decalin
Batch dilatometer 303.15 K

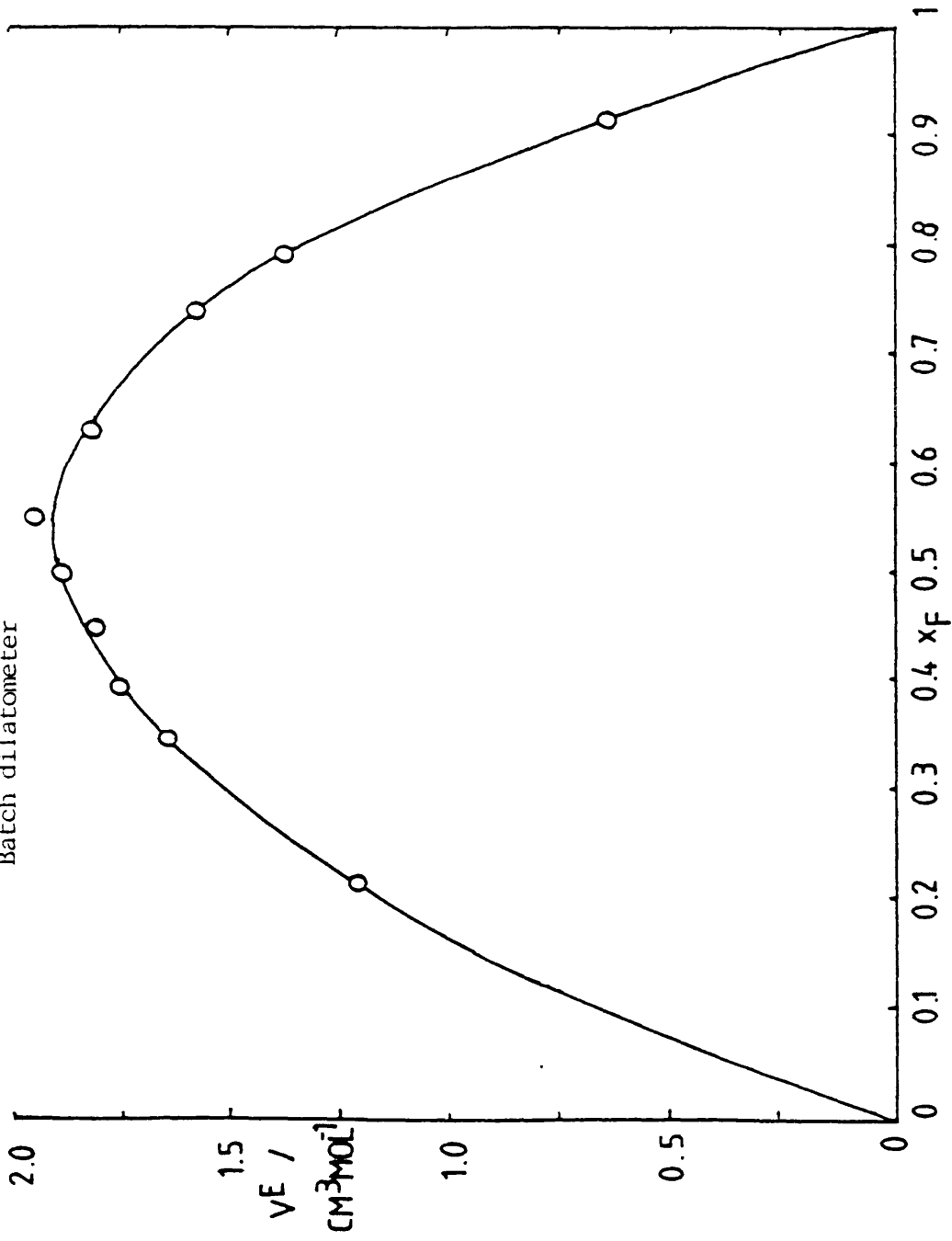


Figure (4.9.8)

Excess volumes for hexafluorobenzene + 2,3-cyclohexenopyridine 303.15 K
Batch dilatometer

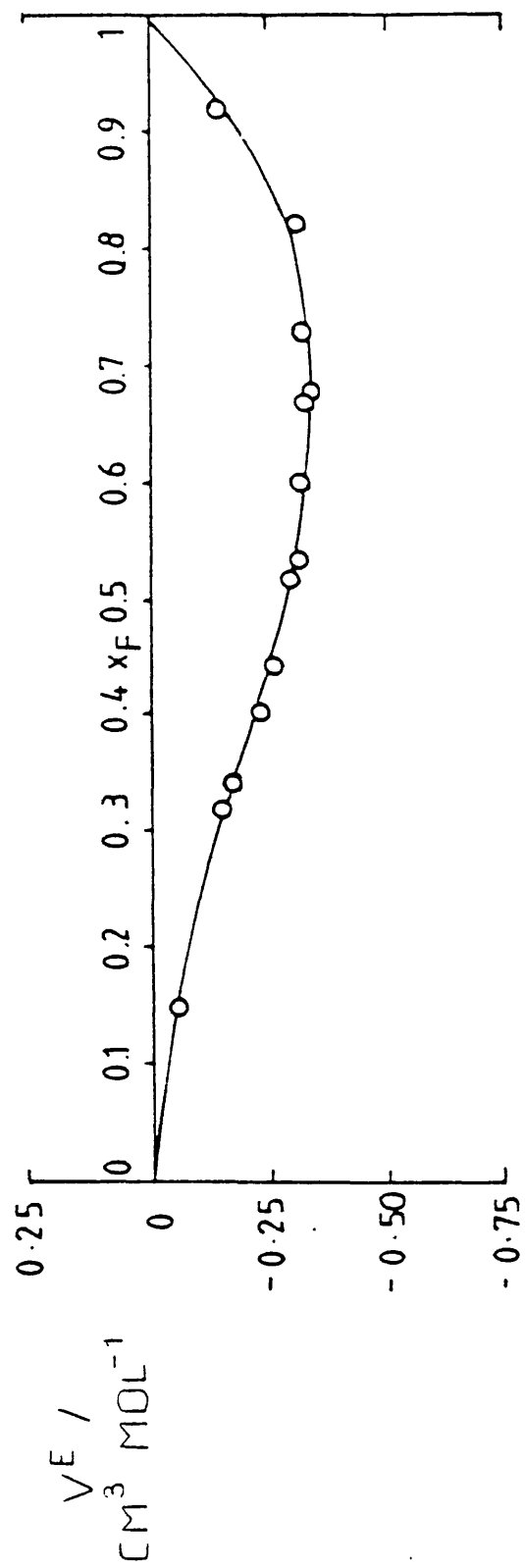


Figure (4.9.9)
Excess volumes for hexafluorobenzene + quinoline 318.15 K
Dilution dilatometer

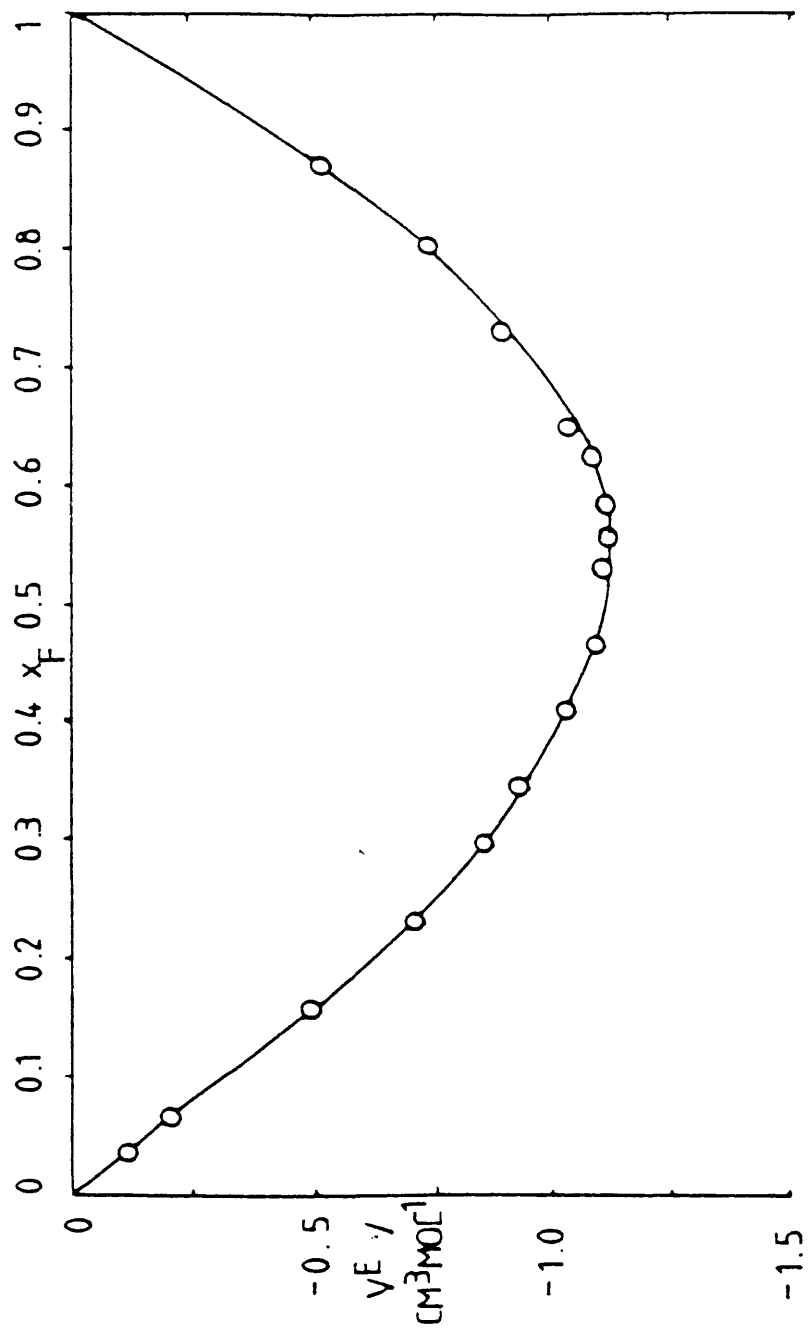
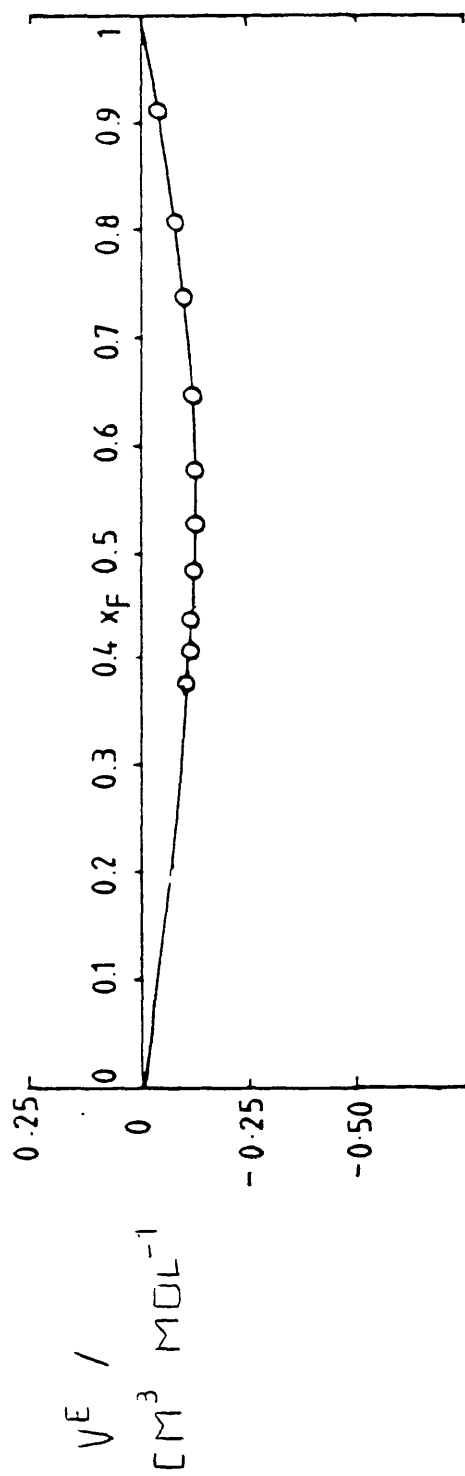


Figure (4.9.10)
Excess volumes for hexafluorobenzene + tetralin 303.15 K
Dilution dilatometer



CHAPTER 5

ENTHALPY MEASUREMENTS

5.1 Introduction

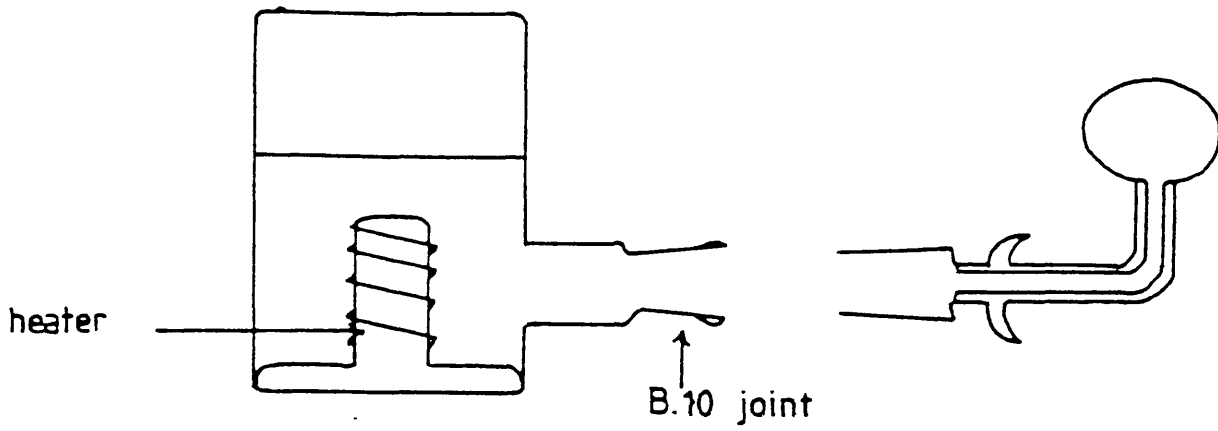
Enthalpy measurements were made by a batch type calorimeter previously used by Osborne (53). It was originally developed by Armitage (58) and was based on a design by Larkin and McGlashan (63), with the A.C. modification of Stubley et al. (64). The calorimeter, shown in figures (5.1.1) and (5.1.2) has been described in detail elsewhere and only brief details are included below.

The A.C. bridge network is diagrammatically represented in figure (5.1.3). This, along with the ancillary equipment has also been described before (53). In the main, the calorimeter was used to determine the excess enthalpies of mixing of hexafluorobenzene + naphthalene related hydrocarbons in the liquid phase, but heats of solution of the solid complex were also measured (section 5.7).

5.2 Operation of calorimeter for excess enthalpy measurements (H^E liq.)

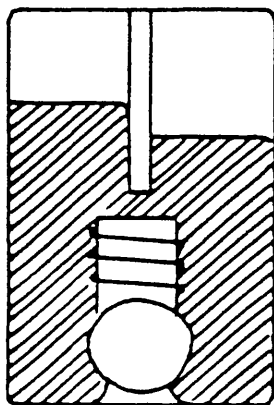
The loading procedure was similar to that employed for the batch dilatometer (see section 4.4). A clean calorimeter vessel was filled with double-distilled mercury, under vacuum. The components (degassed) were injected, one into each side, using syringes fitted with

Figure (5.1.1)



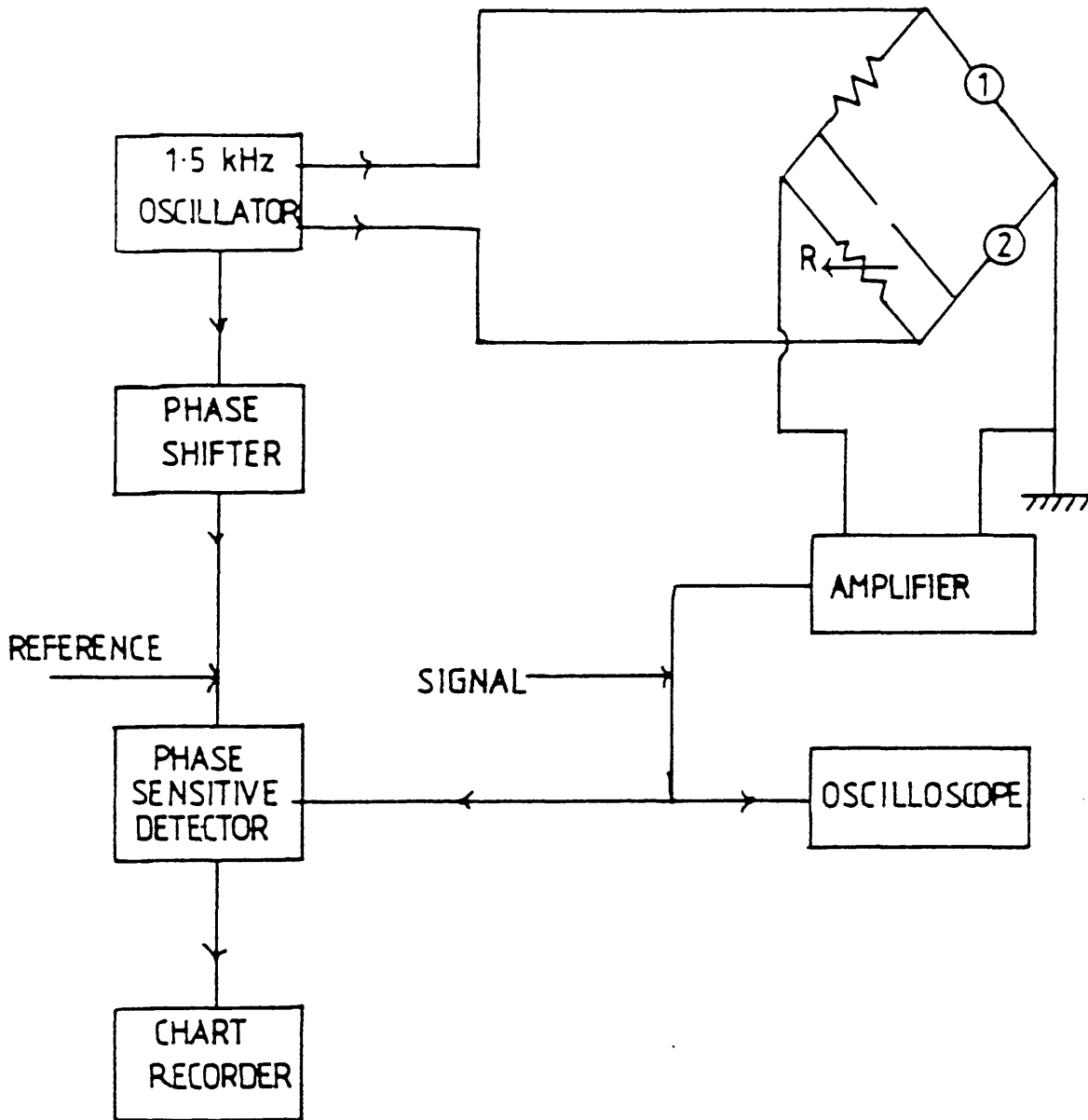
Calorimeter vessel (side view) and expansion bulb

Figure (5.1.2)



Loaded calorimeter vessel (front view)

Figure (5.1.3)



3" curved needles. A lightly greased expansion bulb was worked well into the B.10 joint of the calorimeter and held there using elastic bands. The calorimeter, along with the reference calorimeter (which contained just one of the components, generally hexafluorobenzene) was placed in a polystyrene jacket and connected to the bridge. The jacket was then placed in a watertight stainless steel vessel and lowered into a thermostated bath. Equilibration typically took eight to ten hours and normally the apparatus was left overnight.

5.3 Endothermic measurements of excess enthalpies

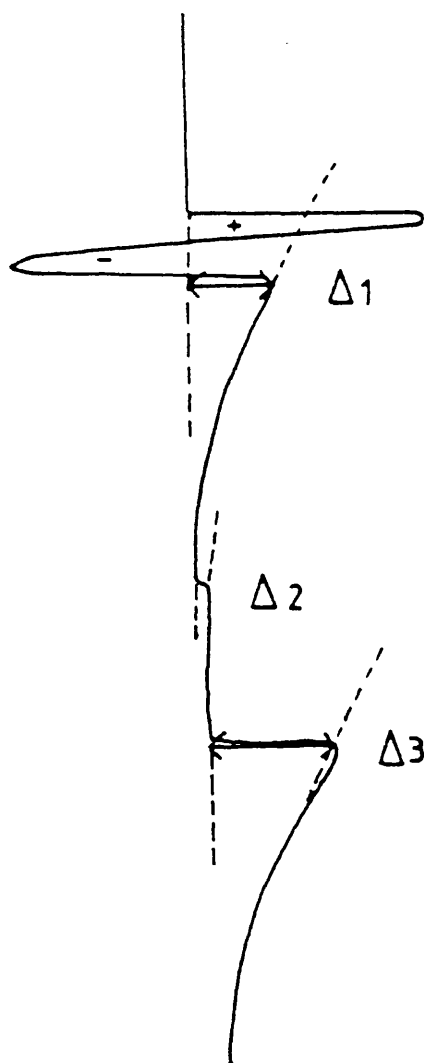
A typical trace is shown in figure (5.3.1).

For both endothermic and exothermic runs, when determining the sign of the deflections, the positive side is taken as the side the pen recorder moves to when electrical energy is introduced. Also calorimeter 1 is the vessel where the actual mixing of components takes place and calorimeter 2 is the reference vessel.

In an endothermic run, electrical energy is put into calorimeter 1 to compensate for the heat taken up by the mixing process in the same calorimeter.

The components are mixed under a pressure which remains effectively constant. Therefore, if $\Delta_1 = 0$ (figure (5.3.1)), the electrical energy introduced equals the enthalpy of mixing.

Figure (5.3.1)



stage 1. mixing. $\Delta_1, I_1, t_1.$

stage 2. stirring correction. $\Delta_2.$

stage 3. calibration. $\Delta_3, I_2, t_2.$

An endothermic trace

We can write

$$\Delta_{\text{mix}} H = I_1^2 R t_1 \quad (5.3.1)$$

If there is not an exact balance, then a term must be subtracted to allow for this. In stage three, a deflection, Δ_3 , is measured for the introduction of a known quantity of electrical energy ($I_2^2 R t_2$). Then, assuming that the deflection is proportional to the energy input, the energy corresponding to the deflection Δ_1 is $(\Delta_1/\Delta_3) I_2^2 R t_2$.

Equation (5.3.1) becomes

$$\Delta_{\text{mix}} H = I_1^2 R t_1 - (\Delta_1/\Delta_3) I_2^2 R t_2 \quad (5.3.2)$$

Stage two is a stirring correction and the small deflection produced, Δ_2 , must be subtracted from Δ_1 and Δ_3 , so that the final expression is

$$\Delta_{\text{mix}} H = I_1^2 R t_1 - \frac{\Delta_1 - \Delta_2}{\Delta_3 - \Delta_2} I_2^2 R t_2 \quad (5.3.3)$$

The molar excess enthalpy, H_m^E , is determined by dividing $\Delta_{\text{mix}} H$ by the total number of moles.

5.4 Exothermic measurements of excess enthalpies

Let the respective heater resistances and heat capacities for calorimeter 1, and 2, be R_1, R_2 and C_1, C_2 .

In stage one, electrical energy is introduced into calorimeter 2 to balance the heat emitted in the exothermic process of calorimeter 1. If this electrical energy exactly compensates (i.e. the temperature rise in both calorimeters is identical), then $\Delta 1 = 0$. Then,

$$\frac{C_1}{C_2} = \frac{\Delta_{\text{exp}} H(\text{calorimeter 1})}{I_1^2 R_2 t_1} \quad (5.4.1)$$

In practice, more heat than necessary is introduced into calorimeter 2 (as shown in figure 5.4.1) resulting in a positive deflection $\Delta 1$. This renders the plot easier to extrapolate (see section 5.5). From stage 4 it is known that an amount of electrical energy ($I_3 R_2^2 t_3$) causes a deflection, $\Delta 4$. Therefore, equation (5.4.1) must be modified to give:

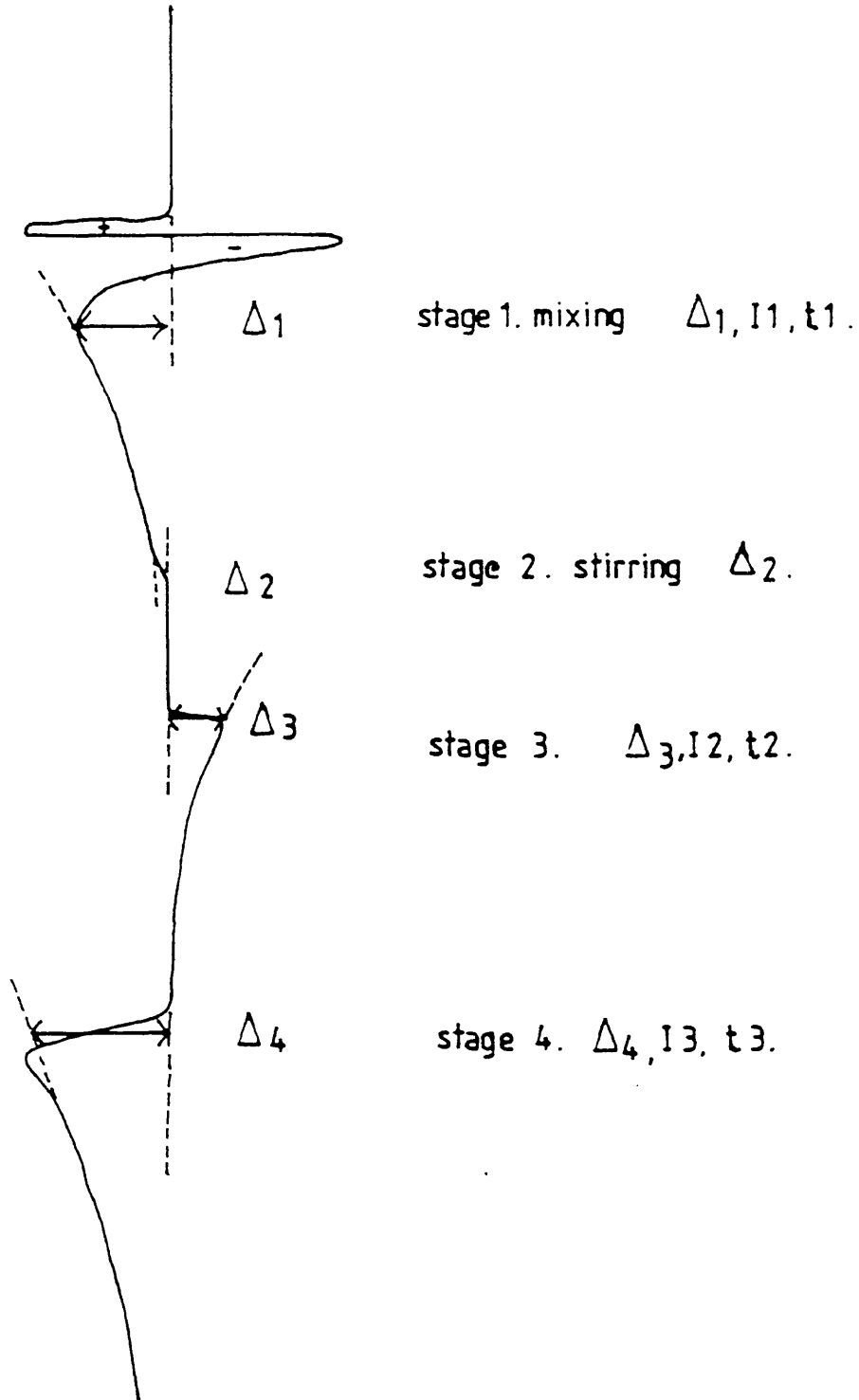
$$\frac{C_1}{C_2} = \frac{\Delta_{\text{exp}} H(\text{calorimeter 1})}{I_1^2 R_2 t_1 - (\Delta 1 / \Delta 4) I_3^2 R_2 t_3} \quad (5.4.2)$$

Stirring correction gives:

$$\frac{C_1}{C_2} = \frac{\Delta_{\text{exp}} H(\text{calorimeter 1})}{I_1^2 R_2 t_1 - \frac{(\Delta 1 - \Delta 2) I_3^2 R_2 t_3}{(\Delta 4 - \Delta 2)}} \quad (5.4.3)$$

The heat capacity ratio can be calculated from stage 3, where electrical energy is put into calorimeters 1 and 2 simultaneously.

Figure (5.4.1)



An exothermic trace

Hence,

$$\frac{C_1}{C_2} = \frac{I_2^2 R_1 t_2}{I_2^2 R_2 t_2 - \frac{(\Delta_3 - \Delta_2) I_3^2 R_2 t_3}{(\Delta_4 - \Delta_2)}} \quad (5.4.4)$$

Combining equations (5.4.3) and (5.4.4) gives:

$$\Delta_{\text{exp H}} = \frac{I_2^2 R_1 t_2 \left\{ \frac{(\Delta_1 - \Delta_2)}{I_1^2 R_2 t_1 - (\Delta_4 - \Delta_2) I_3^2 R_2 t_3} \right\}}{I_2^2 R_2 t_2 - \frac{(\Delta_3 - \Delta_2) I_3^2 R_2 t_3}{(\Delta_4 - \Delta_2)}} \quad (5.4.5)$$

Cancelling R_2 and multiplying by $(\Delta_4 - \Delta_2)$ gives:

$$\Delta_{\text{exp H}} = \frac{I_2^2 R_1 t_2 \left\{ I_1^2 t_1 (\Delta_4 - \Delta_2) - (\Delta_1 - \Delta_2) I_3^2 t_3 \right\}}{I_2^2 t_2 (\Delta_4 - \Delta_2) - (\Delta_3 - \Delta_2) I_3^2 t_3} \quad (5.4.6)$$

Again, H_m^E (J/mol) = $\Delta_{\text{exp H}}/n$.

(where n = the total number of moles).

5.5 Measurement of deflections $\Delta_1, \Delta_2, \Delta_3, \Delta_4$.

When determining the value of a deflection, Δ , we are approximating the pen recorder trace to what we believe is the ideal trace, thereby correcting for heat losses. For deflections Δ_3 , or Δ_4 , the trace is similar

to that depicted in figure (5.5.1a). In figure (5.5.1b) the ideal trace is superimposed onto the original one. The deflection is taken where the areas under the original and ideal traces are the same. (i.e. the positive and negative areas balance).

Deflection $\Delta 2$ (the stirring correction) is generally very small, if present at all, and is measured directly.

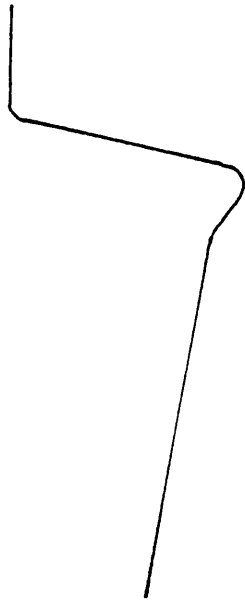
Deflection $\Delta 1$ is more complicated. Consider an exothermic enthalpy of mixing trace. Figures (5.5.2a) and (5.5.2b) show the original trace and the original trace with the ideal trace respectively, for the case where more electrical energy is introduced to balance the exothermic enthalpy of mixing. The deflection is again taken at the point where the positive and negative areas balance.

Figures (5.5.3a) and (5.5.3b) show the original and ideal traces for an exothermic enthalpy of mixing where not enough electrical energy is supplied to balance the heat emitted on mixing.

5.6 Excess enthalpy results

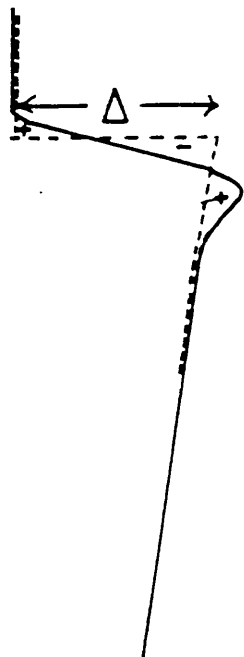
The excess enthalpies (H^E_{liq}) for hexafluorobenzene and various naphthalene compounds, along with compositions (x_F) are listed in tables (5.6.1) to (5.6.10). Measurements were made at 303.15 K where possible. In several cases, however, measurements had to be performed at a temperature just above the melting point of the 1:1

Figure (5.5.1a)



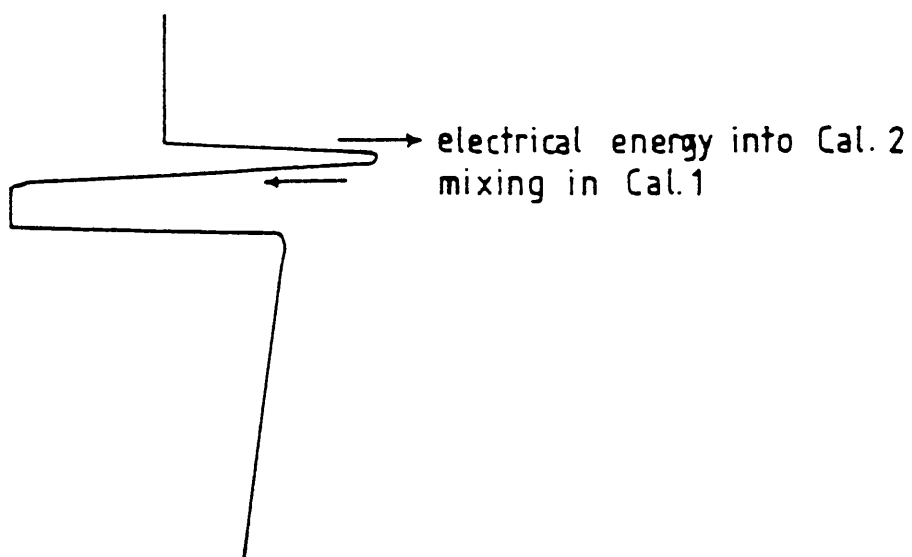
Trace for a Δ_3 , or Δ_4 deflection

Figure (5.5.1b)



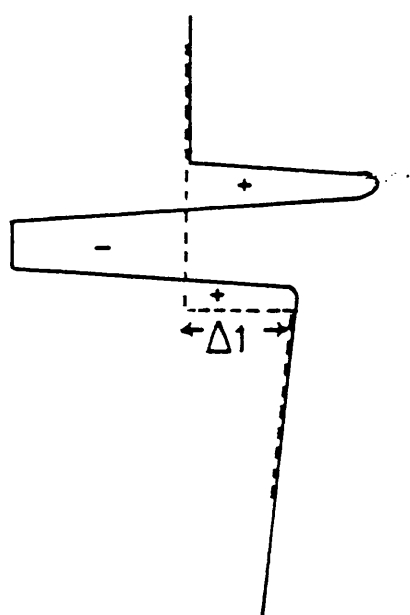
Ideal trace (----) superimposed onto actual trace

Figure (5.5.2a)



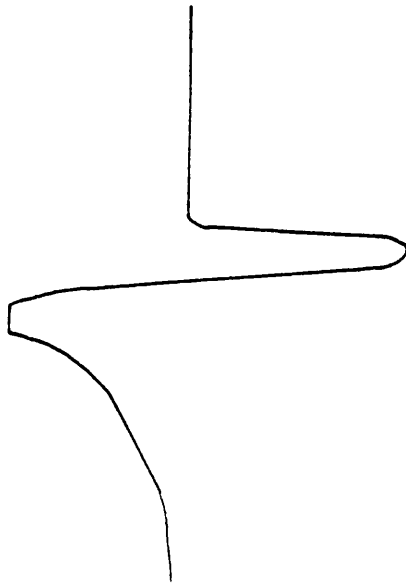
Δl deflection for exothermic mixing (too much electrical energy introduced)

Figure (5.5.2b)



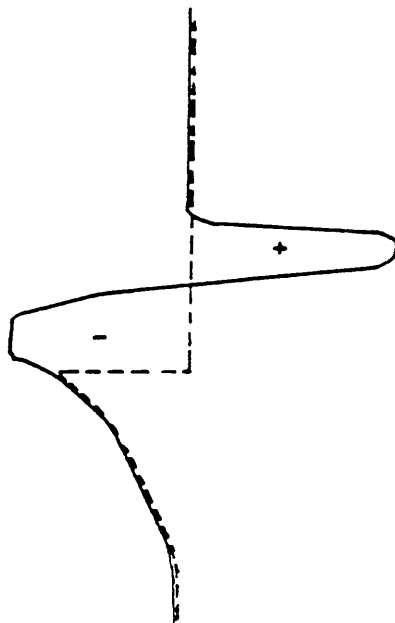
Δl deflection with ideal trace (----)

Figure (5.5.3a)



Trace for Δl deflection for exothermic mixing, where not enough electrical energy is introduced

Figure (5.5.3b)



Δl deflection trace with ideal trace (----)

complex: The hexafluorobenzene + 2-ethylnaphthalene system was studied at 313.15 K, the hexafluorobenzene + 2-methylnaphthalene system at 338.2 K and the hexafluorobenzene + quinoline system at 318.15 K. Since the complex of hexafluorobenzene + 1-methylnaphthalene melts at about 373 K, the full composition range could not be properly investigated. However, some measurements were made at 348.15 K for mole fractions between 0 and 0.15, and between 0.85 and 1.0.

Results were fitted to the function:

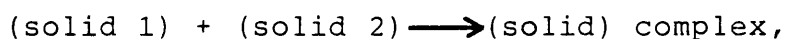
$$H^E / (\text{J/mol}) = x(1-x) \sum_{i=1}^n h_i (1-2x)^{i-1} \quad (5.6.1)$$

(where x = mole fraction of hexafluorobenzene and h_i = parameters.)

As for excess volumes, the parameters (in J mol^{-1}), along with the corresponding minimum standard deviation (in J mol^{-1}) for each system are given in the tables. The smoothed curves with the experimental points are shown in figures (5.6.1) to (5.6.10).

5.7 Enthalpies of solution

In addition to the liquid phase measurements described, it was decided to determine the enthalpy change for the solid state process:



so that an idea of the strength of the solid complex could be ascertained. Accordingly, measurements of the enthalpy of solution of the solid complex in an excess of one or other of the components were made.

Let component 1 = the aromatic hydrocarbon and component 2 = hexafluorobenzene. Suppose n_1 moles of '1', and n_2 moles of '2' are mixed to give a solid complex (z). All the solid complexes studied here are of 1:1 molar ratio, so we will assume that $n_1 = n_2$. Since one mole of '1', and one mole of '2' gives one mole of complex, there are $(n_1 + n_2)/2$ moles of complex. The complex is dissolved in m_2 moles of '2' (acting as a solvent) to give a solution, all at temperature T.

Then,

$$\begin{aligned} \Delta H(\text{measured}) = & n_1 H_1(\text{liq}) + (n_2 + m_2) H_2(\text{liq}) - m_2 H_2^*(\text{liq}) \\ & - n_1 H_1(\text{solid z}) - n_2 H_2(\text{solid z}) \end{aligned} \quad (5.7.1)$$

Consider also the enthalpy of mixing for adding n_1 moles of '1' to $(n_2 + m_2)$ moles of '2' in the liquid phase.

$$\begin{aligned} \Delta H(\text{liq.phase}) = & n_1 H_1(\text{liq}) + (n_2 + m_2) H_2(\text{liq}) - n_1 H_1^*(\text{liq}) \\ & - (n_2 + m_2) H_2^*(\text{liq}) \end{aligned} \quad (5.7.2)$$

Incorporating equation (5.7.1) into (5.7.2) gives:

$$\begin{aligned} \Delta H(\text{measured}) &= \Delta H(\text{liq.phase}) + n_1 H_1^*(\text{liq}) + (n_2 + m_2) H_2^*(\text{liq}) \\ &\quad - m_2 H_2^*(\text{liq}) - n_1 H_1(\text{solid } z) - n_2 H_2(\text{solid } z) \end{aligned}$$

or

$$\begin{aligned} \Delta H(\text{measured}) &= \Delta H(\text{liq.phase}) + n_1 H_1^*(\text{liq}) + n_2 H_2^*(\text{liq}) \\ &\quad - n_1 H_1(\text{solid } z) - n_2 H_2(\text{solid } z) \end{aligned} \tag{5.7.3}$$

But the enthalpy of mixing (solid complex) i.e. n_1 moles of solid '1' + n_2 moles of solid '2' giving the solid complex z , is given by the following:

$$\begin{aligned} \Delta H(\text{solid complex}) &= n_1 H_1(\text{solid } z) + n_2 H_2(\text{solid } z) \\ &\quad - n_1 H_1^*(\text{pure solid}) - n_2 H_2^*(\text{pure solid}) \end{aligned} \tag{5.7.4}$$

Using equation (5.7.4), equation (5.7.3) becomes:

$$\begin{aligned} \Delta H(\text{measured}) &= \Delta H(\text{liq.phase}) + n_1 H_1^*(\text{liq}) + n_2 H_2^*(\text{liq}) \\ &\quad - \Delta H(\text{solid complex}) - n_1 H_1^*(\text{pure solid}) - n_2 H_2^*(\text{pure solid}) \end{aligned} \tag{5.7.5}$$

This can be simplified to :

$$\begin{aligned} \Delta H(\text{measured}) &= \Delta H(\text{liq.phase}) - \Delta H(\text{solid complex}) \\ &\quad + n_1 \Delta_{fus} H_1^* + n_2 \Delta_{fus} H_2^* \end{aligned} \tag{5.7.6}$$

or, alternatively:

$$\begin{aligned} \Delta H(\text{measured}) = & H^E(\text{liq}) \times (n_1 + n_2 + m_2) - H^E(\text{solid complex}) \times (n_1 + n_2) \\ & + n_1 \Delta_{fus} H_1^* + n_2 \Delta_{fus} H_2^* \end{aligned} \quad (5.7.7)$$

(Note that $H^E(\text{solid complex}) = \Delta H(\text{solid complex})/2$)

5.8 Operation

The runs were endothermic and so carried out as described in section 5.3, with the three deflections ($\Delta_1, \Delta_2, \Delta_3$), two currents (I_1, I_2) and two times (t_1, t_2) being noted. The enthalpy calculated (from equation 5.3.4) is now $\Delta H(\text{solution})$, which is equivalent to $\Delta H(\text{measured})$ in equation 5.7.7.

Heats of solution measurements were performed on the 1:1 complexes formed by hexafluorobenzene + 2-methylnaphthalene and + quinoline. In each case, the liquid hydrocarbon was injected into one side of a clean calorimeter in the usual manner. Exactly the correct amount of hexafluorobenzene to form the 1:1 complex was injected using an 'Aglar' micrometer syringe, into the same side of the calorimeter; the volume added could be controlled to ± 0.00005 ml and the mass determined from the density of hexafluorobenzene (65). The complex was melted and allowed to solidify twice to ensure it was homogeneous. The other side of the calorimeter was filled

with a known weight of hexafluorobenzene (enough to dissolve the complex at the temperature; this was easily calculated from the corresponding phase diagram.)

5.9 Results

In equation (5.7.7), $H^E(\text{liq})$ is determined from the relevant $H^E(\text{liq})$ against mole fraction plot (section 5.6), at a hexafluorobenzene mole fraction of $(n_2 + m_2)/(n_1 + n_2 + m_2)$.

The enthalpies of fusion are taken from literature (65,66,67,68) and corrected to the temperature of the thermostated bath, T/K, using the formula:

$$\Delta_{fus} H(T) = \Delta_{fus} H(T^\circ) + \Delta C_p (T - T^\circ) \quad (5.9.1)$$

where T° = the temperature corresponding to the literature enthalpies of fusion. ΔC_p is determined by plotting heat capacity data (66) against temperature, for the liquid and solid pure components ($\Delta C_p = C_p(\text{liq}) - C_p(\text{solid})$).

The results are shown in tables (5.9.1) and (5.9.2).

5.10 Calculation of enthalpy of solid complex

formation, from solid-liquid phase diagram

Recently, Goates, Ott and Reeder (69) published a novel procedure whereby the enthalpy change for the process liquid A + liquid B giving a solid complex AB can

Table (5.9.1)

Hexafluorobenzene + 2-methylnaphthalene (328.15 K)

Number of mols, $n_1 (= n_2)$	Number of mols, m_2	$\Delta H(\text{Solution})$ /J	$H^E/\text{J mol}^{-1}$
1.4103×10^{-3}	5.3695×10^{-3}	32.34	-2812
1.7388×10^{-3}	3.7502×10^{-3}	39.69	-2484
1.0780×10^{-3}	3.8648×10^{-3}	24.22	-2567
1.2694×10^{-3}	4.3362×10^{-3}	28.16	-2371
2.0173×10^{-3}	5.3605×10^{-3}	46.31	-2623
1.4288×10^{-3}	5.0152×10^{-3}	32.46	-2658

Average H^E solid Complex = $-2.60 \text{ kJ mol}^{-1} \pm 0.25 \text{ kJ mol}^{-1}$

Table (5.9.2)

Hexafluorobenzene + quinoline (313.15 K)

Number of mols, $n_1 (= n_2)$	Number of mols, m_2	$\Delta H(\text{Solution})$ /J	$H^E/\text{J mol}^{-1}$
2.2765×10^{-3}	4.9363×10^{-3}	36.35	+1871
2.1910×10^{-3}	5.0664×10^{-3}	35.30	+1810
1.3740×10^{-3}	3.6615×10^{-3}	21.49	+2032
1.4396×10^{-3}	4.1680×10^{-3}	22.24	+2114
1.6673×10^{-3}	3.7523×10^{-3}	26.04	+2063
1.4425×10^{-3}	4.1325×10^{-3}	22.95	+1886

Average H^E Solid Complex = $+1.96 \text{ kJ mol}^{-1} \pm 0.15 \text{ kJ mol}^{-1}$

be calculated from the solid-liquid phase equilibria of the same system (providing the complex is congruently melting). The phase diagram data need to be extremely accurate if a large uncertainty in the enthalpy is to be avoided. Goates et al. tested their procedure on the three systems, tetrachloromethane + benzene, + toluene and + p-xylene.

In this work, we are dealing solely with 1:1 complexes (although others are amenable to the Goates treatment) and so need to consider the diagram (5.10.1). On cooling a solution such as 'x', it freezes at temperature T, depositing the solid complex, AB(s).

('+' refers to the standard state, which is the pure 1:1 solid complex, AB. 'T⁺', therefore is the freezing point of the 1:1 solid complex.)

At temperature T, we have:



$$\text{At equilibrium, } \mu_A(1) + \mu_B(1) = \mu_{AB}(s) \quad (5.10.2)$$

where μ represents chemical potential.

Therefore, if the activity of the solid complex is taken as 1, we can write:

$$\mu_A^\theta(1) + RT \ln x_A \gamma_A + \mu_B^\theta(1) + RT \ln x_B \gamma_B = \mu_{AB}^\theta(s) \quad (5.10.3)$$

where x = mole fraction and γ = activity coefficient.

$$\text{Then, } \Delta_r G^\theta = \mu_{AB}^\theta(s) - \mu_A^\theta(1) - \mu_B^\theta(1) = RT \ln(x_A x_B \gamma_A \gamma_B) \quad (5.10.4)$$

The Gibbs-Helmholtz equation states that at constant pressure:

$$\left\{ \frac{\partial(\Delta G/T)}{\partial T} \right\}_P = -\Delta H/T^2 \quad (5.10.5)$$

From equations (5.10.4) and (5.10.5) we have:

$$\left\{ \frac{\partial(\Delta_r G^\theta/T)}{\partial T} \right\}_P = R \left(\frac{\partial}{\partial T} \right) \ln(x_A x_B \gamma_A \gamma_B) = -\Delta_r H^\theta / T^2 \quad (5.10.6)$$

Integration between the limits of T and T^\dagger (constant P) gives:

$$-\int_{T^\dagger}^T \Delta_r H^\theta dT/T^2 = R \int_{T^\dagger}^T d \ln(x_A x_B \gamma_A \gamma_B) \quad (5.10.7)$$

Assuming $\Delta_r H^\theta$ is constant over the temperature range T to T^\dagger ,

$$\Delta_r H^\theta (T^\dagger - T) / T T^\dagger = R \ln \left\{ \frac{(x_A x_B \gamma_A \gamma_B) \text{ at } T}{(x_A x_B \gamma_A \gamma_B) \text{ at } T^\dagger} \right\} \quad (5.10.8)$$

Figure (5.10.1)

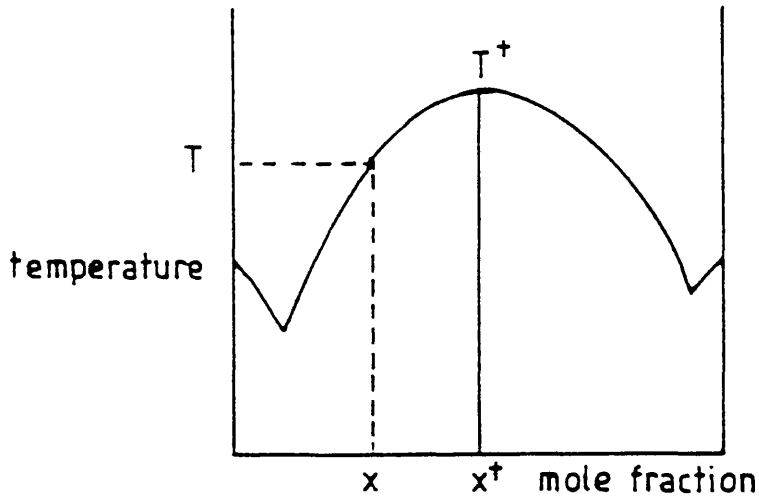
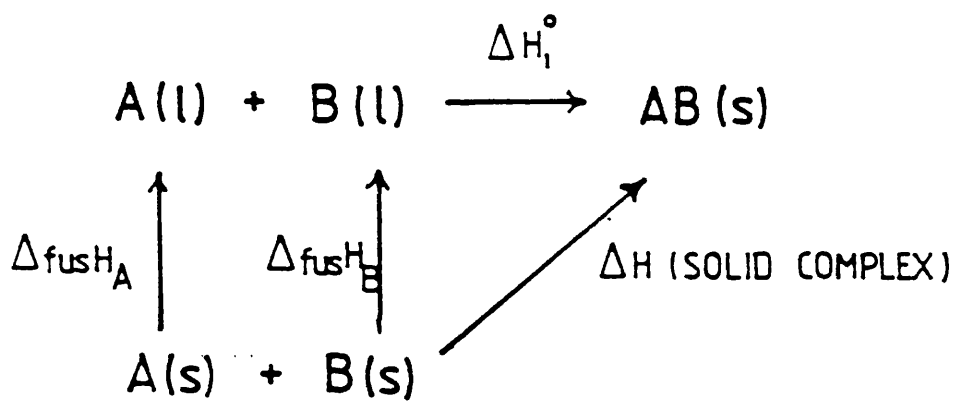


Figure (5.11.1)



Equation (5.10.8) can be divided into two terms for the mole fractions and activity coefficients, so that:

$$\Delta rH^\theta = \Delta rH' + \Delta rH'' \quad \text{where}$$

$$\Delta rH' = (RTT^\dagger)/(T^\dagger - T) \ln \left\{ \frac{(x_A x_B) \text{ at } T}{(x_A x_B) \text{ at } T^\dagger} \right\} \quad (5.10.9)$$

and

$$\Delta rH'' = (RTT^\dagger)/(T^\dagger - T) \ln \left\{ \frac{(\gamma_A \gamma_B) \text{ at } T}{(\gamma_A \gamma_B) \text{ at } T^\dagger} \right\} \quad (5.10.10)$$

At the reference state (x^\dagger, T^\dagger) equations (5.10.9) and (5.10.10) both lead to an indeterminate value (0/0), but both have limits as x and T approach the reference state. The limit of $\Delta rH''$ is zero, so the limit of $\Delta rH'$ can be obtained by plotting its values (calculated from equation (5.10.9)) against $(T^\dagger - T)$ or $x_A x_B$ and extrapolating to $(T^\dagger - T) = 0$. Since, as $x \rightarrow x^\dagger$ there is a greater inaccuracy in calculating $(T^\dagger - T)$, no $\Delta rH'$ value is plotted for a $(T^\dagger - T)$ value of less than 2 K.

5.11 Application

If, as well as the enthalpy change for liquid A + liquid B giving the solid complex AB, the enthalpies of fusion of the pure components (strictly at T^\dagger) are known, then the enthalpy change for solid A + solid B forming the

solid complex AB can be calculated (see figure 5.11.1) and compared with the values obtained from calorimetry (section 5.9).

The $\Delta H(\text{solid complex})$ calculated using the procedure of Goates et al. (and the relevant heats of fusion) are given in table (7.4.1) for the 1:1 complexes of hexafluorobenzene + naphthalene, + 1-methylnaphthalene, + 2-methylnaphthalene and + quinoline. The last two of these systems were also studied calorimetrically and are compared in the discussion (Chapter 7).

Table (5.6.1)

Excess enthalpy of mixing

Hexafluorobenzene + 2-methylnaphthalene

338.15 K

x_F	$H^E / \text{J mol}^{-1}$
0.229	-1402
0.338	-1875
0.409	-2017
0.489	-2183
0.549	-2242
0.658	-2009
0.727	-1916
0.828	-1254

$h(1) = -8809$; $h(2) = 1257$; $h(3) = 9375$

Standard deviation = 86

Table (5.6.2)

Excess enthalpy of mixing

Hexafluorobenzene + 2-ethylnaphthalene

313.15 K

x_F	$H^E / \text{J mol}^{-1}$
0.185	-1216
0.264	-1739
0.372	-2135
0.407	-2264
0.441	-2387
0.447	-2379
0.469	-2515
0.498	-2550
0.505	-2507
0.609	-2270
0.672	-2045
0.737	-1801
0.866	-1017
0.898	-799

$h(1) = -9809$; $h(2) = 191$; $h(3) = 3425$; $h(4) = 1452$

Standard deviation = 87

Table (5.6.3)

Excess enthalpy of mixing
Hexafluorobenzene + quinoline

318.15 K

x_F	$H^E/\text{J mol}^{-1}$
0.246	-635
0.293	-754
0.401	-899
0.417	-902
0.430	-945
0.470	-968
0.550	-999
0.600	-1017
0.683	-926
0.748	-810
0.804	-627

$h(1) = -3983$; $h(2) = 1279$; $h(3) = 480$; $h(4) = -2310$

Standard deviation = 23

Table (5.6.4)

Excess enthalpy of mixing

Hexafluorobenzene + isoquinoline

303.15 K

x_F	$H^E/\text{J mol}^{-1}$
0.130	-178
0.238	-305
0.256	-320
0.368	-445
0.434	-471
0.515	-506
0.559	-525
0.600	-512
0.652	-483
0.736	-432
0.830	-275
0.903	-208

$h(1) = -2034$; $h(2) = 457$; $h(3) = -382$

Standard deviation = 21

Table (5.6.5)

Excess enthalpy of mixing
Hexafluorobenzene + isoquinoline

313.15 K

x_F	$H^E / \text{J mol}^{-1}$
0.153	-218
0.262	-334
0.354	-407
0.434	-442
0.539	-471
0.552	-464
0.601	-452
0.732	-414
0.781	-353
0.792	-361
0.961	-98

$h(1) = -1842$; $h(2) = 373$; $h(3) = 274$

Standard deviation = 11

Table (5.6.6)

Excess enthalpy of mixing
Hexafluorobenzene + tetralin

303.15 K

x_F	$H^E/\text{J mol}^{-1}$
0.153	-481
0.215	-633
0.336	-930
0.441	-1075
0.519	-1129
0.541	-1145
0.606	-1073
0.625	-1074
0.714	-934
0.760	-837
0.813	-694
0.872	-496

$h(1) = -4477$; $h(2) = 641$; $h(3) = 876$

Standard deviation = 17

Table (5.6.7)

Excess enthalpy of mixing

Hexafluorobenzene + cis-decalin

303.15 K

x_F	$H^E / \text{J mol}^{-1}$
0.147	811
0.197	1060
0.282	1358
0.414	1500
0.460	1556
0.535	1563
0.569	1579
0.633	1463
0.684	1407
0.785	1130
0.847	899

$h(1) = 6291; h(2) = -93; h(3) = 1113$

Standard deviation = 40

Table (5.6.8)

Excess enthalpy of mixing

Hexafluorobenzene + trans-decalin

303.15 K

x_F	$H^E / \text{J mol}^{-1}$
0.211	959
0.303	1227
0.443	1433
0.493	1441
0.539	1427
0.587	1407
0.715	1221
0.732	1223
0.847	797
0.967	213

$h(1) = 5780$; $h(2) = -298$; $h(3) = 622$

Standard deviation = 26

Table (5.6.9)

Excess enthalpy of mixing

Hexafluorobenzene + 2,3-cyclohexenopyridine

303.15 K

x_F	$H^E/J \text{ mol}^{-1}$
0.018	6
0.034	-3
0.046	-6
0.071	-45
0.171	-202
0.229	-300
0.269	-380
0.388	-596
0.484	-689
0.538	-700
0.609	-679
0.719	-608
0.732	-599
0.889	-320
0.953	-123

$h(1) = -2780; h(2) = 698; h(3) = 2231; h(4) = 2810; h(5) = -5154;$

$h(6) = -2516; h(7) = -5320$

Standard deviation = 5

Table (5.6.10)

Excess enthalpy of mixing

Hexafluorobenzene + 1-methylnaphthalene

348.15 K

x_F	$H^E / \text{J mol}^{-1}$
0.078	-452
0.098	-607
0.123	-793
0.139	-999
0.874	-940
0.879	-924
0.890	-812
0.911	-614
0.941	-442

No curve fit attempted.

Figure (5.6.1)

Excess enthalpies for hexafluorobenzene

+ 2-methylnaphthalene 338.15 K

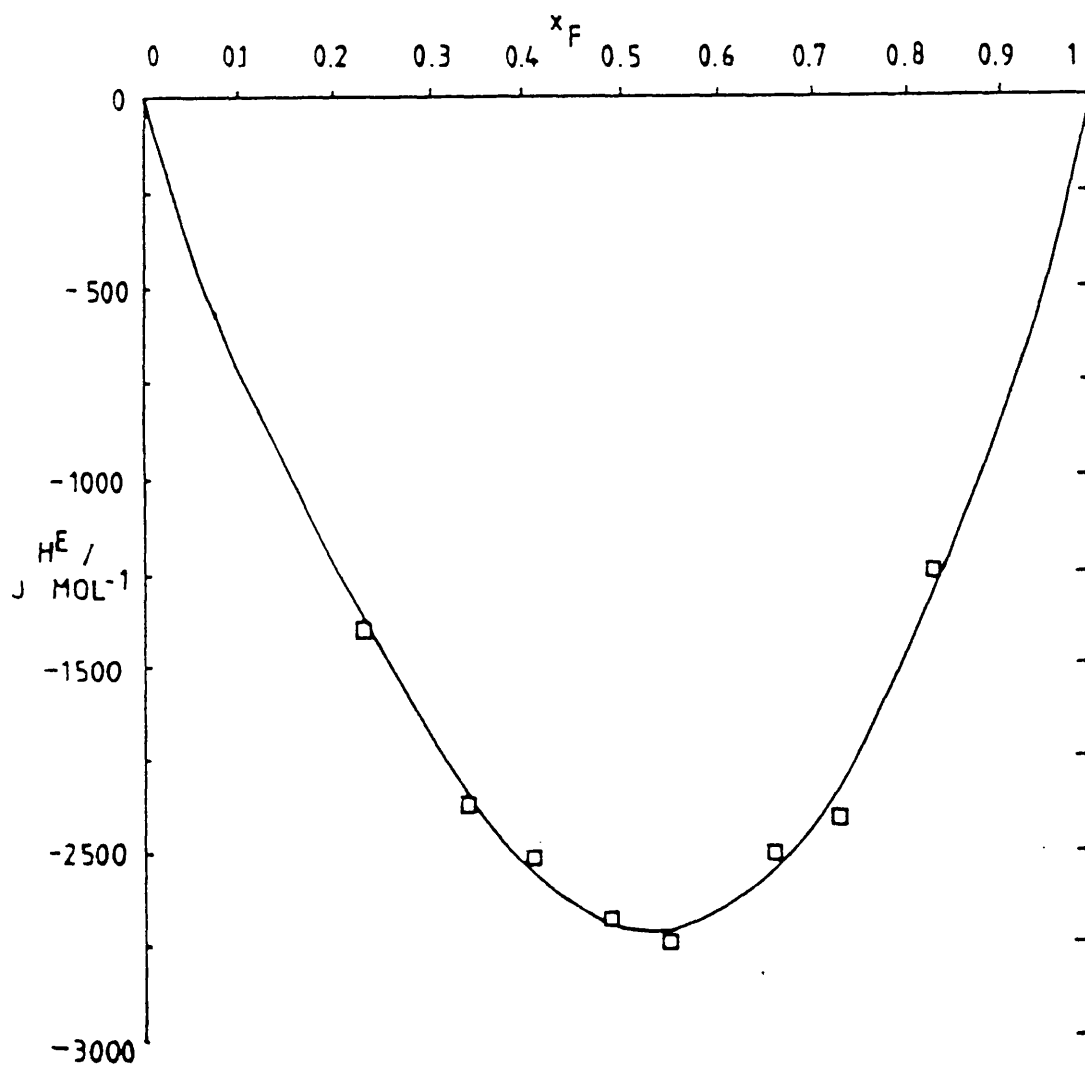


Figure (5.6.2)

Excess enthalpies for hexafluorobenzene

+ 2-ethylnaphthalene 313.15 K

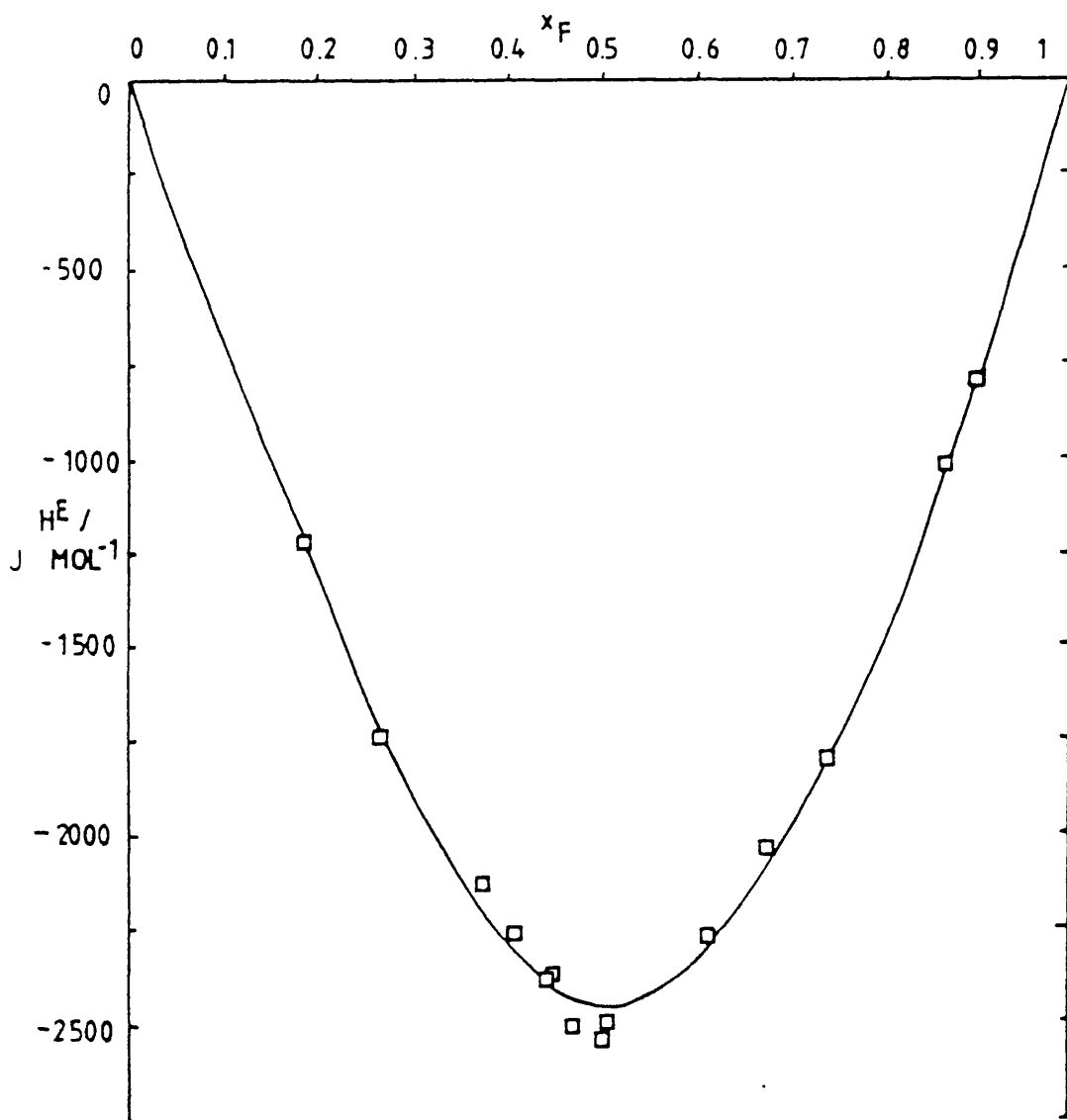


Figure (5.6.3)

Excess enthalpies for hexafluorobenzene

+ quinoline 318.15 K

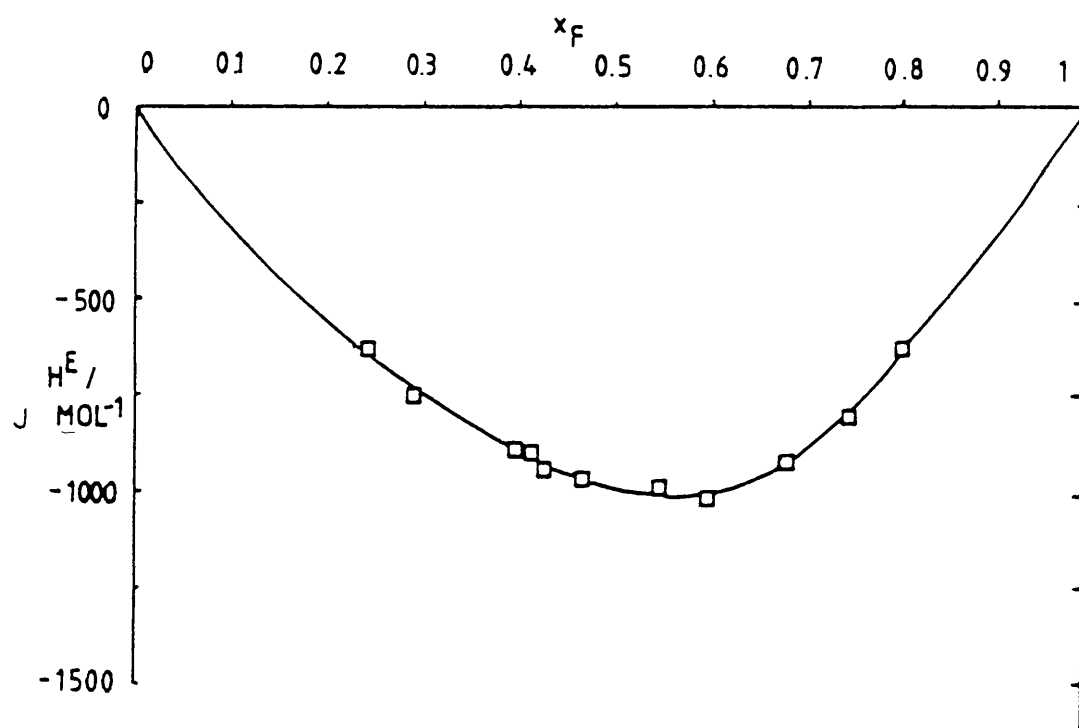


Figure (5.6.4, .5)

Excess enthalpies for hexafluorobenzene
+ isoquinoline

□ C_6F_6 + isoquinoline (303.15K)

○ C_6F_6 + isoquinoline (313.15K)

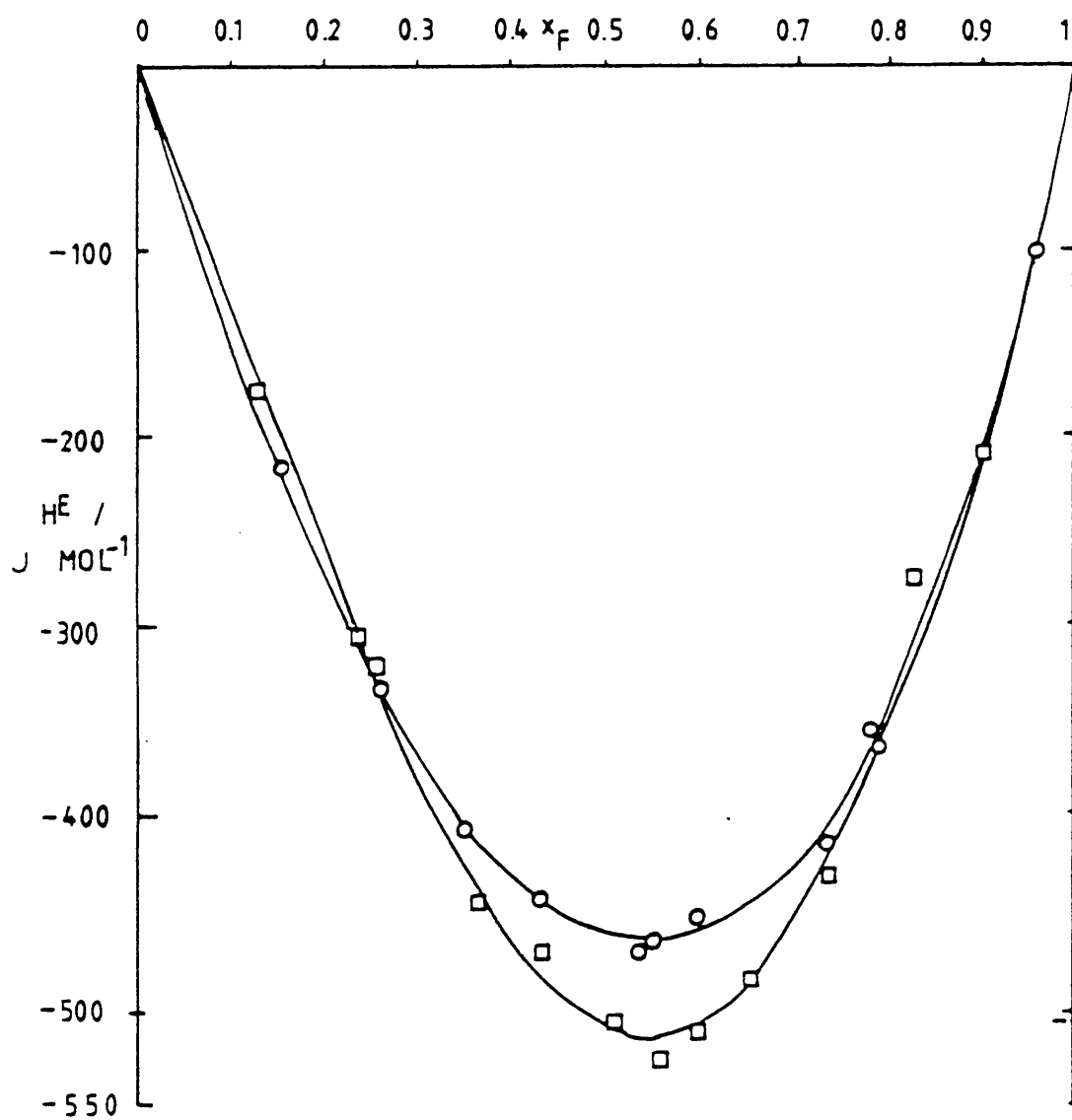


Figure (5.6.6)

Excess enthalpies for hexafluorobenzene

+ tetralin 303.15 K

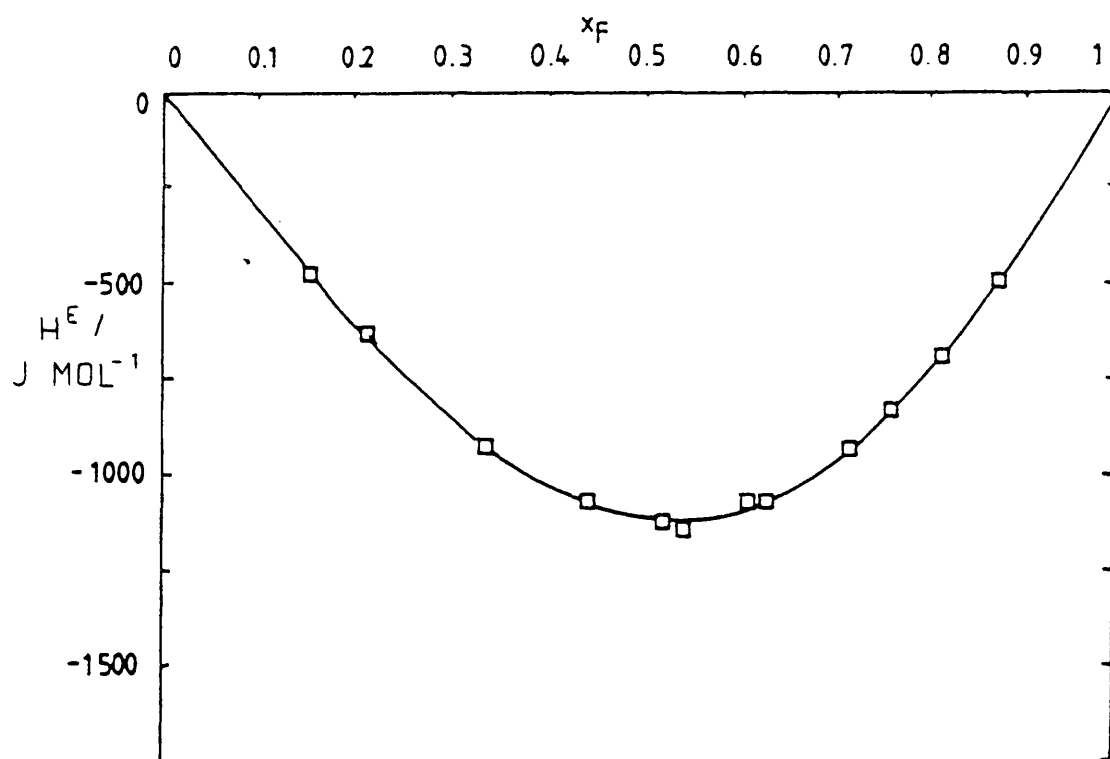


Figure (5.6.7)

Excess enthalpies for hexafluorobenzene

+ cis-decalin 303.15 K

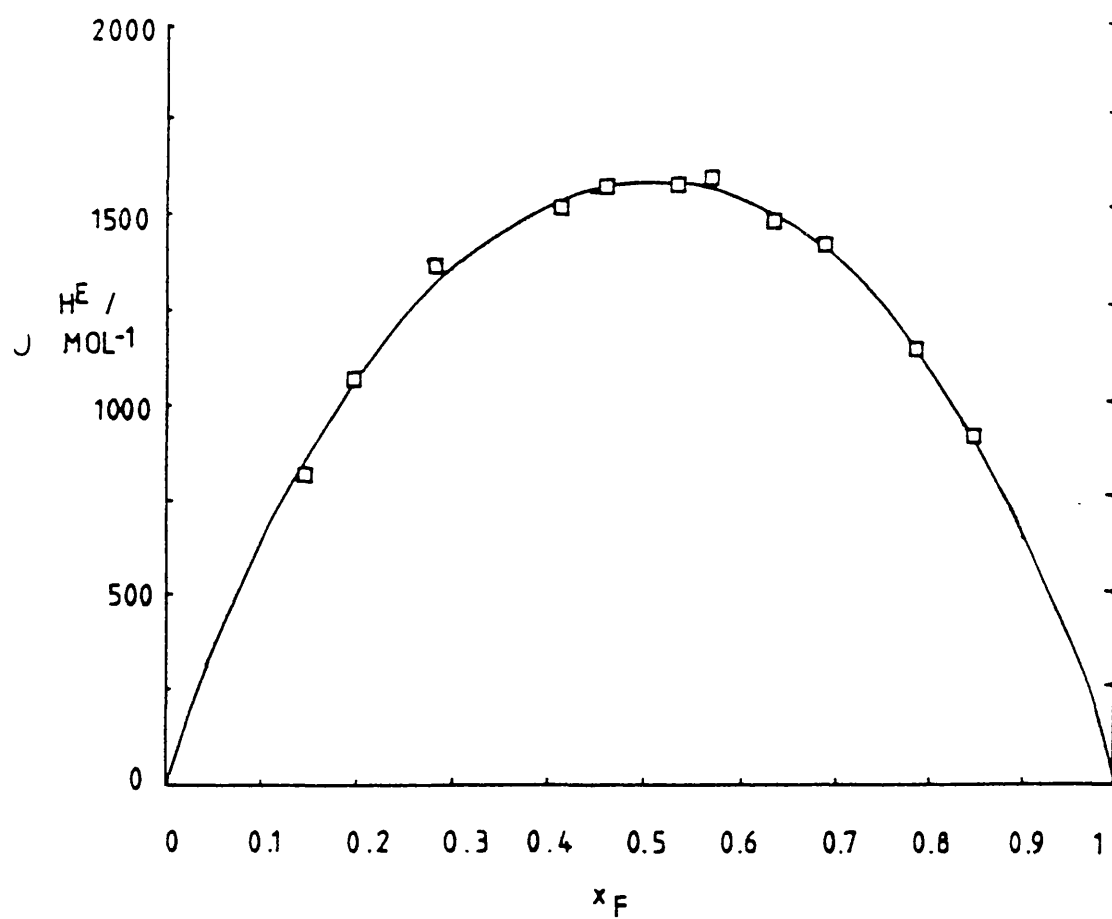


Figure (5.6.8)

Excess enthalpies for hexafluorobenzene

+ trans-decalin

303.15 K

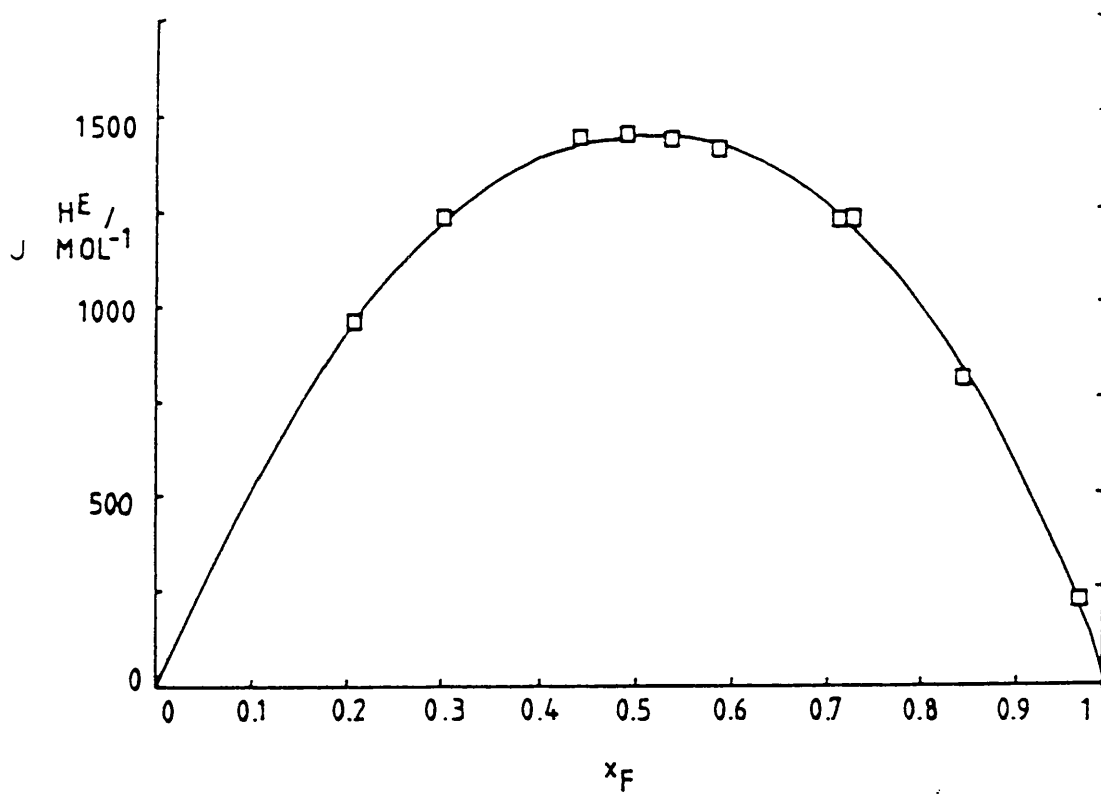


Figure (5.6.9)

Excess enthalpies for hexafluorobenzene

+ 2,3-cyclohexenopyridine 303.15 K

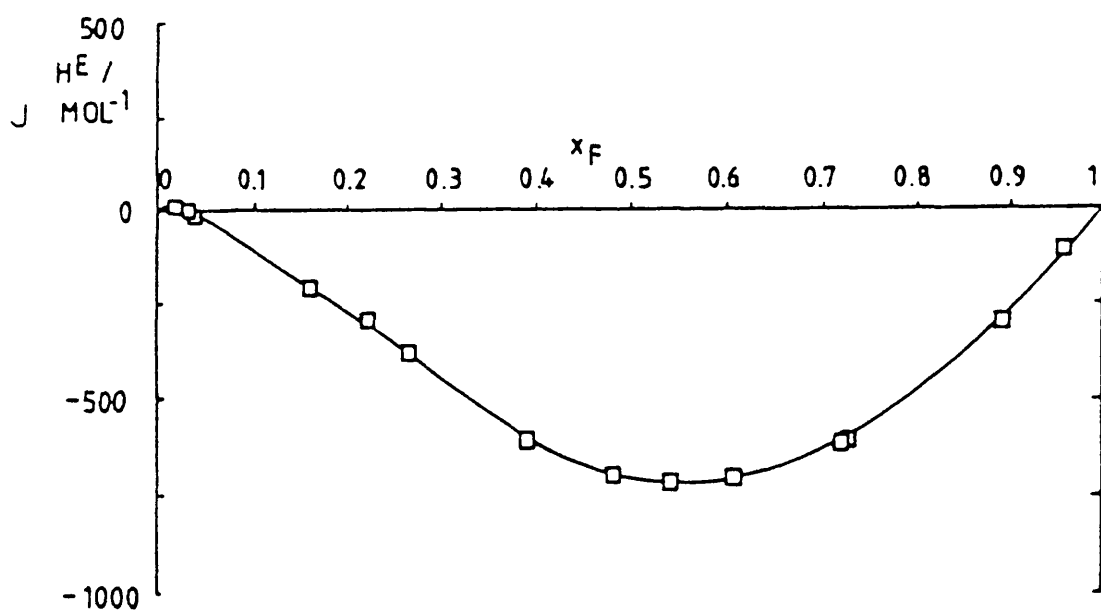
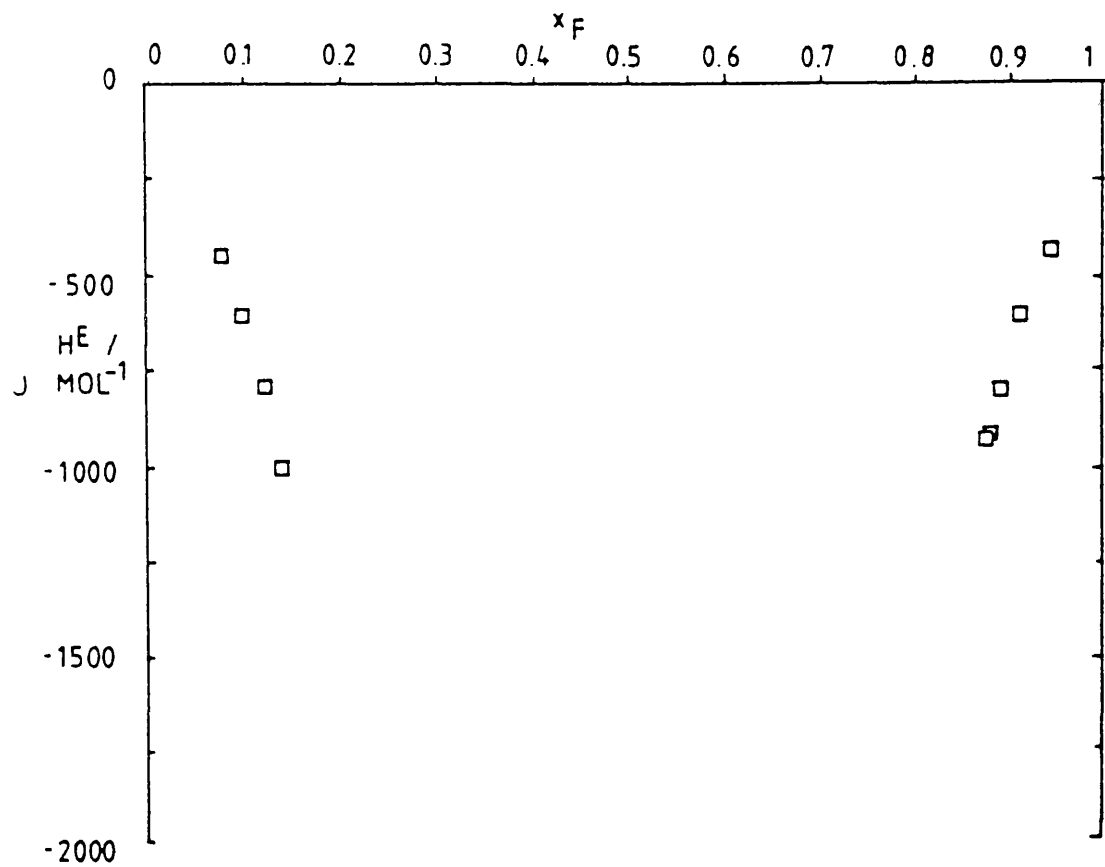


Figure (5.6.10)

Excess enthalpies for hexafluorobenzene
+ 1-methylnaphthalene 348.15 K



measurements only made at mole fractions
between 0, and 0.15, and between 0.85 and 1.

CHAPTER 6

EXCESS GIBBS FUNCTIONS

6.1 Introduction

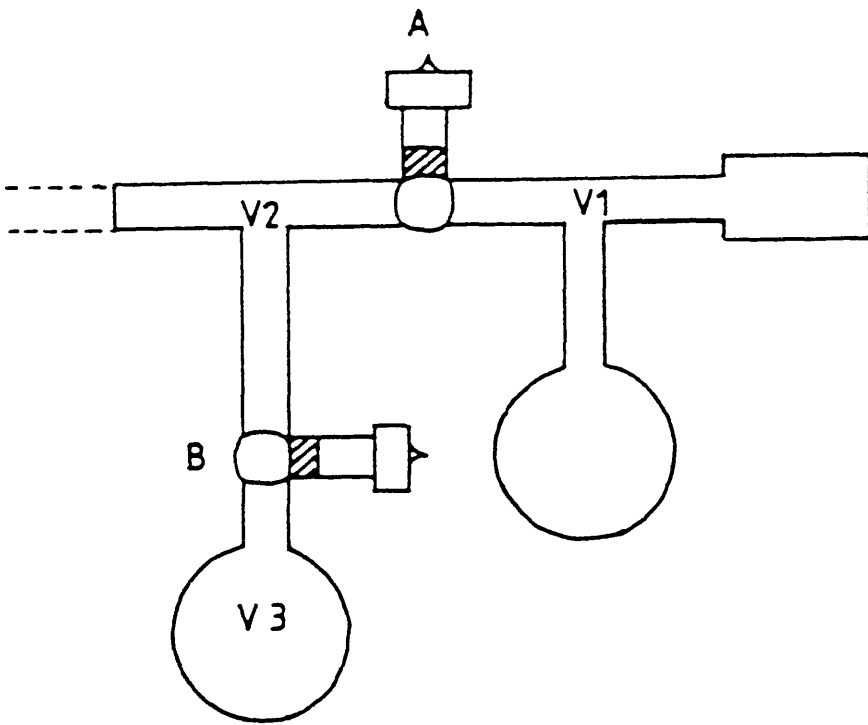
The excess Gibbs function, G^E , was determined from vapour pressure measurements. The static vapour pressure apparatus used to make these measurements was, apart from the cell (figure 6.4.3), the same as that used by Osborne (42,53) and uses a dilution method of mixture preparation. Originally, Osborne's apparatus was a modification of that described by Marsh (70), incorporating a mercury manometer for vapour pressure readings; the manometer was then replaced by a Baratron pressure transducer system.

Only the total composition of the mixture present in the cell and the corresponding vapour pressures were measured. To determine the excess Gibbs function, G^E , (see section 6.3) the activity coefficients must be calculated and to determine these the vapour composition has to be known; this in turn depends on the volume of the vapour space.

6.2 Determination of the vapour space volume

Figure (6.2.1) shows part of the main vacuum line (figure 6.6.1), with a bulb of known volume, V_3 , attached at a B.10 joint. The cell, along with a section of the line that includes the Baratron is the required volume V_1 and contains air at atmospheric pressure P_1 . The rest of the apparatus under investigation (V_2 and V_3) is

Figure (6.2.1)



evacuated.

After the pressure P_1 has been noted, the air is expanded into volume V_2 by opening tap 'A' and a new pressure, P_2 , (corresponding to the volume V_1+V_2) noted. Finally, tap 'B' is opened and a pressure reading P_3 taken for the volume $(V_1+V_2+V_3)$

So, if B is the second virial coefficient of air, we have

$$P_1 V_1 - nBP_1 = P_2 (V_1 + V_2) - nBP_2 \quad (6.2.1)$$

and

$$P_2 (V_1 + V_2) - nBP_2 = P_3 (V_1 + V_2 + V_3) - nBP_3 \quad (6.2.2)$$

Rearranging equation (6.2.2) gives:

$$(P_2 - P_3) (V_1 + V_2) = nB(P_2 - P_3) + P_3 V_3$$

Dividing by $(P_2 - P_3)$ gives:

$$(V_1 + V_2) = nB + P_3 V_3 / (P_2 - P_3) \quad (6.2.3)$$

Substituting equation (6.2.3) into equation (6.2.1) gives:

$$P_1 V_1 - nBP_1 = P_2 P_3 V_3 / (P_2 - P_3) + P_2 nB - nBP_2$$

or

$$P_1 V_1 = P_2 P_3 V_3 / (P_2 - P_3) + P_2 nB + nB(P_1 - P_2)$$

Therefore

$$P_1 V_1 = P_2 P_3 V_3 / (P_2 - P_3) + P_1 nB \quad (6.2.4)$$

The vapour space volume, V_1 , was found to be 94.3 cm^3 with an uncertainty of less than 0.2 cm^3 . The term ' $P_1 nB$ ' was found to alter the value of $P_1 V_1$ by $\pm 0.02\%$ and so was ignored. In practice V_1 will decrease from its calculated value of 94.3 cm^3 as the second component is gradually introduced into the cell.

6.3 Calculation of G^E from vapour pressure data

(Barker method(71))

Expression for activity coefficient

For a liquid in equilibrium with its vapour we can write:

$$\mu_i(\text{liq}, T, P, x) = \mu_i(\text{vap}, T, P, y) \quad (6.3.1)$$

Therefore,

$$\mu_i^*(\text{liq}, T, P) + RT \ln x_i \gamma_i(T, P, x) = \mu_i^\theta(\text{vap}, T) + RT \ln \left\{ \frac{f_i(T, P, y)}{P^\theta} \right\} \quad (6.3.2)$$

Where μ = chemical potential; γ = activity coefficient; f = fugacity; * denotes the pure liquid; θ denotes the standard state.

For a pure liquid exerting a vapour pressure P_i^* we can write:

$$\mu_i^*(\text{liq}, T, P_i^*) = \mu_i^\theta(\text{vap}, T) + RT \ln \left\{ \frac{f_i^*(T, P_i^*)}{P^\theta} \right\} \quad (6.3.3)$$

Subtracting equation (6.3.3) from equation (6.3.2) gives:

$$\mu_i^*(\text{liq}, T, P) - \mu_i^*(\text{liq}, T, P_i^*) + RT \ln x_i \gamma_i(T, P, x) = RT \ln \left\{ \frac{f_i(T, P, y)}{f_i^*(T, P_i^*)} \right\} \quad (6.3.4)$$

Since

$$\left(\frac{\partial \mu_i}{\partial P} \right)_T = V_i^* \quad (6.3.5)$$

(V_i^* = molar volume of pure i)

$$\int_{P_i^*}^P d\mu_i^* = V_i^* \int_{P_i^*}^P dP$$

at constant temperature (if V_i^* is independent of P)

Therefore

$$\mu_i^*(T, P) - \mu_i^*(T, P_i^*) = V_i^*(P - P_i^*) \quad (6.3.6)$$

From equations (6.3.4) and (6.3.6):

$$RT \ln x_i \gamma_i(T, P, x) = RT \ln \left\{ \frac{f_i(T, P, y)}{f_i^*(T, P_i^*)} \right\} - V_i^*(P - P_i^*) \quad (6.3.7)$$

or

$$RT \ln \gamma_i(T, P, x) = RT \ln \left\{ \frac{f_i(T, P, y)}{x_i f_i^*(T, P_i^*)} \right\} - V_i^* (P - P_i^*) \quad (6.3.8)$$

The activity coefficient, γ_i , is corrected to a standard reference pressure, P^θ , using:

$$RT \left(\frac{\partial \ln \gamma_i}{\partial P} \right)_T = (V_i - V_i^*) \quad (6.3.9)$$

Upon integration between the limits P and P^θ we get:

$$RT \ln \gamma_i(T, P^\theta, x) = RT \ln \gamma_i(T, P, x) + (V_i - V_i^*) (P^\theta - P) \quad (6.3.10)$$

For a perfect gas mixture:

$$\mu_i(P.G.T, P, y) = \mu_i^\theta(T) + RT \ln \left\{ \frac{P_i(T, P, y)}{P^\theta} \right\} \quad (6.3.11)$$

Subtracting equation (6.3.11) from the expression for

$\mu_i(\text{vap}, T, P, y)$ in equation (6.3.2) gives:

$$\mu_i(T, P, y) - \mu_i(P.G.T, P, y) = RT \ln \left\{ \frac{f_i(T, P, y)}{P_i(T, P, y)} \right\} \quad (6.3.12)$$

Hence, from a knowledge of equation (6.3.5) we can write:

$$RT \left\{ \frac{\partial}{\partial P} \ln \left(\frac{f_i}{P_i} \right) \right\} = V_i^{\text{vap}} - V_i \text{ (P.G.)} = V_i^{\text{vap}} - \frac{RT}{P} \quad (6.3.13)$$

Integration between the limits of $P = 0$ and P gives:

$$RT \int_{P=0}^P d \ln \left(\frac{f_i}{P_i} \right) = \int_{P=0}^P \left(V_i^{\text{vap}} - \frac{RT}{P} \right) dP \quad (6.3.14)$$

$$RT \ln (f_i / P_i) = \int_{P=0}^P \left(V_i^{\text{vap}} - \frac{RT}{P} \right) dP \quad (6.3.15)$$

Introducing P^θ into equation (6.3.15) and noting that $P_i = P y_i$ means:

$$RT \ln (f_i / P^\theta) = RT \ln (P y_i / P^\theta) + \int_{P=0}^P \left(V_i^{\text{vap}} - \frac{RT}{P} \right) dP \quad (6.3.16)$$

From equations (6.3.8) and (6.3.10),

$$RT \ln \gamma_i (T, P^\theta, x) = RT \ln \left\{ \frac{f_i (T, P, y)}{x_i f_i^* (T, P_i^*)} \right\} - V_i^* (P - P_i^*) + (V_i - V_i^*) (P^\theta - P) \quad (6.3.17)$$

Equation (6.3.15) stated that:

$$RT \ln \left(\frac{f_i}{P_i} \right) = \int_0^P \left(V_i^{\text{vap}} - \frac{RT}{P} \right) dP$$

An expression is needed for V_i^{vap} (the partial molar volume of component i in the vapour).

$$V_i^{\text{vap}} = \left(\frac{\partial V}{\partial n_i} \right)_{T, P, n_j} \quad (6.3.18)$$

Where, for a binary mixture,

$$V = (n_1 + n_2) \left\{ \frac{RT}{P} + B_m \right\} \quad (6.3.19)$$

and the second virial coefficient of the mixture, B_m , is given by

$$B_m = y_1^2 B_{11} + 2y_1 y_2 B_{12} + y_2^2 B_{22} \quad (6.3.20)$$

Therefore,

$$V_i^{\text{vap}} = \frac{RT}{P} + B_m + (n_1 + n_2) \left(\frac{\partial B_m}{\partial n_i} \right)_{T, P, n_2} \quad (6.3.21)$$

From equation (6.3.20) and noting that $y_1 y_2 = (y_2 - y_2^2)$:

$$\left(\frac{\partial B_m}{\partial n_1} \right)_{T, P, n_2} = 2 y_1 B_{11} \left(\frac{\partial y_1}{\partial n_1} \right) + 2 B_{12} \left\{ \left(\frac{\partial y_2}{\partial n_1} \right) - 2 y_2 \left(\frac{\partial y_2}{\partial n_1} \right) \right\} + 2 B_{22} y_2 \left(\frac{\partial y_2}{\partial n_1} \right) \quad (6.3.22)$$

Since $y_1 = n_1 / (n_1 + n_2)$ and $y_2 = n_2 / (n_1 + n_2)$

$$\left(\frac{\partial y_1}{\partial n_1} \right) = \frac{(n_1 + n_2) - n_1}{(n_1 + n_2)^2} \quad \text{and} \quad \left(\frac{\partial y_2}{\partial n_1} \right) = \frac{-n_2}{(n_1 + n_2)^2} \quad (6.3.23)$$

Substituting equation (6.3.23) into (6.3.22) gives:

$$\left(\frac{\partial B_m}{\partial n_1} \right)_{T, P, n_2} = \frac{2 B_{11} y_1 y_2}{n_1 + n_2} + 2 B_{12} \left\{ \frac{2 y_2^2 - y_2}{n_1 + n_2} \right\} - \frac{2 B_{22} y_2^2}{n_1 + n_2} \quad (6.3.24)$$

Substituting equations (6.3.20) and (6.3.24) into equation (6.3.21) gives:

$$V_1^{\text{vap}} = \frac{RT}{P} + y_1^2 B_{11} + 2 y_1 y_2 B_{12} + y_2^2 B_{22} + 2 B_{11} y_1 y_2 - 2 B_{12} y_2 + 4 B_{12} y_2^2 - 2 B_{22} y_2^2 \quad (6.3.25)$$

or

$$V_1^{\text{vap}} = \frac{RT}{P} + B_{11} \left\{ y_1^2 + 2 y_1 y_2 \right\} + B_{22} \left\{ -y_2^2 \right\} + 2 B_{12} \left\{ y_1 y_2 - y_2 + 2 y_2^2 \right\}$$

Since $y_1 = 1 - y_2$, we have:

$$V_1^{\text{vap}} = \frac{RT}{P} + B_{11} \left\{ 1 - y_2^2 \right\} - B_{22} y_2^2 + 2B_{12} \left\{ y_2 - y_2^2 - y_2 + 2y_2^2 \right\}$$

$$V_1^{\text{vap}} = \frac{RT}{P} + B_{11} \left\{ 1 - y_2^2 \right\} - B_{22} y_2^2 + 2B_{12} \left\{ y_2^2 \right\}$$

$$V_1^{\text{vap}} = \frac{RT}{P} + B_{11} + y_2^2 (2B_{12} - B_{11} - B_{22}) \quad (6.3.26)$$

or,

$$V_1^{\text{vap}} = \frac{RT}{P} + B_{11} + 2\delta_{12} y_2^2 \quad (\text{where } 2\delta_{12} = 2B_{12} - B_{11} - B_{22})$$

Equation (6.3.15) now becomes:

$$RT \ln \left(\frac{f_i}{P_i} \right) = \int_0^P B_{ii} dP + \int_0^P 2\delta_{12} (1 - y_i)^2 dP \quad (6.3.27)$$

Therefore,

$$RT \ln \left(\frac{f_i}{P_i} \right) = B_{ii} P + 2\delta_{12} (1 - y_i)^2 P \quad (6.3.28)$$

For a pure gas the second term disappears. So,

$$RT \ln \left(\frac{f_i^*}{P_i^*} \right) = B_{ii} P_i^* \quad (6.3.29)$$

From equation (6.3.17) and using equations (6.3.27) and (6.3.28) we obtain :

$$RT \ln \gamma_i(T, P^\theta, x) = B_{ii} (P - P_i^*) + 2\delta_{12} (1 - y_i)^2 P + RT \ln \left(\frac{P_i}{P_i^*} \right) - RT \ln x_i - V_i^* (P - P_i^*) + (V_i - V_i^*) (P^\theta - P) \quad (6.3.30)$$

or,

$$RT \ln \gamma_i(T, P^\theta, x) = RT \ln \left\{ \frac{P y_i}{x_i P_i^*} \right\} + (B_{ii} - V_i^*) (P - P_i^*) + 2\delta_{12} (1 - y_i)^2 P + (V_i - V_i^*) (P^\theta - P) \quad (6.3.31)$$

$P = P_1 + P_2$, where P_1, P_2 are the partial vapour pressures.

$$P_i = \gamma_i x_i P_i^* \exp \left\{ - \left[(B_{ii} - V_i^*) (P - P_i^*) + 2\delta_{12} (1 - y_i)^2 P + (V_i - V_i^*) (P^\theta - P) \right] / RT \right\} \quad (6.3.32)$$

The basis of the calculation used by Barker (71) is as follows:

We can write,

$$P = \gamma_1 P_1' + \gamma_2 P_2' \text{ where}$$

$$P_i' = x_i P_i^* \exp \left\{ - \left[(B_{ii} - V_i^*) (P - P_i^*) + 2\delta_{12} (1 - y_i)^2 P + (V_i - V_i^*) (P^\theta - P) \right] / RT \right\} \quad (6.3.33)$$

γ = activity coefficient, x = mole fraction, $*$ = pure liquid.

The term P_i' represents the partial vapour pressures if the liquid is ideal, but the vapour, non-ideal.

We can assume that;

$$G^E = x_1 x_2 \left[a + b(x_1 - x_2) + c(x_1 - x_2)^2 + \dots \right] \quad (6.3.34)$$

If $b=c=0$, then we have an equation for a regular solution.

This implies we can write:

$$\ln \gamma_1 = A_1 + B_1 + C_1 + \dots \quad (6.3.35)$$

$$\ln \gamma_2 = A_2 + B_2 + C_2 + \dots \quad (6.3.36)$$

where $A = a/RT$, $B = b/RT$ etc. (A, B etc. are parameters.)

Recalling that $G^E = RT \left\{ x_1 \ln \gamma_1 + x_2 \ln \gamma_2 \right\}$,

and substituting equation (6.3.35) and (6.3.36) into it and using the Gibbs-Duhem equation, we can show that:

$$l = x^2, \quad m = -x^2(1-4x), \quad \text{etc.}$$

$$l = x^2, \quad m = x^2(1-4x), \quad \text{etc.}$$

Since $A = a/RT$, $B = b/RT$ etc., equations (6.3.35) and (6.3.36) become:

$$RT \ln \gamma_1 = a_1 + b_1 + c_1 + \dots \quad (6.3.37)$$

$$RT \ln \gamma_2 = a_2 + b_2 + c_2 + \dots \quad (6.3.38)$$

The total vapour pressure, P , and the liquid mole fraction x are known. A, B and C etc. are calculated by successive approximation. Firstly, it is assumed that (a) the vapour

is ideal, (b) there is a regular solution behaviour.

Therefore $B=C=0$. So,

$$\ln \gamma_1 = Ax_2^2 \quad \text{and} \quad \ln \gamma_2 = Ax_1^2 \quad (6.3.39)$$

So, from equation (6.3.33), we have

$$Ax_2^2 = \ln \left\{ \frac{Py_1}{P_1^*x_1} \right\} \quad (\text{and similarly for } Ax_1^2) \quad (6.3.40)$$

$$P = x_1 P_1^* \gamma_1 + x_2 P_2^* \gamma_2$$

$$P = x_1 P_1^* \exp(Ax_2^2) + x_2 P_2^* \exp(Ax_1^2) \quad (6.3.41)$$

At $x=0.5$:

$$P(x=0.5) = 0.5 \left\{ P_1^* \exp(Ax_2^2) + P_2^* \exp(Ax_1^2) \right\}$$

$$\text{Therefore, } 2P(x=0.5) = (P_1^* + P_2^*) \exp(A/4)$$

$$A = 4 \ln \left\{ \frac{2P(x=0.5)}{P_1^* + P_2^*} \right\} \quad (6.3.42)$$

Using this approximate value of A , we can calculate G^E (equation (6.3.34)), γ , (equation (6.3.39)), P (equation (6.3.41)) and so y (equation (6.3.40)). Using the approximate value of y , the term $\delta_{12} y^2 P$ in equation (6.3.32) can be calculated. This enables P_1' and P_2' (vapour phase imperfections) and so $P(=P_1'+P_2')$ to be calculated.

The pressure residual, R, is defined by

$$R = P(\text{expt.}) - P(\text{calc.})$$

A least squares treatment is carried out, in which the changes in A, B and C etc. which make 'R' as small as possible, are determined.

$$\text{Pressure changes } \delta P = \left(\frac{dP}{dA} \right)_{B,C} \delta A + \left(\frac{dP}{dB} \right)_{A,C} \delta B + \left(\frac{dP}{dC} \right)_{A,B} \delta C = R \quad (6.3.43)$$

To do this, (dP/dA) is required.

$$P = \gamma_1 P_1' + \gamma_2 P_2' \quad \text{equation (6.3.33)}$$

So,

$$\frac{dP}{dA} = P_1' \left(\frac{d\gamma_1}{dA} \right) + P_2' \left(\frac{d\gamma_2}{dA} \right) \quad (6.3.44)$$

If P_1' , and P_2' are constant at constant T and x.
(and $\ln \gamma = A_1 + B_m + C_n + \dots$)

Therefore,

$$\left(\frac{d \ln \gamma_1}{dA} \right)_{B,C} = \frac{1}{\gamma_1} \left(\frac{d\gamma_1}{dA} \right) = 1$$

$$\left(\frac{d\gamma_1}{dA} \right) = 1_1 \gamma_1$$

Equation (6.3.44) now becomes:

$$\frac{dP}{dA} = P'_1 l_1 \gamma_1 + P'_2 l_2 \gamma_2 \quad (\text{constant } T, x, B \text{ and } C) \quad (6.3.45)$$

$$\text{Similarly, } \frac{dP}{dB} = P'_1 m_1 \gamma_1 + P'_2 m_2 \gamma_2 \quad (6.3.46)$$

$$\frac{dP}{dC} = P'_1 n_1 \gamma_1 + P'_2 n_2 \gamma_2 \quad (6.3.47)$$

Using the least squares method and recalling equation (6.3.43), we want the sum:

$$S = \sum_1^N \left\{ R - \left(\frac{dP}{dA} \right) \delta A - \left(\frac{dP}{dB} \right) \delta B - \left(\frac{dP}{dC} \right) \delta C \right\}^2 \quad (6.3.48)$$

for 'N' points to be a minimum.

The condition is : $\left(\frac{\partial S}{\partial \delta A} \right)_{\delta B, \delta C} = 0$, $\left(\frac{\partial S}{\partial \delta B} \right)_{\delta A, \delta C} = 0$, etc.

So,

$$\left(\frac{\partial S}{\partial \delta A} \right)_{\delta B, \delta C} = -2 \sum_1^N \left\{ R - \left(\frac{dP}{dA} \right) \delta A - \left(\frac{dP}{dB} \right) \delta B - \left(\frac{dP}{dC} \right) \delta C \right\} \times \left(\frac{dP}{dA} \right) = 0 \quad (6.3.49)$$

Equation (6.3.49) can be written as:

$$\sum_1^N R \left(\frac{dP}{dA} \right) = \sum_1^N \left\{ \left(\frac{dP}{dA} \right)^2 \delta A + \left(\frac{dP}{dB} \right) \left(\frac{dP}{dA} \right) \delta B + \left(\frac{dP}{dC} \right) \left(\frac{dP}{dA} \right) \delta C \right\} \quad (6.3.50)$$

Repeating the procedure for B and C we obtain the three simultaneous equations of Barker:

$$\begin{aligned} \delta^A \sum_1^N \left(\frac{dP}{dA} \right)^2 + \delta^B \sum_1^N \left(\frac{dP}{dA} \right) \left(\frac{dP}{dB} \right) + \delta^C \sum_1^N \left(\frac{dP}{dA} \right) \left(\frac{dP}{dC} \right) &= \sum_1^N R \left(\frac{dP}{dA} \right) \\ \delta^A \sum_1^N \left(\frac{dP}{dB} \right) \left(\frac{dP}{dA} \right) + \delta^B \sum_1^N \left(\frac{dP}{dB} \right)^2 + \delta^C \sum_1^N \left(\frac{dP}{dB} \right) \left(\frac{dP}{dC} \right) &= \sum_1^N R \left(\frac{dP}{dB} \right) \quad (6.3.51) \\ \delta^A \sum_1^N \left(\frac{dP}{dC} \right) \left(\frac{dP}{dA} \right) + \delta^B \sum_1^N \left(\frac{dP}{dC} \right) \left(\frac{dP}{dB} \right) + \delta^C \sum_1^N \left(\frac{dP}{dC} \right)^2 &= \sum_1^N R \left(\frac{dP}{dC} \right) \end{aligned}$$

The summations are carried out over all 'N' experimental points. Using matrix multiplication the equations can be solved for the unknowns, δ^A , δ^B , δ^C :

$$\begin{bmatrix} \sum_1^N \left(\frac{dP}{dA} \right)^2 & \sum_1^N \left(\frac{dP}{dA} \right) \left(\frac{dP}{dB} \right) & \sum_1^N \left(\frac{dP}{dA} \right) \left(\frac{dP}{dC} \right) \\ \sum_1^N \left(\frac{dP}{dB} \right) \left(\frac{dP}{dA} \right) & \sum_1^N \left(\frac{dP}{dB} \right)^2 & \sum_1^N \left(\frac{dP}{dB} \right) \left(\frac{dP}{dC} \right) \\ \sum_1^N \left(\frac{dP}{dC} \right) \left(\frac{dP}{dA} \right) & \sum_1^N \left(\frac{dP}{dC} \right) \left(\frac{dP}{dB} \right) & \sum_1^N \left(\frac{dP}{dC} \right)^2 \end{bmatrix} \begin{bmatrix} \delta^A \\ \delta^B \\ \delta^C \end{bmatrix} = \begin{bmatrix} \sum_1^N R \left(\frac{dP}{dA} \right) \\ \sum_1^N R \left(\frac{dP}{dB} \right) \\ \sum_1^N R \left(\frac{dP}{dC} \right) \end{bmatrix}$$

Once δ^A , δ^B , δ^C etc. have been determined, new values for A, B and C can be calculated. Since the initial value of B=C=0, the new value for B = B, and C still equals zero. The process is repeated to obtain further improved values of A, B and C.

6.4 The sample preparation line

It is essential in vapour pressure measurements to exclude all traces of water and air from the samples, otherwise readings are spuriously high. Because of this, components were thoroughly dried and degassed before being introduced into the main line

The preparation line used is shown in figure (6.4.1). All taps were of the P.T.F.E type (J.Young, Acton) and were sealed using mercury which was introduced into the annular space between the barrel and the glass using a syringe fitted with a curved needle.

An ampoule (figure 6.4.2) containing one of the components was attached at 'A'. A similar vessel holding the drying agent (P_2O_5) was placed at 'B'. Teflon sleeves (Fisons) sealed with mercury, were used at the B.14 Quickfit connections 'A' and 'B' and this removed the necessity of using grease which may have contaminated samples.

At 'C', either the cell (figure 6.4.3) or the storage ampoule (figure 6.4.4) was connected, again using a teflon sleeve. The cell was used if the involatile naphthalene compound was in 'A' and the ampoule was fitted if the volatile hexafluorobenzene was in 'A'.

Figure 6.4.1)

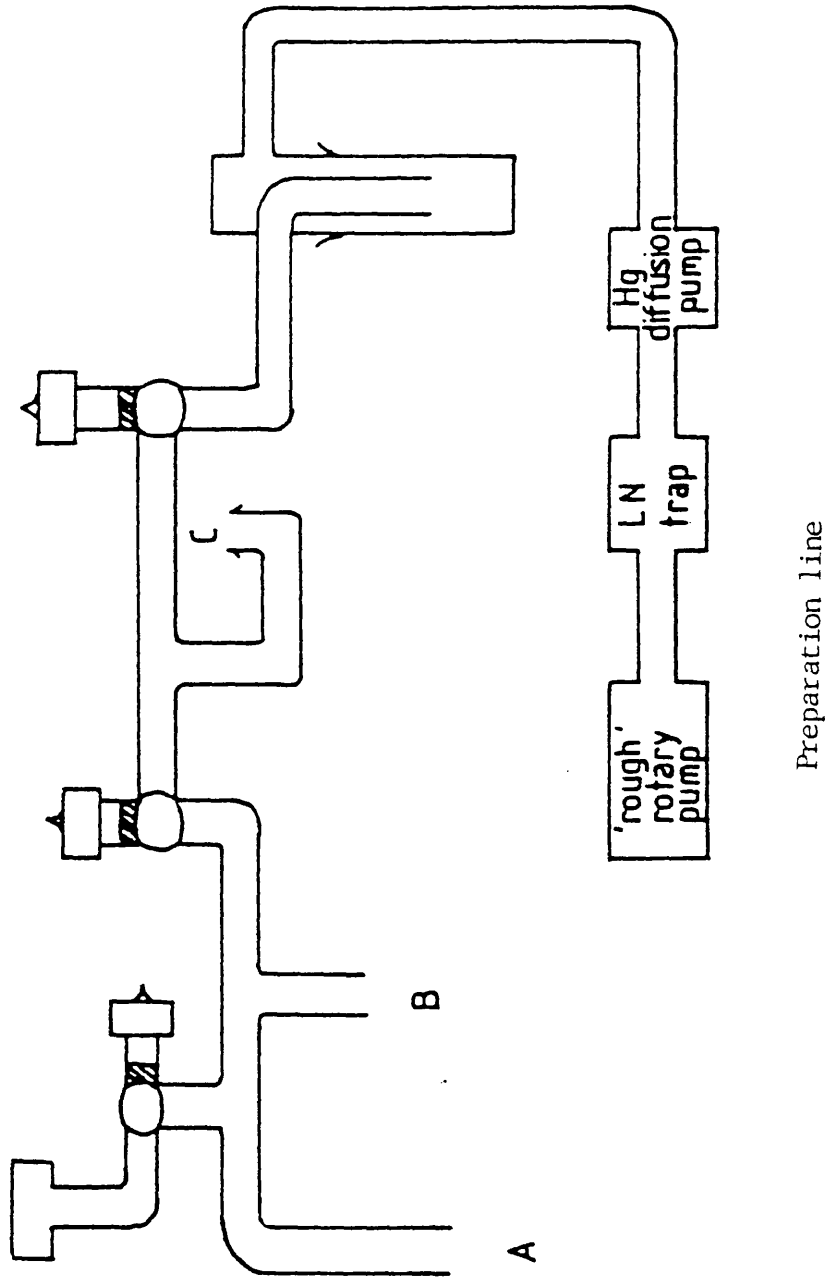


Figure (6.4.2)



Ampoule

Figure (6.4.3)

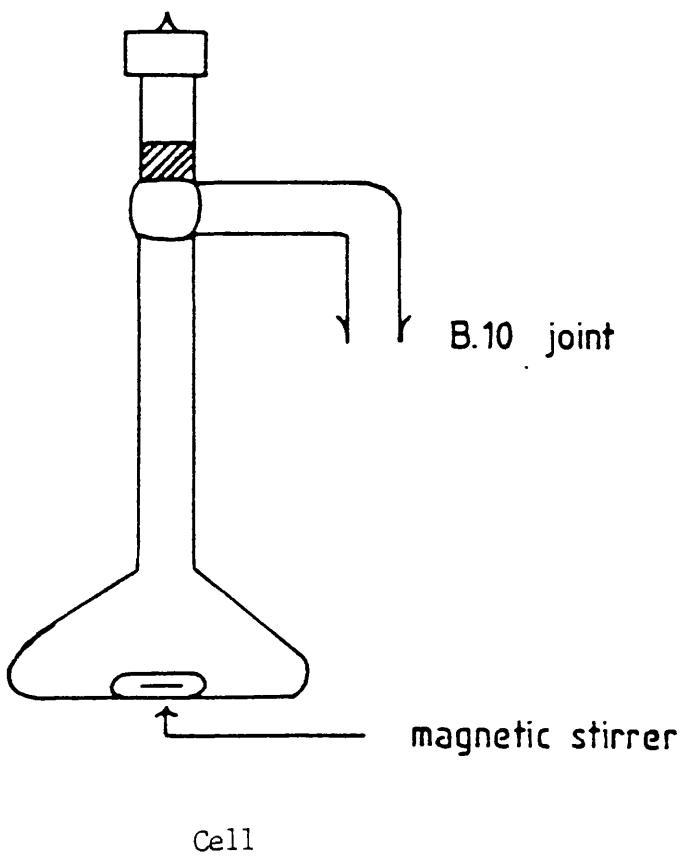
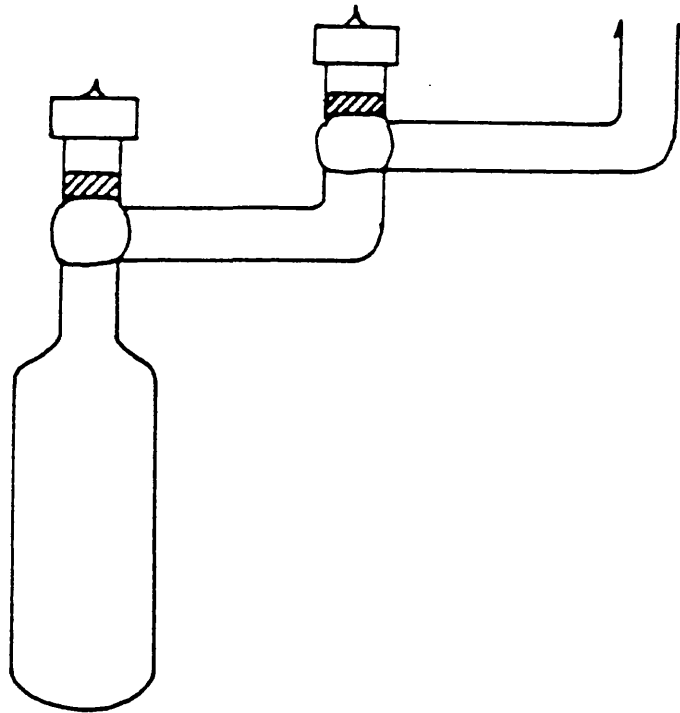


Figure (6.4.4)



Sample Storage Ampoule

The compound in 'A' was frozen with liquid nitrogen, pumped on and thawed. This process was repeated three or four times before distilling the compound onto the P_2O_5 in 'B' by placing a dewar of liquid nitrogen around 'B'. Several more freeze /thaw operations were performed until no bubbles were visible upon thawing. The compound was then distilled over to the cell or ampoule at 'C'. The involatile component was collected in the cell (previously weighed empty and evacuated) and reweighed. From the two weights and buoyancy corrections (section 6.5) the exact weight was deduced.

The volatile component (hexafluorobenzene) can be stored almost indefinitely in the storage ampoule. The weight of it was not required, since it was to be transferred to the burette in the main line from where successive additions were made to the cell. The amount of hexafluorobenzene added was determined from the change in mercury levels in the burette, the diameter (internal) of the burette and the density of hexafluorobenzene (section 6.8).

6.5 Bouyancy corrections to the weight of involatile component

If M_{obs} is the recorded weight of the empty evacuated cell and M_{true} is the actual required weight, then:

$$M_{obs} - V_{weights} \times \rho_{air} = M_{true} - V_{cell} \times \rho_{air} \quad (6.5.1)$$

(where V = volume; V_{cell} = external cell volume; M = mass and ρ = density.)

$$\text{We know that } V_{\text{weights}} = M_{\text{obs}} / \rho_{\text{wts}} \quad (6.5.2)$$

From equations (6.5.1) and (6.5.2) we have :

$$M_{\text{obs}} - \left(\frac{M_{\text{obs}} \times \rho_{\text{air}}}{\rho_{\text{wts}}} \right) = M_{\text{true}} - V_{\text{cell}} \times \rho_{\text{air}}$$

or,

$$M_{\text{obs}} \left(1 - \frac{\rho_{\text{air}}}{\rho_{\text{wts}}} \right) = M_{\text{true}} - V_{\text{cell}} \times \rho_{\text{air}} \quad (6.5.3)$$

We can write a similar expression for the recorded (observed) weight of the cell, evacuated and containing the sample. (M'_{obs})

$$M'_{\text{obs}} \left(1 - \frac{\rho'_{\text{air}}}{\rho_{\text{wts}}} \right) = M'_{\text{true}} - V_{\text{cell}} \times \rho'_{\text{air}} \quad (6.5.4)$$

The true weight of the sample is given by $M'_{\text{true}} - M_{\text{true}}$, which equals:

$$M'_{\text{obs}} \left(1 - \frac{\rho'_{\text{air}}}{\rho'_{\text{wts}}} \right) + V_{\text{cell}} \times \rho'_{\text{air}} - M_{\text{obs}} \left(1 - \frac{\rho_{\text{air}}}{\rho_{\text{air}}} \right) - V_{\text{cell}} \times \rho_{\text{air}}$$

(6.5.5)

It was ensured that all weighings were recorded at the same temperature.

Therefore, $\rho'_{\text{air}} = \rho_{\text{air}}$ and $\rho'_{\text{wts}} = \rho_{\text{wts}}$

Equation (6.5.5) then simplifies to :

$$\text{True sample weight } (= M'_{\text{true}} - M_{\text{true}}) = (M'_{\text{obs}} - M_{\text{obs}}) \left(1 - \frac{\rho_{\text{air}}}{\rho_{\text{wts}}} \right)$$

(6.5.6)

The term $(1 - \rho_{\text{air}} / \rho_{\text{wts}})$ was found to be 0.99984.

Because the cell volume is large compared with that of the sample, it is important to make the weighings at the same temperature, otherwise the term $V_{\text{cell}} \times (\rho'_{\text{air}} - \rho_{\text{air}})$ in equation (6.5.5) becomes significant.

6.6 The vapour pressure apparatus

The apparatus is shown in figure (6.6.1) and apart from the cell has been described in detail before (53).

There are two burettes (see front view of air thermostat, figure 6.6.2) which were constructed from Veridia precision-bore tubing (internal diameter, 1.0 cm). They were housed in an air thermostat made of Perspex, but with a plate glass front to allow a cathetometer to focus on the mercury levels. A temperature of 303.15 K was maintained using a contact thermometer, a heater comprising three resistors in parallel and a fan.

The cell was attached to the line at 'F' by a B.10 Quickfit joint fitted with a teflon sleeve; mercury was used to seal the joint (figure (6.6.1)). Before this method of connection was decided upon, a different method was attempted:

A glass/metal seal was made at 'F' on the line and at the end of the cell. In each case, the metal portion ended in a 'head', as illustrated in figures (6.6.3, .4 and .5). The two metal heads were held together (with two 'o' rings between them to make a seal) using the clamp illustrated in figures (6.6.6 and .7). Unfortunately, this type of connection failed to prevent leaking of air or water. This may have been due to the presence of just two screws, which placed pressure on the 'o' rings at two places, leaving gaps in between for leakage.

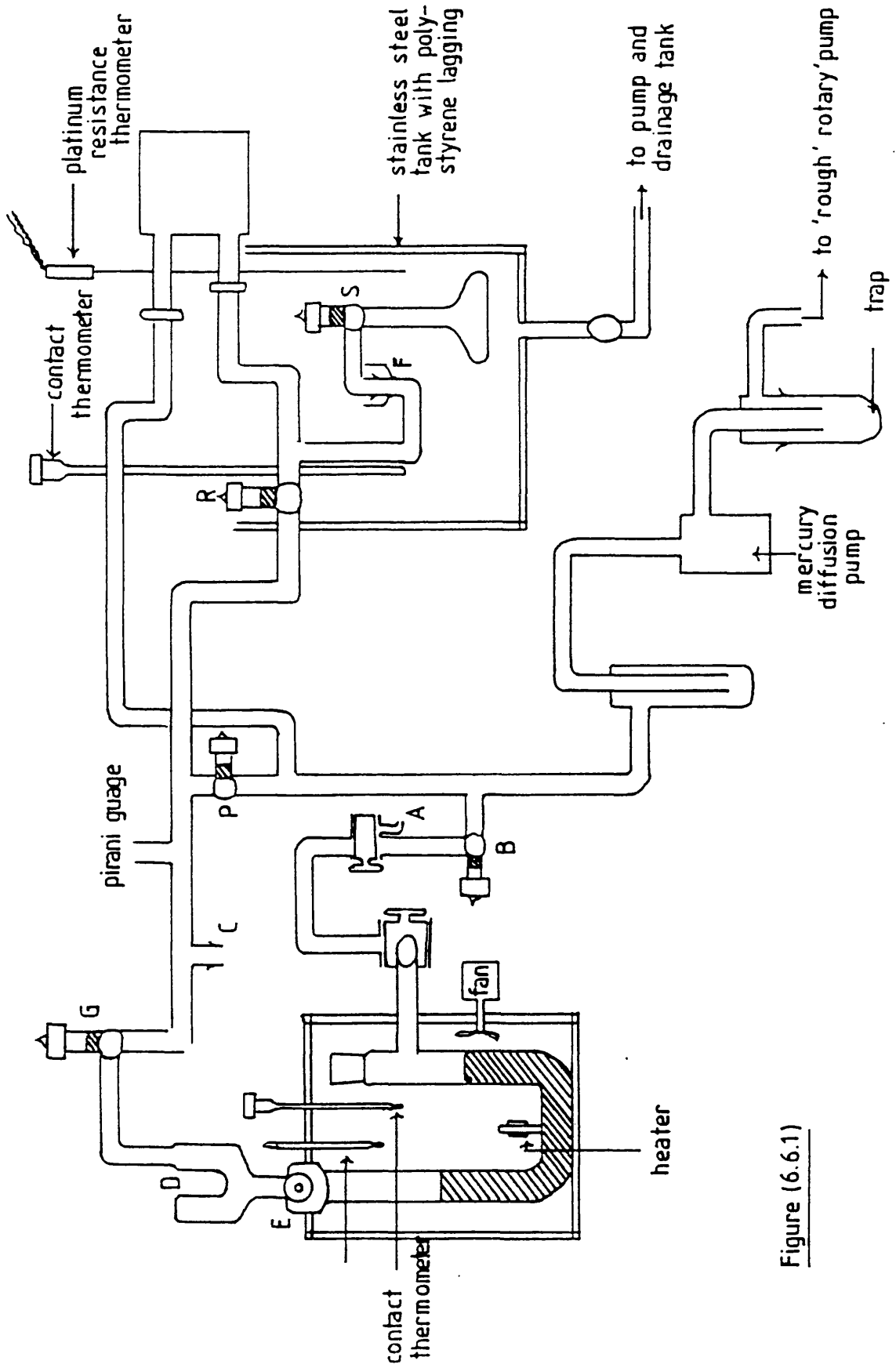
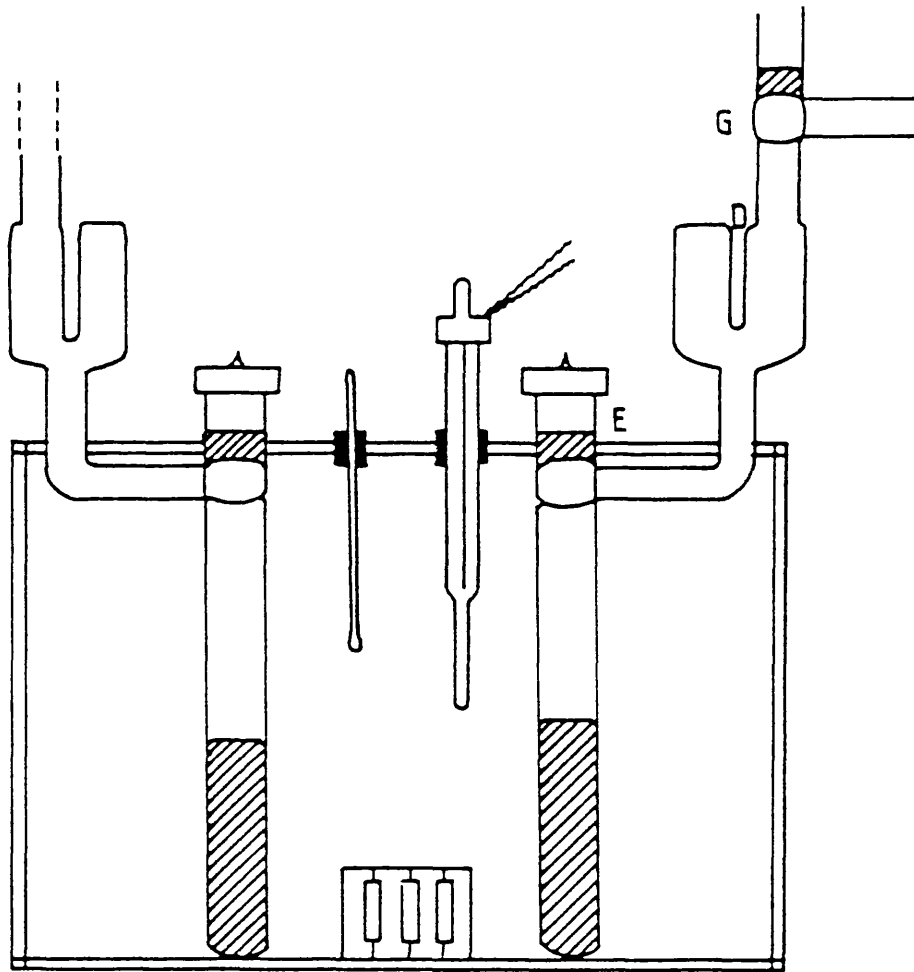


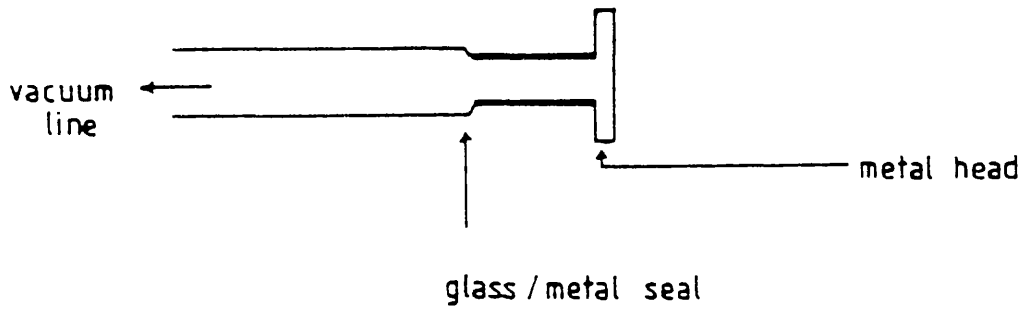
Figure (6.6.1)

Figure (6.6.2)



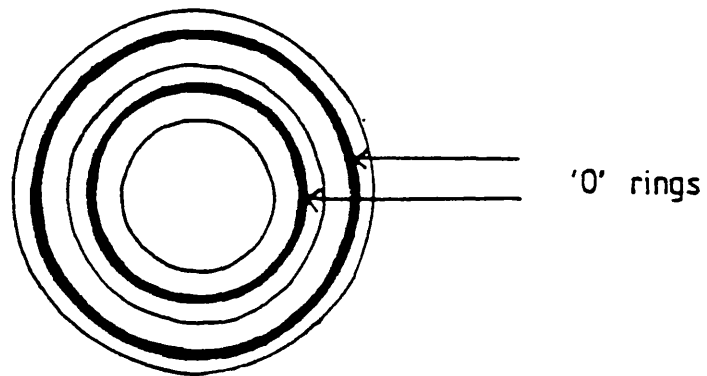
Front view of air thermostat

Figure (6.6.3)



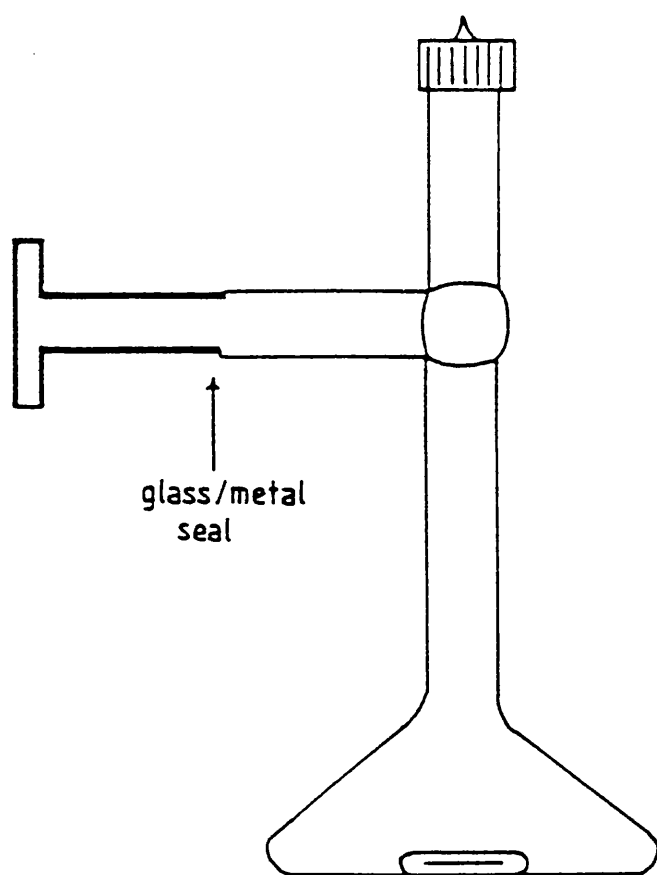
Side view of glass vacuum line / metal seal

Figure (6.6.4)



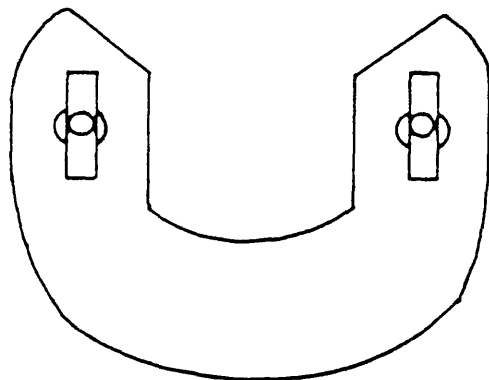
Front view of metal head

Figure (6.6.5)



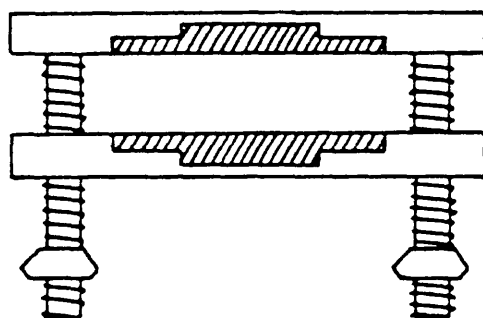
Side view of cell with metal / glass seal

Figure (6.6.6)



Side view of clamp

Figure (6.6.7)



Top view of clamp

The water level in the main tank was raised using water from the drainage tank and a pump (Stuart Turner Ltd. Type 10). The water was heated (using a permanent and intermittent heaters) and stirred using two Gunn stirrers. The temperature of the water was regulated by a contact thermometer. The exact temperature of the bath was recorded to ± 0.005 K by a platinum resistance thermometer (H.Tinsley and Co. Type 51875A) which was connected to a resistance bridge (Automatic Systems Laboratories, Model F.17).

Vapour pressures were measured to ± 0.1 mm Hg using a capacitance pressure transducer system (Baratron). The glass tubes from the reference and cell sides were sealed to separate metal tubes that were linked to the capacitance head (MKS Baratron Type 315BH) via cajon joints with aluminium washers. The 'head' was controlled by its own thermostat (MKS Type 170M-39). Insulated heating tape covered the metal and glass regions of the cell side of the line from the baratron to the water line, so that no distillation of the sample from the cell occurred.

6.7 Loading procedure

The cell containing the involatile component was attached at 'F' (figure 6.6.1), frozen with liquid nitrogen and the sample pumped on by opening taps 'P', 'R' and 'S' for a final degassing. The water level was raised

from the drainage tank by the pump, until it completely covered the cell up to the barrel of the P.T.F.E tap. The water was allowed to reach equilibrium with taps 'R' and 'S' closed. The liquid in the cell was stirred, tap 'S' opened and the steady vapour pressure reading noted. The reading was compared with any literature values (73,74,75,67). Only cis- and trans-decahydronaphthalene had literature values of vapour pressures at the temperatures we operated at; the agreement was good. In the case of tetralin, quinoline and 2-methylnaphthalene, literature values of vapour pressures quoted were for considerably higher temperatures and so only estimates of vapour pressures at our temperatures could be made. The actual readings obtained were consistent with the literature values.

The hexafluorobenzene in the storage ampoule (figure 6.4.4) was then attached at 'C'. The sample was frozen with liquid nitrogen and pumped on (both ampoule taps having been opened). It was then allowed to thaw. With tap 'P' closed and tap 'G' open, liquid nitrogen was placed in the glass finger 'D' in order to distil the hexafluorobenzene onto it. Meanwhile, tap 'B' was opened to create a vacuum behind the mercury column of the burette selected to hold the hexafluorobenzene. In doing so, the mercury level was lowered away from tap 'E'. Tap 'E' was then opened so that upon thawing, the hexafluorobenzene dripped from finger 'D' and onto the mercury in the burette. With tap 'B' closed, tap 'A' was cautiously opened to let air back behind the mercury

column in the burette and so slowly raise the mercury level towards tap 'E'. When the space between tap 'E' and the mercury column was occupied entirely by hexafluorobenzene, tap 'E' was closed and tap 'P' opened, to pump away any excess hexafluorobenzene.

6.8 The run

The sample storage ampoule was removed from 'C' and replaced by an ordinary ampoule containing P_2O_5 . After the vapour pressure of the pure (involatile) component had been noted (section 6.7), liquid nitrogen was placed around the cell to freeze the sample.

The mercury level in the burette was noted from the front of the air thermostat using the cathetometer (Precision Tool and Instrument Co. Ltd.) (the reading being accurate to within ± 0.001 cm). With tap 'P' to the diffusion and rotary pumps closed, and tap 'G' open, tap 'E' was opened and the desired quantity of hexafluorobenzene released. Tap 'E' was closed and the new burette mercury level noted. If the height change is ΔH and the burette has a radius r , then the mass of hexafluorobenzene released is $\pi r^2 \Delta H \rho$ (where ρ is the density of hexafluorobenzene at 303.15 K). Liquid nitrogen was placed under the ampoule at 'C', so that all the released hexafluorobenzene distilled onto the P_2O_5 there. It was frozen and pumped on.

After being allowed to thaw, the hexafluorobenzene in

'C' was distilled into the cell (which had liquid nitrogen around it) by opening taps 'R' and 'S'. The frozen mixture in the cell was briefly pumped on (by opening 'P') before closing taps 'R' and 'S'. The water level was raised, the temperature of the bath allowed to reach equilibrium and the new vapour pressure taken after opening tap 'S'.

The process was repeated until the mole fraction range had been satisfactorily covered.

Because the hydrocarbons used were so involatile, no attempt was made to reverse roles and place the hydrocarbon in the burette and hexafluorobenzene in the cell.

6.9 Results

Tables (6.9.1) to (6.9.5) show the results obtained for the systems studied. In each case, calculated liquid and vapour compositions are presented as hexafluorobenzene mole fractions x_F and y_F . Also listed are the experimental vapour pressures (P_{exp}) and calculated vapour pressures (P_{calc}), G^E , and the parameters, G_j .

The function:

$$\frac{G^E}{RT} = x_F(1-x_F) \left\{ \sum_{j=1}^P G_j (1-2x_F)^{j-1} \right. \quad (6.9.1)$$

is used to fit the data. Standard deviation of experimental vapour pressures from the fitted curve are

given (in N m^{-2}).

The second virial coefficient of hexafluorobenzene (B_{11}) is well documented (65,86,87), but there are no coefficients for the other components. In their absence, estimates were made: In the case of tetrahydronaphthalene (tetralin), the intermediate of the virial coefficients for benzene and cyclohexane at 303.15 K was taken ($B_{22} = -1535 \text{ cm}^3 \text{ mol}^{-1}$). For quinoline, the virial coefficient for pyridine at 318.15 K ($-1500 \text{ cm}^3 \text{ mol}^{-1}$) was used. For 2-methylnaphthalene, the value for toluene at 338.15 K ($-1750 \text{ cm}^3 \text{ mol}^{-1}$) was taken.

To test the effect of B_{22} upon G^E , three different values of B_{22} (-1000 , -1500 and $-2000 \text{ cm}^3 \text{ mol}^{-1}$) were used in analysing the results of the hexafluorobenzene + trans-decalin system (303.15 K), ($B_{22} = -1500 \text{ cm}^3 \text{ mol}^{-1}$) being our estimate for decalin, based upon cyclohexane). The deviation in G^E corresponding to a change in B_{22} of $\pm 500 \text{ cm}^3 \text{ mol}^{-1}$ was $\pm 0.25 \text{ J mol}^{-1}$.

For all systems, B_{12} was assumed to be the arithmetic mean of values B_{11} and B_{22} (pure components). i.e.

$$B_{12} = \frac{B_{11} + B_{22}}{2}$$

The plots of G^E against mole fraction are shown in figures (6.9.1) to (6.9.5). Vapour pressures, plotted

against liquid and vapour mole fractions are shown in figures (6.9.6) to (6.9.10). Table (6.9.6) gives the vapour pressure of the pure components.

6.10 The theoretical determination of excess Gibbs function, G^E , from simple eutectic phase diagrams

Consider a simple eutectic system such as that depicted in figure (6.10.1). T_A^* and T_B^* represent the freezing points of the pure components A and B, and it is assumed that either pure solid A or B separates on freezing. For a component A we can write:

$$\left(\frac{\partial \ln x_A \gamma_A}{\partial T}\right)_P = \frac{\Delta_{fus} H_A}{RT^2} \quad (6.10.1)$$

(where γ is the activity coefficient)

In simple treatments the enthalpy of fusion is assumed to be constant, but in fact it varies with temperature:

$$\Delta_{fus} H_A(T) = \Delta_{fus} H_A(298 \text{ K}) + \Delta C_p(T-298) \quad (6.10.2)$$

where the change in heat capacity (ΔC_p) (which equals $C_p(\text{liquid A}) - C_p(\text{solid A})$) is obtained by plotting heat capacities for the liquid and solid against temperature. The curves are extrapolated and C_p determined for the required temperature.

From equations (6.10.1) and (6.10.2) we have:

$$\left(\frac{\partial \ln x_A \gamma_A}{\partial T}\right)_P = \frac{\Delta_{fus} H_A(298 \text{ K})}{RT^2} + \frac{\Delta C_P(T-298)}{RT^2}$$

Integrating gives:

$$\int_{x_A \gamma_A}^{x_A \gamma_A = 1} d \ln x_A \gamma_A = \frac{\Delta_{fus} H_A(298 \text{ K})}{R} \int_{T_A}^{T_A^*} \frac{dT}{T^2} + \int_{T_A}^{T_A^*} \frac{\Delta C_P dT}{RT} + \frac{(298 \Delta C_P)}{R} \int_{T_A}^{T_A^*} \frac{dT}{T^2}$$

Therefore,

$$\begin{aligned} -\ln x_A \gamma_A &= \frac{\Delta_{fus} H_A(298 \text{ K})}{R} \left(\frac{1}{T_A} - \frac{1}{T_A^*} \right) + \left(\frac{\Delta C_P}{R} \right) \ln \left(\frac{T_A^*}{T_A} \right) \\ &\quad - \frac{(298 \Delta C_P)}{R} \left(\frac{1}{T_A} - \frac{1}{T_A^*} \right) \end{aligned} \quad (6.10.3)$$

Bringing the terms involving $(1/T_A - 1/T_A^*)$ together gives:

$$-\ln x_A \gamma_A = \left\{ \frac{\Delta_{fus} H_A(298 \text{ K}) - 298 \Delta C_P}{R} \right\} \left(\frac{1}{T_A} - \frac{1}{T_A^*} \right) + \left(\frac{\Delta C_P}{R} \right) \ln \left(\frac{T_A^*}{T_A} \right) \quad (6.10.4)$$

We can determine γ_A from equation (6.10.4) for any composition between pure A and the eutectic. A similar expression for B will allow the calculation of γ_B for any composition between pure B and the eutectic.

However, the values for γ_A and γ_B must be corrected to a chosen reference temperature using the expression:

$$\left(\frac{\partial \ln \gamma_A}{\partial T}\right)_{P,x} = -(H_A - H_A^*) / RT^2 \quad (6.10.5)$$

$H_A - H_A^*$ is the difference between the partial molar enthalpy of A in the mixture and the molar enthalpy of pure A.

Since by definition,

$$\begin{aligned} \Delta_{\text{mix}} H_m &= x_A H_A + x_B H_B - x_A H_A^* - x_B H_B^* , \\ \Delta_{\text{mix}} H_m &= x_A (H_A - H_A^*) + x_B (H_B - H_B^*) \end{aligned}$$

We can determine $(H_A - H_A^*)$ by plotting the excess enthalpy (H^E) (which equals $\Delta_{\text{mix}} H_m$, as $\Delta_{\text{mix}} H_m(\text{ideal}) = 0$) against mole fraction (section 4) and drawing a tangent at the given mole fraction.

Only at the eutectic can we determine both γ_A and γ_B directly, using equation (6.10.4), and so find G^E . In order to determine G^E as a function of mole fraction, we need γ_A and γ_B values over the entire composition range. This can be done using the Gibbs-Duhem equation, which may be written in the form:

$$x_A d\mu_A + x_B d\mu_B = 0 \quad (\text{constant temperature and pressure} \\ \text{(and where } \mu = \text{chemical potential)}) \quad (6.10.6)$$

$$\text{Also } \mu_A = \mu_A^* + RT \ln x_A \gamma_A \quad (6.10.7)$$

From equation (6.10.7):

$$d\mu_A = RT d \ln x_A \gamma_A = RT d \ln x_A + RT d \ln \gamma_A \quad (6.10.8)$$

Similarly, for B:

$$d\mu_B = RT d \ln x_B \gamma_B = RT d \ln \gamma_B \quad (6.10.9)$$

Substituting equations (6.10.8) and (6.10.9) into equation (6.10.6) and dividing by 'RT' gives:

$$x_A d \ln x_A + x_A d \ln \gamma_A + x_B d \ln x_B + x_B d \ln \gamma_B = 0 \quad (6.10.10)$$

Since $x_A d \ln x_A + x_B d \ln x_B = 0$, then $x_A d \ln \gamma_A + x_B d \ln \gamma_B = 0$

$$\text{Therefore,} \quad d \ln \gamma_B = -x_A/x_B (d \ln \gamma_A) \quad (6.10.11)$$

Integrating equation (6.10.11) gives:

$$\int_{x_B = \text{Eutectic}}^{x_B} d \ln \gamma_B = - \int_{x_B = \text{Eutectic}}^{x_B} x_A/x_B (d \ln \gamma_A) \quad (6.10.12)$$

In order to evaluate the right hand side of equation (6.10.12), a plot of x_A/x_B against $\ln \gamma_A$ is constructed (figure 6.10.2) and the area under the curve evaluated.

Then, $\ln \gamma_B(x_B) - \ln \gamma_B(x_B = \text{Eutectic}) = - \text{Area.}$ (see figure 6.10.2)

Figure (6.10.1)

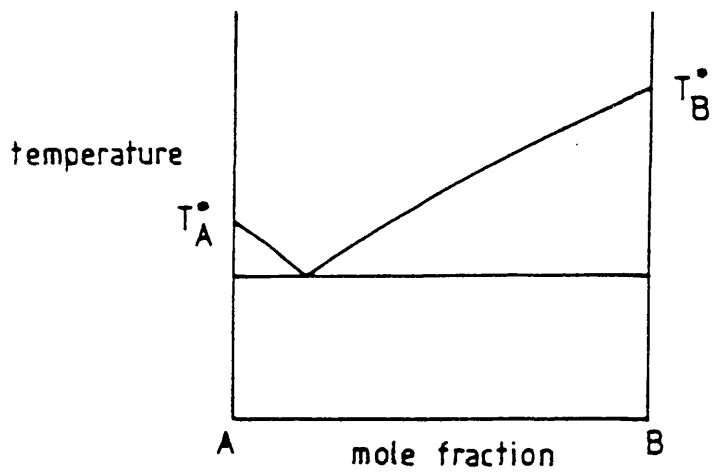
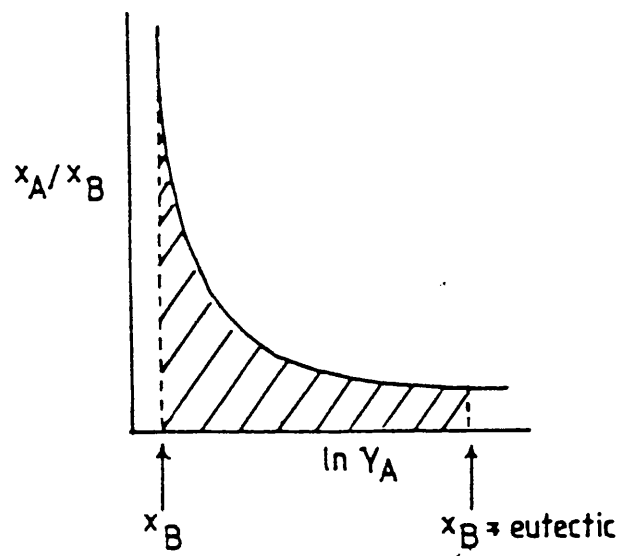


Figure (6.10.2)



Finally, the values of γ_A and γ_B are used to determine G^E , using:

$$G^E = RT \left\{ x_A \ln \gamma_A + x_B \ln \gamma_B \right\} \quad (6.10.13)$$

6.11 Results

In our studies, only the systems hexafluorobenzene + cis-decalin and + trans-decalin are amenable to the above procedure as all other diagrams showed congruently melting complexes. It is also fortunate that reliable enthalpies of fusion (65,66) and heat capacities of solid and liquid phases are available for these compounds. The results are given in tables (6.11.1) and (6.11.2), and plotted together with the corresponding experimental results in figure (6.11.1).

Table (6.9.1)

Excess Gibbs function results

Hexafluorobenzene + 2-methylnaphthalene

338.2 K

x_F	y_F	$P_{\text{exp}}/N \text{ m}^{-2}$	$P_{\text{calc}}/N \text{ m}^{-2}$	$G^E/J \text{ mol}^{-1}$
0.139	0.934	6386	6412	-20
0.213	0.969	9532	9471	-93
0.341	0.980	15905	15982	-200
0.474	0.989	22731	22651	-283
0.646	0.995	32476	32515	-364
0.687	0.996	35436	35539	-369
0.743	0.998	40302	40192	-357
0.786	0.998	44142	44046	-331
0.823	0.999	47235	47345	-294

$G(1) = -0.423$; $G(2) = -0.405$; $G(3) = -0.312$; $G(4) = -0.103$;

$G(5) = 0.717$

Standard deviation = 125 N m^{-2}

Table (6.9.2)

Excess Gibbs function results

Hexafluorobenzene + quinoline

318.2 K

x_F	y_F	$P_{\text{exp}}/N \text{ m}^{-2}$	$P_{\text{calc}}/N \text{ m}^{-2}$	$G^E/J \text{ mol}^{-1}$
0.158	0.953	5412	5387	44
0.222	0.968	7319	7405	79
0.259	0.973	8465	8457	97
0.284	0.976	9172	9134	108
0.338	0.980	10479	10402	126
0.455	0.986	12878	12987	138
0.546	0.990	15051	15035	124
0.583	0.991	15891	15917	115
0.651	0.993	17808	17683	94
0.716	0.995	19424	19457	73
0.763	0.996	20717	20788	59
0.806	0.997	22077	22017	48
0.849	0.998	23184	23226	38

$G(1) = 0.202$; $G(2) = -0.119$; $G(3) = -0.178$; $G(4) = 0.235$;

Standard deviation = 78 N m^{-2}

Table (6.9.3)

Excess Gibbs function results

Hexafluorobenzene + tetralin

303.2 K

x_F	y_F	$P_{\text{exp}}/N \text{ m}^{-2}$	$P_{\text{calc}}/N \text{ m}^{-2}$	$G^E/\text{J mol}^{-1}$
0.054	0.580	1199	1189	-19
0.159	0.823	2519	2527	-42
0.217	0.871	3226	3269	-53
0.284	0.907	4119	4078	-66
0.471	0.954	6239	6235	-118
0.514	0.961	6839	6740	-133
0.580	0.969	7479	7569	-156
0.655	0.979	8585	8590	-178
0.689	0.982	8945	9096	-185
0.732	0.986	9759	9755	-190
0.757	0.988	10185	10174	-190
0.778	0.990	10625	10531	-188
0.804	0.992	11052	10962	-183

$$G(1) = -0.203 ; G(2) = -0.277 ; G(3) = -0.242$$

$$\text{Standard deviation} = 78 \text{ N m}^{-2}$$

Table (6.9.4)

Excess Gibbs function results
Hexafluorobenzene + cis-decalin

303.2 K

x_F	y_F	$P_{exp}/N \text{ m}^{-2}$	$P_{calc}/N \text{ m}^{-2}$	$G^E/J \text{ mol}^{-1}$
0.252	0.956	8479	8467	675
0.384	0.966	10092	10097	860
0.434	0.968	10492	10522	901
0.641	0.975	11825	11743	879
0.743	0.979	12265	12258	748
0.758	0.979	12305	12339	722
0.776	0.980	12425	12444	686
0.887	0.987	13158	13192	408
0.900	0.988	13238	13299	368
0.933	0.975	12937	12976	394

$G(1) = 1.471$; $G(2) = 0.136$; $G(3) = 0.071$

Standard deviation = 49 N m^{-2}

Table (6.9.5)

Excess Gibbs function results

Hexafluorobenzene + trans-decalin

303.2 K

x_F	y_F	$P_{exp}/N \text{ m}^{-2}$	$P_{calc}/N \text{ m}^{-2}$	G^E/Jmol^{-1}
0.213	0.900	7332	7337	499
0.293	0.920	8679	8677	630
0.419	0.937	10065	10034	762
0.533	0.945	10758	10816	794
0.553	0.947	10905	10931	790
0.620	0.952	11358	11311	760
0.691	0.957	11798	11725	692
0.733	0.960	11918	11987	636
0.819	0.969	12598	12600	482
0.859	0.975	12932	12926	394

$G(1) = 1.259$; $G(2) = 0.098$; $G(3) = -0.070$

Standard deviation = 50 N m^{-2}

Table (6.9.6)

Vapour pressures of pure components

<u>Compound</u>	<u>Vapour pressure/N m⁻²</u>	<u>Temp/K</u>
Hexafluorobenzene	14305	303.15
2-methylnaphthalene	453	338.15
Quinoline	306	318.15
Cis-decalin	466	303.15
Trans-decalin	893	303.15
Tetralin	533	303.15

Figure (6.9.1)
Excess Gibbs functions for
Hexafluorobenzene + 2-methylnaphthalene 338.15 K

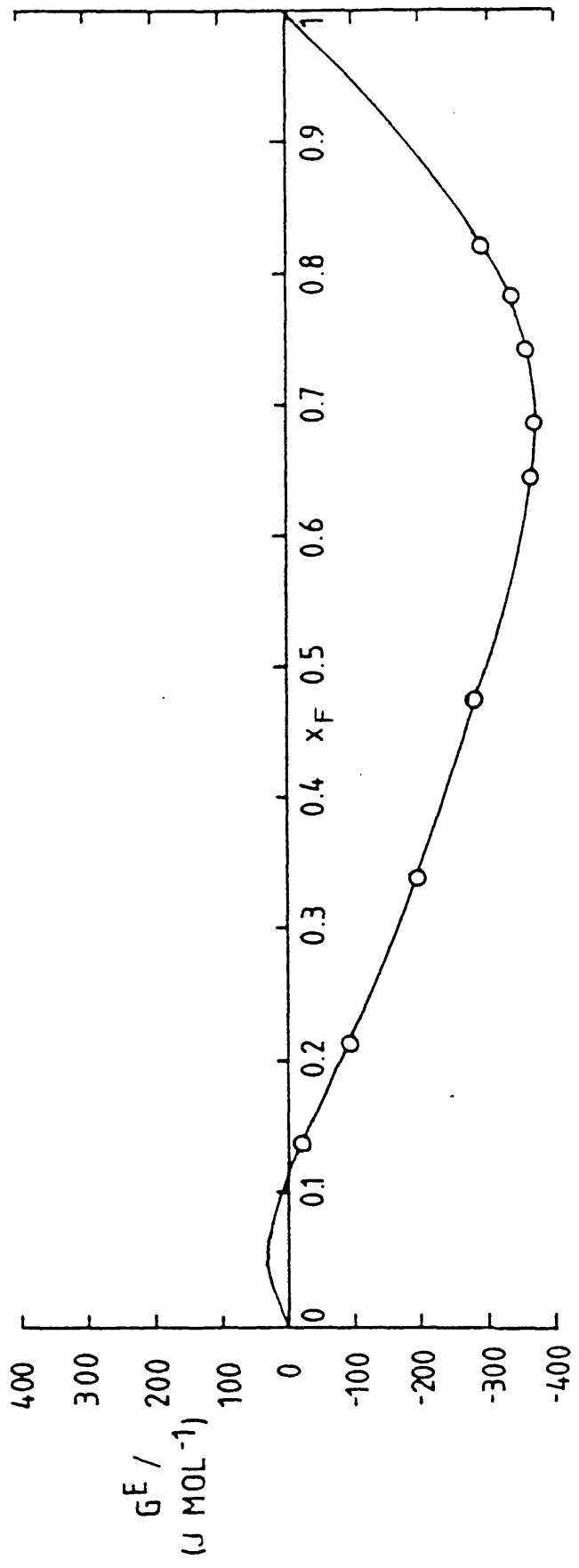


Figure (6.9.2)
Excess Gibbs Functions for
Hexafluorobenzene + quinoline 318.15 K

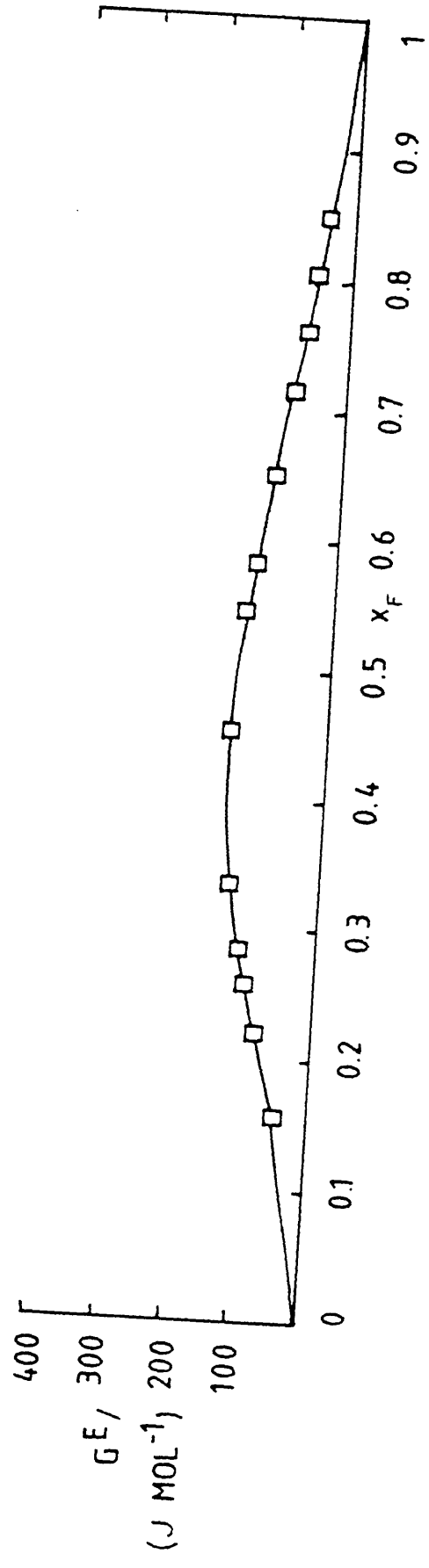


Figure (6.9.3)
Excess Gibbs function for
Hexafluorobenzene + tetralin 303.15 K

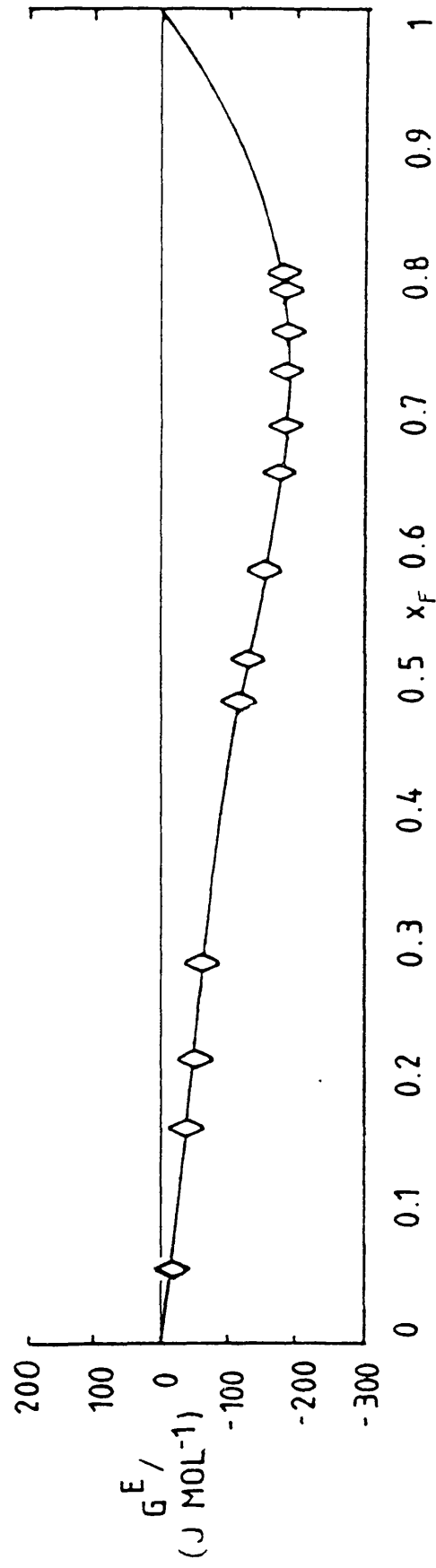


Figure (6.9.4)
Excess Gibbs functions for
Hexafluorobenzene + cis-decalin 303.15 K

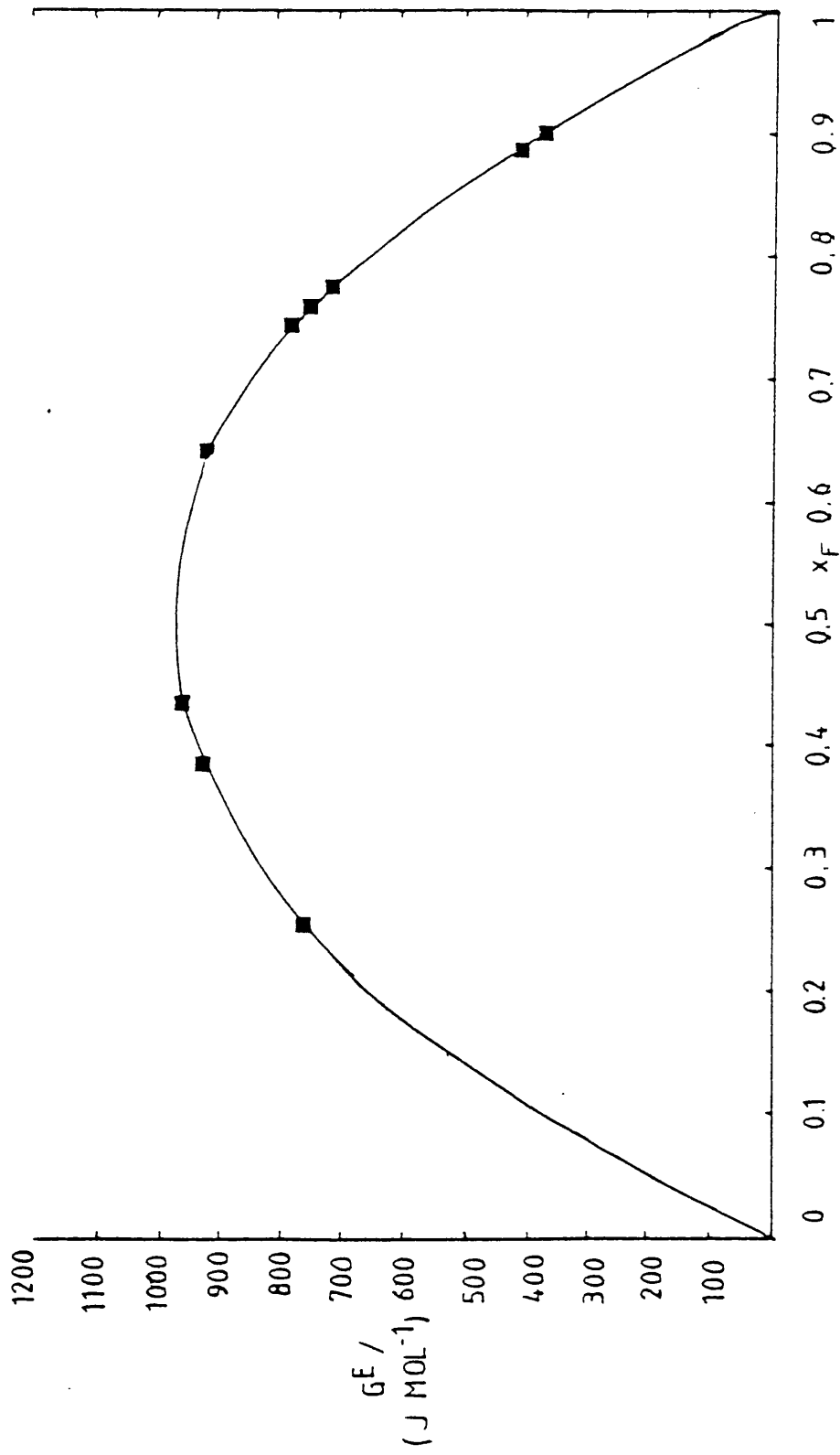


Figure (6.9.5)
Excess Gibbs functions for
Hexafluorobenzene + trans-decalin 303.15 K

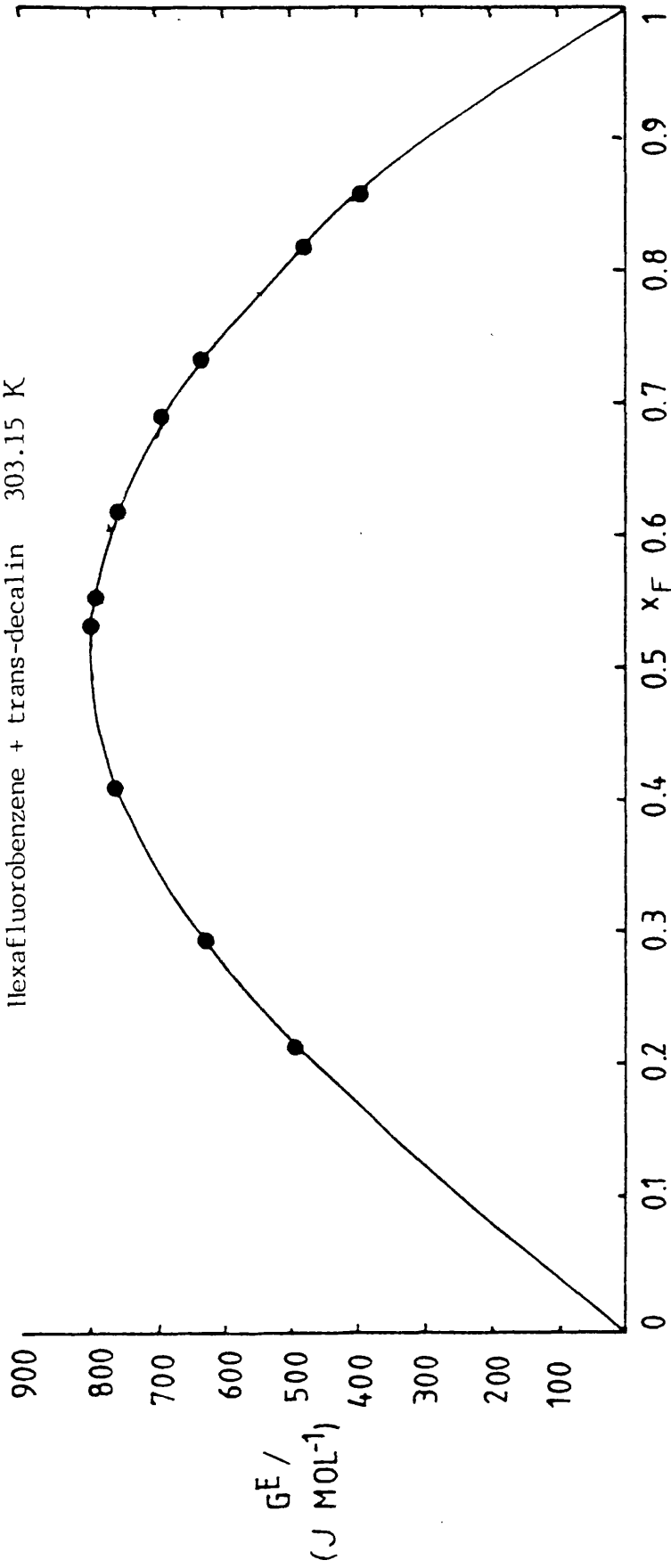


Figure (6.9.6)

Vapour pressure v. liquid and vapour mole fractions
Hexafluorobenzene + cis-decalin 303.15 K

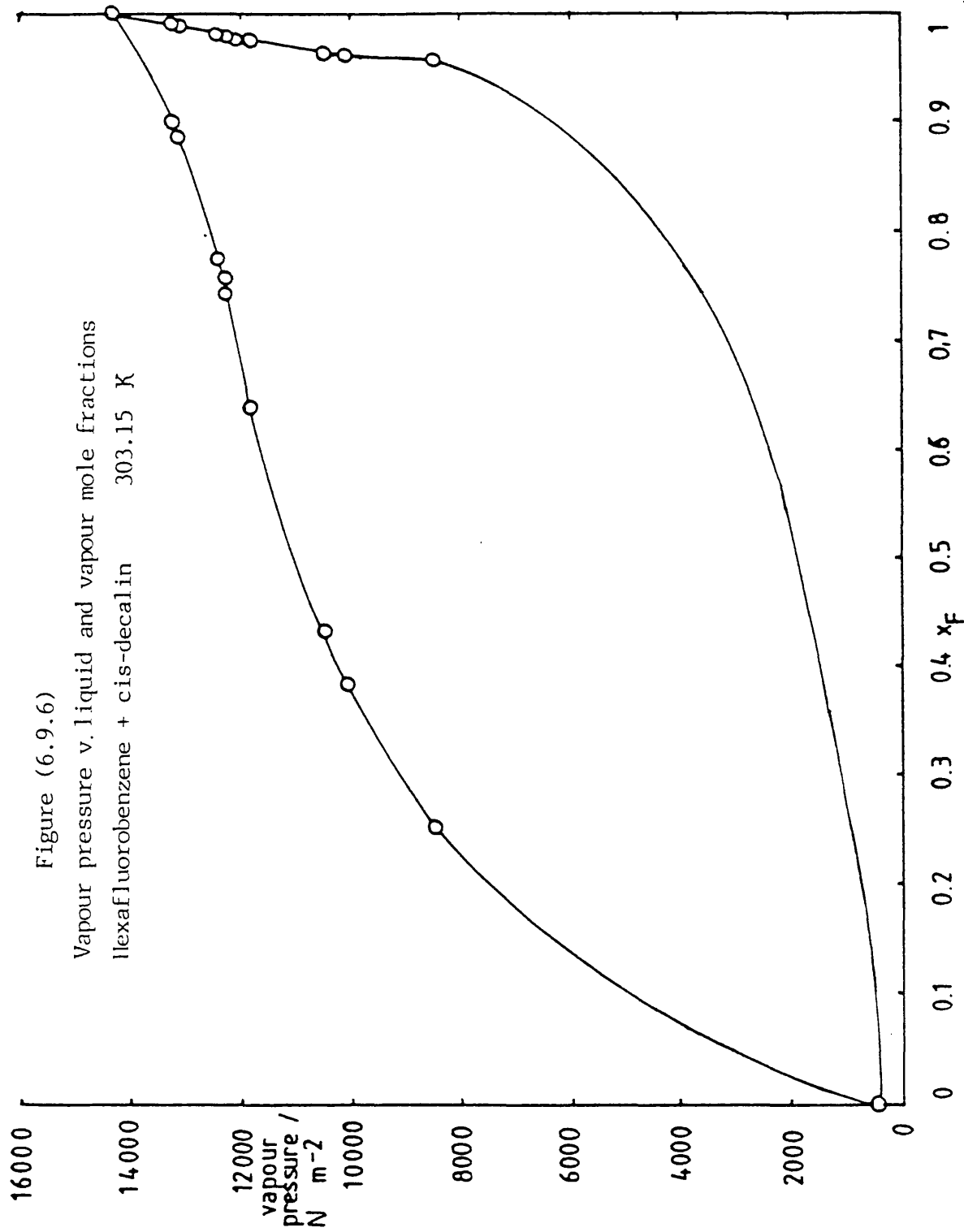


Figure (6.9.7)

Vapour pressure v. liquid and vapour mole fractions
Hexafluorobenzene + trans-decalin 303.15 K

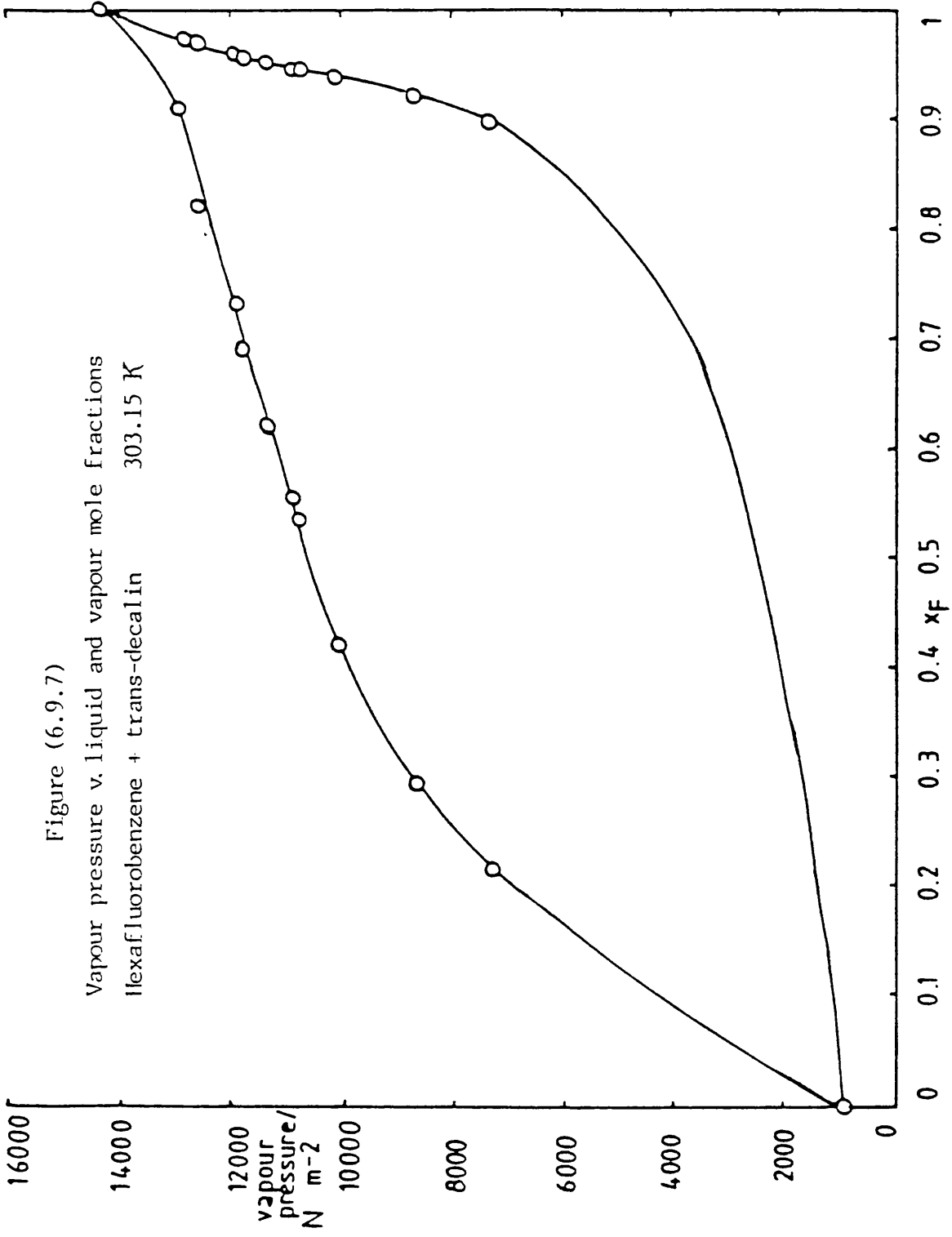


Figure (6.9.8)

Vapour pressure v. liquid and vapour mole fractions
Hexafluorobenzene + quinoline 318.15 K

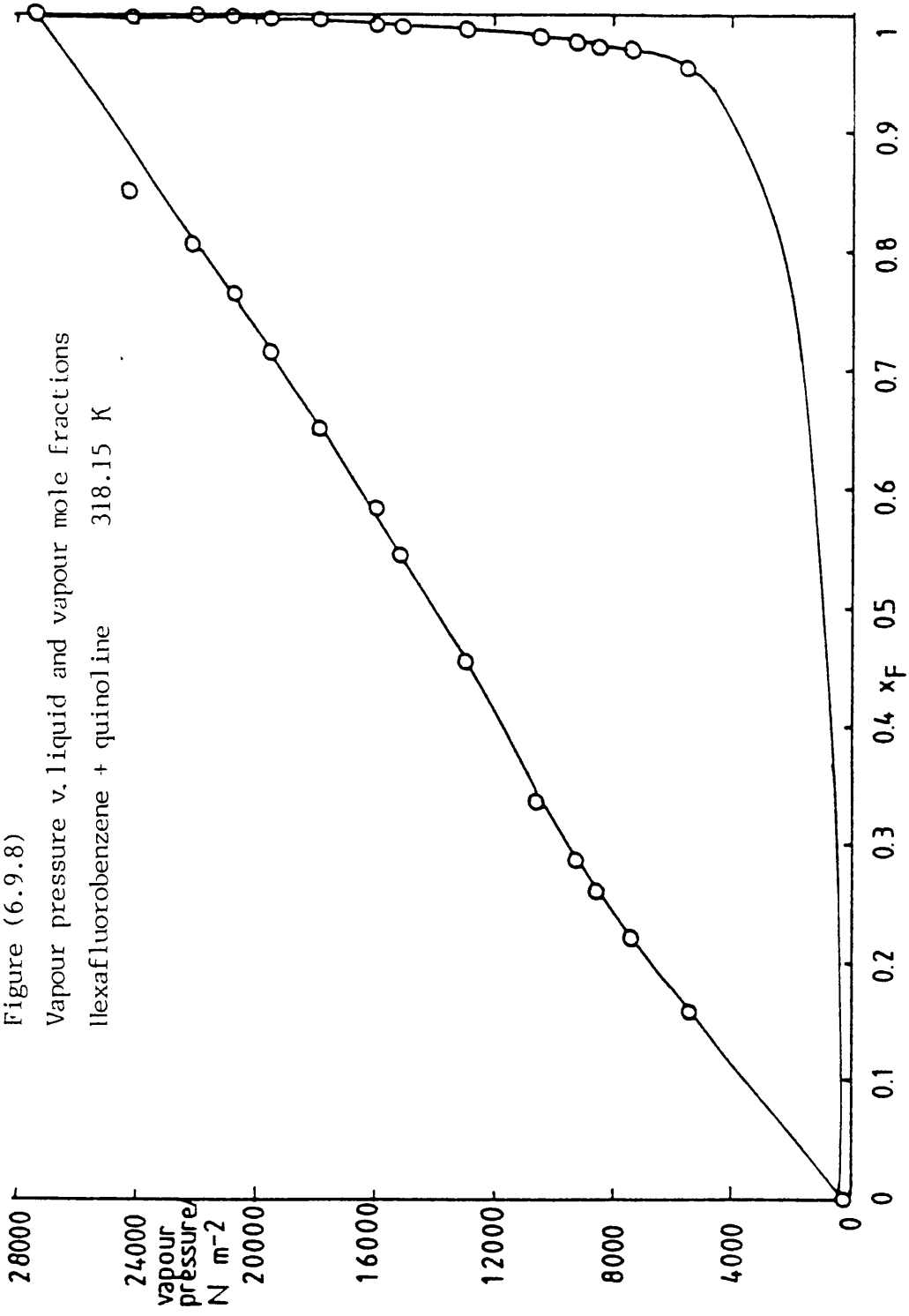


Figure (6.9.9)
Vapour pressure v. liquid and vapour mole fractions
hexafluorobenzene + tetralin
303.15 K

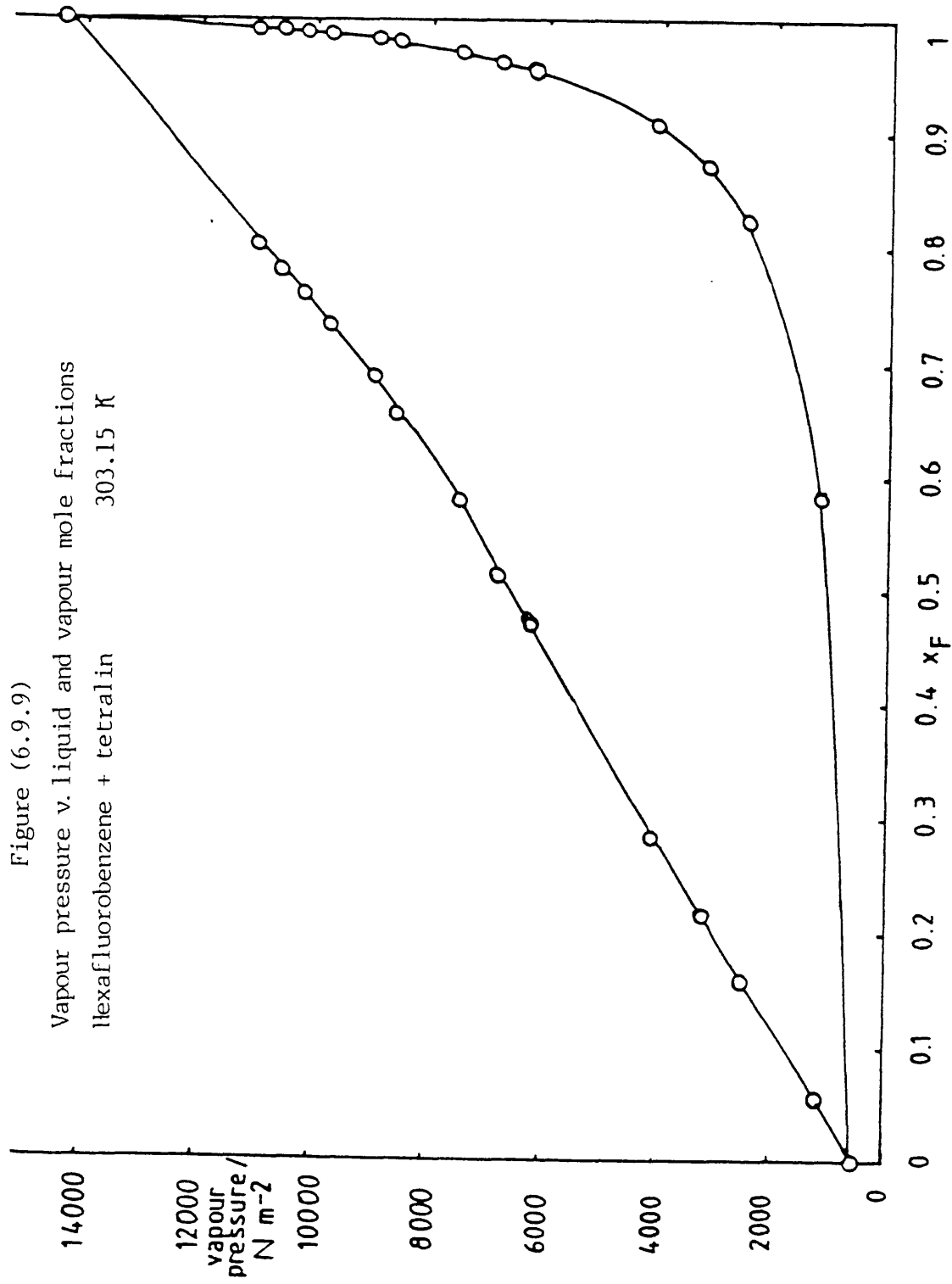


Figure (6.9.10)

Vapour pressure v. liquid and vapour mole fractions

Hexafluorobenzene + 2-methylnaphthalene 338.15 K

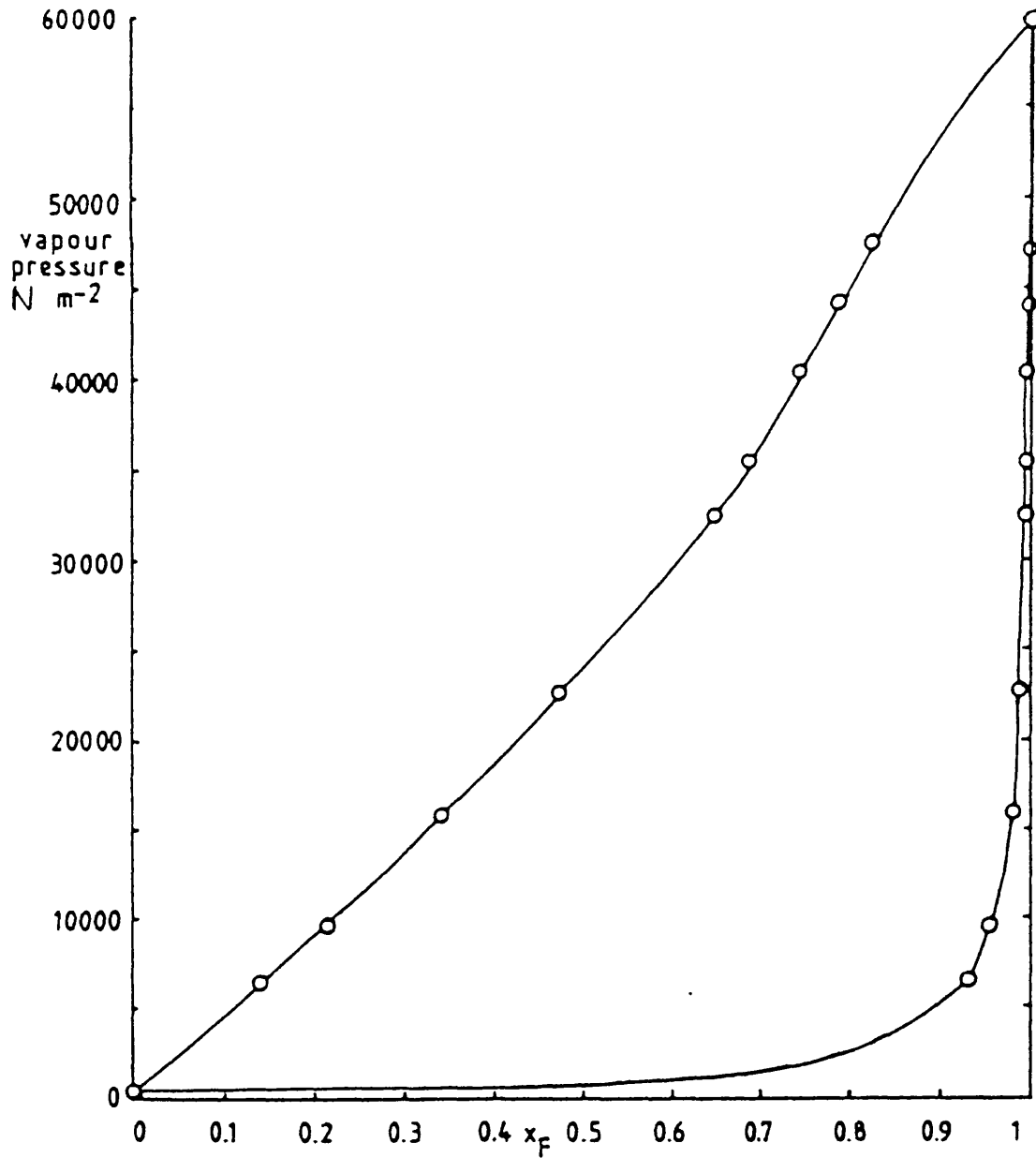


Table (6.11.1)

Excess Gibbs functions calculated from phase diagram data

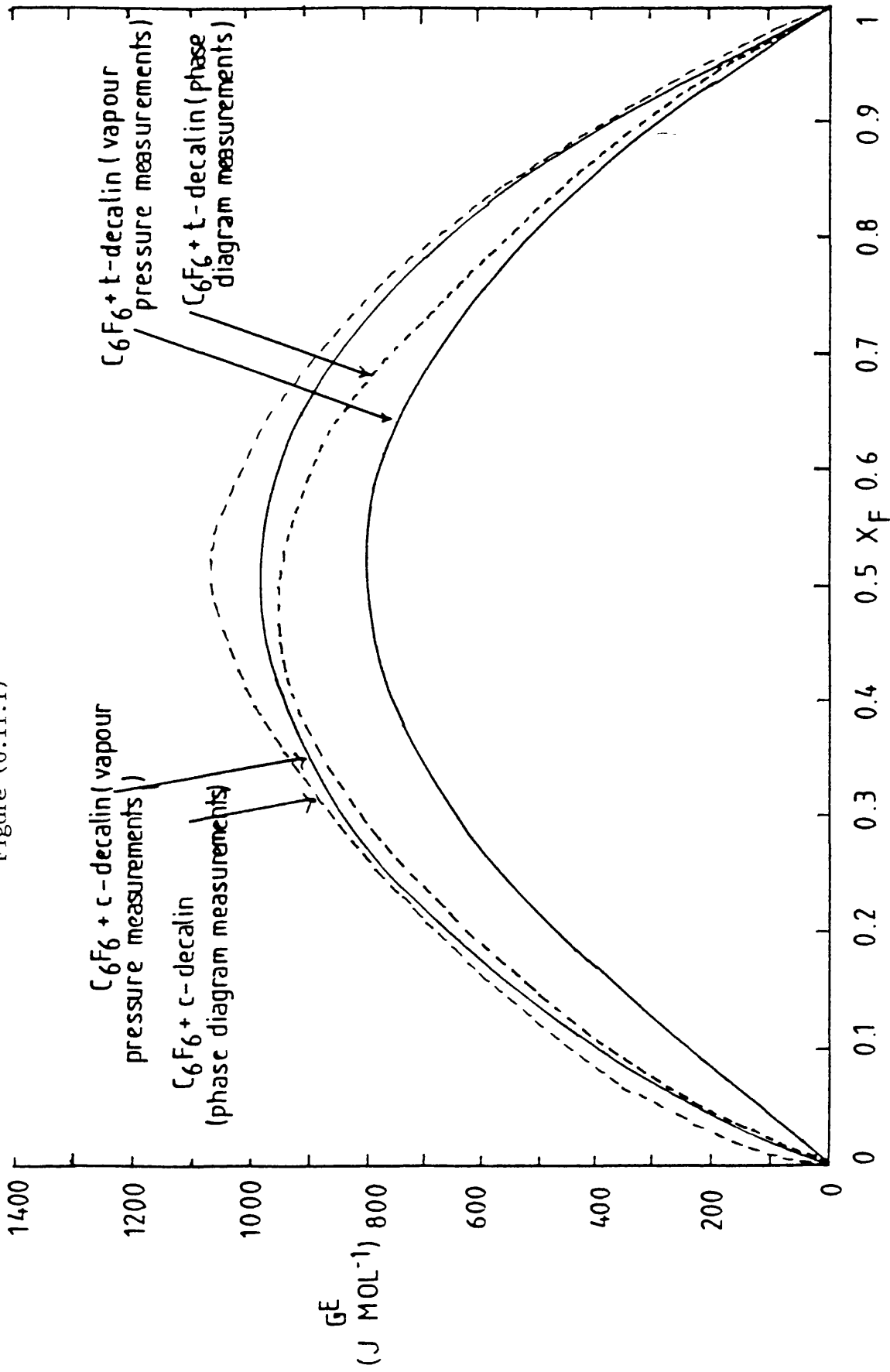
Hexafluorobenzene + cis-decalin:

$x_{\text{C}_6\text{F}_6}$	$\gamma_{\text{C}_6\text{F}_6}$	$\gamma_{\text{c-decalin}}$	$G^E/\text{J mol}^{-1}$
0.060	3.3624	1.0265	245
0.150	3.4230	1.0405	550
0.250	2.5590	1.0987	770
0.350	1.9971	1.2213	938
0.500	1.5190	1.5275	1061
0.650	1.2410	1.9845	958
0.750	1.1295	2.4160	786

Hexafluorobenzene + trans-decalin:

$x_{\text{C}_6\text{F}_6}$	$\gamma_{\text{C}_6\text{F}_6}$	$\gamma_{\text{t-decalin}}$	$G^E/\text{J mol}^{-1}$
0.097	3.2755	1.0353	369
0.150	2.8818	1.0527	510
0.250	2.2531	1.1203	726
0.400	1.6803	1.3037	924
0.500	1.4317	1.4659	934
0.535	1.3684	1.5486	936
0.650	1.2063	1.8156	833

Figure (6.11.1)



CHAPTER 7

DISCUSSION

7.1 Solid-liquid phase equilibria

In Chapter 3, it was shown that hexafluorobenzene forms congruently melting complexes with naphthalene and quinoline type compounds, all of the 1:1 molar ratio variety. Methylnaphthalenes in particular form very strong complexes with hexafluorobenzene, although the 1-methylnaphthalene complex melts about 35 K higher than the 2-methylnaphthalene complex. Dahl (28) stated that unlike pure solid hexafluorobenzene, where molecules occupy a perpendicular arrangement to each other (45, 88), in solid complexes of this type a parallel alternate layer arrangement exists. In any one layer of methylnaphthalene molecules (which has a parallel layer of interacting hexafluorobenzene molecules above and below) it can be seen that 1-methylnaphthalene molecules pack better amongst themselves than 2-methylnaphthalene molecules (figure 7.1.1).

If geometry is important in these complexes then replacing the 'C-Me' group of methylnaphthalenes by a nitrogen with a lone pair (which is comparable in size to a 'C-Me' group) should not affect the complex too much. Indeed, both quinoline and isoquinoline give congruently melting 1:1 complexes (see figures 3.5.3 and 3.5.4), although they appear to be not as strong. These systems can be compared with the two systems hexafluorobenzene + toluene, and hexafluorobenzene + pyridine, where the

Figure (7.1.1)
Packing in a layer of 1-methylnaphthalene
molecules

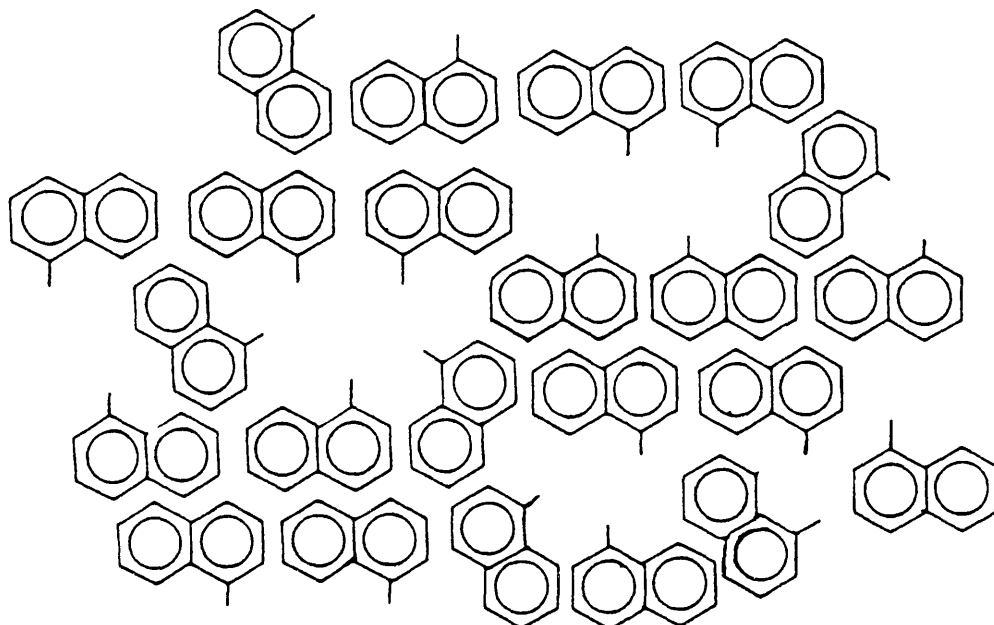
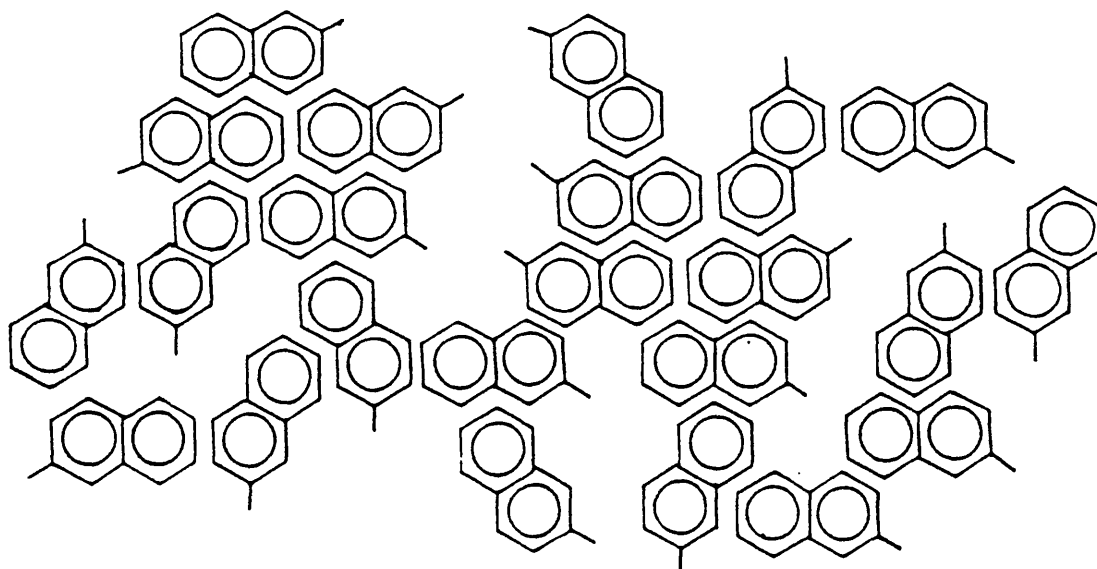


Figure (7.1.2)
Packing in a layer of 2-methylnaphthalene
molecules



former gives a congruent melting point complex (16), but the latter only an incongruently melting complex (32).

The complex hexafluorobenzene + 2-ethylnaphthalene also forms a congruently melting complex, but this is not as high melting as the 2-methylnaphthalene complex due to the increasing aliphatic character (figure 3.5.2).

The non-aromatic equivalent of benzene, cyclohexane, gave a eutectic diagram with hexafluorobenzene (16). Similarly, it was noted that the two alicyclic equivalents of naphthalene (cis-, and trans-decahydronaphthalene (decalin)) gave simple eutectic diagrams with hexafluorobenzene (figures 3.5.6 and 3.5.7).

1,2,3,4,-tetrahydronaphthalene (tetralin), possessing one aromatic and one alicyclic ring, is the intermediate of naphthalene and decalin. Despite the large proportion of alicyclic character, the phase diagram with hexafluorobenzene still boasts a congruently melting complex (figure 3.5.5). This finding is not so surprising though, if one notices that tetralin is much closer in shape to the planar naphthalene than to decalin. Also, tetralin can be thought of as a benzene molecule with its π -electron density increased by the inductive effect from the attached alicyclic ring.

The results obtained for pentafluorocyanobenzene (PFCB) + 1-, and + 2-methylnaphthalene give weight to the idea of π - π^* interactions existing in these complexes (see

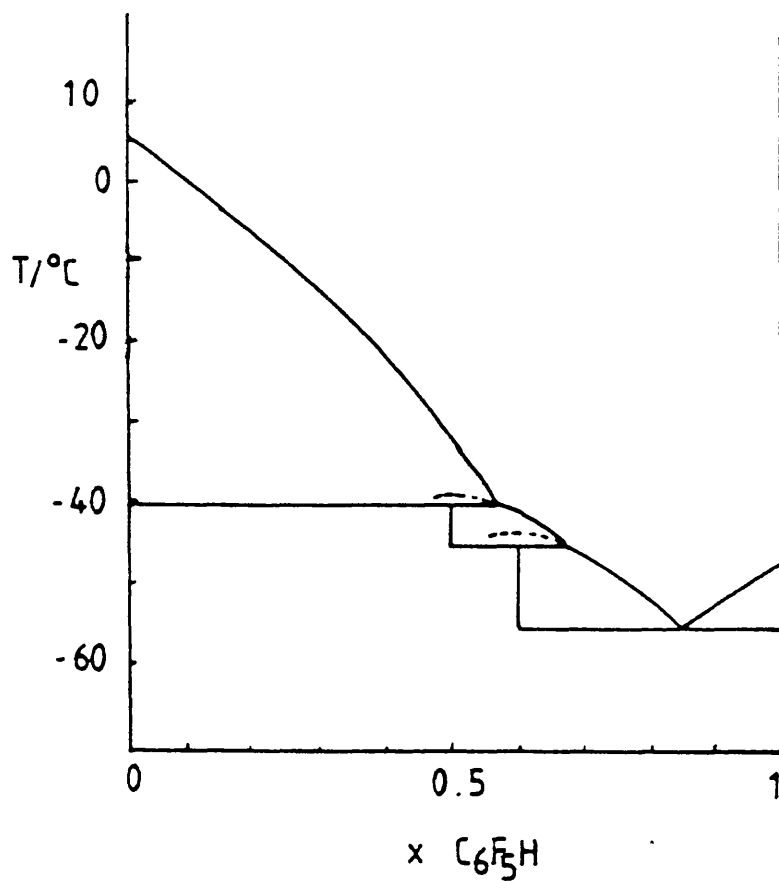
HOMO/LUMO interactions, Chapter 1). The cyanide group is a better electron acceptor and so PFCB should interact more strongly with the electron donating aromatic hydrocarbon. The results show that the melting point of the 1:1 complex is some 20 K higher in each case, than with hexafluorobenzene (figures 3.5.9 and 3.5.10).

Pentafluorobenzene + 2-methylnaphthalene gives a congruently melting complex, despite the large difference in melting temperatures (75 K) of the pure components (figure 3.5.11). This behaviour contrasts with that of pentafluorobenzene + benzene (19) which shows an incongruently melting complex and where the difference in melting points of the pure components is only 45 K (figure 7.1.3).

The phase diagram of hexafluorobenzene + 2,3-cyclohexenopyridine (2,3-CHP) is incomplete due to excessive supercooling, but it appears that a simple eutectic exists with no evidence of complex formation (figure 3.5.8). Similar difficulties prevented the determination of the PFCB rich region of the PFCB + 2-methylnaphthalene diagram (figure 3.5.10). (A freezing temperature apparatus incorporating a cooled metal rod to encourage freezing, such as the one used by Brindley et al.(76), may have overcome these problems).

Figure (7.1.3)
Solid liquid phase diagram
Pentafluorobenzene + benzene

Work of Duncan and Swinton.⁽¹⁹⁾



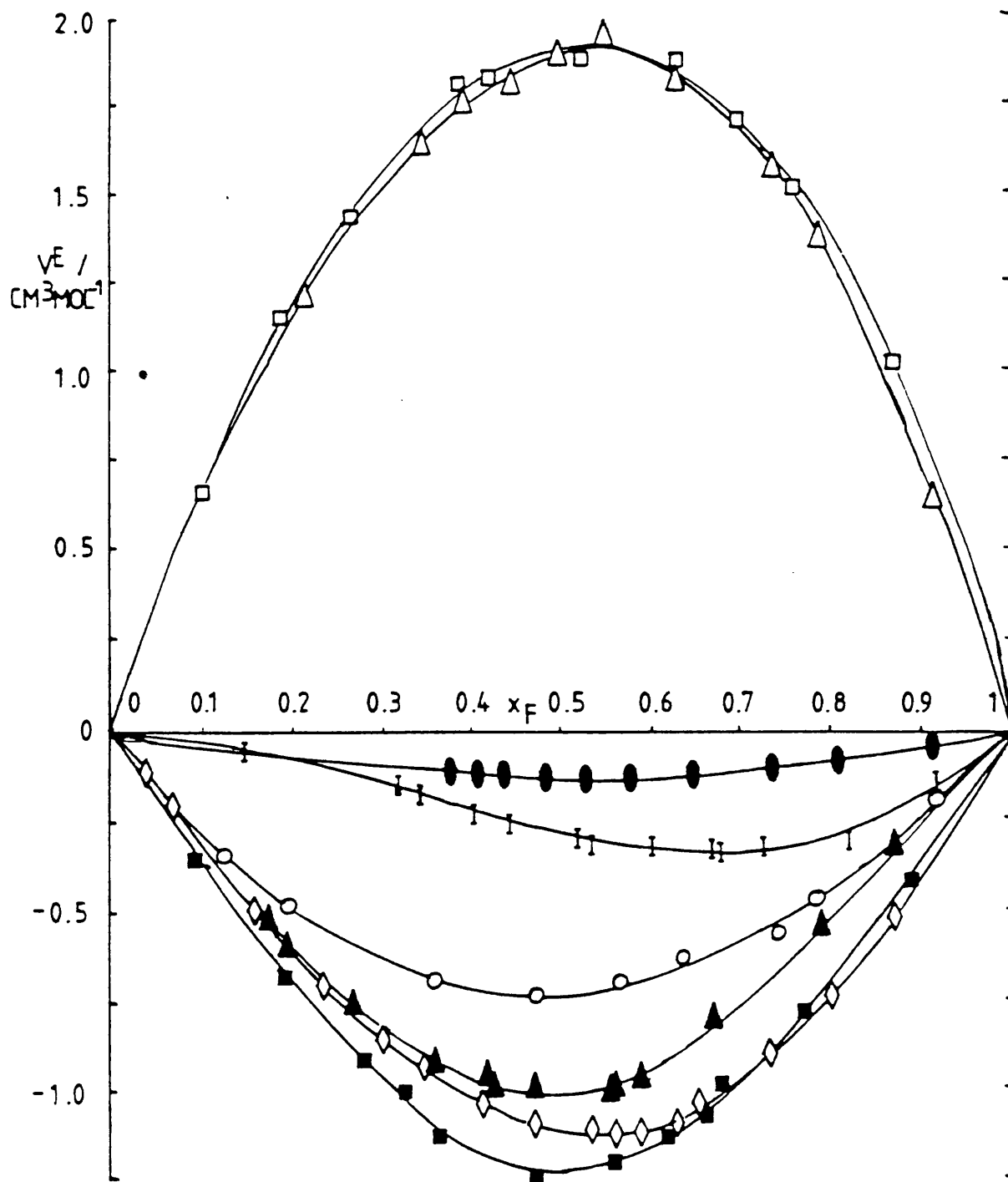
7.2 Excess volumes

Binary systems in which specific interactions occur are characterized by negative (or more precisely, more negative) excess volumes, v^E . The systems hexafluorobenzene + 2-methyl and + 2-ethylnaphthalene, + quinoline, + isoquinoline and + tetralin, all exhibit negative excess volumes of mixing (figure 7.2.1), with the most negative v^E being for the system hexafluorobenzene + 2-methylnaphthalene ($V = -1.25 \text{ cm}^3\text{mol}^{-1}$ at $x = 0.5$ and 338.15 K). The system hexafluorobenzene + 2,3-CHP also possesses negative excess volumes, despite there being no evidence of complex formation in the phase diagram.

Hexafluorobenzene + cis-, and + trans-decalin, where only dispersion forces are involved and the unlike interactions are particularly weak, give positive excess volumes (in each case, about $+1.9 \text{ cm}^3\text{mol}^{-1}$ at $x = 0.5$ and 303.15 K). This can be compared with the v^E of $2.56 \text{ cm}^3\text{mol}^{-1}$ ($x = 0.5$ and 313.2 K) for the hexafluorobenzene + cyclohexane system (17) (figure 7.2.2).

Cis-decalin (figure 7.2.3) approximates less to a planar molecule (like naphthalene) than trans-decalin (figure 7.2.4) and if packing in alicyclic hydrocarbons + aromatic fluorocarbon systems is like that in aromatic hydrocarbon + aromatic fluorocarbon systems, it might be anticipated that the excess volume for hexafluorobenzene + cis-decalin would be more positive. This is not the case.

Figure (7.2.1)
Excess volumes of mixing



KEY FOR FIGURE (7.2.1) [EXCESS VOLUMES]

- C_6F_6 + cis-decalin (303.15 K)
- △ C_6F_6 + trans-decalin (303.15 K)
- C_6F_6 + tetralin (303.15 K)
- ⌈ C_6F_6 + 2,3-cyclohexenopyridine (303.15 K)
- C_6F_6 + isoquinoline (303.15 K)
- ▲ C_6F_6 + 2-ethylnaphthalene (318.15 K)
- ◇ C_6F_6 + quinoline (318.15 K)
- C_6F_6 + 2-methylnaphthalene (338.15 K)

Figure (7.2.2)
Excess volumes of mixing (17)

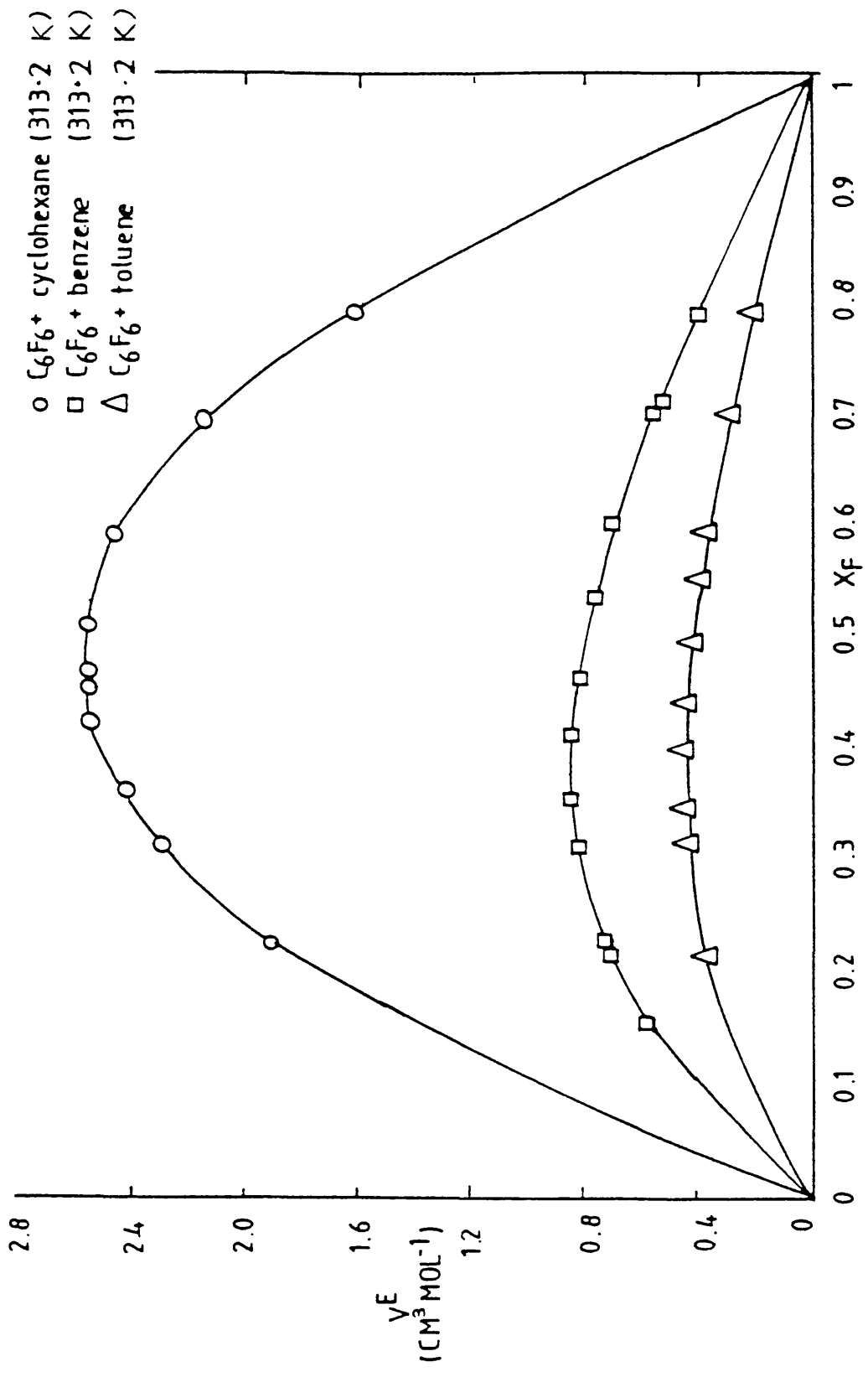
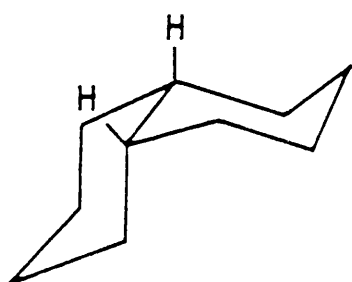
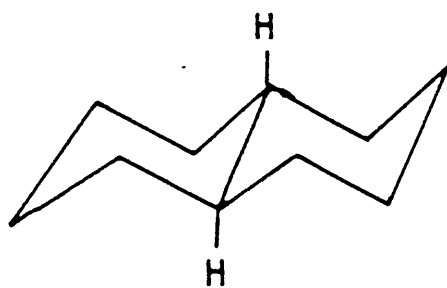


Figure (7.2.3)



Cis-decalin

Figure (7.2.4)



Trans-decalin

If it is assumed that tetralin is the intermediate of 2-methylnaphthalene and decalin (in the absence of excess volume data for hexafluorobenzene + naphthalene) one might speculate that the excess volume at $x = 0.5$ for hexafluorobenzene + tetralin would be about $0.3 \text{ cm}^3\text{mol}^{-1}$ (half way between -1.25 and $+1.9 \text{ cm}^3\text{mol}^{-1}$, the values at $x = 0.5$ for hexafluorobenzene + 2-methylnaphthalene, and + decalin respectively). In fact, hexafluorobenzene + tetralin gives negative volumes of mixing ($-0.125 \text{ cm}^3\text{mol}^{-1}$ at $x = 0.5$), which may point to the basic unit of two six-membered rings joined at two adjacent carbons (where at least one ring is aromatic) packing favourably with hexafluorobenzene. However, the value of V^E is not necessarily a reliable guide to the strength of intermolecular interactions; the partial molar volumes of components, for instance, affect V^E .

For each system, the excess volumes were measured at one temperature only. i.e. $(\partial V^E/\partial T)_p$ was not determined. The contribution to V^E from complex formation should decrease with an increase in temperature resulting in positive values of $(\partial V^E/\partial T)_p$ if complex formation occurs.

The systems hexafluorobenzene + decalin, + tetralin and + isoquinoline were studied at 303.15 K. If hexafluorobenzene + decalin is taken as the non-complexing equivalent of the other two systems (i.e. the V^E for hexafluorobenzene + decalin = V_p^E), then the contribution to the excess volume from complexing (V_c^E) for these two

systems can be calculated. (as $V^E = V_p^E + V_c^E$, see Chapter 1). This gives some indication of the strength of the two complexes. For hexafluorobenzene + isoquinoline, $V_c^E = -2.65 \text{ cm}^3\text{mol}^{-1}$ ($x = 0.5$, 303.15 K) and for hexafluorobenzene + tetralin, $V_c^E = -2.03 \text{ cm}^3\text{mol}^{-1}$ ($x = 0.5$, 303.15 K). If we assume V^E to be independent of temperature, then an estimate of V_c^E for hexafluorobenzene + 2-methylnaphthalene (for which V^E was measured at 338.15 K, not 303.15 K) can be made; $V_c^E = -3.12 \text{ cm}^3\text{mol}^{-1}$ ($x = 0.5$) indicating the complex to be stronger.

From the work of Duncan, Sheridan and Swinton (17) (whose volumes were measured at 313.15 K) and Barlatier et al. (77) (whose hexafluorobenzene + pyridine volumes were recorded at 303.15 K), an estimate of V_c^E for hexafluorobenzene + benzene, + toluene and + pyridine can be made assuming that hexafluorobenzene + cyclohexane is the non-complexing equivalent of each system. V_c^E for hexafluorobenzene + benzene = $-1.76 \text{ cm}^3\text{mol}^{-1}$ ($x = 0.5$), but by introducing the methyl group onto the benzene V_c^E decreases to $-2.15 \text{ cm}^3\text{mol}^{-1}$ ($x = 0.5$) which is similar to the V_c^E for hexafluorobenzene + tetralin.

It is also of interest to compare the above behaviour with that of hexafluorobenzene and the 'n' donor, N,N, - dimethylaniline (DMA). DMA mixes with hexafluorobenzene to give a V^E of $-0.48 \text{ cm}^3\text{mol}^{-1}$ at $x = 0.5$ and 323.15 K (85). Taking hexafluorobenzene + isopropyl-cyclohexane (IPCH) as the non-complexing equivalent system ($V^E = 2.1 \text{ cm}^3\text{mol}^{-1}$ at $x = 0.5$ and

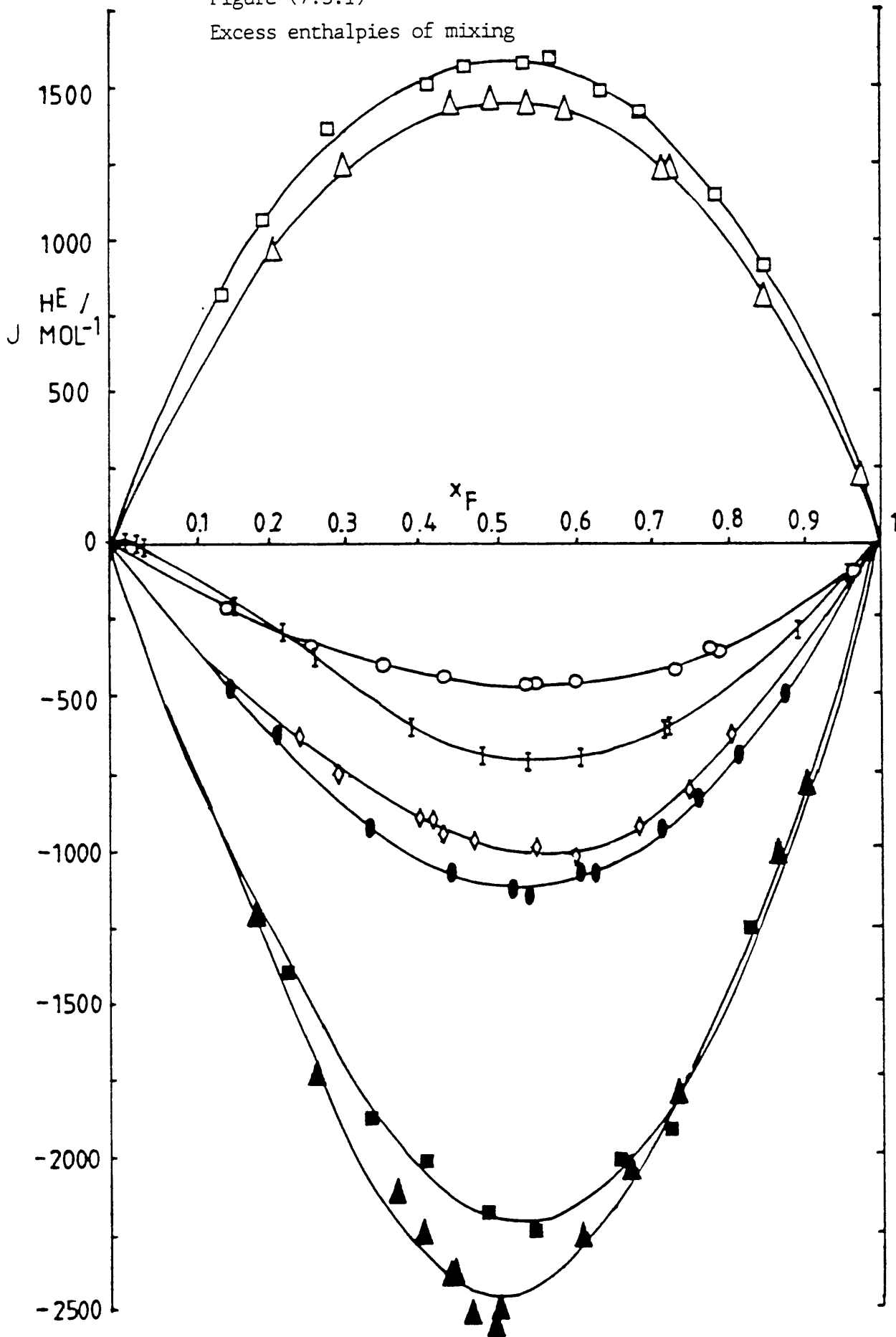
T = 323.15 K) means V_C^E for hexafluorobenzene + DMA is $-2.58 \text{ cm}^3\text{mol}^{-1}$.

Some excess volume measurements at 348.15 K were attempted on the hexafluorobenzene + 1-methylnaphthalene system in the liquid region (i.e. $x = 0 - 0.15$, and $x = 0.85 - 1$) in order to estimate the V^E plot. Although always negative, the values obtained were too scattered to enable even an indication of V^E at $x = 0.5$ to be made.

7.3 Excess enthalpies

A similar trend to that found with excess volumes emerges with excess enthalpies. Mixtures of hexafluorobenzene + substituted naphthalenes, + quinoline, + isoquinoline and + tetralin all give negative excess enthalpies over the whole composition range (figure 7.3.1), which is again indicative of strong specific interactions. The tetralin system shows surprisingly exothermic behaviour ($H^E = -1125 \text{ J mol}^{-1}$ at $x = 0.5$ and 303.15 K) and is more exothermic than the quinoline system in contrast to the excess volumes. The most negative excess enthalpy at $x = 0.5$ is obtained with hexafluorobenzene + 2-ethylnaphthalene (-2450 J mol^{-1} at 318.15 K); it is surprising at first that this system should be more exothermic than the hexafluorobenzene + 2-methylnaphthalene system (-2200 J mol^{-1} at $x = 0.5$, 338.15 K) despite the longer side chain. However, the ethyl group has a larger inductive effect than the methyl group. Both systems though are substantially more

Figure (7.3.1)
Excess enthalpies of mixing



KEY FOR FIGURE (7.3.1) [EXCESS ENTHALPIES]

- C_6F_6 + cis-decalin (303.15 K)
- △ C_6F_6 + trans-decalin (303.15 K)
- C_6F_6 + isoquinoline (313.15 K)
- I C_6F_6 + 2,3-cyclohexenopyridine (303.15 K)
- ◇ C_6F_6 + quinoline (318.15 K)
- C_6F_6 + tetralin (303.15 K)
- C_6F_6 + 2-methylnaphthalene (338.15 K)
- ▲ C_6F_6 + 2-ethylnaphthalene (318.15 K)

negative than hexafluorobenzene + benzene and + toluene (19) (see figure 7.3.2) where $H^E = -426$, and -1151 J mol^{-1} respectively, (at $x = 0.5$, and 303.15 K). Although quinoline and isoquinoline show exothermic heats of mixing with hexafluorobenzene (figure 7.3.1), pyridine, when mixed with hexafluorobenzene gives an H^E of $+330 \text{ J mol}^{-1}$ (13), ($x = 0.5$, 298.15 K).

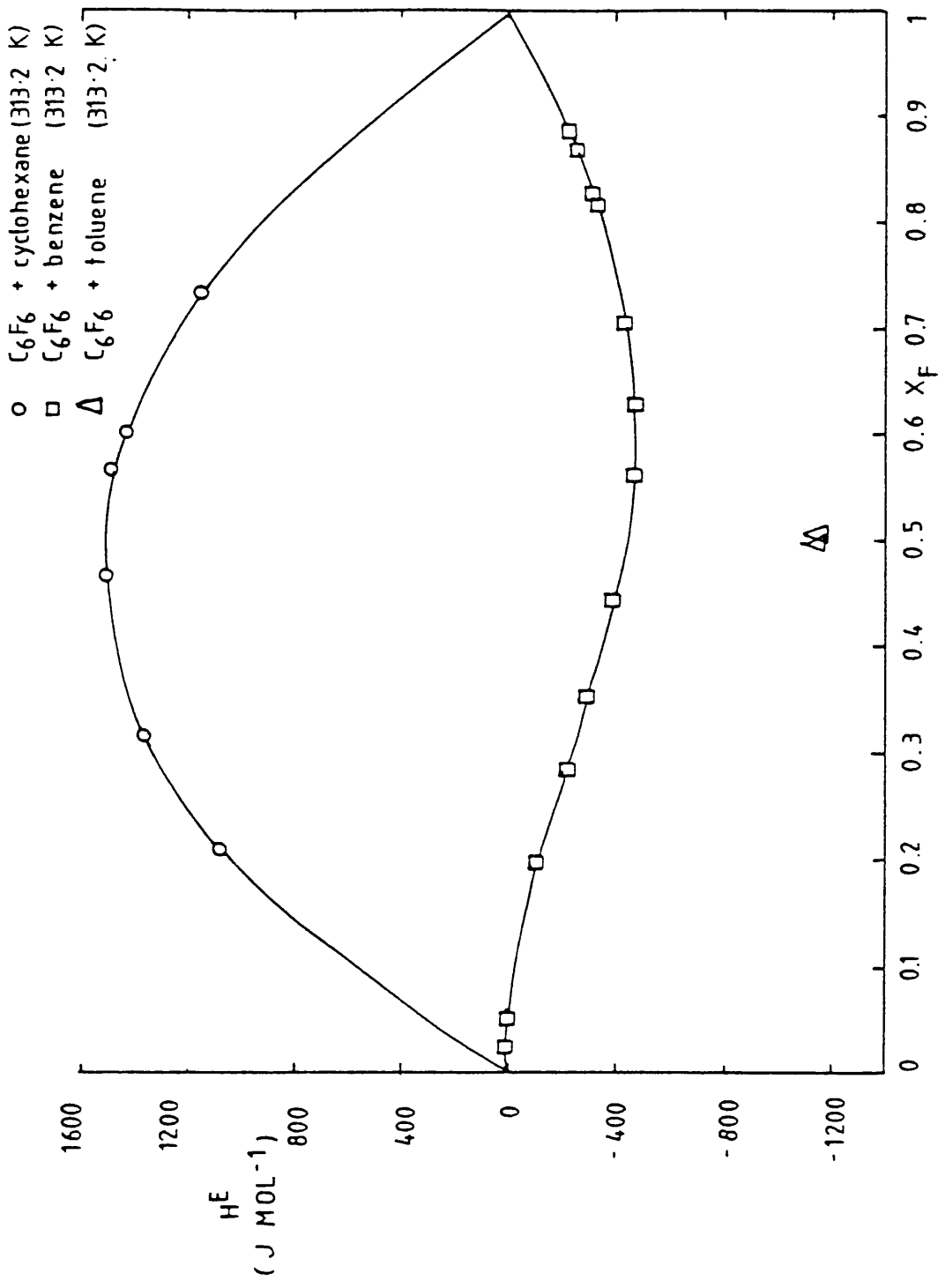
Cis- and trans-decalin again give large positive deviations from ideality when mixed with hexafluorobenzene (figure 7.3.1). This can be compared with hexafluorobenzene + cyclohexane, where $H^E = 1580 \text{ J mol}^{-1}$ at $x = 0.5$ and 303.15 K (figure 7.3.2).

The system hexafluorobenzene + 2,3-CHP shows negative excess enthalpies except at very low hexafluorobenzene mole fractions (figure 7.3.1).

The excess enthalpies for hexafluorobenzene + 1-methylnaphthalene (measured at 348.15 K and so only determined in the liquid mole fraction regions $x = 0 - 0.15$, and $x = 0.85 - 1$) indicate that the H^E at $x = 0.5$ would be in the same area as that of hexafluorobenzene + 2-methylnaphthalene which was measured at 338.15 K .

The excess heat capacity, C_p^E , ($= (\partial H^E / \partial T)_p$) was only determined for hexafluorobenzene + isoquinoline, for which the excess enthalpies were measured at two temperatures (303.15 K and 313.15 K). The value of $+5 \text{ J K}^{-1} \text{ mol}^{-1}$ is

Figure(7.3.2) Excess enthalpies (work of Andrews, Morcom, Duncan, Swinton & Pollock) (8)



evidence for complexing, as a higher temperature means a weakening of any specific interactions, leading to a more positive enthalpy change and a positive value of C_p^E .

As for excess volumes, it is possible to estimate the contribution to the excess enthalpy due to specific complexing interactions (H_c^E). Trans-decalin is taken as the non-complexing equivalent of the complexing aromatic series as it approximates better to the planar aromatic naphthalene molecule. H_c^E gives an idea of the strength of the complex and here indicates that hexafluorobenzene + tetralin ($H_c^E = -2558 \text{ J mol}^{-1}$, $x = 0.5$, 303.15 K) complexes more strongly than hexafluorobenzene + isoquinoline ($H_c^E = -1948 \text{ J mol}^{-1}$, $x = 0.5$, 303.15 K). The value for hexafluorobenzene + tetralin is comparable with that for hexafluorobenzene + toluene ($H_c^E = -2731 \text{ J mol}^{-1}$, $x = 0.5$, 303.15 K), but the H_c^E for hexafluorobenzene + isoquinoline is more negative (i.e. shows a greater contribution to H^E from chemical interactions) than the hexafluorobenzene + pyridine system ($H_c^E = -1250 \text{ J mol}^{-1}$, $x = 0.5$, 303.15 K). Again, if dependence on temperature is not considered too important and is ignored, H_c^E for hexafluorobenzene + 2-methylnaphthalene can be estimated; the value of -3345 J mol^{-1} , ($x = 0.5$) indicates a much stronger complex.

Armitage (13,78) measured the excess enthalpies for the systems hexafluorobenzene + DMA and + IPCH. From these data, an H_c^E value for hexafluorobenzene + DMA of -3040 J mol^{-1} ($x = 0.5$) was calculated.

7.4 Enthalpies of solution

As mentioned previously, the enthalpy change for the process



was measured calorimetrically (Chapter 5) and compared with calculated values (where the enthalpy change for liquid A + liquid B giving a solid complex was calculated from solid / liquid phase diagram data. A knowledge of the relevant enthalpies of fusion allowed the enthalpy change for equation (7.4.1) to be found). The theoretical basis of the treatment of Goates (69) is outlined in Chapter 5, section 10.

Only the systems hexafluorobenzene + 2-methylnaphthalene and + quinoline were considered by both methods and the agreement was not good (Table 7.4.1).

In the Goates, Ott and Reeder method used to determine the enthalpy change for liquid + liquid giving a solid complex, freezing points on both sides of the phase diagram were used by them and an accuracy of ± 0.03 K was claimed (except on steep parts of the curve, where the accuracy fell to ± 0.1 K). The phase diagrams reported in this thesis are very steep, due to the strong nature of the complexes, and so the accuracy of Goates et al. cannot be attained; as a result, points on the plots of $\Delta H'$

Table (7.4.1)

A comparison of $\Delta H(\text{Solid Complex})$ determined from calorimeter measurements, and from the calculation of Goates et al. (69)

System	$\Delta H (1+1 \rightarrow s)$ (Goates treatment) /kJ mol ⁻¹	$\Delta H(\text{Solid Complex})$ (Goates treatment) /kJ mol ⁻¹	$\Delta H(\text{Solid Complex})$ (Calorimeter) /kJ mol ⁻¹
Hexafluorobenzene			
+ 2-'Me'naphthalene	-20 ± 3	+4.6 ± 3	-5.2 ± 0.5
Hexafluorobenzene			
+ quinoline	-31 ± 1	-8.0 ± 1	+3.8 ± 0.3
Hexafluorobenzene			
+ 1-'Me'naphthalene	-30 ± 1	-9.5 ± 1	
Hexafluorobenzene			
+ naphthalene	-27 ± 1	+3.6 ± 1	
Hexafluorobenzene			
+ benzene	-18 ± 1.5	+3.3 ± 1.5	+1.0 ± 0.3

against $(T^\dagger - T)$ (see Chapter 5, section 10) were scattered, and extrapolations to $T^\dagger - T = 0$ (which determines the enthalpy change) very inaccurate. (figures 7.4.1, .2, .3, .4 and .5). In addition, Goates' assumption that the plot of $\Delta H' \text{ v } (T^\dagger - T)$ is linear may be unjustified. Furthermore, solid solution regions may exist (figure 7.4.6), which would invalidate the basic treatment of Goates et al. An additional minor contribution to the large discrepancy between calorimetry and calculated values is the fact that although the Goates calculated values are for temperature T^\dagger (melting point of the 1:1 complex), our calorimetric measurements are made necessarily at a temperature below this (see Chapter 5, section 8).

The value of ΔH for liquid + liquid \rightarrow solid complex (calculated from phase diagram data) and the resultant ΔH (solid complex) are given in table (7.4.1) for the systems hexafluorobenzene + 1-methyl and + 2-methylnaphthalene, + naphthalene, + quinoline and + benzene; in the case of hexafluorobenzene + naphthalene, since McLaughlin and Messer gave no data with their phase diagram (39), freezing temperatures on one side of the diagram only were redetermined in this laboratory (figure 3.5.12).

Brennan and Swinton (79) used a scanning calorimeter to show that the enthalpy change associated with equation (7.4.1) for hexafluorobenzene + benzene was $1.0 \pm 0.3 \text{ kJ mol}^{-1}$. (i.e. small and positive, which was proposed as evidence for stabilization by geometrical packing effects enhanced by weak electrostatic forces). From the phase

Figure (7.4.1)

Hexafluorobenzene + 2-Methylnaphthalene

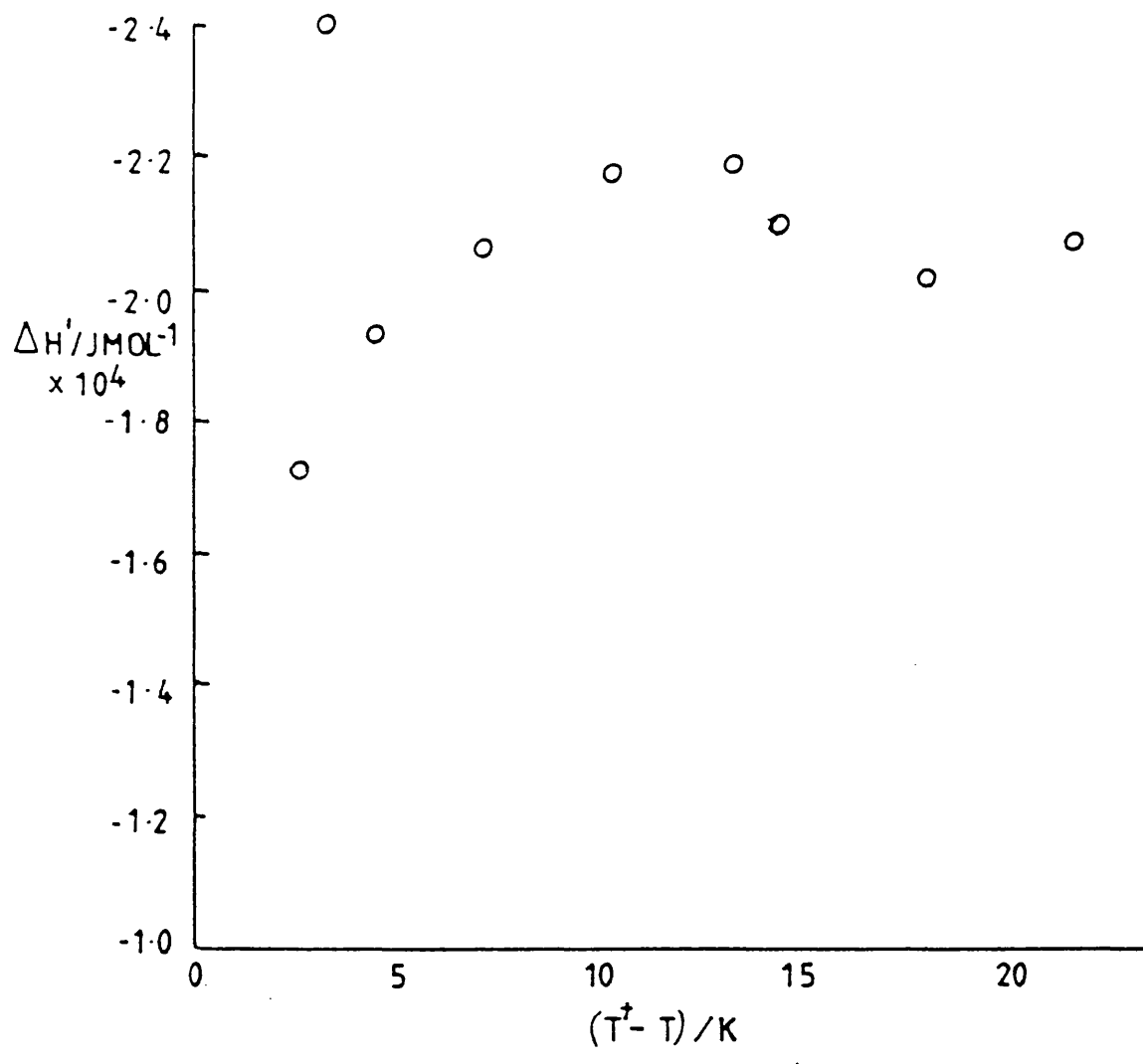


Figure (7.4.2)

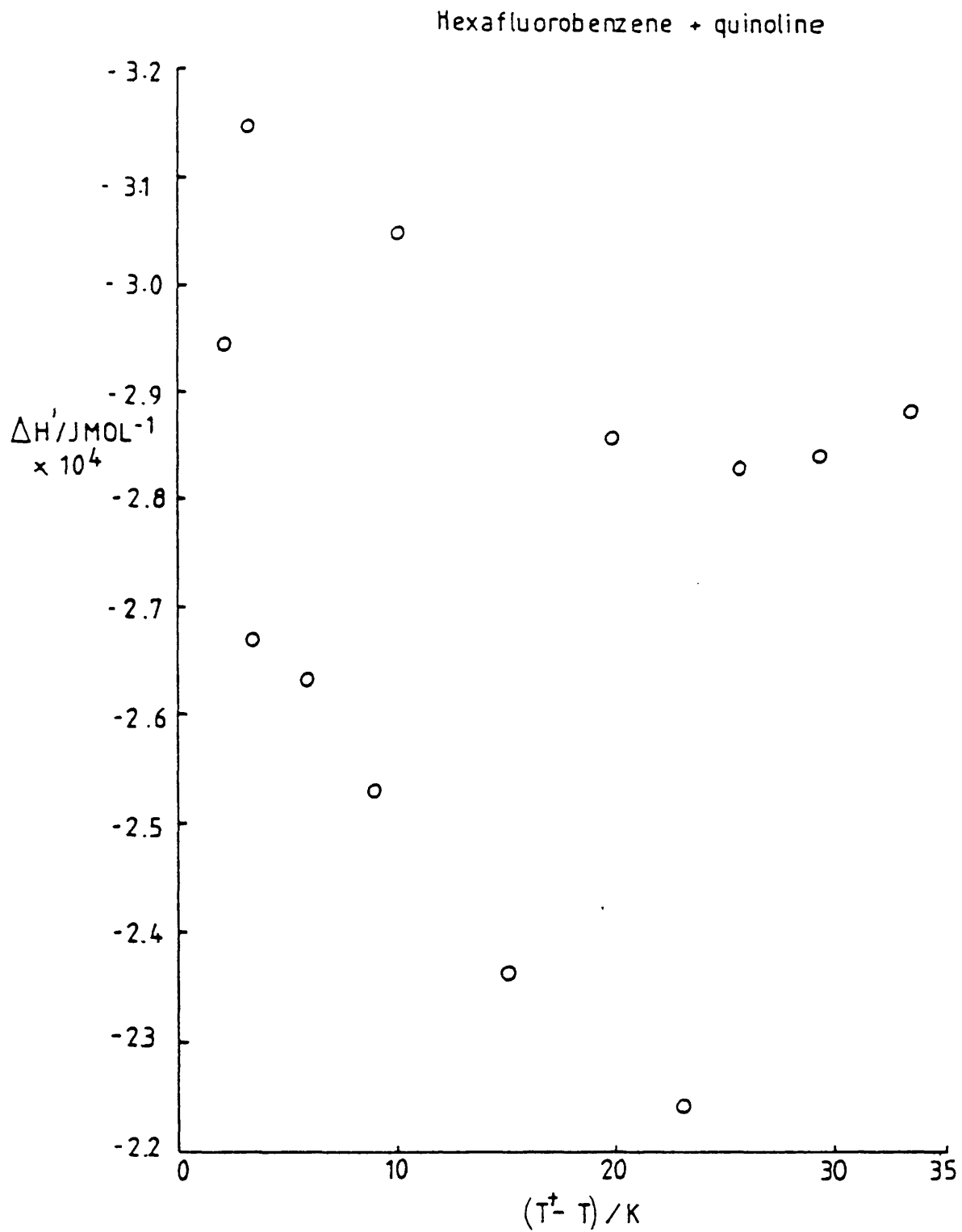


Figure (7.4.3)

Hexafluorobenzene + 1-Methylnaphthalene

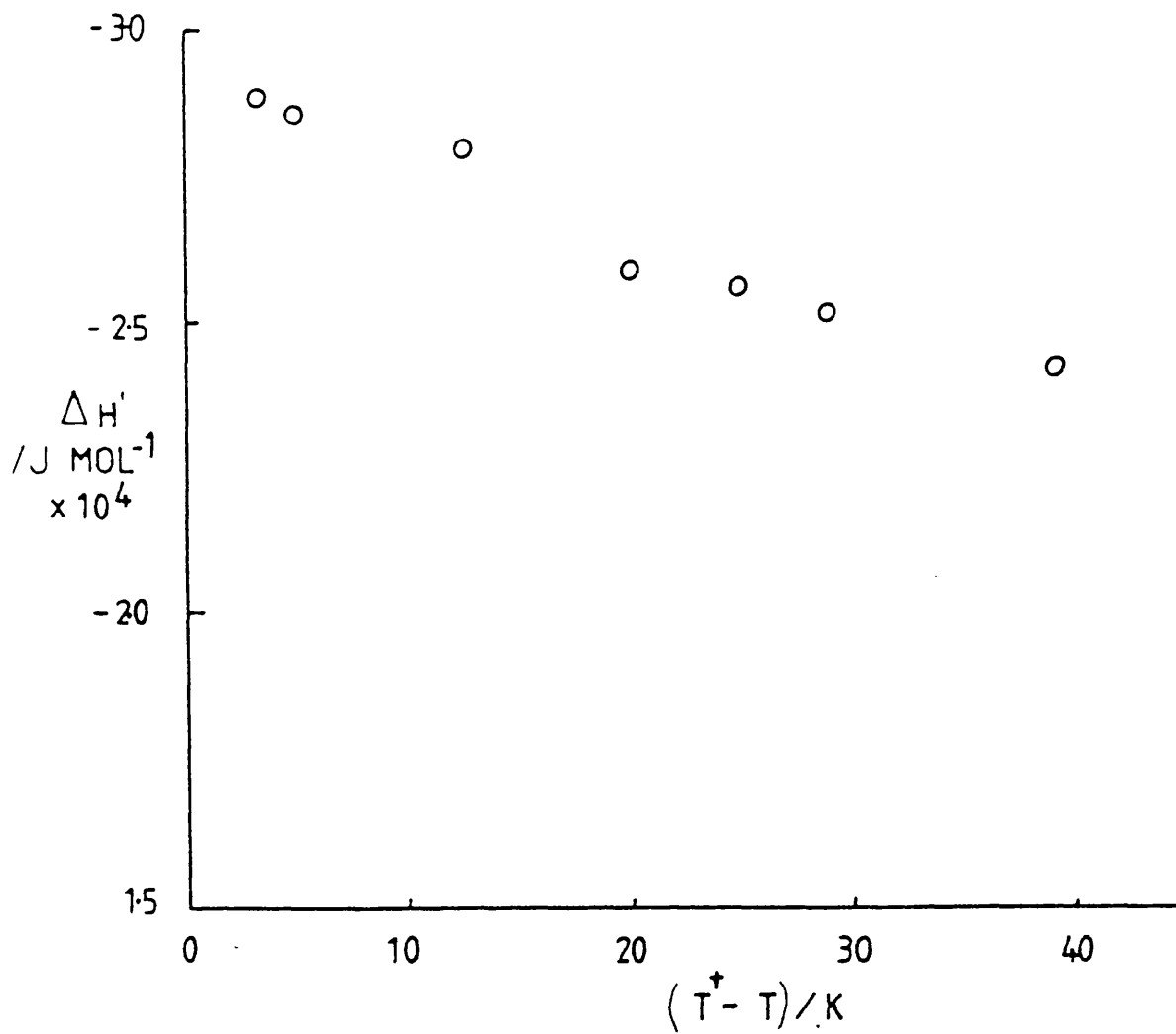


Figure (7.4.4)

Hexafluorobenzene + naphthalene

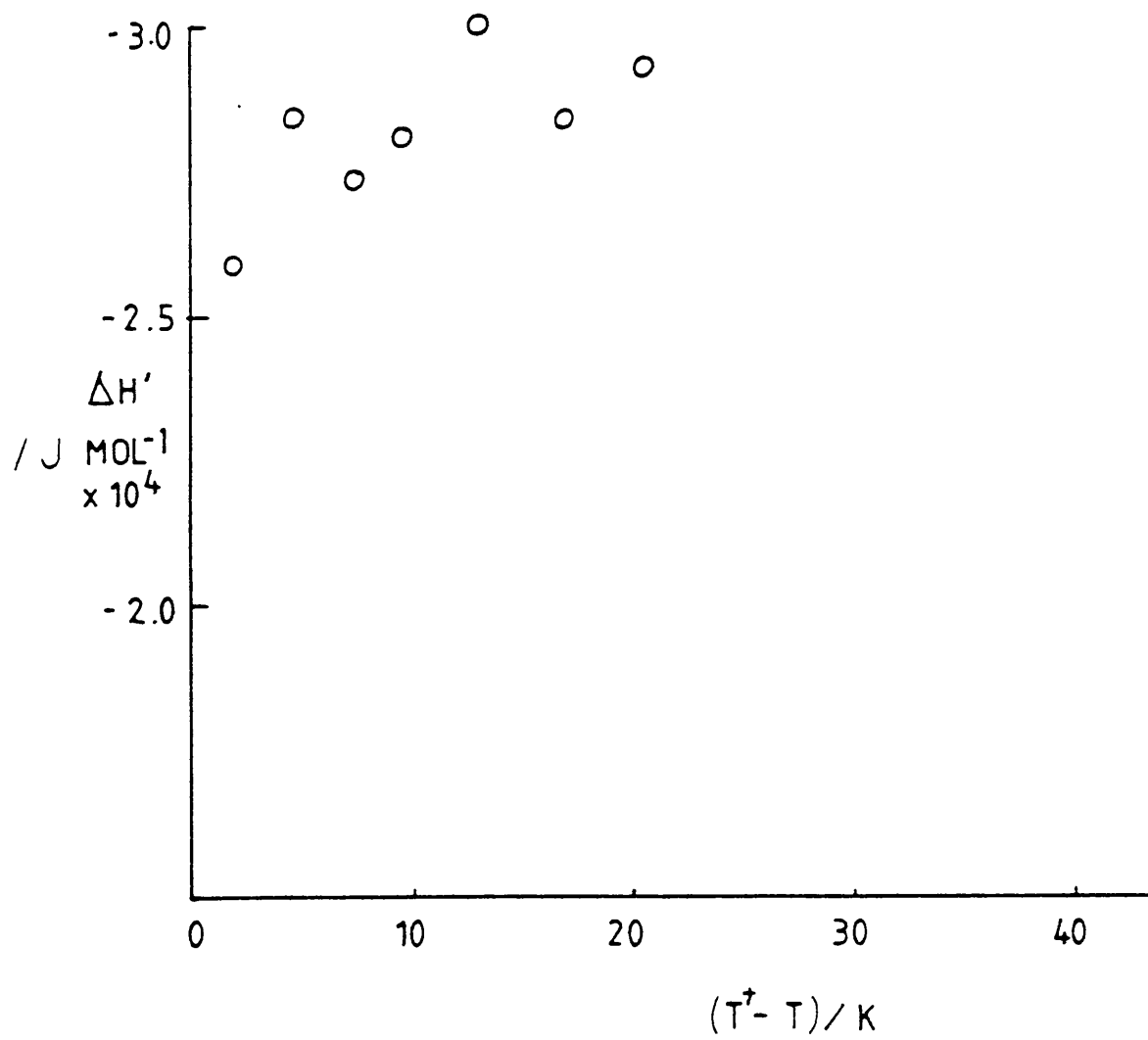
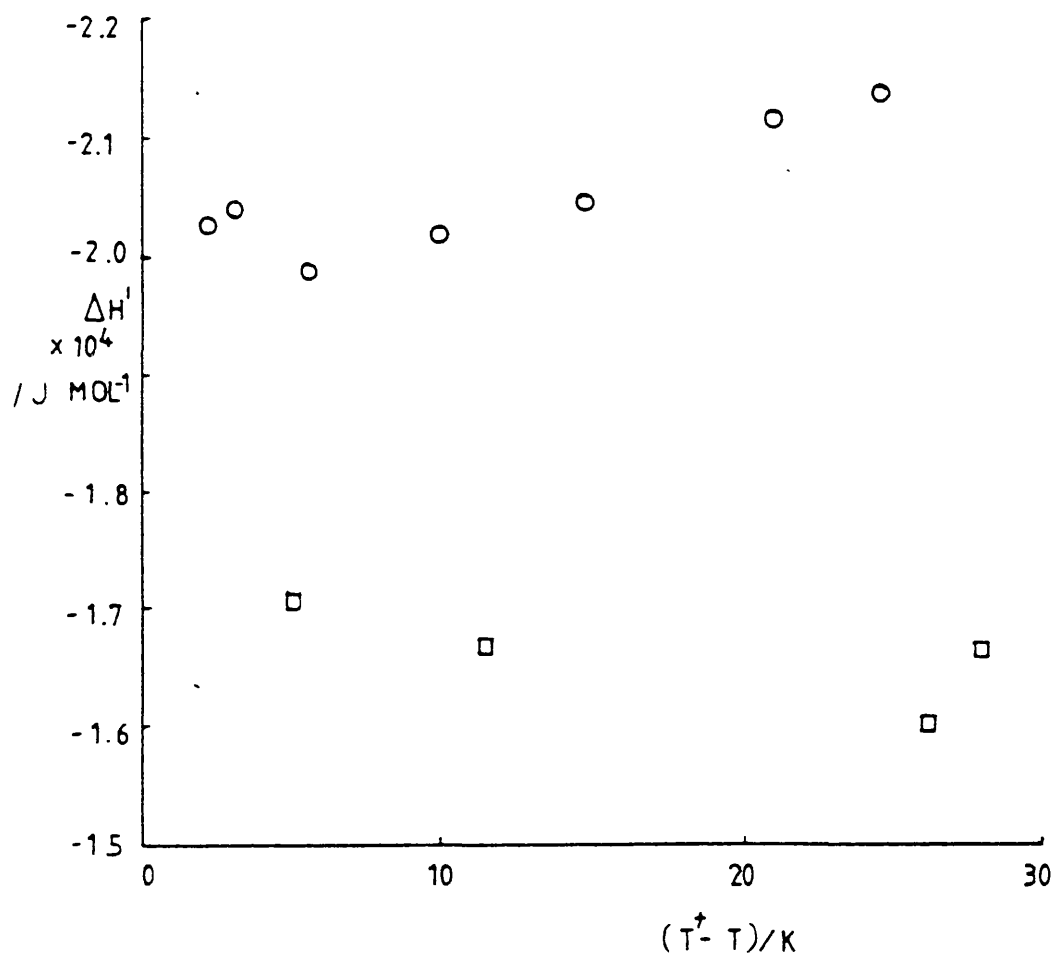


Figure (7.4.5)

Hexafluorobenzene + benzene



○ = points determined from benzene excess side of phase diagram.

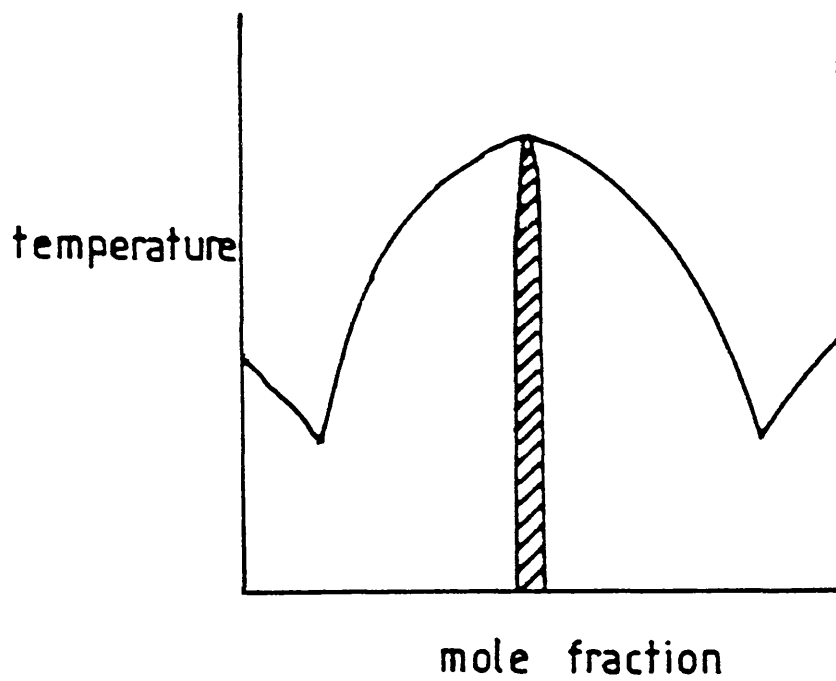
□ = points determined from hexafluorobenzene excess side.

diagram for hexafluorobenzene + benzene measured by Goates et al. (32), we calculated the enthalpy change for liquid + liquid \rightarrow solid complex (see figure 7.4.6); a value of $-18.5 \text{ kJ mol}^{-1}$ ($\pm 1.5 \text{ kJ mol}^{-1}$) was obtained. From a knowledge of the enthalpies of fusion and heat capacities of the two components (65,80), the enthalpy of formation of the solid complex was found (figure 5.11.1). The value of $+3.34 \text{ kJ mol}^{-1} \pm 1.5 \text{ kJ mol}^{-1}$ is in reasonable agreement.

$\Delta H(\text{solid complex})$ values determined from phase diagrams reported in this thesis using the treatment of Goates do not generally seem to be sensible: For hexafluorobenzene + 1-methylnaphthalene, a $\Delta H(\text{solid complex})$ of -9.5 kJ mol^{-1} was calculated, showing the solid complex to be stronger than that formed from hexafluorobenzene + benzene. But the value of $+4.6 \text{ kJ mol}^{-1}$, calculated for the hexafluorobenzene + 2-methylnaphthalene system, indicates a complex of similar strength to that formed with hexafluorobenzene + benzene and + naphthalene, and so is probably too high. Conversely, the $\Delta H(\text{solid complex})$ calculated for hexafluorobenzene + quinoline (-8 kJ mol^{-1}) seems too low.

As mentioned before, the calorimeter was used to determine the $\Delta H(\text{solid complex})$ of just two systems (hexafluorobenzene + 2-methylnaphthalene, and + quiniline). The values obtained appear more reasonable, and are certainly more reliable, than those determined from phase diagram data, i.e. the complex with

Figure (7.4.6)



Phase diagram for congruently melting point complex (1:1)
showing region of solid solution

2-methylnaphthalene is predicted as being stronger than the quinoline complex.

7.5 Excess Gibbs function: vapour pressure measurements

The excess Gibbs functions for the five systems determined from vapour pressure measurements are presented in Chapter 6 (section 9) and are shown together in figure (7.5.1). The values correlate well with the excess volume and enthalpy results.

Hexafluorobenzene + cis- and + trans-decalin give large positive excess Gibbs functions (970 J mol^{-1} and 802 J mol^{-1} respectively, at $x = 0.5$ and 303.15 K). When phase separation occurs, G^E/RT is approximately 0.5 (i.e. $G^E \approx 1200 - 1300 \text{ J mol}^{-1}$ at $x = 0.5$) so the system hexafluorobenzene + cis-decalin is approaching phase separation. A study of the simple eutectic phase diagram (figure 3.5.6) supports this, since it shows a near horizontal region at the middle mole fractions. Hexafluorobenzene + quinoline, as expected, exhibits a much less positive excess Gibbs function (135 J mol^{-1} at $x = 0.5$ and 318.15 K) due to complex formation. Hexafluorobenzene + tetralin has a slightly negative G^E (-125 J mol^{-1} , $x = 0.5$ and 303.15 K) and as expected, hexafluorobenzene + 2-methylnaphthalene possesses the most negative G^E , -298 J mol^{-1} (at $x = 0.5$ and 338.15 K).

We may again draw a comparison with the corresponding systems involving monocyclic hydrocarbons (figure 7.5.2).

Figure (7.5.1)

Excess Gibbs functions

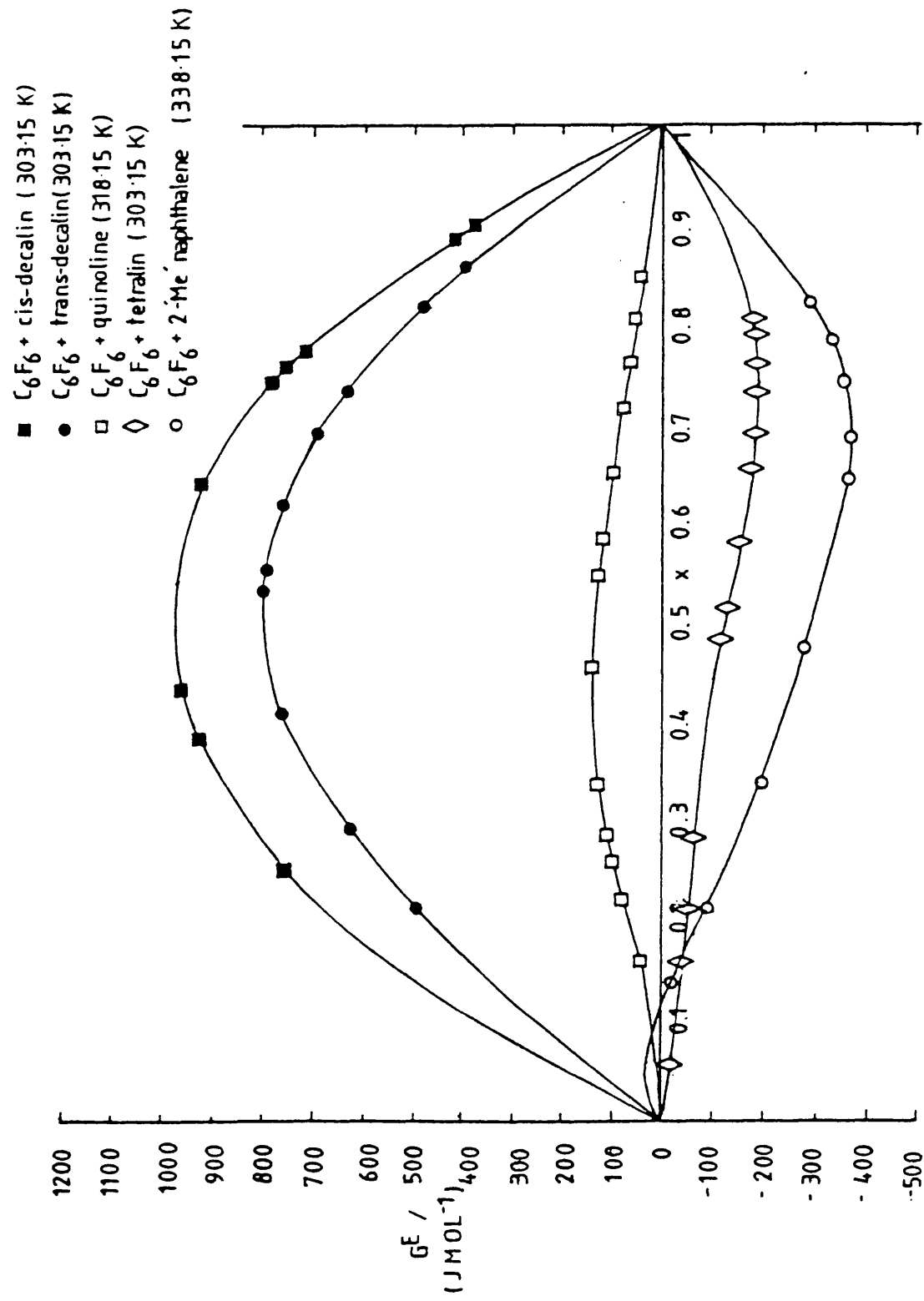
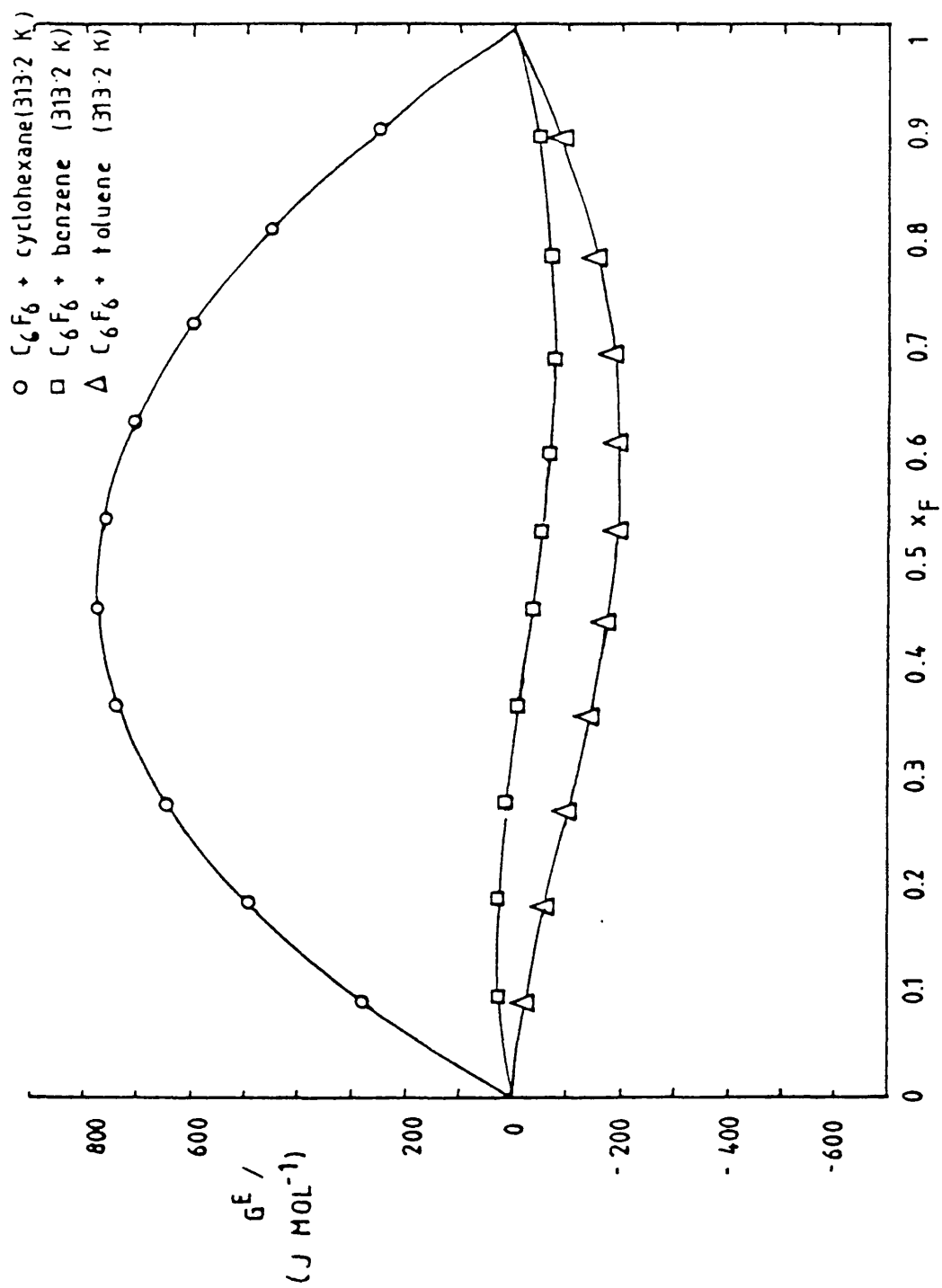


Figure (7.5.2)
Excess Gibbs functions (work of Gaw & Swinton)^(14,15)



The alicyclic cyclohexane gives a large positive G^E when mixed with hexafluorobenzene (15), (800 J mol^{-1} at $x = 0.5$ and 303.15 K) whereas benzene and toluene both show negative G^E values (14), (-60 and -210 J mol^{-1} respectively at $x = 0.5$ and 303.15 K).

For comparison N,N -dimethylaniline + hexafluorobenzene gives a G^E of -206 J mol^{-1} ($x = 0.5$ and 322.52 K) upon mixing with hexafluorobenzene. Isopropylcyclohexane + hexafluorobenzene has a G^E of $+752 \text{ J mol}^{-1}$ ($x = 0.5$ and 323.15 K) (85).

Since, for each of the five systems, excess enthalpies as well as excess Gibbs functions are available, plots of TS^E against mole fraction can be constructed. These are shown in figure (7.5.3). Hexafluorobenzene + tetralin, + quinoline and + 2-methylnaphthalene all show negative excess entropies, indicative of ordering associated with complex formation.

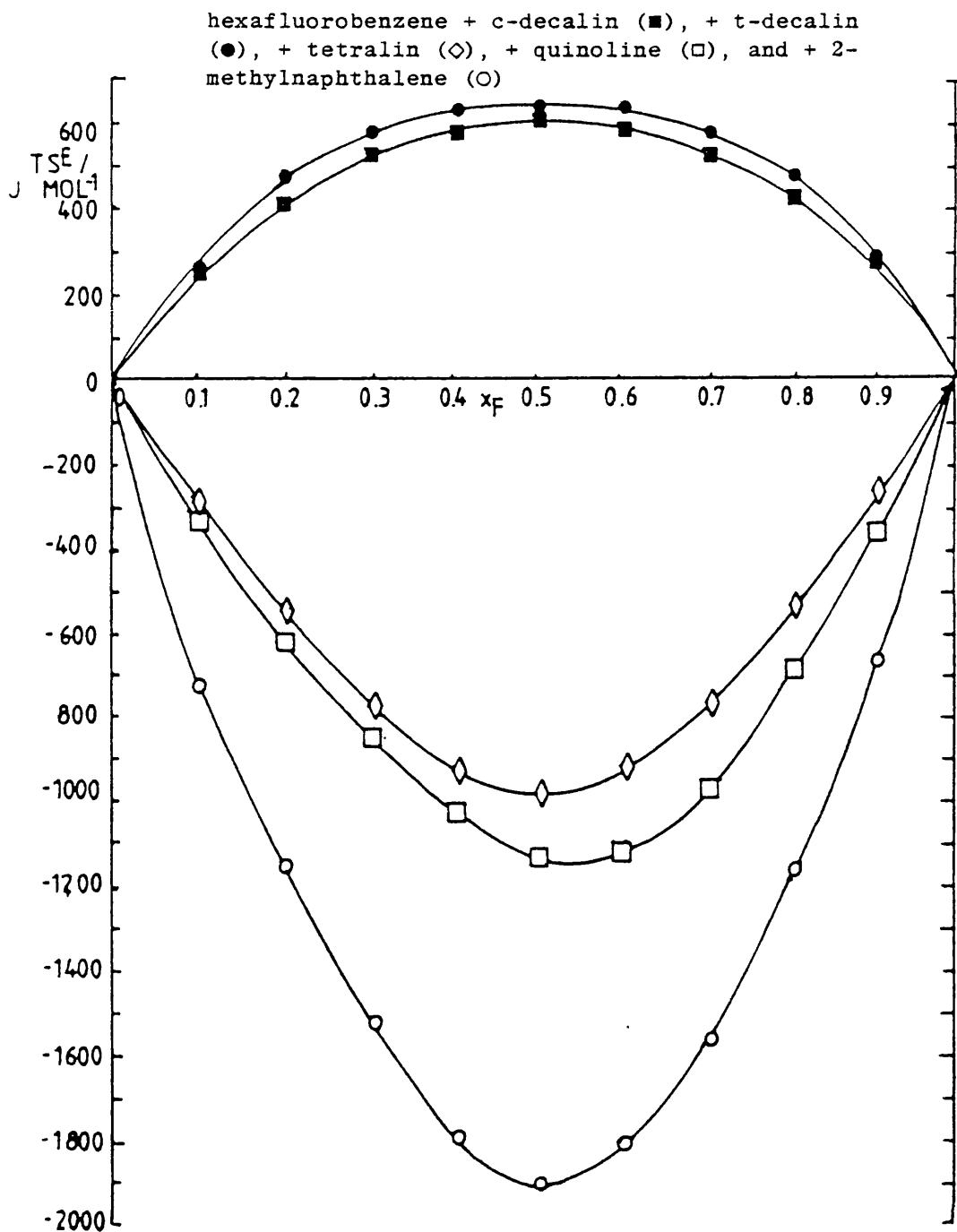
7.6 Excess Gibbs functions determined from solid-liquid phase diagrams

There are few systems for which G^E has been determined both from vapour pressure measurements and solid / liquid phase equilibria studies. One that has is the system benzene + p -xylene (81), where an uncertainty of $\pm 3 \text{ J mol}^{-1}$ was claimed on G^E values determined from the phase diagram; a good agreement with G^E values obtained from vapour pressure readings was found (82).

Figure (7.5.3)

Plot of TS^E v mole fraction

(calculated from G^E and H^E data)



Ott, Goates et al.(83) have recently discussed in detail the determination of G^E by both methods and have shown that a very careful analysis is needed in order to obtain good agreement between the two methods.

In the present work we have calculated G^E for hexafluorobenzene + cis- and + trans-decalin from our solid-liquid phase diagrams and the details of the calculation are presented in Chapter 6 (section 10). The values obtained by the two methods are shown in figure (6.11.1). The agreement is fairly good, although the values obtained from the solid-liquid phase equilibria are higher by some 100 J mol^{-1} in each case. The values obtained from vapour pressure measurements are undoubtedly more reliable, simply because all the readings were made at a chosen temperature (303.15 K in the present case). In order to calculate G^E from the solid-liquid phase diagram, it is necessary to convert measurements made at the freezing temperatures to 303.15 K. Nevertheless, it is possible to obtain reliable G^E values from solid-liquid phase equilibria studies provided the following conditions are met:-

1. It is assumed that the phase diagram shows a simple eutectic with no regions of solid solution.

2. Reliable enthalpies of fusion and heat capacities as a function of temperature of both solid and liquid forms of the pure components are available.

3. Reliable excess enthalpy measurements, as a function of temperature, are needed in order to convert the

activity coefficients (determined at the freezing points) to the chosen temperatures.

However, this method shows considerable promise and may be used more in the future.

7.7 Preliminary spectroscopic studies

In an attempt to prove the existence of $\pi-\pi^*$ interactions in hexafluorobenzene + naphthalene complexes, preliminary ultra - violet spectroscopy experiments were conducted using a Perkin Elmer 340 spectrophotometer.

The system hexafluorobenzene + 1-methylnaphthalene seemed to be the most likely to give an absorption peak due to charge transfer and so a 0.1 M solution of the potential electron acceptor, hexafluorobenzene, and a 10^{-4} M solution of 1-methylnaphthalene (both in n-hexane) were prepared. (The solution concentrations used were those suggested by Beaumont (84) and ensured that all of the aromatic hydrocarbon would complex with the hexafluorobenzene).

The twin compartment cells used are depicted in figure (7.7.1). To begin with, both cells contained the two solutions separated as shown. One cell was placed in the reference side and the other in the sample side of the spectrophotometer. Both cells were positioned so that the direction of light was that shown in the figure and the spectrum run. The cell on the sample side was then

Figure (7.7.1)

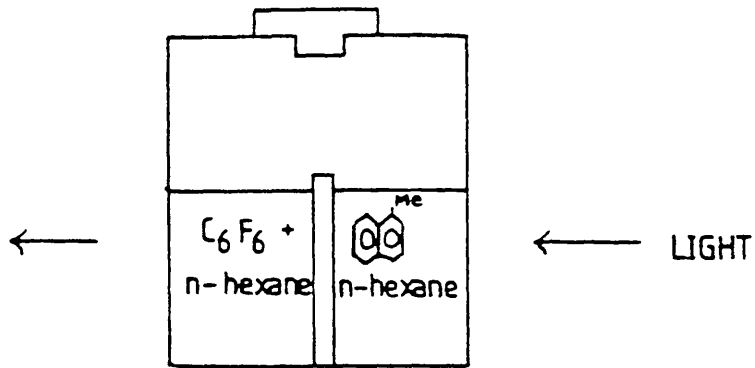
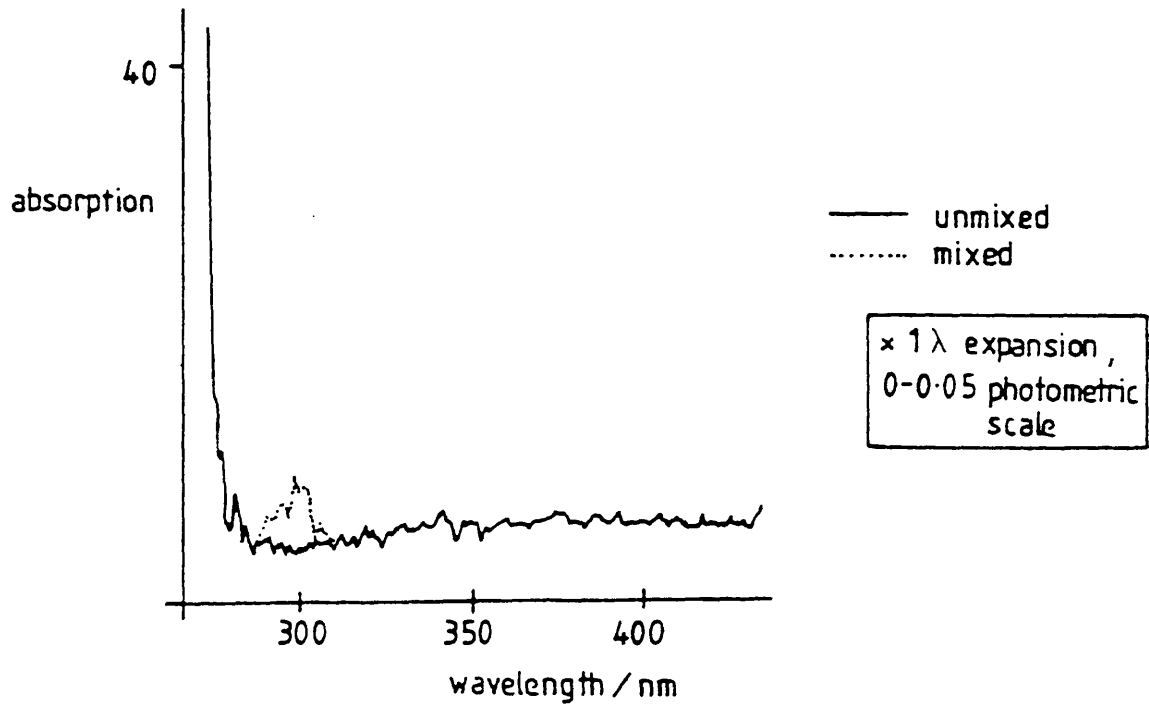


Figure (7.7.2)



carefully inverted several times to mix the two solutions, replaced in the instrument, and a new spectrum run. Very little difference existed between the two spectra, although a very small peak emerged at about 300 nm, as shown in figure (7.7.2).

7.8 Conclusion

Mixtures of hexafluorobenzene and naphthalene-type compounds form very strong 1:1 molar ratio congruent melting point complexes and possess negative V^E , H^E and G^E values.

It is possible that the basic unit of two six-membered rings joined at two adjacent carbons, where at least one ring is aromatic, is of the correct geometry for interaction with hexafluorobenzene. The fact that introducing a methyl group into these aromatic hydrocarbons (e.g. 1-, or 2-methylnaphthalene) seems to enhance the stability of the complex, may point to the presence of charge-transfer interactions. However, future work might include studies of V^E, H^E , for hexafluorobenzene + methylated naphthalenes, tetralins and decalins, which would allow plots of X^E against 'n' (where n = number of methyl groups attached to the hydrocarbon) to be constructed and compared with Powell's results (7).

Further weight to the idea that charge-transfer ($\pi-\pi^*$) interactions occur in these complexes is given by the work done on pentafluorocyanobenzene (PCFB) systems:

Both 1- and 2-methylnaphthalene give stronger (higher melting point) complexes with PCFB than hexafluorobenzene. Also a consideration of HOMO/LUMO overlap (see Chapter 1 and reference 13) seems to support the existence of charge-transfer interactions in aromatic fluorocarbon + naphthalene systems, whilst offering an explanation for their absence in aromatic fluorocarbon + benzene systems.

The little ultra - violet spectroscopy carried out was inconclusive and clearly more work can be done here, maybe even looking for peaks in the infra - red region.

Swinton (17) measured the induced dipole moment of hexafluorobenzene in mixtures with aromatic hydrocarbons. The values obtained, of 0.3 - 0.4 D (298 K), were smaller than anticipated, if π - π^* interactions were present. It would be interesting to repeat this work on hexafluorobenzene + naphthalene mixtures.

It is likely that charge-transfer does play a part in the specific chemical interactions (as do electrostatic forces between the π -quadrupole of the aromatic hydrocarbon and the C-F bond dipole) in hexafluorobenzene + naphthalene complexes; the geometry of the aromatic hydrocarbon is also important.

REFERENCES

1. R.L. Scott, J.Amer.Chem.Soc.,1948,70,4090.
2. R.L. Scott, J.Phys.Chem.,1958,62,136.
3. J.A.Godsell et al., Nature,1956,178,199.
4. J.S.Rowlinson and "Liquid and Liquid Mixtures",
F.L.Swinton, 3rd Ed. Butterworths,1982.
5. C.R.Patrick and Nature,1960,187,1021.
G.S.Prosser,
6. G.M.Brooke, J.Burdon, J.Chem.Soc.,1960,1768.
M.Stacey and J.C.Tatlow,
7. R.L.Powell and J.Chem.Thermodynamics,
F.L.Swinton, 1970,2,87.
8. A.W.Andrews, K.W.Morcom, J.Chem.Thermodynamics,
W.A.Duncan, F.L.Swinton 1970,2,95.
and J.M.Pollock,
9. T.G.Beaumont and J.Chem.Soc.,1967,1131.
K.M.C.Davis,
10. T.G.Beaumont and Nature,1968,218,865.
K.M.C.Davis,
11. D.V.Fenby, I.A.McLure J.Phys.Chem.,1966,70,602.
and R.L.Scott,
12. D.V.Fenby and R.L.Scott, J.Phys.Chem.,1967,71,4103.
13. D.A.Armitage and Trans.Faraday Soc.,
K.W.Morcom, 1969,65,688.
14. W.J.Gaw and F.L.Swinton, Trans.Faraday Soc.,
1968,64,2023 .
15. W.J.Gaw and F.L.Swinton, Trans.Faraday Soc.,
1968,64,637.

16. W.A.Duncan and F.L.Swinton, Trans.Faraday Soc., 1966,62,1082.
17. W.A.Duncan, J.P.Sheridan and F.L.Swinton, Trans.Faraday Soc., 1966,62,1090.
18. M.W.Hanna, J.Amer.Chem.Soc.,1968,90,285.
19. W.A.Duncan and F.L.Swinton, J.Phys.Chem.,1966,70,2417.
20. B.J.Skillern de Bristowe and D.Stubley, J.Chem.Thermodynamics, 1973,5,865.
21. B.J.Skillern de Bristowe and D.Stubley, J.Chem.Thermodynamics, 1973,5,121.
22. P.J.Howell, B.J.Skillern de Bristowe and D.Stubley, J.Chem.Thermodynamics, 1972,4,225.
23. D.Hall and K.W.Morcom, J.Chem.Thermodynamics, 1975,7,407.
24. J.M.T.Brindley, K.W.Morcom and C.G.Osborne, J.Chem.Thermodynamics, 1979,11,687.
25. D.Hall, K.W.Morcom and J.M.T.Brindley, J.Chem.Thermodynamics, 1974,6,1133.
26. C.Y.Leong, D.E.Jones and D.V.Fenby, J.Chem.Thermodynamics, 1974,6,609.
27. J.C.A.Boeyens and F.H.Herbstein, J.Phys.Chem.,1965,69,2153.
28. T.Dahl, Acta.Chem.Scand.,1971,25,1031.
29. T.Dahl, Acta.Chem.Scand.,1972,29,170.
30. T.Dahl, Acta.Chem.Scand.,1972,26,1569.
31. T.Dahl, Acta.Chem.Scand.,1973,27,995.

32. J.R.Goates, J.B.Ott, J.Chem.Thermodynamics,
and J.Reeder, 1973,5,135.
33. J.R.Goates, J.B.Ott, J.Chem.Thermodynamics,
and J.Reeder, 1974,6,281.
34. J.R.Goates, J.B.Ott, J.Chem.Thermodynamics,
and J.Reeder, 1974,6,489.
35. J.B.Goates, J.B.Ott, J.Chem.Soc. (Faraday Trans.),
J.Reeder and R.B.Shirts, 1974,70 (7),1325.
36. A.W.Andrews J.Chem.Thermodynamics,
and K.W.Morcom, 1971,3,519.
37. A.W.Andrews, D.Hall J.Chem.Thermodynamics,
and K.W.Morcom, 1971,3,527.
38. M.L.Martin and J.Chem.Thermodynamics,
R.S.Murray, 1972,4,723.
39. E.McLaughlin and J.Chem.Soc. (A),1966,10,1106.
C.E.Messer,
40. E.Kenyon-Blair, J.Chem.Thermodynamics,
G.A.Griffith, P.R.Jackson 1983,15,1001.
and K.W.Morcom,
41. T.Kelly and F.L.Swinton, J.Chem.Thermodynamics,
1974,6,435.
42. C.G.Osborne and J.Chem.Thermodynamics,
K.W.Morcom, 1981,13,235.
43. E.Aznar, B.Ruiz and J.Chem.Thermodynamics,
C.Gutierrez, 1985,17,1121.
44. T.Dahl, Acta.Cryst.,1977,B33,3021.
45. F.L.Swinton, Molecular Complexes,
ed.R.Foster, P.Elek, London,
1974,Vol 2 .

46. R.Foster, Organic charge Transfer
Complexes, Acad. Press, 1969.
47. R.Foster and C.A.Fyfe, J.Chem.Soc.Chem.Comm.,
1965, 642.
48. J.Milfrom, J.Phys.Chem., 1959, 63, 1843.
49. W.L.Masterton et al, J.Chem.Thermodynamics,
1971, 3, 243.
50. J.D.Ray, Rev.Sci.Instr., 1957, 28, 200.
51. E.A.Guggenheim and Physicochemical Calculations,
J.E.Prue, N.Holland Publ.Co., 1956, 195.
52. J.Kendall et al., J.Amer.Chem.Soc., 1921, 43, 1481.
53. C.G.Osborne, Ph.D Thesis, Leicester
University 1981.
54. E.F.G.Herrington, J.Chem.Soc., 1950, 50, 199.
55. L.H.Adams, International Critical Tables,
Vol.57,
56. A.W.Andrews, Ph.D Thesis, Leicester
University, 1971.
57. D.A.Armitage, Trans.Faraday Soc.,
M.J.Blandamer, M.J.Foster 1968, 64, 1193.
N.J.Hidden, K.W.Morcom,
M.C.R.Symons and M.J.Wootten,
58. R.Martin, Ph.D Thesis,
Leicester University, 1978.
59. R.H.Stokes, B.J.Levien, J.Chem.Thermodynamics,
and K.N.Marsh, 1970, 2, 43.
60. G.A.Bottomley and J.Chem.Thermodynamics,
R.L.Scott, 1974, 6, 973.
61. M.K.Kumaran and J.Chem.Thermodynamics,
M.L.McGlashan, 1977, 9, 259.

62. D.A.Armitage, Ph.D Thesis,
Leicester University,1968.
63. J.A.Larkin and J.Chem.Soc.,1961,3425.
M.L.McGlashan,
64. E.A.Faulkner, J.Chem.Soc.,1965,2837.
M.L.McGlashan and
D.Stubley,
65. J.F.Counsell, Trans.Faraday Soc.,
J.H.S.Green,J.L.Hales 1965,61,212.
and J.F.Martin,
66. J.P.McCullough, J.Phys.Chem.,1957,61,1105.
H.L.Finke et al.,
67. J.Timmermans, Physico-chemical constants of pure
organic compounds,Volumes 1 and 2,
Elsevier,1965.
68. G.S.Darks, S.S.Todd J.Amer.Chem.Soc.,1936,58,398.
and W.A.Moore,
69. J.R.Goates, J.B.Ott J.Chem.Thermodynamics,
and J.Reeder, 1985,17(7),665.
70. K.N.Marsh, Trans.Faraday Soc.,
1968,64,883.
71. J.A.Barker, Aust.J.Chem.,1953,6,207.
72. W.F.Seyer and C.W.Mann, J.Amer.Chem.,1945,67,328.
73. S.Young, J.Chem.Soc., (LONDON),1985,55,483.
74. W.Herz and P.Shuftan, Z.Physik Chem.,1922,101,269.
75. C.R.Patrick and Trans.Faraday Soc.,
G.S.Prosser, 1964,60,700.
76. D.A.Armitage, J.Chem.Thermodynamics,
J.M.T.Brindley,D.J.Hall 1975,7,97.
and K.W.Morcom,

77. A.Barlatier et al., Compt.Rend.,1971,C273,1473.
78. D.A.Armitage, Trans.Faraday Soc.,
T.G.Beaumont,K.M.C.Davies, 1971,67,2548.
D.J.Hall and K.W.Morcom,
79. J.S.Brennan and J.Chem.Soc.Faraday Trans.I.,
F.L.Swinton, 1974,70,1965.
80. G.D.Oliver et al., J.Amer.Chem.Soc.,1948,70,1502.
81. J.B.Ott, J.R.Goates J.Chem.Thermodynamics,
and R.B.Grigg, 1979,11,1167.
82. J.B.Ott, K.N.Marsh J.Chem.Thermodynamics,
and R.H.Stokes, 1980,12,493.
83. J.B.Ott, J.R.Goates J.Chem.Thermodynamics,
1986,18,107.
84. T.G.Beaumont, Ph.D Thesis, Leicester
University,1969.
85. D.A.Armitage, J.Chem.Thermodynamics,
J.M.T.Brindley and 1978,10,581.
K.W.Morcom,
86. D.R.Dounslin,R.H.Harrison, J.Chem.Thermodynamics,
and R.T.Moore, 1969,1,581.
87. J.H.Dymond and E.B.Smith, The Virial Coefficients
of Pure Gases and Mixtures,
Clarendon Press,Oxford,1980.
88. N.M.D.Brown and J.Chem.Soc.Chem.Comm.,1974,770.
F.L.Swinton,

Philip R. Jackson

Thermodynamic studies of
binary mixtures involving
aromatic fluorocarbons

SUMMARY

Solid-liquid phase diagrams have been determined for binary systems of hexafluorobenzene + naphthalene-type compounds, and indicate strong 1:1 congruently melting point complexes. Hexafluorobenzene + cis- and + trans-decalin were found to give simple eutectic phase diagrams.

Excess enthalpies, excess volumes and excess Gibbs functions have been measured for the same hexafluorobenzene + naphthalene-type compound mixtures and are large and negative, which is characteristic of systems where specific interactions take place. This contrasts with the large positive excess functions found with hexafluorobenzene + decalin systems, where only dispersion forces are assumed present.

The excess Gibbs function for hexafluorobenzene + trans- and cis-decalin have been determined theoretically from freezing point data as well as directly from vapour pressure measurements.

A batch calorimeter, besides being used for excess enthalpy measurements, has been employed in determining heats of solution, which lead to a value for the enthalpy change for the process, solid + solid \rightarrow complex.

The possibility of charge-transfer interactions occurring in hexafluorobenzene + naphthalene-type compound systems has been discussed in terms of HOMO/LUMO overlap considerations and is supported by the observation that pentafluorocyanobenzene forms stronger (higher melting point) complexes with 1- and 2-methylnaphthalene, than hexafluorobenzene does.